WEST POMERANIAN
UNIVERSITY OF TECHNOLOGY
IN SZCZECIN

FACULTY OF MECHANICAL ENGINEERING AND MECHATRONICS

Institute of Materials Science and Engineering

Sandra Paszkiewicz

POLYMER HYBRID NANOCOMPOSITES CONTAINING CARBON NANOPARTICLES. *IN SITU* SYNTHESIS AND PHYSICAL PROPERTIES

PhD Thesis

Szczecin, 2014

Reference commission:

Supervisor:	Professor Zbigniew Rosłaniec PhD, DSc
Promoter:	Anna Szymczyk PhD, DSc
Assistant-promoter:	Ryszard Pilawka PhD
Referents:	Professor Karl Schulte PhD
	Professor Jarosław Janicki PhD, DSc

The research described in this thesis was funded by National Science Centre project NCN No N N507 218340 entitled: ”Polymer hybrid nanocomposites containing graphene and carbon nanotubes – nanostructure, mechanical and electrical properties”.

I would like to thank:
Prof. Zbigniew Rosłaniec, for his valuable comments and assistance that served me in preparing this work, my promoter Dr. Anna Szymczyk, for invaluable assistance during the course of the doctorate and my assisting promoter Dr. Ryszard Pilawka, and all co-workers, colleagues for their valuable guidance and kindness.

.

To my fiancé and my family

Table of content

List of abbreviations and symbols

CB	carbon black
CMG	chemically modified graphene
CNF	carbon nanofibers
CNT	carbon nanotubes
CRG	chemically reduced graphene
CRGO	chemically reduced graphene oxide
DWCNT	double-walled carbon nanotubes
EG	expanded graphite
FLG	few layer graphene
f-CRGO	functionalized chemically reduced graphene oxide
f-GO	functionalized graphene oxide
f-GP	functionalized graphene
GD	graphene derivatives
GNP	graphite nanoplatelets
GNF	graphite nanoflakes
GNR	graphene nanoribbons
GNS	graphite nanosheets
GO	graphene/graphite oxide
GOn	graphene oxide nanosheets
GP	graphene
MGP	multi-graphene platelets
MWCNT	multi-walled carbon nanotubes
MMT	montmorillonite
RGO	reduced graphene oxide
SLG	single layer graphene
SWCNT	single-walled carbon nanotubes
TEGO	thermally expanded graphite oxide
TRG	thermally reduced graphene
TRGO	thermally reduced graphene oxide

ABS	acrylonitrile -butadiene-styrene terpolymers
EP	epoxy
LCE	liquid crystalline epoxide
HDPE	high-density polyethylene
PA	polyamide
PANI	polyaniline
PBT	poly(butylene terephthalate)
PC	polycarbonate
PE	polyethylene
PEE	poly(ether esters)
PEI	polyetherimide
PET	poly(ethylene terephthalate)
PLA	poly(lactic acid)
PI	polyimide
PMMA	poly(methyl methacrylate)
PP	polypropylene

PS	polystyrene
PTT	poly(trimethylene terephthalate)
PTT-PTMO	poly(trimetylene terephthalate)-*block*-poly(tetramethylene oxide)
PTMG	poly(tetramethylene oxide) glycol
PTMOT	poly(tetramethylene ether glycol terephthalate)
PU	polyurethane
PVA	poly(vinyl alcohol)
PVF	poly(vinyl fluoride)
PVDF	poly(vinylidene fluoride)
RPUF	rigid polyurethane foam
TPE	thermoplastic elastomer
TT	trimethylne terephthalate unit/sequence

AFM	atomic force microscope
CVD	chemical vapour deposition
DMTA	dynamic mechanical thermal analysis
DSC	differential scanning calorimetry
HiPco	high-pressure CO conversion
TEM	transmission electron microscopy
TGA	thermal gravimetric analysis
SAXS	small angle x-ray scattering
SEM	scanning electron microscopy
WAXS	wide angle x-ray scattering

C, %	solution concentration
H, Sh	Shore hardness
E, MPa	Young's modulus
T_g, ^oC	glass transition temperature
T_c, ^oC	crystallization temperature
T_m, ^oC	melting temperature
X_c, %	degree of crystallinity

Preface

One of the most currently developing directions of cognitive and applied works is the research on nanocomposites, particularly on polymer nanocomposites. Polymer nanocomposites are obtained by modifying the traditional materials by dispersing the fillers in a polymer matrix with dimensions of a few nanometers. They are therefore complex systems with two or more phases (continued and dispersed) with an explicit separation surface from which the dispersed component is characterized by at least one dimension in the nanometer scale [1] [2]. The study of interfacial interactions at the nano level are among the most important topics of research and development in the field of materials science [1] [3]. The interest in such materials stems from the fact that the introduction of the filler nanoparticles, having at least one dimension not exceeding 100 nm, to polymer matrix enables to design and manufacture of materials with extremely high or new physical properties, with very limited involvement of the filler. Introduction to the polymer matrix the "nanofiller", depending on its type, has to make the improvement of mechanical properties, thermal, optical and barrier. Polymer nanocomposites, consisting of additives and polymer matrices, including thermoplastics, thermosets and elastomers, are considered to be an important group of relatively inexpensive materials for many engineering applications. Two or more materials are combined to produce composites that possess properties that are unique and cannot be obtained each material acting alone. Significant improvement in properties of composites depends mainly on: the size and shape of the nanofiller particles, specific surface area, the degree of development of the surface, the surface energy and the way the spatial distribution of nanoparticles in the polymer matrix [2]. As nanofillers may be used materials differing with regard to the chemical nature (organic and inorganic), the physical structure (such as amorphous, crystalline) and particle shape (1D-linear rods, such as carbon nanotubes, 2D-lamellar, e.g. nanoclay (MMT), 3D-"powder") [2]. The major advantages of polymer nanocomposites include: increased stiffness (without loss of toughness), increased thermal and dimensional stability, increased fire resistance, improved barrier effect, good optical properties and for nanocomposites involving carbon nanotubes and graphene - an additional electrical conductivity. Except those mentioned advantages, the nanocomposites have certain drawbacks, which include high cost, difficulty in obtaining a high and uniform level of dispersion in the polymer and nanofiller tendency to agglomerate [1] [3].

So far, the greatest interest among researchers and innovative groups aroused nanocomposites containing carbon nanotubes. The discovery in 2004, the new carbon allotrope, namely graphene, due to its extraordinary physico-chemical properties attracted much attention on nanocomposites with its participation. Graphene is an atomically thick, two-dimensional (2-D) sheet composed of sp2 carbon atoms arranged in a honeycomb structure [4] with a carbon–carbon bond length of 0.142 nm [5]. Electrons in graphene behave like massless relativistic particles, which contribute to very peculiar properties such as an anomalous quantum Hall effect and the absence of localization [6]. Graphene has indicated a variety of intriguing properties including high electron mobility at room temperature (250 000 cm^2/Vs) [7] [8], and unlike CNT, chirality is not a factor in its electrical conductivity, exceptional thermal conductivity (5000 Wm^{-1} K^{-1}) [9], and superior mechanical properties with Young's modulus of 1 TPa and ultimate strength of 130 GPa [8]. These properties in

addition to extremely high surface area (theoretical limit: 2630 m^2/g) and gas impermeability [10] demonstrate graphene's great potential for improving electrical, mechanical, thermal, and gas barrier properties of polymers. Graphene does not occur free-standing because of its instability and tendency to form three-dimensional structures (for example, fullerenes and nanotubes). Graphenes can be obtained from graphite, but that the loosened structure of graphite has become the graphene, it is necessary to use micromechanical methods [11]. A type of 2D graphitic nanofiller consisting of stacked graphene layers are graphite nanoplatelets (GNP), also called graphite nanosheets (GNS) and graphite nanoflakes (GNF), or just simply exfoliated or expanded graphite (EG). The stacked layers are bonded to each other by weak Van der Waals forces with a constant interlayer distance of about 0.34 nm. Carbon nanotubes, similarly as graphene, have extremely high strength properties: tensile strength, up to ~ 500 GPa and the elastic modulus reaches 7-8 TPa. With a small diameter (1-80 nm) and a large aspect ratio (L/D exceeds 10 000) are potentially attractive material for reinforcing polymers, ceramics and metals [12] [13] [14], which was also confirmed by previous studies of the research team of the Institute of Materials Science and Engineering WUT on PTT nanocomposites reinforced with carbon nanotubes (MWCNT, SWCNT) [15] [16].

Interesting from the point of view of their impact on the enhancement effect seems to be the introduction of two types of carbon nanofillers such as graphene (a plate filler - 2D) and CNT (a fibrous filler / linear 1D). This is confirmed by some of the literature data, where, for example, the strengthening effect (increase in elastic modulus and hardness) was observed after the introduction of a few layer functionalized graphene (0.6 wt%) into the matrix of PVA and PMMA [17] [18]. The PVA composites reinforced with few layer graphene (FLG)/SWCNT (0.2/0.4 wt %, E = 9.33 GPa, H = 366 MPa) had significantly higher values of the Young's modulus and hardness than the composites containing SWCNT (0.6 % by weight, E = 7.8 MPa, H = 290 MPa) and an unmodified PVA (E = 0.66 GPa, H = 38 MPa) [19]. In the case of thermoplastic composites changes in physical properties can be attributed not only to the extraordinary characteristics of graphene and carbon nanotubes, but also to their effects on the crystal structure of the polymer. The effect of the addition of filler on the ability to crystallize of semicrystalline polymers was already noted. The secretes of the dispersed phase distributed in polymer matrix become active nucleation centers, stimulating the growth of crystallites. The amount of the crystalline phase substantially affect the mechanical properties of the composite [20] [21]. Reducing the size of the precipitates and the increase in their number in the volume of the system leads to an increase in nucleation, thereby resulting in smaller crystallites. Fine-grained structure gives better results in mechanical properties. Another effect of the introduction of graphene (similarly as in the case of CNT) may be changes of physical changes temperatures. This is due to the fact that the presence of nanoparticles in the polymer, influence the mobility of the polymer chains, which in some cases resulted in increasing the glass transition temperature T_g and crystallization temperature Tc. For instance, the addition of 1 wt %. of functionalized graphene into poly(acrylonitrile) caused an increase in T_g of 50 °C, in the case of nanocomposites based on poly(methyl methacrylate)/ GNS (0.05 wt %) of approximately 30 °C [19]. In the case of nanocomposites based on PVC containing GNS and / or CNT increasing of degree of crystallinity of the polymer after the introduction of nanofiller was observed [20]. The

synergic effect of addition of three types of carbon nanostructures graphene nanoplatelets (GNPs), carbon black (CB) and CNTs originates not only from the dispersion promotion of fillers due to the unique geometric structure of the individual conductive carbon material, but also from the effective link of both the narrow and broad gaps between graphite sheets by the spherical CB and long flexible CNTs, resulting in the formation of excellent conducting network in the matrix [22].

According to the specific application, CNT/graphene derivatives/polymer nanocomposites can be classified as structural or functional composites. For the structural composites, the unique mechanical properties of CNTs and EG/FLG, such as the high modulus, tensile strength and strain to fracture, are explored to obtain structural materials with much improved mechanical properties. As for hybrid CNT/GD/polymer functional composites, many other unique properties of nanofiller, such as electrical, thermal, optical and damping properties along with their excellent mechanical properties, are utilized to develop multi-functional composites for applications in the fields of heat resistance, chemical sensing, electrical and thermal management, photoemission, electromagnetic absorbing and energy storage performances, etc.

It is an open question to completely understand the synergistic effect brought about by the combinations of nanofillers with different shapes. As an outlook, the variation of the graphene derivatives (expanded graphite - EG, few layer graphene- FLG) to CNT ratio may lead to even more improved mechanical, electrical and barrier properties by adjusting an optimum microstructure.

The aim of this work is to develop the novel electrically conductive hybrid graphene and carbon nanotubes polymer nanocomposites while maintaining balanced mechanical and thermal properties. The main objective will be to examine the effect of the addition of graphene and carbon nanotubes on the morphology, interphase interaction, mechanical and electrical properties of nanocomposites, and as a result to conclude the graphene and carbon nanotubes polymer strengthening mechanism. Also, identify the characteristics of specific, indicating the functional nature of the obtained nanocomposites.

INTRODUCTION

1. Carbon nanotubes

1.1. General characterization

Carbon nanotubes (CNT) first reported by Iijima [23] possess high flexibility [24], low mass density [25] and large aspect ratio (typically ca. 300-1000). Owning superior mechanical properties, such as a Young's modulus of 1.0 TPa [26] [27] a theoretical critical strain of 20% or higher, and ideal tensile strength of about 100 GPa [28] carbon nanotubes (CNTs) have been perceived as the strongest material in nature for about 2 decades. The unique combination of mechanical, electrical, and thermal properties that make nanotubes excellent candidates to substitute or complement the conventional nanofillers in the fabrication of multifunctional polymer nanocomposites. Depending on their structural parameters, SWCNT can be metallic or semiconducting, which further expands their range of applications.

Carbon nanotubes are long cylinders of covalently bonded carbon atoms. The ends of the cylinders may or may not be capped by hemifullerenes [29]. There are two basic types of CNT: single-walled carbon nanotubes (SWCNT) and multiwalled carbon nanotubes (MWCNT) (Figure 1). SWCNT can be considered as a single graphene sheet (graphene is a monolayer of sp2-bonded carbon atoms) rolled into a seamless cylinder. The carbon atoms in the cylinder have partial sp3 character that increases as the radius of curvature of the cylinder decreases. MWCNT consist of nested graphene cylinders coaxially arranged around a central hollow core with interlayer separations of ~0.34 nm, indicative of the interplane spacing of graphite [30]. A special case of MWCNT is double-walled carbon nanotubes (DWCNT) that consist of two concentric graphene cylinders. DWCNT are expected to exhibit higher flexural modulus than SWCNT due to the two walls and higher toughness than regular MWCNT due to their smaller size [31].

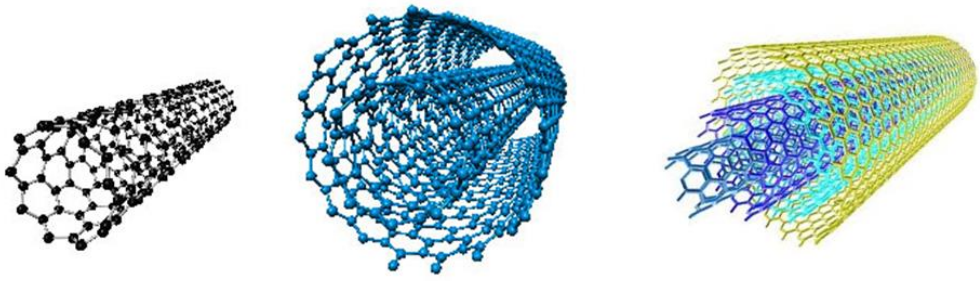

Fig. 1 Schematic diagrams showing different types of CNTs: a) SWCNT, b) DWCNT and c) MWCNT [32]

The nanotubes can be filled with foreign elements or compounds, e.g., with C60 molecules, to produce hybrid nanomaterials which possess unique intrinsic properties, such as transport properties [31]. These hybrid nanomaterials currently have limited availability, but as production increases this might be a new opportunity for polymer nanocomposites.

The various ways of rolling graphene into tubes are described by the tube chirality (or helicity or wrapping) as defined by the circumferential vector, $\overrightarrow{C_h} = n\overrightarrow{a_1} + m\overrightarrow{a_2}$ (Figure 2),

where the integers (*n, m*) are the number of steps along the unit vectors (*a*b1 and *a*b2) of the hexagonal lattice [33]. Using this (*n, m*) naming scheme, the three types of orientation of the carbon atoms around the nanotube circumference are specified as arm chair (*n*) *m*), zigzag (*n*) 0 or *m*) 0), or chiral (all others). The chirality of nanotubes has significant impact on its transport properties, particularly the electronic properties. All armchair SWCNT are metallic with a band gap of 0 eV. SWCNT with *n* -*m*) 3*i* (*i* being an integer and ≠0) are semimetallic with a band gap on the order of a few meV, while SWCNT with $n - m \neq 3i$ are semiconductors with a band gap of ca. 0.5-1 eV [34]. Each MWCNT contains a variety of tube chiralities, so their physical properties are more complicated to predict.

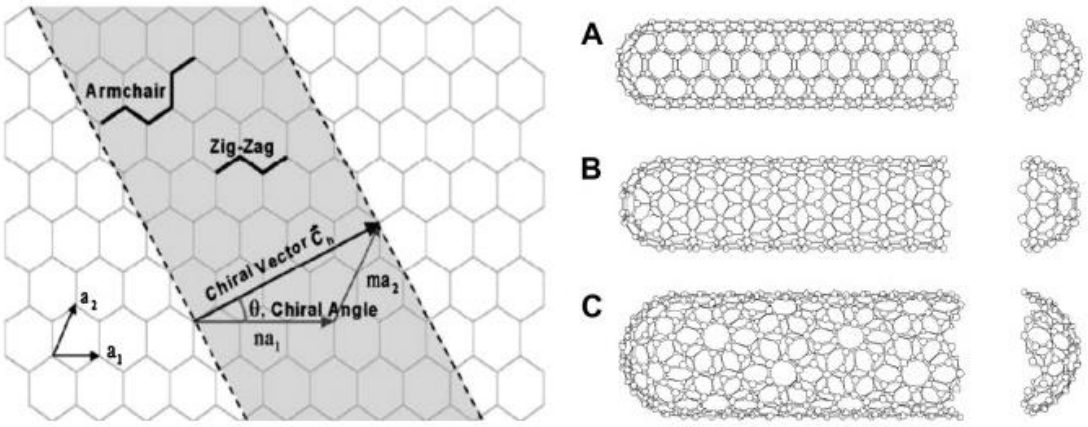

Fig. 2 Schematic diagram showing how a hexagonal sheet of graphene is "rolled" to form a carbon nanotube with different chiralities (A: armchair; B: zigzag; C: chiral) [33] [35].

1.2. Processing of carbon nanotubes for composite materials

CNTs (single- or multi-walled) can be produced using different methods, which mainly involve gas phase processes. The optimal conditions for nanotube generation using electric arc-discharge technique involve the passage of a direct current (80–100 A) through two high-purity graphite (6–10 mm OD) electrodes separated by ~1–2 mm, in a high-purity He and Ar atmosphere (500 Torr) [36], metal powders (only for producing SWCNTs); thus the costs associated with the production of SWCNTs and MWCNTs are high. Although the crystallinity of the material is also high, there is no control over dimensions (length and diameter) of the tubes. Unfortunately, by-products such as polyhedral graphite particles (in the case of MWCNTs), encapsulated metal particles (for SWCNTs), and amorphous carbon are also formed [37]. High-power laser vaporization (YAG type) of pure graphite targets inside a furnace at 1200 ^{o}C, in an Ar atmosphere is capable of generating MWCNTs [38]. In order to generate SWCNTs using the laser technique, it is necessary to add metal particles as catalysts to the graphite targets. Unfortunately, the laser technique is not economically advantageous because the process involves high-purity graphite rods, the laser powers required are high (in some cases two laser beams are required), and the amount of nanotubes that can be produced per day is not as high as some of the methods discussed above. In electrolysis method, which involves a liquid phase process is able to produce MWCNTs [39]. The liquid-phase electrolytic method has not been widely used probably because the nanotube

yield is difficult to control. In addition, the technique has not been able to produce SWCNTs. However, additional studies need to be carried out because this route may be advantageous owing to the low cost involved. Hydrocarbon (e.g., methane, acetylene, naphthalene, etc.) decomposition over metal catalysts (e.g., Co, Ni, Fe, Pt and Pd deposited on substrates such as silicon, graphite, or silica), is able to produce fullerenes, CNTs, and other sp2-like nanostructures. This process is also known as chemical vapor deposition (CVD). Compared with arc and laser methods, CVD might offer more control over the length and structure of the produced nanotubes, and the process appears scalable to industrial quantities. In addition to high-energy lasers, arc-discharge, and thermal routes, solar energy offers an alternative to produce CNTs. In this method to produce SWCNTs and MWCNTs a solar energy is focused on carbon-metal target in an inert atmosphere [40]. This method is potentially advantageous but further research needs to be carried out because the quality of the products is highly sensitive to the pressure, carrier gas, and carbon-metal ratio.

The chemical modification and solubilization of carbon nanotubes represent an emerging area in the research on nanotubes-based materials. Understanding nanotube suspensions is vital to controlling various solvent-based processes (phase separation, chemical derivatization, etc.) associated with preparing nanotube/polymer composites because the initial nanotube dispersion can impact the nanotube dispersion in the polymer matrix [29]. Local strain in carbon nanotubes, which arises from pyramidalization and misalignment of the π-orbitals of the sp2- hybridized carbon atoms, makes nanotubes more reactive than a flat graphene sheet, thereby paving the way to covalently attach chemical species to nanotubes [41]. This covalent functionalization of nanotubes can improve nanotube dispersion in solvents and polymers and furthermore can provide a means for engineering the nanotube/polymer interface for optimal composite properties. A noteworthy drawback of covalent functionalization is the disruption of the extended π conjugation in nanotubes. While the impact of disrupted π conjugation is limited for mechanical and probably thermal properties, the impact on electrical properties is expected to be profound because each covalent functionalization site scatters electrons. Noncovalent functionalization is an alternate method for tuning the interfacial properties of nanotubes [42] [43].

2. Polymer nanocomposites containing carbon nanotubes

The polymer nanocomposites using carbon nanotubes as a filler were first reported in 1994 [44]. Earlier nanocomposites used nanoscale fillers such as carbon blacks, silicas, clays, and carbon nanofibers (CNF) to improve the mechanical, electrical, and thermal properties of polymers. The combination of high-aspect ratio, small size, strength, stiffness, low density, and high conductivity makes CNTs perfect candidates as fillers in polymer composites. The properties of polymer nanocomposites containing carbon nanotubes depend on several factors in addition to the polymer: synthetic process used to produce nanotubes; nanotube purification process (if any); type and amount of impurities in the nanotubes; diameter, length, and aspect ratio of the nanotube objects in the composite (isolated, ropes, and/or bundles); nanotube orientation in the polymer matrix [29]. Fabrication of carbon nanotube/polymer composite methods have predominantly focused on improving nanotube dispersion because the better

nanotube dispersion in the polymer matrices is, the greater improvement in properties has been found.

2.1. Preparation of CNT/polymer nanocomposites

The widely applied methods to produce nanotubes/polymer composites are as follows: solution blending, melt blending, *in situ* polymerization and others: latex technology, solid-state shear pulverization and coagulation spinning methods. Solution blending is the most common method for fabricating polymer nanocomposites because it is both amenable to small sample sizes and effective. This method involves three major steps: disperse nanotubes in a suitable solvent, mix with the polymer (at room temperature or elevated temperature), and recover the composite by precipitating or casting a film. To obtain metastable suspensions of nanotubes or nanotube/polymer mixtures in different solvents high-power ultrasonication can be used. However, high-power ultrasonication for a long period of time shortens the nanotube length, i.e., reduces the aspect ratio, which is detrimental to the composite properties [45]. One variation of the solution blending method uses surfactants to disperse higher loadings of nanotubes [46] [47]. But using surfactants to improve nanotube dispersion can be problematic because the surfactant remains in the resulting nanocomposite and might degrade transport properties and they can also alter the polymer matrix [48]. One alternative to surfactant-aided dispersion is nanotube functionalization to improve dispersion and interfacial adhesion to the polymer matrix. The next method of preparing CNT/polymer composites, melt blending, is generally less effective (in comparison to solution blending) at dispersing nanotubes in polymers and is limited to lower concentrations due to the high viscosities of the composites at higher nanotube loadings. Melt blending uses high temperature and high shear forces to disperse nanotubes in a polymer matrix and is most compatible with current industrial practices. To improve the processability, electrical, magnetic and optical properties of CNTs, some conjugated or conducting polymers are attached to their surfaces by *in situ* polymerization. As in the solution mixing, functionalized nanotubes can improve the initial dispersion of the nanotubes in the liquid i.e. monomer, solvent and consequently in the composites. Furthermore, *in situ* polymerization methods enable covalent bonding between functionalized nanotubes and the polymer matrix using various condensation reactions. Zhu et al. [49] prepared epoxy nanocomposites by this technique using end-cap carboxylated SWCNT and an esterification reaction to produce a composite with improved tensile modulus (*E* is 30% higher with 1 wt % SWNT). On the other hand, Nogales et al. [50] used an *in situ* polycondensation reaction process to achieve low percolation thresholds in SWCNTs and thermoplastic poly(butylene terephthalate) (PBT) composites and the percolation threshold is about 0.2 wt % of SWCNTs. Furthermore, Hernandez et al. [51] prepared PET/SWCNTs nanocomposites by two different methods: direct mixing and *in situ* polymerization and samples prepared by *in situ* polymerization show a low percolation threshold for electric conductivity of Φ_c = 0.048 wt % of SWCNT. High-performance structural composites based on CNTs and polymer have also been prepared by in situ polymerization. Jia et al. [52] first synthesized PMMA/CNT composites by *in situ* polymerization of MMA with CNTs present. Later, Park et al. [53], Velasco-Santos et al. [54], and Jang et al. [55] polymerized *in situ* polyimide (PI)/SWCNT, PMMA/MWCNT, and liquid crystalline epoxide (LCE)/MWCNT

composites. PI/SWCNT composite films were anti-static and optically transparent with significant conductivity enhancement (10 orders) at a very low loading (0.1 vol %). However, Wiśniewska et al. [56] [57] presented the influence of the presence of carbonaceous nanoparticles on the course of radical polymerization and the properties of reaction products. It has been shown that SWCNTs distinctly changed the course of polymerisation of vinyl monomers and, depending on their kind, SWCNTs' reactivity occurred as an inhibitor in S polymerisation and a retarder in MMA polymerization.

Note that as polymerization progresses and the viscosity of the reaction medium increases, the extent of *in situ* polymerization reactions might be limited. Instead of avoiding the high viscosities of nanotube/polymer composites, some researchers have decreased the temperature to increase viscosity to the point of processing in the solid state. Solid-state mechanochemical pulverization processes (using pan milling [58] or twin-screw pulverization [59]) have mixed MWCNT with polymer matrices. Pulverization methods can be used alone or followed by melt mixing. Nanocomposites prepared in this manner have the advantage of possibly grafting the polymer on the nanotubes, which account in part for the observed good dispersion, improved interfacial adhesion [58], and improved tensile modulus [58] [59]. An innovative latex fabrication method for making nanotube/polymer composites disperses nanotubes in water (SWCNT require a surfactant, MWCNT do not) and then adds a suspension of latex nanoparticles [60] [61]. Freeze-drying and subsequent processing of this colloidal mixture produces composites with uniform dispersion of nanotubes even in a highly viscous matrix like high molecular weight polystyrene [60]. This method allows to prepare polymers that can be synthesized by emulsion polymerization or formed into artificial latexes, e.g., by applying high-shear conditions. To obtain nanotube/polymer composites with very high nanotube loadings, a "coagulation spinning" method to prepare composite fibers comprising predominately nanotubes has been developed [62]. This method disperses SWCNT using a surfactant solution, coagulates the nanotubes into a mesh by wet spinning it into an aqueous poly(vinyl alcohol) solution, and converts the mesh into a solid fiber by a slow draw process.

In common with conventional fiber composites, both mechanical properties, such as stiffness and strength, and functional properties, such as electrical, magnetic and optical properties, of polymer/CNT nanocomposites are linked directly to the alignment of carbon nanotubes in the matrix. Nanotube alignment can be achieved prior to composite fabrication where aligned nanotubes are incorporated into a polymer matrix by *in situ* polymerization [63] [64]. Furthermore, *in situ* polymerization can be carried out in the presence of an external field (e.g., a magnetic field [65]), where viscosity of the nanotube-monomer suspension affects the degree of alignment. Carbon nanotubes can also be aligned during or after the composite fabrication by mechanical stretching [66], spin-casting [67], wet spinning, melt fiber spinning [68], and electrospinning [69] [70], where the last two methods allow you to obtain the greatest degree of alignment.

The physical properties of nanotube/polymer nanocomposites, are determined from the nanotube and polymer characteristics as well as from the microstructures produced while fabricating and processing these nanocomposites. The optimal microstructure for one physical property might not be the best microstructure of another physical property.

2.2. Influence of carbon nanotubes on selected properties of polymer nanocomposites

Mechanical properties

Carbon nanotubes exhibit excellent mechanical properties with tensile strength of 50-200 GPa and Young's modulus of 1 TPa. The combination of these unique mechanical properties along with the high aspect ratio, low density and high surface area make CNTs an ideal candidate for reinforcement in composite materials.

Both SWCNTs and MWCNTs have been utilized for reinforcing thermosetting polymers, such as epoxy and polyurethane resins, as well as thermoplastic polymers, including polyethylene, polypropylene, polystyrene, polyesters, etc. In general, the tensile modulus and strength of polymer-rich nanotube composites are found to increase with nanotube loading, dispersion, and alignment in the matrix. In addition to dispersion, there are other major requirements that need to be satisfied for effective reinforcement of CNTs in composites : they include a high aspect ratio and interfacial interactions between carbon nanotubes and polymer matrix. However, the results at low concentrations of nanotubes tend to stay far behind the idealized theoretical predictions of the rule of mixtures [71] and the Halpin-Tsai model [72]. For instance, Haggenmueller et al. [68] received an improvement in the tensile modulus of PE fiber from 0.65 to 1.25 GPa for PE/0.5 wt % SWCNT (aspect ratio ~380) composite. Assuming the modulus of SWCNT is 1 TPa, the Halpin-Tsai model would predict the modulus of nanocomposite to be ~16 GPa at this nanotube loading. At higher nanotube concentration, the scope of improvement in mechanical properties can be limited by high viscosity of the prepared nanocomposites. The differences between the predictions and the experimental results occur from the imperfect dispersion and poor load transfer. Nanotubes agglomeration impact the diameter and length (observed decrease in aspect ratio, a parameter in model) and reduce the modulus of the filler (another parameter in model) with respect to isolated nanotubes. For example, polystyrene nanocomposites reinforced with well-dispersed 1.0 wt % CNTs of a high aspect ratio had more than 35 % and 25 % increases in elastic modulus and tensile strength, respectively [73].

Indeed, dispersion is the foremost important issue in producing CNT/polymer nanocomposites. Many different techniques have been employed for CNT dispersion i.e.: ultrasonication, calendaring process, ball milling, stir and extrusion etc. The technique employed for CNT dispersion can influence, to a large extent, on the mechanical properties of CNT/polymer nanocomposites. A good dispersion not only determine the mechanical performance of composites but also makes more filler surface area available for bonding with polymer matrix and prevents the aggregated filler from acting as stress concentrator. It should be also noted, that the dispersion states of CNT in polymer matrix depends strongly from the magnification and scale. For conventional composites, ‘‘dispersion” is generally defined as even distribution of fillers in a matrix medium without aggregates. In contrast, for CNT/polymer nanocomposites, dispersion has two aspects: (a) disentanglement of CNT bundles or agglomerates, which is nanoscopic dispersion and (b) uniform distribution of individual CNTs or their agglomerates throughout the nanocomposites, which is more of a micro- and macroscopic dispersion [74]. A smaller diameter of CNT can enhance the degree of CNT alignment due to the greater extensional flow; and a higher CNT content decreases

their alignment because of the CNT agglomeration and restrictions in motion from neighboring CNTs [75]. However, note that the aligned composites have very anisotropic mechanical properties, i.e., the mechanical properties along the alignment direction can be enhanced, whereas these properties are sacrificed along the direction perpendicular to this orientation.

As for fiber-reinforced polymer composites, the external load applied to CNT/polymer composites have to be transferred to the CNTs, allowing them to take the major share of the load [76]. Functional moieties on nanotubes typically provide better interfacial load transfer via bonding and/or entanglement with the polymer matrix. The chemical bonding between SWNT and the obtained polymer matrix with only ~0.3 % grafting density, predicted by molecular simulation, can increase the shear strength of a polymer-nanotube interface by over an order of magnitude [77]. Experimentally, a 145 % increase in tensile modulus and 300 % increase in yield strength with 1 wt % fluorinated SWCNTs in a poly(ethylene oxide) matrix was obtained [78]. In fact, at low SWCNTs loadings (<0.5 wt %) the experimental Young's moduli of these composite fibers approximate the Halpin-Tsai predictions for an aligned composites, and the tensile strength is higher than the theoretical rule of mixture estimate. This suggests that the covalent bonding at the nanotube/polymer interface can be very effective in strengthening the material.

Electrical properties

Electrically conducting polymer nanocomposites with a volume conductivity higher than 10^{-10} S/cm are considered to be an important group of relatively inexpensive materials that can be utilized in many engineering fields (Fig. 3a), for instance electrically conducting adhesives, electromagnetic interference shielding materials for electronic devices, antistatic coatings and films, thermal interface etc. [79] [80] [81].

The percolation theory can be used to explain the electrically conducting behavior of composites consisting of conducting fillers and insulating matrices. When the conductive filler content is gradually increased, the transition from insulator to conductor can be observed. The critical filler content where the measured electrical conductivity of the composites sharply jump up by several orders of magnitude due to the formation of continuous electron paths or conducting networks is known as a percolation threshold. Below the percolation transition range, electron paths do not exist and the electrical properties are dominated by the matrix material. Above the percolation transition range, multiple electron paths exist in the matrix so that the electrical conductivity of the composite often shows a saturation plateau (Fig. 3b) [82] [83].

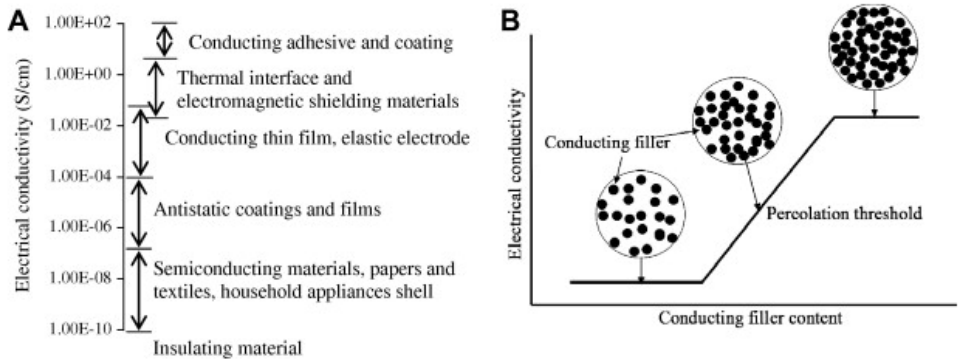

Fig. 3 Typical applications of conducting composites (A) and a schematic of percolation phenomenon and conducting network in conducting composites (B) [74].

The concentration of the conducting filler must be above the percolation threshold in order to achieve conducting networks in the composite. To achieve percolation threshold, conventional conductive fillers such as carbon black (CB), exfoliated graphite and carbon fibers that are usually micro-meter scale materials, need to added in content as high as 10-50%, resulting in a composite with poor mechanical properties and a high density. To minimize aforementioned problem the incorporation of CNT might give a solution. In comparison to traditional conductive fillers, CNT possess unique advantages i.e. high aspect ratio and excellent electrical conductivity, which in turn facilitate the formation of conducting networks and thus transform the insulating polymer to a conducting composite at a low CNT content, often as low as 0.5 wt % (or even lower) (Fig. 4).

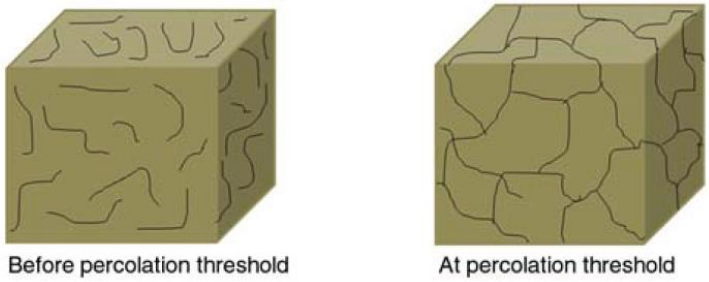

Fig. 4 A schematic presentation for the arrangement of CNTs before percolation threshold and at percolation threshold in polymer nanocomposites [84].

Fig. 5 presents the percolation threshold of CNTs based nanocomposites with different polymer matrices [85]. The transition from insulator to a conductor for most polymer matrixes is observed when the CNT concentration is below 5 wt %. However, the values of percolation threshold for CNT/epoxy nanocomposites varied from 0.002 to 7 vol %. [76] [86] [87] [88], influenced by processing techniques used, to produce the nanocomposites, type of the nanotubes (SWCNTs or MWCNTs) and nanotubes characteristics: aspect ratio [89], dispersion [46] and alignments [90] [91]. Note that the well-dispersed CNTs gave rise to 50 times higher conductivities than the entangled ones [85] and generally have higher aspect ratios than nanotube aggregates. There is a critical value of CNT aspect ratio, above which the percolation threshold was sensitive to dispersion state, while below which the percolation threshold increased rapidly with decreasing aspect ratio. Furthermore, slight aggregation produces a lower percolation threshold by increasing the local interactions between nanotubes [89] [92]. Alignment of the nanotubes in polymer matrix also affects the electrical

conductivity and its percolation threshold. When the nanotubes are highly aligned in the composites, there are fewer contacts between the tubes, which results in a reduction in electrical conductivity and a higher percolation threshold as compared to those in a composite with randomly oriented nanotubes [93].

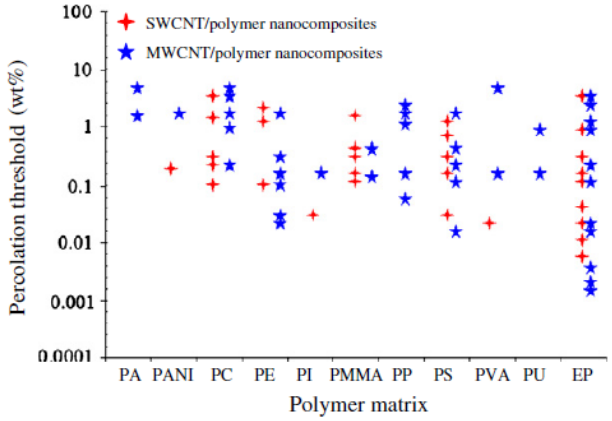

Fig. 5 Percolation thresholds of CNT/polymer nanocomposites [85].

Many reports have shown that functionalization of CNTs affects tremendously the electrical conductivity of nanocomposites: proper functionalization facilitates the CNT dispersion and the formation of conducting networks in composites, resulting in lowered percolation threshold of nanocomposites. It is generally known that chemical functionalization disrupts the extended π-conjugation of nanotubes and hence reduces the electrical conductivity of isolated nanotubes. In addition, functionalization of CNTs using acids of a high concentration can severely damage and fragment CNTs into smaller pieces with decreased aspect ratios. For instance, nanocomposites based on amino-functionalized CNT showed a typical percolation behavior, although the conductivities were in general lower than those containing pristine or untreated CNTs [94]. However, there are also several researches which report that functionalization can improve the electrical properties of the composites [95] [96] [97] [98]. It seems that the disadvantages of functionalization with respect to SWNT conductivity are prevailed by the improved dispersion enabled by functionalization.

The CNT/polymer nanocomposites commonly possess electrical conductivity in the range of 10^{-5} to 10^{-3} S/cm above the percolation threshold [15] [51] [99]. With the increasing content of CNT above the percolation threshold, the electrical conductivity can be marginally enhanced, but the solution viscosity becomes too high to produce void-free composites with CNT content higher than 1.0 wt %. This restrains the utilization of CNT/polymer nanocomposites for applications where high CNT contents are necessary. Thus, processing techniques that improves the electrical conductivity of nanocomposites below or near the percolation threshold became relevant to producing highly conducting composites. Buldum et al. [100] and Stadermann et al. [101] indicated, based on simulation results, that the contact resistance of CNTs in polymer composites played an important role in enhancing the conductivity of nanocomposites. Ma et al. [94] confirmed those studies and showed that the nanocomposites with silver decorated CNTs exhibited a significantly higher conductivity above the percolation threshold than those containing pristine CNTs. A high electrical

conductivity value of 0.81 S/cm was achieved with 0.5 wt % of silver decorated CNT. It was also shown that the silver nanoparticles were tightly attached onto the defect sites of CNT surface, compensated the negative effect (caused by the amino functionalization) by enhancing the conductivity of CNT and reducing the contact resistance of CNT junctions in matrix.

Rheological properties

Rheology is the study of the flow behavior of a material under conditions in which they flow rather than elastic or plastic deformation. The study of the viscoelastic properties of CNT/polymer composites have both practical importance related to composite processing and scientific importance as a probe of the composite dynamics and microstructure [29]. The rheological properties of nanotubes/polymer nanocomposites depend on several major factors such as: characteristics of the filler loading, aspect ratio and dispersion, polymer molecular weight, and the interfacial interaction between the polymer and filler [102] [103] [104] [105]. The two commonly used techniques to characterize the rheological properties of CNT/polymer composites is storage modulus and variations of viscosity as the function of frequency. It has been observed [106] that with an increasing concentration of carbon nanotubes the viscosity of the polymer system drastically changed above certain value (Fig. 6).

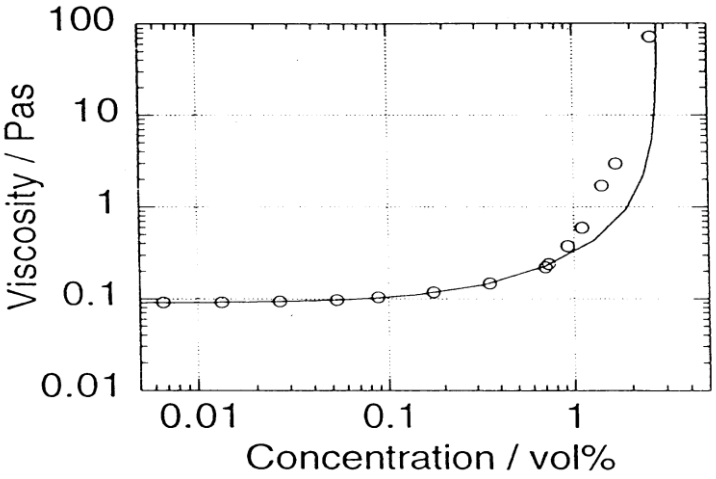

Fig. 6 Increase of viscosity of aqueous oxidised-CNT suspension [106].

It was also observed, that at low frequencies, the fully relaxed polymer chains exhibit the typical Newtonian viscosity plateau but with the increase of CNT content the low-frequency complex viscosity significantly increases, indicating that the relaxation of polymer chains in the nanocomposites is effectively restrained by the presence of CNT [105]. With the increase of frequency and CNT loading the storage modulus also gradually increased, indicating a transition from viscous liquid to solid-like behavior. The concentration at which CNT/polymer nanocomposite shows a transition from a rheological state (where the viscosity or storage modulus changes significantly with increasing filler content) to a solid-like behavior (where the viscosity or storage modulus is insensitive or has only a slight variation

with increasing filler content) is known as the rheological percolation threshold [103] [104] [105].

The strong dependence between the rheological percolation threshold and temperature was reported [107]. It has been suggested that that the superposition of the entangled polymer network and the combined nanotube-polymer network rather than the nanotube network alone dominates the rheological properties. Whereas, the electrical percolation threshold, which is not dependent on the temperature, requires contacts of carbon nanotubes to form solid conducting networks where the temperature effect becomes marginal. The content of CNTs required to form a rheological percolation threshold should be much lower than that for electrical percolation, so the polymer chains contribute strongly to the rheological response of nanocomposites [103] [108].

The rheological response of CNT/polymer nanocomposites with CNTs content below the percolation threshold can be used as an indirect measurement to show the dispersion of carbon nanotubes in polymer matrix. In general, the better the dispersion of CNT, the lower the viscosity is. For instance, it was already reported that the functionalization of CNT can be successfully used to reduce the viscosity of the CNT/epoxy suspension [109] and to lower the rheological percolation threshold of nanocomposites due to the better dispersion [110]. This group also showed that for the nanocomposites containing functionalized CNT the storage moduli at low frequencies were also higher, indicating better load transfer between the CNTs network and the polymer. The effect of functionalization on re-agglomeration of CNTs in an epoxy matrix can be affected by rheological changes. It was observed that the CNTs without any functionalization started to re-agglomerate upon application of curing temperature, whereas the amino-functionalized CNTs remained uniformly dispersed over the whole curing process, indicating a beneficial effect of functionalization on the stability of CNTs dispersion even at a high temperature [111].

Thermal properties

The thermal conductivity of a material is dominated by atomic vibrations or phonons, and the conduction by electrons is generally irrelevant for insulating materials [112]. The thermal conductivity of CNT/polymer nanocomposites depends on several factors such as content, aspect ratio, dispersion of CNTs and their interfacial interactions with polymer matrix. The exquisite thermal properties of CNTs including high thermal conductivity and good thermal stability, led to the expectation that CNTs could make useful functional fillers to rectify the thermal properties of polymers. Nanocomposites with good thermal conductivity have potential applications in printed circuit boards, connectors, thermal interface materials, heat sinks, and other high-performance thermal management systems. Some enhancements have been observed when employed CNT as thermal conducting filler to polymer matrix. For instance, SWCNT/epoxy nanocomposites showed 70 % and 125 % increases in thermal conductivity at 40 K and room temperature, respectively, with 1 wt % SWCNTs [113], while introduction of 0.1-1.0 wt % of MWCNTs to epoxy resin enhanced the thermal conductivity of epoxy resin by about 40 % [114]. However, also some reports exposed that the thermal conductivities of CNT/polymer composites showed only a marginal improvement compared

with the electrical conductivities with the same CNT content were already presented. Taking into consideration the differences in transport mechanisms between the thermal and electrical conductivities of composites, Moniruzzaman et al. [29] proposed that the phonons (major carriers for thermal conduction) were much more probably to travel through the matrix rather than through the CNT networks because the different thermal conductivity of CNT and polymer, i.e. about 10^4 W/(m·K) with $K_{CNT} \approx 10^3$ and $K_{polymer} \approx 10^{-1}$ W/(m·K), is much smaller than that of the electrical conductivity, i.e. in the range of 10^{15}–10^{19} with $\sigma_{CNT} \approx 10^2$–$10^6$ and $\sigma_{polymer} < 10^{-13}$ S/cm.

A significant influence of thermal conductivity of CNT/polymer composites has aspect ratio due to two main factors: (i) for a given volume fraction, the number of CNT–polymer–CNT contacts increases with decreasing aspect ratio, which in turn reduces the influence of high interfacial thermal resistance between CNTs and polymer matrix [115], (ii) increasing the aspect ratio of CNTs shifts the phonon dispersion towards lower frequencies, resulting in a better CNT-liquid thermal coupling [116]. Another important factor that affects the thermal conductivity is the interfacial adhesion between CNT and polymer matrix. The enhanced CNT–polymer interfacial interactions can inhibit the phonon transportation along CNTs, and increased the interfacial thermal resistance by affecting the damping behavior of the phonons' vibration [117].

Besides the thermal conductivity, the addition of CNT to polymer matrix can also rectify the thermal stability (thermal decomposition temperatures), glass transition and melting temperature and as well as flame-retardant properties through their constraint effect on the polymer segments and chains. Similar as described above for thermal conductivity, many factors such as CNT type, aspect ratio and dispersion, its interfacial interactions with polymer matrix governed these thermal properties. For instance, epoxy/silane functionalized MWCNT with 0.25 wt % loading showed sharp transition temperature from 147 to 161 ^oC, which was even higher than that of the nanocomposites containing CNTs without functionalization [76]. However, when incorporated CNTs into thermoplastic matrix this capability becomes more pronounced since CNTs can act as the nucleation agents for crystallization of polymers. For example, Probst et al. found that carbon nanotubes can nucleate crystallization of poly(vinyl alcohol) at concentrations as low as 0.1 wt% [118], while Anand et al. [119] showed that melt compounded SWCNT act as effective nucleating agents for PET crystallization. The crystallization behavior of polypropylene (PP) in the presence of single walled carbon nanotubes (SWCNTs) has also been reported [120] [121]. Nogales et al. also found that SWCNTs did not influence the crystal structure of PBT [50], but they did not evaluate the influence on crystallization rate. Velasco-Santos et al. [54] added into poly(methyl methacrylate) (PMMA) matrix 1.0 wt % well-dispersed SWCNTs and gave rise to a 40 ^oC increase in glass transition temperature of PMMA, whereas Kashiwagi et al. [122] observed the increase by 12 ^oC of the thermal decomposition temperature of polypropylene at peak weight loss with 2 vol % MWCNTs. The flammability of CNT/polymer composites was also observed and found that SWCNT have the highest capability to reduce the mass loss rate of the composite MWCNT are the second most effective in comparison to CNF and carbon black [123]. The mechanisms behind this enhancement can be understood from two points: [123] [124] [125]: (i) the networks containing CNT act as a heat shield for the neat polymer below the layer, thus significantly

reducing the heat release rate of nanocomposites and (ii) the incorporation of CNT into a polymer leads to an enhanced thermal stability of nanocomposites, thus effectively inhibits the formation of cracks or openings that compromise the flame-retardant effectiveness of nanocomposites during burning. Poorly dispersed CNTs or very low concentration of CNTs resulted in the formation of a discontinuous layer consisting of fragmented islands with sizes from 1 to 10 mm. Note that the functionalization of CNT will further reduce the flammability of nanocomposites as it will not only enhance the dispersion of CNT in the polymer matrix, but also enhance the thermal stability of nanocomposites.

The high cost of CNTs, especially SWCNTs, in comparison to other fillers like graphite, CB and carbon fibers, limits the widespread applications of CNT-based conducting composites. Therefore, nanocomposites containing hybrid fillers of CNTs and other inexpensive particles were developed in recent years [126] [127] [128] [129]. Hybrid fillers with unique geometric shapes and different dispersion characteristics may offer a new way to lower the final cost of CNT-based nanocomposites with multi-functional properties.

3. Graphene and graphene derivatives

3.1. General characterization

Graphene is an atomically thick, two-dimensional (2-D) sheet composed of sp^2 carbon atoms arranged in a honeycomb structure [4] with a carbon–carbon bond length of 0.142 nm [5] (Fig. 6). Electrons in graphene behave like massless relativistic particles, which contribute to very peculiar properties such as an anomalous quantum Hall effect and the absence of localization [6]. Graphene has indicated a variety of intriguing properties including high electron mobility at room temperature (250 000 cm^2/Vs) [7] [8], and unlike CNT, chirality is not a factor in its electrical conductivity, exceptional thermal conductivity (5000 Wm^{-1} K^{-1}) [9], and superior mechanical properties with Young's modulus of 1 TPa and ultimate strength of 130 GPa [8]. These properties in addition to extremely high surface area (theoretical limit: 2630 m^2/g) and gas impermeability [10] demonstrate graphene's great potential for improving electrical, mechanical, thermal, and gas barrier properties of polymers.

A type of 2D graphitic nanofiller consisting of stacked graphene layers are graphite nanoplatelets (GNP), also called graphite nanosheets (GNS) and graphite nanoflakes (GNF), or just simply exfoliated or expanded graphite (EG). The stacked layers are bonded to each other by weak Van der Waals forces with a constant interlayer distance of about 0.34 nm [130].The thickness of GNPs varies from a few to several dozens of nanometers, as compared to their diameter, usually in the microscale, which leads to the high specific surface area of GNPs (with a theoretical value of 2630–2965 m^2/g [131]) and high aspect ratios. The diameter and thickness GNPs could be by a number of techniques, such as intercalation, oxidation, heat treatment, microwave irradiation, ultrasonic treatment etc. [132] [133] [134] [135]. In comparison to other classic 2D nanofillers, such as nanoclays, GNPs have lower mass density, and are highly thermally and electrically conductive, due to the sp^2 hybridized carbons in the monolayer graphenes within the GNPs. The graphene nanoplatelets also possess superior mechanical properties with a reported modulus of 1.1 TPa and strength of 125 GPa [136].

Therefore, GNPs, the cost-effective nanofiller, are truly ideal for improving polymer's properties and obtaining multifunctionalities for practical applications.

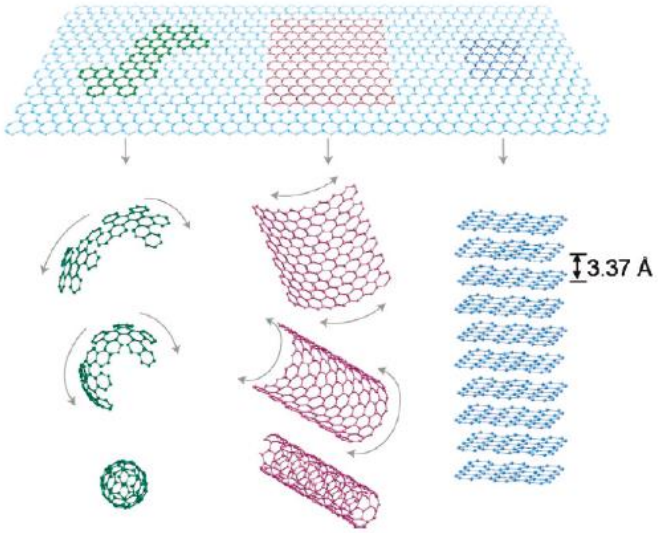

Fig. 7 Graphene, the building block of all graphitic forms, can be wrapped to form the 0-D buckyballs, rolled to form the 1-D nanotubes, and stacked to form the 3-D graphite [137]**.**

3.2. Methods for preparation of graphene and graphene derivatives

There are different methods for preparation of graphene sheets that can be divided into two main routes: bottom-up and top-down processes. In bottom-up processes, graphene sheets are synthesized by a variety of methods such as: chemical vapor deposition (CVD) [138] [139] [140] [141], arc discharge [142] [143], epitaxial growth on SiC [144] [145] [146] [147], chemical conversion [148] [149] [150], reduction of CO [151], unzipping of carbon nanotubes [152] [153] and many more. CVD and epitaxial growth often produce small amounts of large-size, defect-free graphene sheets. These methods can be more attractive than for example mechanical cleavage [7] for production of graphene sheets for fundamental studies and electronic applications but are not adequate to provide large amount of nanofillers preferably with modified surface structure for polymer nanocomposites. In top-down processes, graphene and modified graphene sheets are produced by separation/exfoliation of graphite or graphite derivatives (such as graphite oxide or graphite fluoride [154]). Generally, these methods are suitable for large scale production required for polymer composite applications and offer significant economic advantages over bottom-up methods. Fig. 8 shows a block diagram which summarizes the different routes reported for production of graphene or modified graphene starting from graphite or GO.

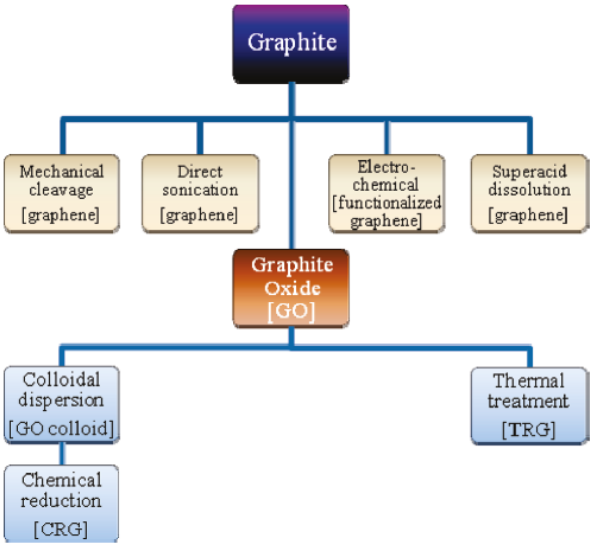

Fig. 8 Top-down methods for production of graphene and modified graphene starting from graphite or via graphite oxide (GO) [4].

Alkali metal [131] or acid [155] [156] intercalated graphite can be expanded upon the heat treatment to produce thicker (~100 nm) form of 2-D carbon known as expanded graphite (EG), which is commonly used as a filler for polymer composites. However, EG still bears layered structure of graphite. Recently, a thinner form (~10 nm) of EG known as graphite nanoplatelets (GNP) was produced by either thermal expansion of fluorinated graphite intercalation compounds [157] or microwave radiation of acid-intercalated graphite followed by pulverization using ball milling or ultrasonication [158]. Due to the large diameter and rigidity of graphite flakes are preserved in this process, GNP can improve electrical conductivity and mechanical properties of polymers at substantially smaller loadings than graphite or EG [159] [160].

Direct exfoliation of graphite.

Recently, graphite has been directly exfoliated to single- and multiple-layer graphene via sonication in the presence of polyvinylpyrrolidone [161] or N-methylpyrrolidone [11], electrochemical functionalization of graphite assisted with ionic liquids [162], and through dissolution in superacids [163]. The direct sonication method have the ability to be scaled up to produce large quantities of single- and multiple-layer graphene or functionalized graphene that can be used for composite applications. Nevertheless, separation of the exfoliated graphene sheets from the bulk graphite might be a challenge. Fig. 9 summarizes different routes of the graphite structure modification after different treatments.

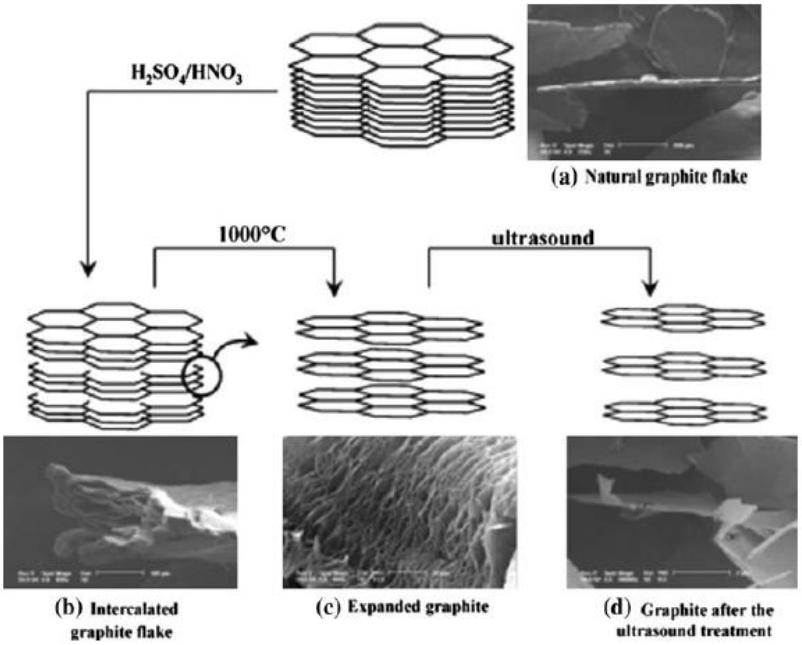

Fig. 9 Scheme of the graphite structure modification after different treatments [130].

Graphite oxide.

Currently, one of the most promising methods for large scale production of graphene is exfoliation and reduction of graphite oxide. It was first prepared over 150 years ago by Brodie [164]. However, graphite oxide was also produced using different variations of Staudenmaier [165] and Hummers methods in which graphite is oxidized using strong oxidants such as $KMnO_4$, $KClO_3$ and $NaNO_2$ in the presence of nitric acid or its mixture with sulfuric acid. Analogous to graphite, which is composed of stacks of graphene sheets, graphite oxide is composed of graphene oxide sheets stacked with an interlayer spacing between 6 and 10 Å depending on the water content [136]. The model of Lerf-Klinowski [166] describes GO as built of pristine aromatic "islands" separated from each other by aliphatic regions containing epoxide and hydroxyl groups and double bonds as shown in Fig. 10. Graphite oxide has an approximate C/O/H atomic ratio of 2/1/0.8 [164]. During oxidation graphene oxide sheets undergo unzipping resulting in size reduction compared to the parent graphite flake size [167].

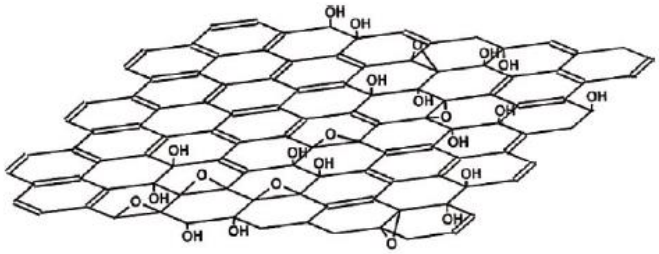

Fig. 10 Structure of GO (a) consisting of aromatic islands separated by aliphatic regions containing oxygen bonded carbons as described by the Lerf-Klinowski model [67].

A number of different methods currently exist for the exfoliation and reduction of GO to produce chemically modified graphene. The term "chemically modified" is chosen because complete reduction of graphene oxide to graphene has not yet been observed [4]. In chemical

reduction methods a stable colloidal dispersion of GO is produced followed by chemical reduction of the exfoliated graphene oxide sheets. Stable colloids of graphene oxide can be obtained using variety of solvents such as water, alcohol (and other protic solvents), but also polar aprotic solvents like isocyanate [168], octadocylamine [169] or treating with surfactants [170] [171]. Colloidal graphene oxide or the organically treated version can chemically reduced producing chemically reduced graphene (CRG) using hydrazine [168] [172], dimethylhydrazine [173], hydroquinone [174] etc. Reduction of graphene oxide restores electrical conductivity but it still remains: C/O atomic ratio of ~ 10/1 [170]. However, the main drawback that limits application of this method is the hazardous nature and cost of the chemicals used in reduction. An alternative method to produce chemically modified graphene sheets without the need for dispersion in a solvent and which leads to restoration of the electrical conductivity with reported electrical conductivity of a compacted film with density 0.3 g/cm^3 ranging between 10 and 20 S/cm [175] compared to 6000 S/cm for defect-free single graphene sheets [176] is a thermal reduction process. Thermally reduced graphene oxide (TRG) can be produced by rapid heating of dry GO under inert gas and high temperature [175] [177] [178] [179]. Heating GO in an inert environment at 1000 ^{o}C for 30 s leads to reduction and exfoliation of GO, producing TRG sheets. Exfoliation, which leads to volume expansion of 100 - 300 times, takes place when the pressure generated by the gas (CO_2) evolved due to the decomposition of the epoxy and hydroxyl sites of GO exceeds van der Waals forces holding the graphene oxide sheets together, producing very low-bulk-density TRG sheets. About 30 % weight loss is associated with the decomposition of the oxygen groups and evaporation of water [175]. 80 % of the TRG sheets are single layers with an average size of about 500 nm independent of the starting GO size, but due to the structural defects these sheets are highly wrinkled [175] [178]. TRG has C/O ratio of about 10/1 compared to 2/1 for GO [178] and high surface area of 1700 m^2/g. This ratio has been increased up to 660/1 through heat treatment at higher temperature (1500 ^{o}C) or for longer time [180].

4. Polymer nanocomposites containing graphene derivatives

The discovery of graphene and graphene derivatives with its combination of extraordinary physical properties and ability to be dispersed in various polymer matrices has created a new class of polymer nanocomposites that have shown immense potential applications in the fields of electronics, aerospace, automobile, defense industries, green energy, etc., due to its exceptional reinforcement in composites. Graphene based polymer nanocomposites can be prepared in many different ways, but the most common synthesis strategies of preparing graphene/polymer nanocomposites are three synthesis routes: 1. Solution mixing, 2. Melt blending and 3. *In situ* polymerization.

4.1. Synthesis of graphene/polymer nanocomposites

Solution mixing

Solution mixing is the most direct method to prepare polymer composites. The method consists of three main steps: 1. The filler dispersion in a suitable solvent using for example ultrasonication, 2. Incorporation of the polymer and 3. Solvent removal by distillation or evaporation [181] [182]. During this preparation process, the polymer covers graphene sheets and when the solvent is evaporated or distilled off, the graphene sheets reassemble, sandwiching the polymer to form polymer nanocomposites [183]. The compatibility of the polymer and nanofiller to the employed solvent plays the critical role in achieving a good dispersion. The solution mixing can be used to obtain polymer nanocomposites with a range of polymers such as: poly(vinyl fluoride) (PVF) [184], poly(ethylene) (PE) [185], poly(vinyl alcohol) (PVA) [186] [187], Poly(methylmethacrylate) (PMMA) [188], Polyurethane (PU) [189] etc. However, removal of the solvent is a critical issue. Due to the oxygen functional groups, graphene oxide can be directly mixed with water soluble polymers like PVA. GO-PVA composites have been prepared [182] by direct addition of PVA powder into the exfoliated aqueous dispersion of GO. The fully exfoliated and clearly well-dispersed GO sheets in the PVA matrix with only few restacks were observed with Field Emission Scanning Electron Microscopy (FESEM). The molecular level of GO dispersion in PVA matrix has been also confirmed by XRD.

The solubility and interaction between GO and polymer matrix can be improved by chemical functionalization. Using solution mixing technique various types of polar polymers like PAN, PAA, PMMA have been successfully mixed with functionalized graphene oxide (f-GO) [190] [191]. Functionalization of graphene sheets may stabilize dispersion in water and in organic solvents with reducing the agglomeration. Ultrasonication may help to receive a homogeneous dispersion of graphene sheets, however long exposure time to ultrasounds may induce defects in graphene which are detrimental to the composite properties [192].

The attached oxygen groups on the surface of graphene can break the conjugated structure and localize π-electrons leading to decrease of both carrier mobility and carrier concentration and modifying the electronic structure of graphene. Therefore GO is a typical insulator exhibiting a sheet resistance of about 10^{12} Ω/sq or higher [193]. To restore the conjugated network of graphene which results in recovery of its electrical conductivity and other properties, the reduction process can be used. *In situ* reduction may be used to restore the conductivity and prevent restacking since the presence of polymers in the solution mixture during the reduction [194]. For instance, the dramatic enhancement of electrical conductivity for the *in situ* reduced GO-Nafion nanocomposites by exposure to hydrazine has been reported [195].This enhancement of electrical conductivity indicated a sufficient accessibility of the inorganic GO sheets to the reducing agent, through the nanochannels formed by the polymeric ionic domains. The chemical reduction has been successfully used to prepare other polymers such as vinyl acetate/vinyl chloride copolymers [196]. However, the adequate reducing agents are needed to be selected depending on the type of polymer as *in situ* reduction may cause degradation of polymer [197].

Melt blending

The second often used technique to obtain polymer nanocomposites, especially for thermoplastic polymers, with graphene derivatives is melt blending process. This technique is more practical and versatile and uses a high temperature and shear force to disperse fillers in the polymer matrix. A range of composites based on polystyrene (PS) [198], polypropylene (PP) [199] [200], poly(vinylidene fluoride) (PVDF) [201], have been prepared using this technique. High temperature that softens the polymer matrix allows easier dispersion of reinforcing phase. Melt blending is free from toxic solvents but is also less effective in dispersing graphene in the polymer matrix especially at higher filler loadings due to the increased viscosity of the composites [192]. Another disadvantage of this technique is rolling, buckling or even shortening of graphene sheets during mixing due to the strong shear forces which result in reducing its aspect ratios which is not beneficial for better dispersion [194]. Bao et al. [202] have successfully prepared graphene/poly(lactic acid) (PLA) nanocomposites with improved properties. They observed well-dispersed graphene and significantly improved crystallinity, rate of crystallization, mechanical properties, electrical conductivity and fire resistance of obtained nanocomposites. On the other hand, Kim et al. [203] have noted that addition of graphene to polyethylene didn't improve electrical conductivity nearly up to 1.2 vol % of nanofiller loading.

In situ polymerization

To prepare polymer/graphene composites, the *in situ* polymerization technique is particularly attractive, as it enables control over both the polymer architecture and the final structure of the composites. This technique is often used to prepare graphene polymer nanocomposites such as PMMA [204], Nylon 6 [205], PU [206], poly (butylene terephthalate) (PBT) [207], epoxy [208] [209], polyaniline (PANI) [210], PE [211] etc. The key point of this approach relies on good dispersion of graphene or its derivative in the monomer or solvent, followed by *in situ* polymerization initiated either by heat or by the addition of a suitable compound. The intercalation of monomers into the layered structure of graphite, during *in situ* polymerization, increases interlayer spatial distance and exfoliates graphene platelets producing well-dispersed graphene sheets throughout the polymer matrix after polymerization. *In situ* polymerization technique enables the covalent bonding between the functionalized sheets and polymer matrix through various chemical reactions. Major nuisance of this technique is the viscosity increase with the progress of polymerization which hinders manipulation and limits load fraction [181] [194]. Furthermore, in certain cases the process is carried out in the presence of solvents, hence solvent removal is a crucial issue similar to the solvent mixing technique [194]. The investigation of Zaman et al. [212] showed a general approach to make highly dispersed graphene/polymer nanocomposites with good control over the structure and achievement of the lowest electrical conductivity percolation threshold for epoxy ever reported, by adopting *in situ* polymerization technique to prepare chemically modified graphene/epoxy composites.

4.2. Influence of graphene derivatives on selected properties of polymer nanocomposites

Mechanical properties

The experimental discovery of graphene as a new nanomaterial with its intrinsic strength of ~130 GPa and elastic modulus of 125 GPa, has opened an interesting and novel area in material science in recent years. Defect-free graphene is the stiffest material ever reported, however despite some structural distortion, the measured elastic modulus of CRG sheets is still as high as 0.25 TPa [8]. Actually, better comprehension of chemistry and intrinsic properties of graphene with different preparation approaches has led scientists to devise graphene filled composites with enhanced mechanical, electrical, thermal and barrier properties. Same as other composites, the range of the improvement is referred to many factors such as the reinforcement phase concentration and the distribution in the host matrix, interface bonding and the reinforcement phase aspect ratio. The foremost facet of these nanocomposites is that all the property enhancements are obtained at a very low filler loading in the polymer matrix [182]. Table 1 presents the percentage enhancement in the mechanical properties of graphene based polymer nanocomposites in relation to the base polymer matrix. It can be noted from the Table 1 that the incorporation of graphene to polymer matrices can significantly affect their mechanical properties. Nevertheless, the extent of improvement is different for different matrices. For instance, the tensile strength increase alters from ~0.9 MPa for graphene/epoxy at 1.0 wt % [213], 77 MPa for CRGO/PE at 3.0 wt % [214], and 150 MPa for functionalized CRGO/PVA at 3.0 wt % [186]. This variability is mostly due to the structure and intrinsic properties of graphene, its surface modifications, the type of polymer matrix and also different preparation process **[**215**]**. Despite the fact that graphene has the highest theoretical strength, it has shown poor dispersion in polymer matrices due to restacking as well as its low wettability, resulting in a decrease in mechanical properties of reinforced nanocomposites. Graphene oxide is commonly used to improve mechanical properties of graphene based nanocomposites, because of its excellent mechanical properties (i.e. Young's modulus of GO monolayer is 207.6 ± 23.4 GPa [216]), abundant functional groups which simplify strong interfacial interactions and load transfer from the host polymer to GO and ability to significant change of Van der Waals interactions between GO sheets, facilitating their easier dispersion in polymer matrices [217]. El Achaby *et al.* [218] have prepared graphene oxide nanosheets (GOn) / PVDF nanocomposite films by solution casting method with various GOn contents in dimethylformamide (DMF). The GOn were homogenously dispersed and distributed throughout the polymer matrix due to the strong and specific interaction between carbonyl group (C=O) in GOn surface and fluoride group (CF_2) in PVDF. The property enhancements was related to the strong and specific interfacial interaction that resulted in the adsorption of macromolecular chains of PVDF on to the GOn surface.

The strong interfacial interaction between graphene platelets and polymer matrix is relevant for effective reinforcement. Poor interfacial adhesion may result in lower composite strength properties. Covalent and non-covalent functionalization of graphene based materials can be used to promote the interaction between the matrix and graphene platelets. Hydrogen

bond interactions and Van der Waals interactions were reported to be responsible for the improvement of mechanical properties [219] [220] [221].

Not only physical interactions can improve the properties of composites but also the chemical tailoring of the interface between filler and polymer matrix which may provide the most effective increase of the interfacial shear strength for improving stress transfer due to the formation of covalent bonds [182]. Cai D. et al [222] showed GO covalently bonded to PU via the formation of urethane bonds (-NH-CO) from the reaction between the hydroxyl groups (-OH) on the surface of the GO and -NCO groups on the ends of PU chains (Fig. 11) which led to the increase in toughness by 50 % at 1 wt % loading without losing its elasticity.

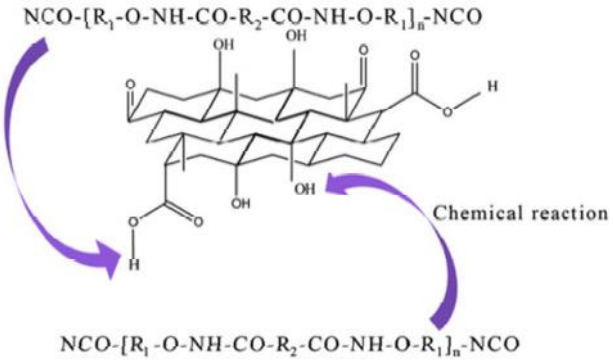

Fig. 11 The schematic illustration for the formation of the covalent bonds between the GO and PU matrix [222].

Except the intrinsic properties and interfacial interactions between graphene and polymer matrix, a wrinkled topology of graphene can enhance mechanical interlocking and adhesion to the host polymer [181] [215] [223]. It has been reported [224] that the wrinkled structure of graphene, which was different from the rectangular shape assumed by the Halpin-Tsai model, may play a significant role in reinforcement (experimental results showed 13% higher value for Young's modulus than the theoretically predicted from the model).

Besides the mechanical reinforcement, the improvement in creep [225], fatigue [217], [226] [227], fracture toughness [217] [224], impact strength [228] of graphene/polymer nanocomposites have been also reported.

Table 1 Mechanical properties of graphene-polymer nanocomposites [229].

Matrix	Filler	Filler loading (wt %a, vol % b)	Fabrication process	% increase compared to neat polymer				Reference
				Tensile strength	Elastic modulus	Fracture energy (GIC)	Fracture toughness (KIC)	
Epoxy	f-GP1	0.489b	*In situ*	~-22.6	~26.7	~296	~55.3	[209]
	f-GP1	1.5a	*In situ*		~7.7		~55	[230]
	TRGO2	0.1a	*In situ*	20			25	[231]
	f-GP1	4.0a	*In situ*	-15	21.6	200	100	[232]
	GP3			-23	7.4	104.3	50	
	TRGO2	0.1a	*In situ*	40	31	126	53	[224]
	f-GP1	1.0a	*In situ*	30	50		Negligible	[233]
	TRGO2	0.125a	*In situ*	~45	~50	115	65	[217]
	GNR4	0.3a	*In situ*	22	30		Marginally increased	[234]
	GO	0.1a	*In situ*	12	~4	29	28	[235]
	GP3	1.0a	*In situ*	0.9	22.6			[213]
	GO	1.0a	Solution	~0.5	~3.6			[185]

	TRGO2	1.0a	blending Solution blending		-8.9		[203]
	CRGO5	3.0a	Melt blending	77	87		[214]
PU	f-GP1	0.5a	Melt blend. Sol. blend. *In situ*		~49.1 ~98.4 ~14.7		[189]
PVA	CRGO5	1.8b	Solution blending	150	~940		[186]
	f-CRGO6	3.0a	Solution blending	177	86	235	[236]
PVAc	GO f-GO7	0.7a	Solution blending	~38.7 ~55.3	~-9.35 -11.7		[237]
PP	CRGO5	1.0	Melt blending	75	75		[199]
PMMA	GO CGRO5	2.0a	*In situ*	15.0 -1.9	29.9 35.8		[204]

[1]Functionalized graphene, [2]Thermally reduced GO, [3]Graphene, [4]Graphene nanoribbons, [5]Chemically reduced GO, [6]Functionalized CRGO, [7]Functionalized GO

Electrical properties

Table 2 summarizes the electrical and thermal properties of graphene based polymer nanocomposites according to the literature data with respect to pure polymer matrix.

One of the most fascinating properties of single layer graphene is its very high electrical conductivity. When graphene is used as nanofiller with the insulating polymer matrix, it can provide percolated pathways for electron transfer, making the composites electrically conductive. Graphene based composite materials exhibit a nonlinear increase of the electrical conductivity as a function of the filler content at certain amount of filler loading, known as percolation threshold. There is several factors that affect the electrical conductivity and the percolation threshold of nanocomposites such as the filler's concentration, processing method, the presence of functional groups and aspect ratio of graphene sheets, distribution in the matrix, wrinkles and folds etc. [181] [192]. The current flow in graphene based materials takes place via tunneling between thin polymer layers surrounding the nanosize particles, and this tunneling resistance claimed to be the limiting factor in the composite conductivity [238]. The single layer graphene (pristine graphene) has high electrical conductivity but the difficulty in manufacturing large amount by mechanical exfoliation and thereby high cost limits its use. To eliminate the oxygen functional groups and partially restore the electrical conductivity, making reduced graphene oxide suitable for preparing conducting composites, the reduction process of graphene oxide can be utilized. It has been already noted that thermally reduced GO has higher electrical conductivity than chemically reduced GO due to the absence of oxygenated functional groups [192]. Kim et al. [189] have showed that in PU/graphene nanocomposites the lower percolation threshold of < 0.5 vol % was obtained for thermally reduced graphene oxide while > 2.7 vol % for graphite. On the other hand, Shen et al. [239] has revealed that electrical conductivity of rGO-g (2.5×10^3 S/m) (chemical reduction using glucose) is higher by four orders of magnitude compared to the conductivity of TRGO (2.8×10^{-1} S/m), much higher than that of GO (2.7×10^{-7} S/m). The lower conductivity of TRGO was suggested to be due to the presence of oxygenated species and the

smaller sp^2 domains created by thermal reduction of GO which makes it intractable to restore the conducting network in reduced graphene.

Table 2 Electrical and thermal properties of graphene/polymer nanocomposites [229].

Matrix	Filler	Filler loading (wt %[a], vol %[b])	Fabrication process	Electrical properties		Thermal properties		Reference
				Percolation threshold ([a]-wt %, [b]-vol %)	Surface resistance[a] (Ω)/Electrical conductivity[b] (Sm^{-1})	% increase in thermal conductivity	Thermal resistivity[a] (MΩ)/Thermal conductivity (W/m·K)	
Epoxy	f-GP[1]	1.5[a]	*In situ*			~25		[209]
	f-GP[1]		*In situ*	0.244[b]				[212]
	CRGO[2]		*In situ*	0.52[b]				[240]
PMMA	Graphene	1.0[a]	*In situ*			23.8		[213]
	CRGO[2]		*In situ*	0.62[b]				[241]
	f-GO[3]		*In situ*	0.26[b]	$2.47x10^{-5b}$			[242]
PE	TRGO[4]		Solution blending	0.16[b]				[188]
	TRGO[4]	1.0[a]	Solution blending		$2.0x10^{8a}$			[203]
PU	Graphene		*In situ*	3.8[b]				[211]
	f-GP[1]	0.5	Melt blend.	>0.5[b]				[189]
			Sol. blend.	<0.3[b]				
			In situ	>0.5[b]				
PVA	f-CRGO[5]	3.0[a]	Solution blending	0.37[b]	$0.9x10^{-2b}$			[236]
PVDF	TRGO[4]		Solution blending	4.5[a]				[184]
	TRGO[4]		Solution blending	0.016[b]				[243]
PBT	Graphene	0.5 1.0	Solution blending				760 50	[207]
PANI	CRGO[2]	10.0a	Solution blending		$8.38x10^{-4a}$ $11.92x10^{2b}$			[244]

[1]Functionalized graphene, [2]Chemically reduced GO, [3]Functionalized GO, [4]Thermally reduced GO, [5]Functionalized chemically reduced GO.

Recently, Zhang et al. [188] have examined the effect of surface chemistry of graphene (oxygen content) on electrical conductivity of PMMA/graphene nanocomposites. It has been noted that the percolation threshold increases with increasing content of oxygen of graphene sheets. PMMA nanocomposites with the lowest oxygen content in graphene showed a dramatic increase in electrical conductivity from 3.33×10^{-14} S/m with 0.4 vol % to 2.38×10^{-2} S/m with 0.8% and even up to 10 S/m at 2.67 vol % of graphene. This rapid transition from insulator to semiconductor was due to the formation of an interconnected graphene network. Despite above presented results the presence of oxygen-containing groups on graphene surface has been proved to disrupt its graphitic sp^2 network and decrease its intrinsic conductivity. In general, the higher oxygen content is, the lower intrinsic conductivity can be observed. Furthermore, Pham et al. [241] reported an interesting study on simple, environmentally friendly approach for preparing highly conductive poly(methyl methacrylate) - reduced graphene oxide (PMMA-RGO) composites with low percolation threshold of 0.16 vol% and electrical conductivity of ~64.1 S/m at 2.7 vol % by self-assembly of positively charged PMMA latex particles and negatively charged graphene oxide sheets through electrostatic interactions, followed by hydrazine reduction. Whereas, the effect of temperature on electrical conductivity of PVDF/graphene composite was investigated by Ansari et al.

[245]. A gradual increase in resistivity with temperature followed by a sharp increase was observed when PVDF reached the melting point. As the temperature approaches the melting point of the polymer, the distance between particles increases (due to volume expansion of the matrix), leading to a sharp increase in resistance. On the other hand, the PVDF/TRGO composites showed the gradual decrease of resistivity with the increasing temperature and above the melting point a dramatic decrease of resistivity. This negative temperature coefficient behavior of PVDF/TRGO composite was ascribed to the higher aspect ratio of TRGO that leads to contact resistance predominating over tunneling resistance. Generally, contact resistance can predominate when the number of contacts increases either because of an increase in the number of particles or an increase in the aspect ratio.

Thermal properties

The exceptional thermal properties of graphene-based fillers have been harnessed to improve the thermal conductivity, thermal and dimensional stability and cause large shifts in the T_g of the host polymer. Pristine graphene have shown high thermal conductivity due to the strong C-C covalent bonds and phonon scattering; is known for the highest thermal conductivity with room temperature value ~3000 W/m·K when suspended [9] [246] and approximately 600 W/m·K when supported on a SiO_2 substrate [247]. Unlike CNTs, the sheet-like geometry of graphene-based materials may provide lower interfacial thermal resistance and thus produce larger conductivity improvements in polymer composites [248] [249]. Table 3 provides comparison of thermal conductivity determined for graphene with the exceptional data reported for CNTs [9] [250] [251] [252]. The geometry of GNPs and graphene filler may also impart significant anisotropy to the thermal conductivity of polymer nanocomposites [253], with the measured in-plane conductivity about ten times higher than the cross-plane conductivity [254] [255]. Other factors such as aspect ratio, orientation and dispersion of graphene sheets will also affect thermal properties of composites.

Table 3 Room Temperature Thermal Conductivity in Graphene and CNTs [9].

sample type	K (W/mK)	method	comments	ref
SLG	~4840-5300	optical	Individual; suspended	Baladin et al. [9]
MW-CNT	>3000	electrical	Individual; suspended	Kim et al. [250]
SW-CNT	~3500	electrical	Individual; suspended	Pop et al. [251]
SW-CNT	1750-5800	thermocouples	bundles	Hone et al. [252]

Thermal conductivity studies of graphene-based materials were largely focused on different polymer matrices such as: epoxy matrix composites [248] [254] [256] [257] [258], PMMA [188] [259], PP [208], PC [260] etc. (Table 2).

Aside from being used to impart thermal conductivity, GNPs and various CMGs fillers can also endow other unique properties such as thermal stability (as typically defined by the maximum mass loss rate measured by thermogravimetric methods) to composites [261] [262] [237], even GO can enhance the overall composite thermal stability versus the neat polymer [263] [264] , despite being thermally unstable itself. Yan et al. [265] observed that inclusions of GNSs into rigid polyurethane foam (RPUF) increase the T_g whereas decrease the Tan δ of PU, where both T_g

and Tan δ interpret the mobility and movement capacity of polymer molecule chain segments. The presence of GNSs highly impedes the polymer chain motion via strong interfacial interactions and acts as "physical crosslink" during the glass transition, which evidently improves the stiffness and heat resistance of the nanocomposites.

A significant number of studies on nanoclay-filled composites have suggested improved thermal stability trends with increased levels of exfoliation and interfacial adhesion [266]. Increases in the onset of (non-oxidative) degradation of 20-30 ^{o}C and higher have been reported with GO-derived fillers [221] [267] [268]. Thermal degradation stability improvement of several polymer matrices, such as HDPE [228], poly (arylene ether nitrile) (PEN) [269], polycarbonate (PC) [270] with graphene as nanofiller has been studied. For instance, the degradation temperature of PS composite increased with graphene content and a maximum increase of 16 °C was observed for the 20 wt % composite [271].

The negative coefficient of thermal expansion (CTE) of graphene [272] [273], along with its high specific surface area and high stiffness, can significantly lower the coefficient of thermal expansion (CTE) of a polymer matrix [274]. The reduction of CTEs, as high as 31.7 %, below T_g was observed for incorporation of 5 % GO into epoxy [258]. Compared with CNTs, GNPs were reported to decrease the CTE of PP in two directions instead of one when aligned in the matrix [253].

Rheological properties

Investigation of nanocomposite rheology is important for the understanding of processing operations but it can also be useful for nanocomposite microstructure examination [275] [276] [277]. In linear viscoelastic rheology measurements, the low-frequency moduli may supply information on the graphene dispersion; for example, the presence of a low-frequency storage modulus (G`) plateau is indicative of rheological percolation due to formation of a 'solidlike' elastic network of filler [278]. The onset of a frequency-independent G` can also coincide with other phenomena, like the loading at which a large decrease in the linear viscoelastic strain limit is observed [279]. The percolation threshold determined from linear viscoelastic rheology measurement can be used to approximately quantify dispersion in terms of an equivalent aspect ratio of idealized platelets [279] [280]. In general, G` has been found to increase across the frequency range with dispersion of rigid nanoplatelets, coherent with reinforcement. Additionally, changes in the dynamic moduli have been widely examined in nanocomposites based of GNP and GO-derived fillers using dynamic mechanical analysis (DMA) temperature scans [135] [256] [281].

Furthermore, orientation of chemically modified graphene (CMG) platelets may affect the onset of rheological percolation, as well-dispersed, randomly oriented platelets would be expected to percolate at lower concentration than well-dispersed, aligned platelets. One method that promotes the randomization of filler orientation is thermal annealing above the T_g of the polymer. For instance, Kim et al. [279] observed that the rheological percolation threshold of a TEGO / polycarbonate composite was lowered from 1.5 vol % to 0.5 vol % by annealing for several hours. In addition, orientation of the platelets, induced by high strain, lowered the melt elasticity, while the following annealing steps were noted to restore the solid-like behavior of the composites melt. Thence, annealing of the composites following

molding operations may provide a way to improve properties that benefit from randomly oriented (rather than aligned) platelets, such as the percolation threshold for electrical conductivity.

Lower solution viscosity of composites have been reported with GNP nanofillers compared to CNTs [248], which may be for solution-based processing techniques. It was suggested that at sufficiently high concentration, entanglement of CNTs in polymer matrix could result in unwanted large viscosity increases, whereas platelets can more easily slide past one another thus moderating the viscosity increase [282]. Nevertheless, the solution viscosities of CMG/epoxy composites have been found to increase essentially with filler concentration, which could inhibit the formation of the crosslinked epoxy network [283]. It has been already reported the functionalization, which enhance the compatibility of the nanofiller with polymer matrix, may also help to moderate the solution viscosity of composites with increased nanofiller loading [256]. In particular, GO composite solutions may exhibit electro-rheological properties, a characteristic of insulating colloidal particles in insulating media where increases in solution viscosity due to morphological changes can be observed upon application of an electric field [264].

Barrier properties

The incorporation of graphene derivatives i.e. GNPs, GO etc. can significantly reduce gas permeation through a polymer nanocomposites compared to the neat polymer matrix. A percolating network of platelets can create a 'tortuous path' which inhibits molecular diffusion through the matrix, thus resulting in significantly reduced permeability (Fig. 12) [274]. However, some recent studies on permeability of CMG/PS nanocomposites suggest that at low loading (e.g. <0.05 wt %) the reduction in permeability of the composite is mainly caused by a reduction in gas solubility in the composite, with diffusion effects becoming more momentous at higher loading [284]. The platelets orientation may further enhance barrier properties perpendicular to their alignments, whilst higher aspect ratios of platelets correlate with increased barrier properties [274].

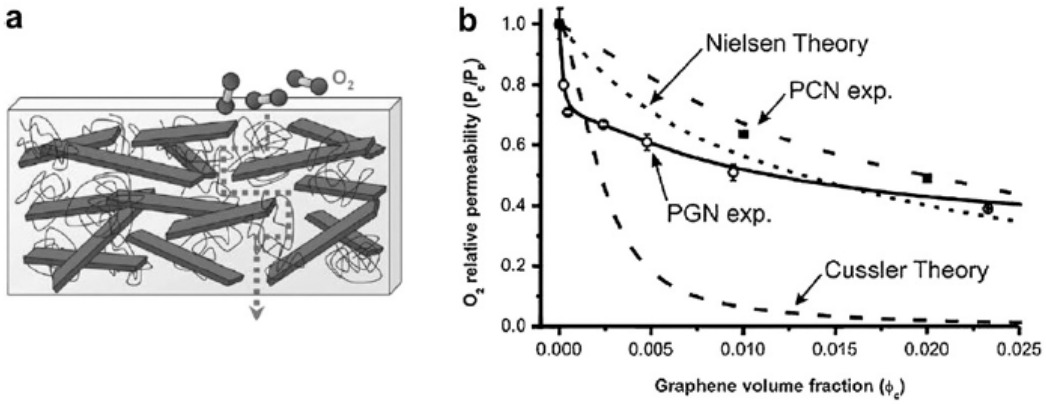

Fig. 12 (a) Illustration of formation of a 'tortuous path' of platelets inhibiting diffusion of gases through a polymer composite (Nielsen model). (b) Measurements of oxygen permeability of CMG/PS ('PGN') and montmorillonite/PS ('PCN') composites as a function of filler loading, compared with two theoretical models of composite permeability [284].

Graphene derivative fillers have been widely investigated in various permeation studies [189] [228] [253] [261] [279] [284]. For nanocomposites based on thermoplastic matrices results include a 20 % reduction in oxygen permeability for PP with 6.5 wt % of GNP [253], and a 39 % reduction in the nitrogen permeability of a PC/TEGO nanocomposite at ~3.5 wt % loading [279]. As shown in Fig. 10, PS/CMG nanocomposite were reported to exhibit a lower oxygen permeability than PS composites with exfoliated montmorillonite at the same loading [284]. In comparison to this study, a phenyl isocyanate-functionalized GO platelets were noted to confer improved barrier properties relative to TEGO, with up to a 99 % reduction in nitrogen permeability observed at approximately 3.7 wt % loading in comparison to an 81 % reduction for TEGO at equivalent loading. Peculiarly, the barrier properties in this study correlated with modulus improvement implying better filler alignment or higher aspect ratio for the functionalized GO composites [189].

5. Polymer hybrid nanocomposites with carbon nanomaterials

Hybrid composites have lately attracted the attention of researchers with different mixtures being tried out e.g. MWCNT with carbon black [19] [285] few layer graphene with single walled CNT and nanodiamonds [19] and MWCNT with graphene platelets [213] etc.

Graphene, a single-atomic layer of carbon hexagons, can be stacked into graphite or rolled up into cylindrical CNTs. They are mutually complementary in both structure and properties and yet share many common properties such as ultrahigh mechanical strength and electrical conductivity [229]. However, they still possesses their drawbacks. CNTs have superior mechanical properties but only when dispersed uniformly and forming a network to achieve sufficient percolation for electrical conductivity. Whereas, graphene has remarkably high electron mobility at room temperature but causes problem of its restacking [286] [287]. Zhang et al. [288] classified the graphene-CNT hybrids into three types, CNTs adsorbed horizontal to the graphene sheets (GNS), CNTs adsorbed perpendicular to the GNS and CNT wrapped with GNS.

Yang et el. [213] design a strategy to improve the mechanical properties and thermal conductivity of epoxy multi-graphene platelets (MGPs) filled composites by combining one-dimensional multi-walled carbon nanotubes (1-D MWCNTs) and 2-D MGPs. They showed, that the long and tortuous MWCNTs can bridge adjacent MGPs and inhibit their aggregation, resulting in an increased contact surface area between MGP/MWCNT structures and the polymer (Fig. 13). A remarkable synergetic effect between the MGPs and MWCNTs on the enhanced mechanical properties and thermal conductivity of these epoxy composites was demonstrated. Kumar et al. [289] have reported a remarkable increase in thermal and electrical conductivities of polyetherimide (PEI) containing the hybrid ternary systems of GNPs and MWCNTs in equal amounts at a fixed loading of 0.5 wt %. In the case of thermal conductivity, composites containing hybrid fillers exhibited a 45 % increase whereas composites with only GNPs or MWCNTs exhibited improvement of 22 % and 9 %, respectively as compared to pure PEI. Additionally, Sumfleth et al. [285] studied the potential of CB and MWCNT as conductive fillers in an epoxy polymer. It was observed that ternary systems including CB and MWCNT were produced resulting in a hybrid structure and revealed an electrical behavior similar to the binary MWCNT system. The different behaviors

of the carbon nanoparticles-modified systems were compared using percolation theory. Since the conductivities at high filler contents and the percolation exponent of the ternary CB/MWCNT-epoxy and the binary MWCNT-epoxy were similar, it was likely that MWCNT dominated the percolation dynamics and the formation of the network structure in ternary CB/MWCNT-epoxy. Besides that, CB might shortcut some parts of the MWCNT network branches.

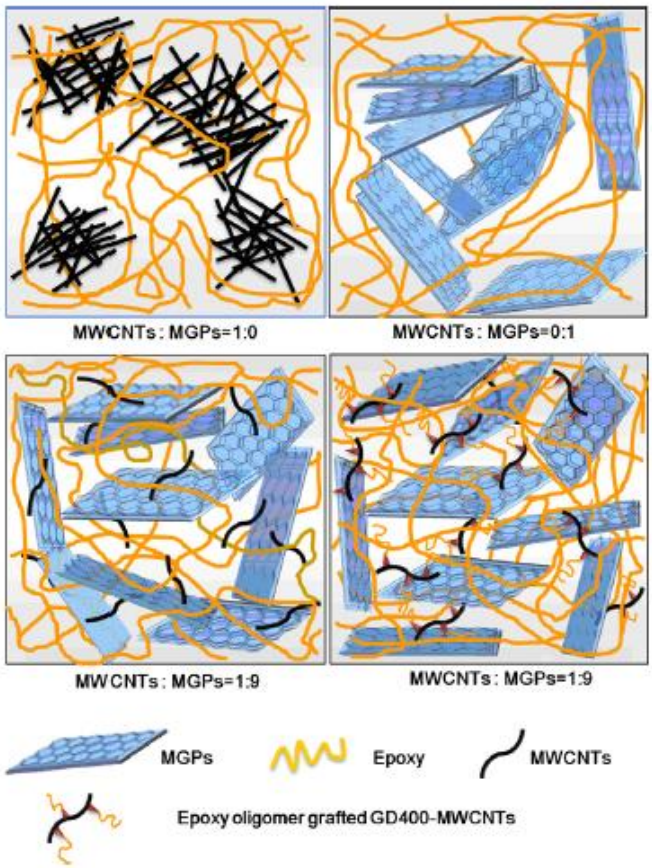

Fig. 13 The model of microstructural scheme in epoxy composites with various weight ratios of MWCNTs and MGPs [213].

Whereas, Ma P.-C. et al. [290] reported that that when CB nanoparticles were added into the nanocomposites containing CNTs, the gaps between the CNTs were effectively filled and the CNTs were linked together, resulting in the formation of solid conducting networks (Figure 14). A low percolation threshold was achieved with hybrid fillers of 0.2 % and 0.2 % CB. It was observed that the distinct geometric shapes and aspect ratios as well as different dispersion characteristics of the two conducting fillers offered unique synergy, giving rise to the enhanced electrical conductivity of nanocomposites and also great enhancement of the ductility and fracture toughness of hybrid nanocomposites while maintaining high flexural modulus and strength. Furthermore, a synergistic effect between two-dimensional few-layer graphene (FLG) and one-dimensional MWCNT on the electrical conductivity was found [291].

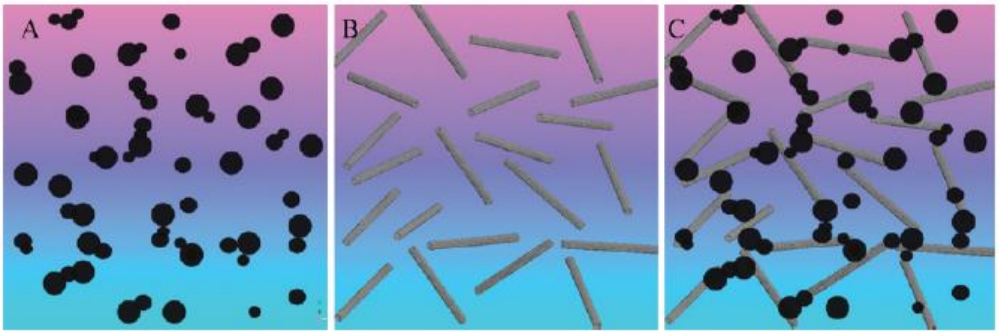

Fig. 14 Schematics of conducting networks in nanocomposites containing hybrid fillers of CB and CNT with the individual filler contents below the respective percolation thresholds: (A) CB only; (B) CNT only; (C) hybrid fillers of CB and CNT [290]

A synergistic effect of combining SWNTs and GNPs (maximizing at a ratio of approximately 3:1 of GNPs:SWNTs) was reported, with TEM observations by the authors used to attribute the effect to the morphology of the filler blend in which the SWNTs bridged across adjacent GNP platelets, forming an extended network of filler in direct contact (Fig.15) [248].

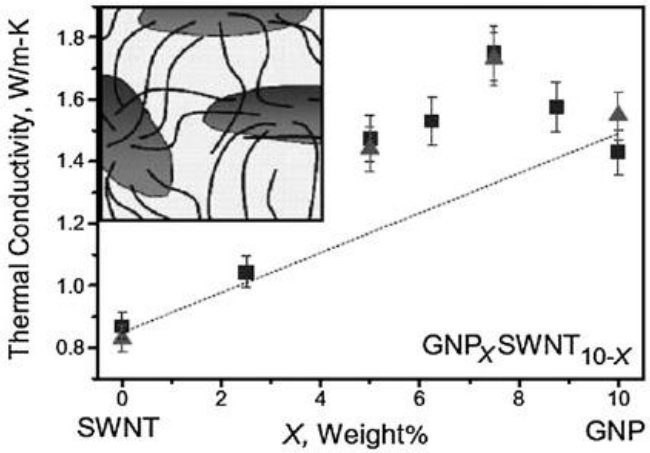

Fig. 15 Combination of graphite nanoplatelets (GNP) and single-walled carbon nanotubes (SWNTs) synergistically improve the thermal conductivity of epoxy. TEM studies established the presence of SWNTs bridging between dispersed GNPs (as shown in the schematic, inset) which may be responsible for the effect [248]**.**

A synergistic effect on the electric conductivity enhancement of epoxy composites was achieved by the addition of three fillers including GNPs, CB and CNTs [292]. The synergy originated not only from the dispersion promotion of fillers due to the unique geometric structure of the individual conductive carbon material, but also from the effective link of both the narrow and broad gaps between graphite sheets by the spherical CB and long flexible CNTs, resulting in the formation of excellent conducting network in the matrix. The percolation threshold of the nanocomposites filled with GNP0.7CB0.1CNT0.2was only 0.2 wt %, while those with GNP0.9CB0.1 and GNPs were 0.5 wt % and 1 wt % respectively. In order to fully understand the synergistic effect among the three kinds of carbon conductive fillers, a schematic illustration has been provided by authors (Fig. 16) [292].

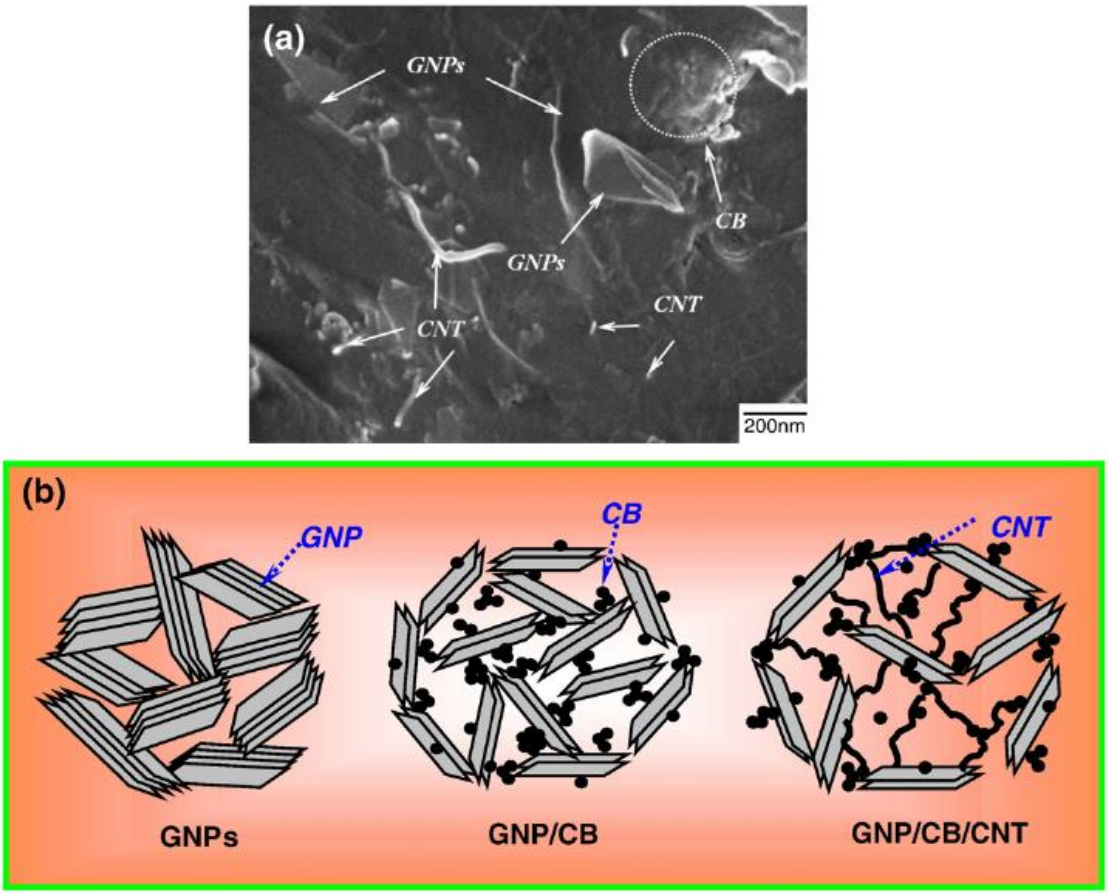

Fig. 16 SEM image of the GNP0.7CB0.1CNT0.2/EP composite (a) and schematic illustrations for the synergistic effect among GNPs, CB and CNTs (b). Three specimens of each type were tested, and the standard error was±5 % [292]**.**

It is an open question to completely understand the synergistic effect brought about by the combinations. As an outlook, the variation of the graphene derivatives (EG, FLG) to CNT ratio may lead to even more improved electrical properties by adjusting an optimum microstructure.

6. Applications of polymer hybrid nanocomposites

Among the potential areas of application of nanocomposites containing carbon nanofillers dominate electrotechnical, electronic, automotive, aerospace and sports industry. Owning to their unique electrical and mechanical properties as well as large surface area (especially in case of graphene nanosheets) hybrid carbon nanostructures have emerged as a new class of promising materials attractive for potential applications in actuators, solar cells, field-emission devices, field effect transistors, supercapacitors and batteries [293] [294] [295] [296] [297] [298] [299]. Recently, the combination of one-dimensional CNTs and two-dimensional GN sheets to design hierarchically structured composites has been extensively studied in lithium ion batteries [296], supercapacitors [300] [301] and transparent conductors [302] [303] and [304]. A simple approach was developed for preparing a flexible GN/MWCNT (16 wt % MWCNTs) film with MWCNTs uniformly sandwiched between GN sheets [305]. GN/MWCNT film shows high specific capacitance (265 $F \cdot g^{-1}$ at 0.1 $A \cdot g^{-1}$), good rate capability (49 % capacity retention at 50 $A \cdot g^{-1}$) and excellent electrochemical stability (3%

capacity loss after 2000 cycles). Such performance indicated that the GN/MWCNT film could be an important electrode in the fabrication of flexible energy storage devices.

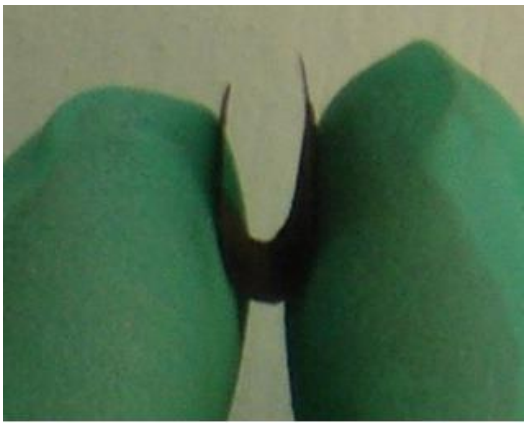

Fig. 17 Photograph of the flexible GN/MWCNT film (16 wt % MWCNTs) [305].

Great improvements in performance have been observed in these materials as CNTs can bridge the defects for electron transfer and expand the layer distance between GN sheets. Therefore, the inclusion of CNTs is expected to improve the unique potential of GN film as a freestanding electrode for supercapacitors. A particularly attractive option is to design and develop hybrid films based on graphene sheets as electrodes for energy-storage applications [306] [307]. In this context, it is critical to tailor the hybrid film properties by controlling their composition and architecture at nano/micrometer scale. For energy storage applications, therefore, it is highly desirable to use one-dimensional (1D) carbon nanotubes (CNTs) to physically separate 2D GNs to preserve graphene's high surface area. Yu et al. [308] reported their recent investigation of the fabrication of large-area multicomponent hybrid films by sequential self-assembly of functionalized 2D graphene sheets and 1D CNTs via electrostatic interactions onto various substrates, suitable for electrochemical measurements. The resultant hybrid films exhibited a nearly rectangular cyclic voltammogram, even at a high scan rate of 1 V/s with an average specific capacitance of 120 F/g.

Significant property enhancement has been observed in these materials with the existence of CNTs which are believed to bridge the defects for electron transfer and, in the meantime, to increase the basal spacing between graphene sheets. Recently, a novel 3D carbon material, consisting of parallel graphene layers stabilized by vertically aligned CNTs in between the graphene planes, has been designed by computational mode. Monte Carlo simulations revealed that this novel material doped with lithium cations can reach hydrogen storage capacity of 41 $g \cdot L^{-1}$, which would meet the D.O.E's volumetric target for mobile applications under ambient conditions [309].

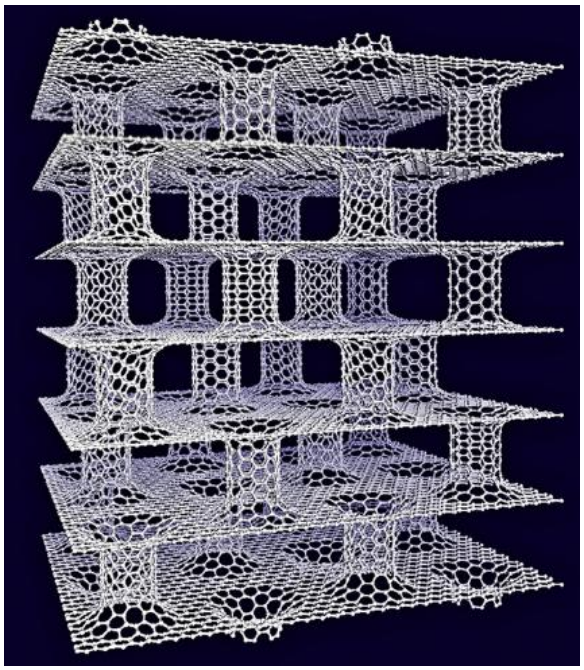

Fig. 18 Pillared graphene: a building-like three-dimensional structure for hydrogen storage [309]**.**

Since the intrinsic dielectric constant of most polymers is very low, the integration of carbon nanotubes (CNTs) into the polymers provides an attractive and promising way to reach a high dielectric constant owing to their outstanding intrinsic physical performances. However, these CNT-based composites usually suffer from high dielectric loss, low breakdown strength and the difficulty to tailor the dielectric constant. Therefore, Wu et al. [310] designed and fabricated a new class of candidates composed of graphene oxide-encapsulated carbon nanotube (GO-e-CNT) hybrids. The obtained GO-e-CNT–polymer composites not only exhibit a high dielectric constant and low dielectric loss, but also have a highly enhanced breakdown strength and maximum energy storage density. Moreover, the dielectric constant of the composites can be tuned easily by tailoring the loading of GO-e-CNTs.

Furthermore, Jha et al. [311] demonstrated the potential of 2D graphene – 1D carbon nanotube hybrid nanomaterials as catalyst support material for the dispersion of 3D nanocrystalline PtRu electrocatalysts for direct methanol fuel cell (DMFC) applications since it’s attracting much attention and interest due to its potential application in portable and small devices.

Although the nanocomposites market is largely focused on applications now under development in carbon nanotubes, which have had more time for development than applications in graphene, researchers in the nanocarbon field are expecting that with time graphene applications will eventually become increasingly important. The aim of many research studies is nowadays to develop novel polymer hybrid nanomaterials, consisting of carbon nanofillers with different shapes (1D and 2D) in polymer matrices. Hybrid nanocomposites will give potentially novel properties through synergetic effects between fillers and the matrix.

The above data indicate the huge potential posed by the polymer nanocomposites and their importance in the twenty-first century technology materials.

7. The aim and main objectives of dissertation

Based on the literature review the following thesis of this PhD dissertation has been established, that it is possible to obtain uniform distribution of graphene and carbon nanotubes in polymer matrix by mechanically dispersing them in liquid substrate (monomer), and then conducting polycondensation process in the presence of graphene or/and carbon nanotubes. To prepare nanocomposites, several types of graphene derivatives (expanded graphite, few layer graphene) and single walled carbon nanotubes will be used. The greatest improvement in properties (obtaining functional materials) in the polymer nanocomposite can be obtained only when nanofillers are de-agglomerated, uniformly dispersed in polymer matrix and interphase interactions provide the greatest possible interaction strength between the dispersed phase (reinforcement), and the polymeric matrix.

The main objective of the study is to investigate the effect of the addition of graphene and carbon nanotubes with graphene on the morphology, interphase interaction, electrical, mechanical and barrier properties of nanocomposites and consequently draw conclusions about the creation the percolation paths and strengthening mechanism of polymers with graphenes and carbon nanotubes**.** Also the specific features that indicate the functional nature of the obtained nanocomposites will be identified. Determination of the conditions for obtaining nanocomposites with the participation of graphene and carbon nanotubes with graphene during the synthesis of polyesters and copolyether-esters may form the basis for the development of the technology and obtain these materials in a pilot scale or industrial scale.

The cognitive objective is mainly to establish the impact of the chemical structure and the structure of graphene and carbon nanotubes and their reciprocal arrangement in the polymer matrix, interphase interactions on the strengthening mechanism of nanocomposite (mechanical properties) and the mechanism of the creation of structures that affect the permeability to gases and vapors and electrical conductivity. Another objective is to investigate the effect of carbon nanotubes and graphene on the supermolecular structure of the polymers constituting the matrix of the nanocomposite.

To achieve the overall goal of the project the following partial objectives are defined:

- Characterization of graphene/CNT system;
- Study on the dispersion state of the nanoparticles in the nanocomposites and its dependence on the processing conditions (flow, flow-capillary dimensions, temperature and pressure molding);
- Determining the proper mixing and dispersion of nanofillers in the polymer system obtained by *in situ* polycondensation process, including the knowledge necessary to carry out the reaction in an industrial environment;
- The study of the manufacturing process of the functional material (improved mechanical and barrier properties), taking into account the desired shape of the final product;

- The study of physical and processing properties of prepared nanocomposites and analysis of the possibility of their utilization;
- The study of the effect of graphene and carbon nanotubes addition on mechanical, electrical and barrier properties of polymer hybrid nanocomposites;
- The study of the supermolecular structure of the obtained nanocomposites;
- Testing of the properties of the final materials and the comparison of these nanocomposites with commercially available materials.

The general plan of research is to prepare polymer nanocomposites by *in situ* polycondensation based on poly(ethylene terephthalate) (PET), poly(trimetylene terephthalate) (PTT) and poly(trimethylene terephthalate-*block*-tetramethylene oxide) block copolymer (PTT-PTMO) with poly(trimetylene terephthalate) as a rigid segment. The interest of the research was also focused on the enhancement of the dispersion of the nanoparticles in the hybrid systems by mean of graphene/CNT in polymers and the interfacial adhesion between the filler and the matrix material.

EXPERIMENTAL

8. Reagents for polymer synthesis

For both polyesters: poly(ethylene terephthalate) (PET), poly(trimethylene terephthalate) (PTT) and poly(trimethylene terephthalate-*block*-tetramethylene oxide) (PTT-PTMO) elastomer synthesizes the following chemicals were used as presented in Table 4.

Table 4 The list of raw materials and reagents used for synthesis of polymer composites

Name	Designation at work	Producer
dimethyl tereftalate	DMT	Sigma-Aldrich
1,2-ethanediol	ED	Sigma-Aldrich
1,3-propanenediol	PDO	Sigma-Aldrich
poly(tetramethylene oxide) glycol with molecular weight of 1000 g/mol	PTMO	Terathane 1000, DuPont, USA
zinc acetate $Zn(CH_3COO)_2$ (catalyst)	ZC	Sigma - Aldrich
antimony trioxide Sb_2O_3	AT	Sigma - Aldrich
tetrabutyl orthotitaniate	TBT	Fluka
Irganox 1010 (phenol stabilizer)	Irganox	Ciba-Geigy, Switzerland

9. Specification and characterization of nanoparticles

The single walled carbon nanotubes (SWCNT, purity of 90wt%) were purchased from Cheap Tubes Inc. (Brattleboro, USA). From providers' data: the SWCNTs were produced in a high-yield catalytic process based on chemical vapour deposition (CCVD) with an outer diameter of 1-2nm, inner diameter of 0.8-1.6nm and about 5-30μm of length.

The single walled carbon nanotubes KNT 95 were purchased from Grafen Chemical Industries (Grafen Co.), a leader in the fabrication and application of carbon nanomaterials located in Ankara, TURKEY. From providers data: diameter: <2 nm, EC: > 100 S/cm, length: 5 – 30 μm, purity: >95%, surface area: 380 m^2/g.

Expanded graphite (EG I) (added to PET), provided by Polymer Institute SAS was prepared by thermal expansion (SGL Carbon SE, Germany); average thickness of the expanded agglomerates was 450-560 nm. Graphene platelets size ranged from 16 μm to 46 μm (99 %). C1s XPS spectra in 40eV of EG I: sp2-C: 67.13 %; sp3-C: 5.93 %; C-O: 2.78 %; π-π*: 10.46 %, π-π*: 13.71 %. Expanded graphite II added to poly(trimethylene terephthalate) was also provided by Polymer Institute of Slovak Academy of Science with platelets size of around 50 μm. XPS analysis provide following information: C1s: 99.21 % and O1s: 0.79 %. Additionally, to determine the effect of particle size on barrier properties of EG500 (flake size of 500 μm was applied, obtained in an analogous manner as EG I and EGII. The preparation process of nanofillers provided by Polymer Institute of SAS is described at [312]

Graphene (<1nm) was purchased from ANGSTRON Materials (Dayton, Ohio, USA). From providers data: a graphene powder that has less than three graphene layers, and has x-y dimensions of 10 μm at most. The carbon content is ~97.0 %, and the oxygen content is

~2.10%. Graphene has a specific surface area of 400 – 800 m^2/g and true density ≤ 2.20 g/cm^3. This product is suitable for conductive composites, barriers, energy cells, solar cells, transparent electrodes, nanocomposites, heat radiation, capacitors, conductive inks, and organic semiconductor applications.

Few layer graphene (FLG) was provided by Institut de Chimie et Procédés pour l'Énergie, l'Environnement et la Santé (ICPEES), Strasbourg, France. The synthesis of FLG consists of mechanical ablation of pencil lead on a harsh glass surface with simultaneous ultrasonication followed by a purification to remove the inorganic binder present in the pencil lead. The detailed characterization of the nanofiller used in the thesis is presented in [313].

10. Equipment for the preparation of polymers and polymer composites

The equipment for polymer composites preparation consisted of: equipment for dispersion of carbon nanofillers, consisted of dispersing devices (Fig. 19 a and b); equipment for synthesis of polymers and composites, consisted of polycondensation reactor and cooling-receiving device. Preparation of carbon nanofillers in liquid substrates was carried out using two types of mixers: ultra-high speed stirrer high (Ultra-Turrax® T25) and ultrasonic homogenizer (*S*onopuls HD 2200, Bandelin). Additionally, in case of graphene derivatives, ultra-low power sonic bath was used.

Mechanical stirrer is equipped with a dispersing head and an electric motor which drives it. Launching the mixer causes, that the system gets dispersed axially between the two planes of the head, the outer stationary (stator) and implementing internal rotation at very high speed set point setting (rotor).

In this way the fluid flow is forced in both direction of rotation, and radially through the slots in both planes (Fig. 19c).

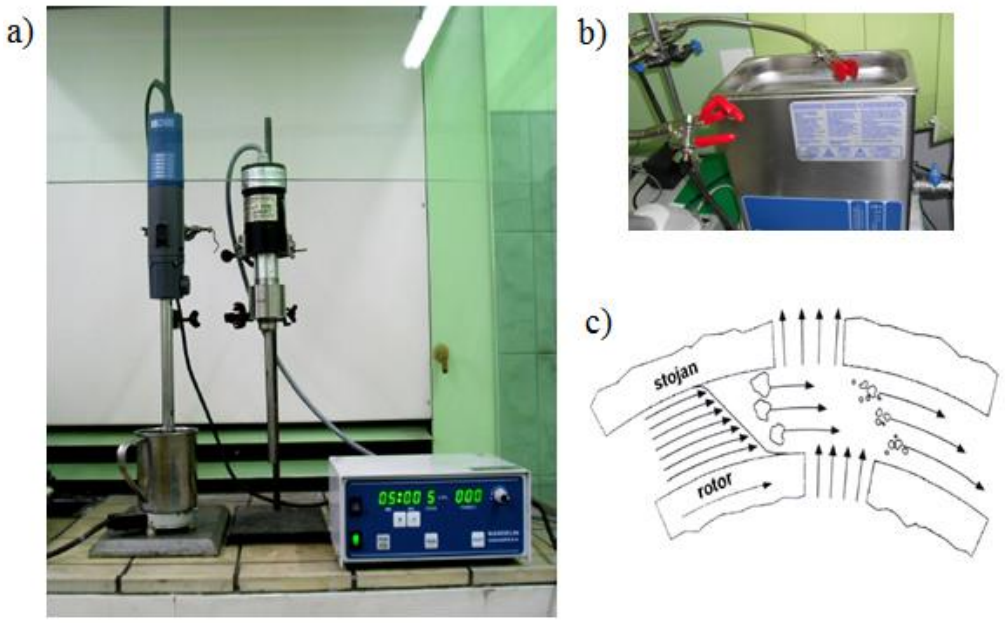

Fig. 19 The equipment for preparation of nanofiller dispersion in liquid substrates: a) high-speed stirrer (Ultra-Turax T25) and sonicator (Homogenizer HD 2200, Sonoplus); b) an ultra-power lower sonic bath (BANDELIN, Sonorex digitec; c) scheme of dispersion process using high-speed stirrer.

Acceleration which marks dispersed system generates very high shear forces and the shear occurring in the intensive turbulence and further mixing of the dispersion. With respect to the liquid substrate and carbon nanofillers introduced to the system, the effect of the mechanical stirrer is to seclude existing beams/sheets and ensuring the distribution of nanoparticles in the entire volume of the substrate. In an ultrasonic homogenizer to obtain a good dispersion of nanoparticles in liquid media, a high density of ultrasonic energy on the sonotrode is used. The generator converts the collected mains voltage with a frequency range of 50 - 60 Hz into the voltage of high frequency of 20 kHz. It provides a high frequency constant in time and an ultrasound high power. Connected to the generator, transducer, equipped with a high oscillatory system, converts the supplied energy from the generator to mechanical vibrations at a constant frequency (20 kHz), while the transmitter is assembled with the sonotrode. Through it and its tip occurs repeated mechanical reinforcement of the amplitude of the ultrasound, influence on a substance in which it is immersed.

The use of ultrasonic vibration on the dispersion is to restack the existing agglomerates of nanotubes and nanosheets.

Nanocomposites and pure polymers were prepared by *in situ* polymerization in the polycondensation reactor (Autoclave Engineers, Pennsylvania, USA) capacity of 1000cm^3 (Fig. 20).

During the synthesis the reaction mixture is in the cylinder which is made of stainless steel and equipped with an anchor stirrer. The rotational speed of the stirrer is regulated and torque measurement is based on measuring the power consumed by the motor which drives the stirrer.The progress of the polymerization reaction phase is determined by the increase of torque stirrer. Thermocouple placed in the cylinder allows the direct measurement of the temperature of the reaction mixture. The heating cylinder is divided into three zones of temperature control in each stage of the synthesis of the polymer / composite. Directly from the cylinder is led out the cooling system that allows discharging condensation by-products, e.g. water, alcohol, glycol, etc., resulting in the individual process steps. To control the pressure in the reactor is used an inert gas (nitrogen) and the vacuum pump depending on the needs. If required pressure introduced into the reactor is nitrogen, it is applicable during the extrusion stage of the finished polymer. When vacuum is required, high-performance vacuum pump equipped with a valve needle is used, allowing the gradual lowering of the pressure. This counteracts the rapid increase in the volume of the reaction mixture and clogging of the condenser system.

a)

b)

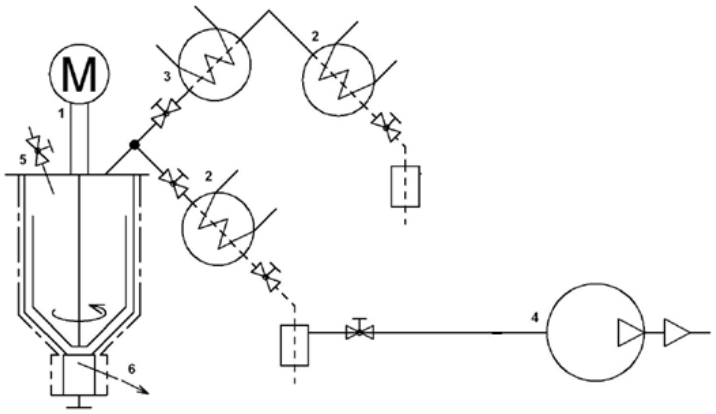

Fig. 20 Photo (a) and a scheme (b) of polycondensation reactor used to prepare polymers and polymer nanocomposites: 1) horseshoe agitator; 2) and 3) condensers' system; 4) vacuum pump, 5) valve control system and pressure generation in the cylinder with a nitrogen inlet 6) nozzle.

The obtained product in the ductile form can be extruded from the rector with the nozzle, equipped with separate heating system. The polymer in the form of a strand falls down by gravity into the water bath and then is wound on a spool driven electrically. The prepared material is granulated, dried and subjected to further processing operations. All equipment used for the synthesis of polymer composites is the equipment of the Department of Polymer Materials WUT.

11. Synthesis of polymers

Synthesis of thermoplastic polyesters

The syntheses of thermoplastic polyesters: poly(ethylene terephthalate) and poly(trimetylene terephthalate) (Fig. 21) were performed in steel reactor (Autoclave Engineers, Pennsylvania,

USA) with a capacity of 1000 cm^3. Due to the similarities between the synthesis processes of both polymers their scheme for PET can be used describes both.

1 step – Transestrification between dimethyl terephtalate (DMT) and ethanediol to bis(2-hydroxyethyl) terephthalate.

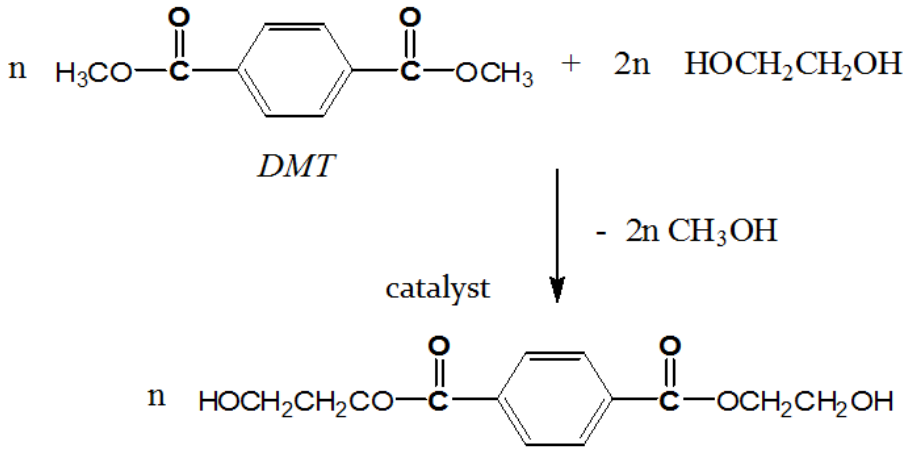

2 step- Polycondensation of bis(2-hydroxyethyl) terephthalate to poly(ethylene terephthalate).

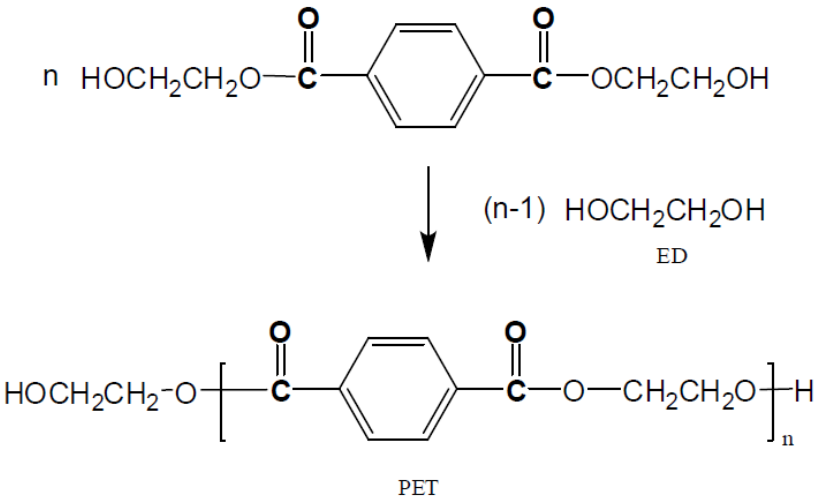

In case of synthesis of PTT transesterification reactions took place between dimethyl terephtalate (DMT) and 1,3-propanediol resulting in formation bis*(*3-hydroxypropyl) terephthalate (BHTP) that then undergo a condensation polymerization reaction, leading to the formation of poly (trimethylene terephthalate) with the effluence of 1,3-propanediol as a by- product.

The substantial differences in obtaining thermoplastic polyesters included the use of different catalysts. In case of PET, zinc acetate and antimony dioxide were used as catalyst in transestryfication and polycondensation reactions respectively. Whereas in case of poly(trimetylene terephthalate) and in both steps of *in situ* polymerization, tetrabutyl

orthotitaniate was used as catalyst. The second fundamental difference accounted for the values of polycondensation process temperatures. PTT was synthesized at the temperature of 260 ^{o}C, while PET at about 15^{o}C higher temperature, i.e. 275^{o}C.

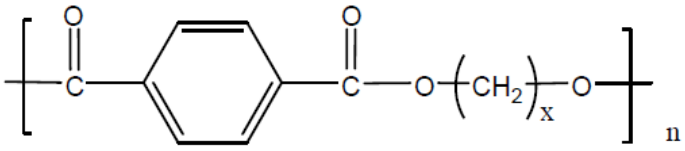

Fig. 21 Molecular formula of synthesized polyesters: x= 2 - PET, x=3 – PTT.

The amounts of reactants used in the synthesis were selected depending on the assumed amount of the final product, according to the calculations (Table 5).

The polymerization process was conducted in two stages. In the first stage, the dispersion of SWCNTs/EG or hybrid system (EG+SWCNTs) in ED, DMT and zinc acetate catalyst was charged into1L steel reactor (Autoclave Engineers Inc, USA) equipped with a vacuum pump, condenser, and cold trap for collecting the by-products. Transesterification reaction took place between dimethyl terephtalate (DMT) and ethanediol under nitrogen flow at atmospheric pressure and in a temperature range of 160÷180^{o}C. The ethanediol was used in 50 mol % excess over the dimethyl ester. The methanol formed during the transestrification was distilled off and collected. The first stage of the polymerization process was finished when the amount of formed methanol was close to the theoretical one. Then the second stage was begun: antimony dioxide as catalyst was added, the pressure was gradually lowered to about 0.1 hPa and the polycondensation was carried out at temperature of 275^{o}C and under continuous stirring (stirrer speed 40 min^{-1}). The progress of the polymerization was monitored by measuring the changes of viscosity of the polymerization mixture, i.e. an increase in torque stirrer values during the polycondensation. The reaction was considered complete when the viscosity of the system increased to 14Pa·s. The obtained polymer/nanocomposite was extruded from the reactor under nitrogen flow in the form of polymer wire.

Table 5 The amount of raw materials used to obtain 100g of PET and PTT

Estimated weight of the obtained polymer (PET)	**100 g**
DMT mass: $m_{DMT}=M_{DMT}(m_{PET}/M_{PET})$	101.04 g
ED mass: $m_{ED}=M_{ED}(m_{PET}/M_{PET})$	48.44 g
OC mass: 0.25 wt % m_{DMT}	0.25 g
TA mass: 0.25 wt % m_{DMT}	0.25 g
Amount of effluent CH_3OH obtained during transestrification (theoretical)	33.3 g
M_{DMT}= 194 g/mol, M_{PET}= 192 g/mol (molar weight of mer); M_{ED}=1.5 x 62= 193 g/mol; M_{CH3OH}= 2 x 32= 64 g/mol; (used multipliers are due to the reaction stechiometry)	
Estimated weight of the obtained polymer (PTT)	**100 g**
DMT mass: $m_{DMT}=M_{DMT}(m_{PTT}/M_{PTT})$	94.17 g
PDO mass: $m_{PDO}=M_{ED}(m_{PTT}/M_{PTT})$	73.78 g
TiBu mass: 0.25 wt % m_{DMT}	0.24 g
Amount of effluent CH_3OH obtained during transestrification (theoretical)	31.07 g
M_{DMT}= 194 g/mol, M_{PTT}= 206 g/mol (molar weight of mer); M_{PDO}=2 x 76= 152 g/mol; M_{CH3OH}=2 x 32= 64 g/mol; (used multipliers are due to the reaction stechiometry)	

Synthesis of block copoly(ether-ester) (PTT-*block*-PTMO)

PTT-PTMO block copolymer was synthesized according to the same procedure as previously described for PET and PTT.The only difference was that when the first step of reaction was completed, poly(tetramethylene oxide) glycol with molecular weight of 1000 g/mol was added. The chemical formula of the synthesized copolymer is shown in Figure 22.

Multiblock poly(ether–ester) (PEE) based on poly(butylene terephthalate) (PBT) as rigid segments and poly(tetramethylene oxide) (PTMO) as soft segments have been intensively studied [314] [315]. Due to their excellent mechanical properties, like strength and elastic properties in a wide temperature range they are of special interest. The PBT-*block*-PTMO copolymers are available as commercial products (Elitel^{TM}, Arnitel, Hytrel®, DSM etc.). Recently a study on a novel family of polyester thermoplastic elastomers based on PTT has been conducted [316] [317].

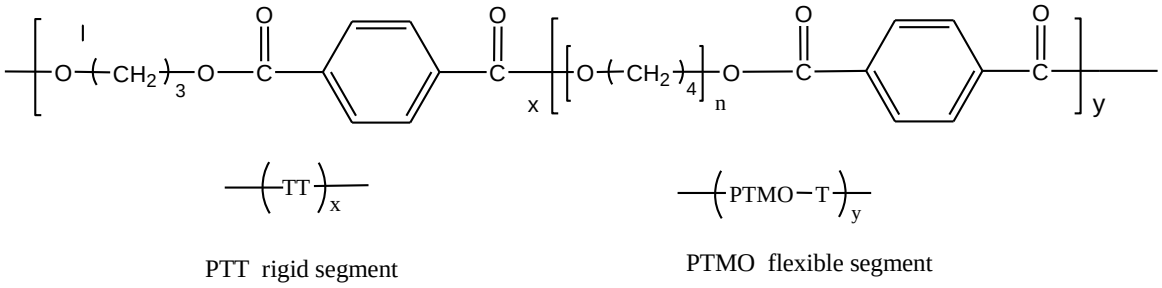

Fig. 22 Chemical structure of block copoly(ether ester) (PTT-*block*-PTMO).

1 step – Transestrification between dimethyl terephtalate (DMT) and 1,3-propanediol to bis(2-hydroxypropyl) terephthalate (BHPT). During this stage, except of BHPT its low molecular weight oligomers can be formed.

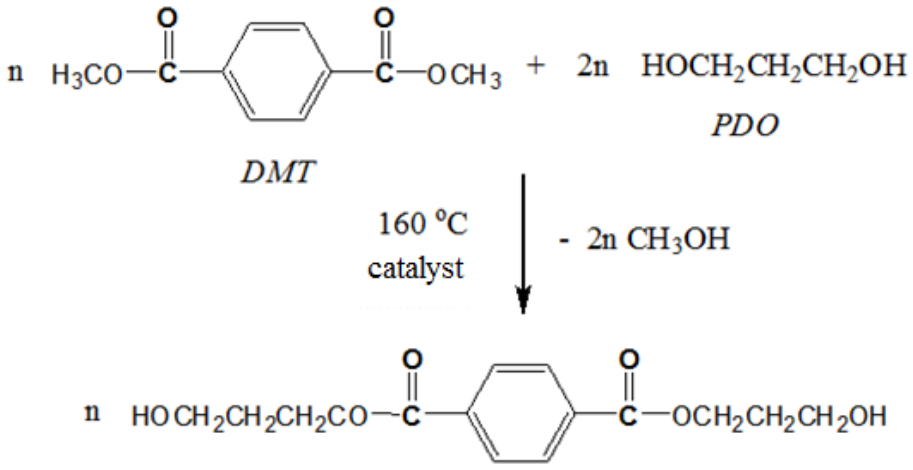

2 step- Polycondensation of bis(3-hydroxypropyl) terephthalate and its oligomers with poly(tetramethylene ether glycol terephthalate) (PTMO-T) unit to PTT-*block*-PTMO copolymer. The obtained block copolymer is presented as a random copolyester (TT units and PTMO-T units).

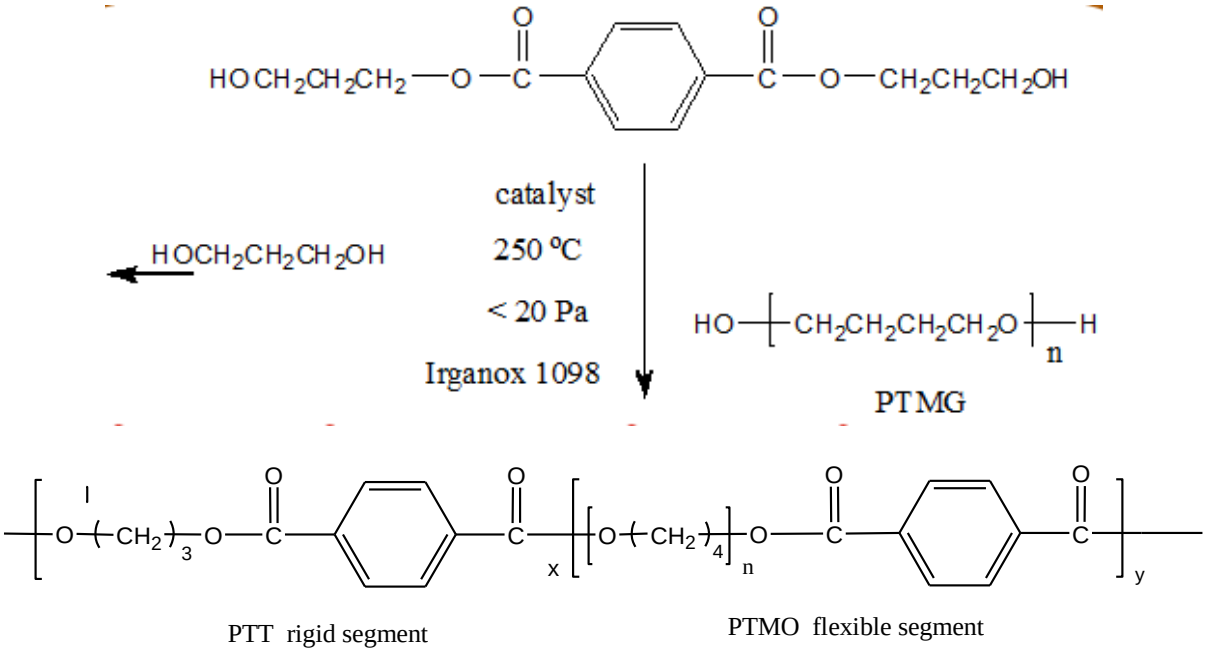

PTT rigid segment PTMO flexible segment

where x, y- degree of polymerization of rigid and flexible segments respectively [316].

The amounts of reactants used in the synthesis were selected depending on the assumed amount of the final product, according to the calculations (Table 6). Nanocomposites were synthesised by melt transesterification and subsequently polycondensation as follows. In the first stage, an appropriate amount of nanofiller (Graphene Ang, SWCNT) was dispersed in 250 ml of PDO using ultra-high speed stirrer high (Ultra-Turrax® T25) and ultrasonic homogenizer *(*Sonopuls HD 2200, Bandelin). Completed time of dispersing was 30 min. Additionally, in case of Graphene Ang, ultra-low power sonic bath was used for 8h. Then the dispersion of nanofillers in PDO, DMT and TBT catalyst was charged into1L steel reactor (Autoclave Engineers Inc, USA) equipped with a vacuum pump, condenser, and cold trap for collecting the by-products. The transesterification reaction was carried out under a constant flow of nitrogen at 165°C in the presence of catalyst (TBT, 0.15 wt% in relation to DMT) for one and half hour. During the reaction, methanol was distilled off. The conversion of the transesterification reaction was calculated by monitoring the amount of effluent methanol. When the reaction of DMT with PDO reach conversion level of 90 %, PTMG was introduced in the reactor, together with Irganox 1010 (0.5 wt% of total comonomers mass) and second portion of catalyst (TBT, 0.10 wt% in relation to DMT), and in subsequent step the reaction mixture was heated slowly under reduced pressure. The second step, melt polycondensation was carried out at 250 °C and under reduced pressure of 15-20 Pa. The stirring torque change was monitored in order to estimate the melt viscosity of the product. Synthesis was finished when melt rich a fixed value of melt viscosity corresponding to high molecular weight copolymer. The obtained nanocomposite was extruded from reactor under nitrogen, cooled to room temperature in water bath and granulated. The neat PTT-PTMO copolymer was synthesized following the same procedure, without nanofillers. The content of rigid segments based on PTT was 50 wt% and the content of soft segments based on PTMO was 50 wt%.

Table 6 The amount of raw materials used to obtain 100g of PTT-*block*-PTMO

Estimated weight of the obtained polymer (PTT-*block*-PTMO)	**100 g**
DMT mass	58.16 g
PDO mass	28.9 g
PTMO mass	48g
Catalyst mass: TiBu 0,25 wt % m_{DMT}	0.15 g
Stabilizer mass: 0,5 wt % m_{PEE}	0.5 g
Calculations performed for a copolymer having a weight ratio of soft segments to the rigid of*: PTT/PTMO 50:50 wt/wt;*	
Substrates molar mass was calculated from the stoichiometric reaction of the polymers for *PTT-b-PTMOT – 1881.9 g/mol; x=5.48 x – amount (in moles) of PTT on y=1 soft segment of PTMOT); M_{DMT}=194 g/mol, M_{PTMO}=1000 g/mol; M_{PTT}=206 g/mol; M_{PDO} – 76 g/mol;*	

12. Samples preparation

Before the preparation of test samples the obtained composite materials were granulated and dried in a vacuum drier at 120 ^{o}C for 4 hours . Due to the high sensitivity to moisture of the polyesters during processing, drying of the composites based on PET and PTT took place immediately before the processing process.

Samples for determining the mechanical properties were made using injection molding machine Boy 15 (Dr. BOY, Germany) with a mold clamping force of 150 kN. The polymer material was injected into a 10-soccet mold (Fig 23 a). The dimensions of the measured profiles correspond to the standardized dimensions (profile type 3) according to the PN-ISO 37 standard, while expanded the grip parts of the dumb bell shape samples (Fig. 23 b). It was due to the better samples deposition in the jaws of the testing machine, and the possibility of using surface for other indications/ measurements. The injection molding parameters (Table 6) were selected depending on the type of polymer matrix and based on the guidelines of the PN-EN ISO 294 standard, and the plastic melting point was determined on the basis of DSC measurements.

The above mentioned dumb bell shape samples were used to determine the tensile measurements. The cut out sections of samples were used to determine the density and for thermal analysis (DSC, TGA). Before performing the measurement samples of tested materials were conditioned according to the standard PN-EN ISO 291 + AC1.

Samples for X-ray scattering (WAXS) and dielectric spectroscopy were carried out using a hydraulic press (Collin P 200E) at a temperature of 15 °C (260 °C for PET and for PTT at 245 °C) higher than the melting temperature determined by DSC. Terms of pressing: pressure 15 bar, warm-up time 1 min, pressure 1 min, cooling 1 min. To prevent the molten material from sticking to the plates, kapton tape was used for polyesters (PET, PTT) and PTFE tape for PTT-b-PTMO. The obtained amorphous films for dielectric test (crystallization tests, the electrical conductivity) of a thickness of 200-250 μm were sputtered of thin film of gold having a diameter of 2 cm.

a) b)

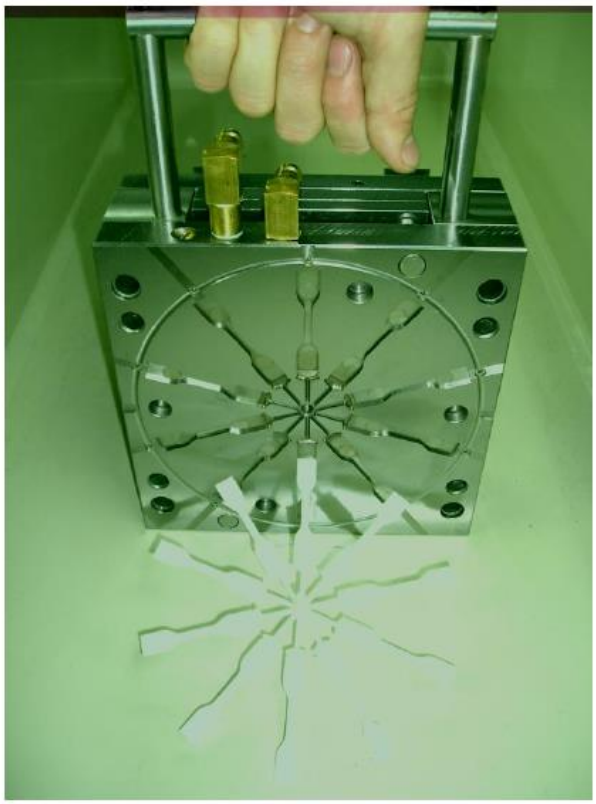

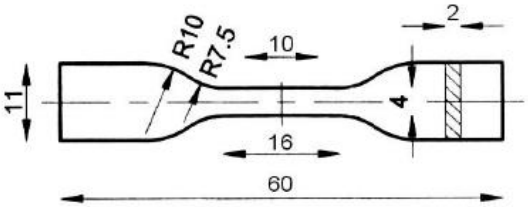

Fig. 23 Photo of 10-soccet injection molding form to prepare samples for tensile tests, designed in the Department of Polymer Materials (a), the dimensions of the custom specimens for determinations of mechanical properties (b).

Table 6 The injection molding process parameters of polymer nanocomposites and polymers (copolymers) on the injection molding machine Boy 15

Material	Temp. of heating zones [^{o}C]			Form temperature [^{o}C]	Pressure [MPa]	
	I	II	III		injection	hold
PET	245	260	270	30	70	25
PET/EG	245	260	270	30	70	35
PET/SWCNT	245	260	270	30	70	35
PET/EG+SWCNT	245	260	270	30	70	35
PTT	235	240	245	30	70	25
PTT/EG	235	240	245	30	70	30
PTT/SWCNT	235	240	245	30	70	30
PTT/EG+SWCNT	235	240	245	30	70	30
PTT-PTMO	210	215	220	30	60	20
PTT-b-PTMO/G	210	215	220	30	65	25
PTT-b-PTMO/SWCNT	210	215	220	30	65	25
PTT-b-PTMO/G+SWCNT	210	215	220	30	65	25

.

13. Investigation methods

13.1. Morphology and structure

The structure of nanocomposites was observed by scanning electron microscopy (SEM, JEOL JSM 6100). The samples were cryofractured in liquid nitrogen, and then vacuum coated with a thin gold film before the test. Transmission electron microscopy (TEM) analysis was carried out by a JEOL JEM-1200 Electron Microscope using an acceleration voltage of 80 kV. The TEM samples (thickness of about 100-150 nm) were obtained by cutting of tensile specimen's perpendicular to flow direction under cryogenic conditions using Reichert Ultracut R ultramicrotome with a diamond knife.

Raman spectroscopy experiments were performed by using a Renishaw Raman InVia Reflex Spectrophotometer, with excitation at 785 nm (diode laser), and a resolution of 2 cm^{-1}.

13.2. Thermal properties

Thermal and thermo-oxidative stability of investigated polymer nanocomposites were evaluated by thermogravimetry (TGA 92-16.18 Setaram) using the system to measure the simultaneous TG-DSC. Measurements were carried out in inert atmosphere (argon) an oxidizing atmosphere i.e. dry, synthetic air (N_2 : O_2 = 80 : 20 vol %). The study was conducted at a heating rate of 10 ^{o}C/min in the temperature range from 20 to 700 ^{o}C. Measurements were conducted in accordance with the principles contained in the PN-EN ISO 11358:2004. The thermal decomposition kinetics was examined by Freeman-Carroll method [318] using equation:

$$\frac{\Delta \ln(d\alpha/dt)}{\Delta \ln(1-\alpha)} = n - (E_a/R)\frac{\Delta \ln(1/T)}{\Delta \ln(1-\alpha)} \qquad (1)$$

where: α is the degree of conversion. The degree of conversion is given by $\alpha = (m_0-m)/(m_0-m_f)$, where m is the weight of sample and the subscripts 0 and f to the values at the beginning and at the end of the weight loss event of interest. Furthermore, $d\alpha/dt$ denotes the decomposition rate or weight loss rate, E_a stands for the activation energy, n is order of reaction, R is the gas constant, and T symbolizes the absolute temperature.

By plotting a graph of $\Delta \ln(d\alpha\text{-}dt)/\Delta \ln(1-\alpha)$ versus $\Delta T^{-1}/\Delta \ln(1-\alpha)$, a straight line was obtained, and the slope and intercept are equal to $-E_a/R$ and n, respectively

The thermal transitions of the polymers were measured with differential scanning calorimetry (DSC, TA Instrument Q-100).

.

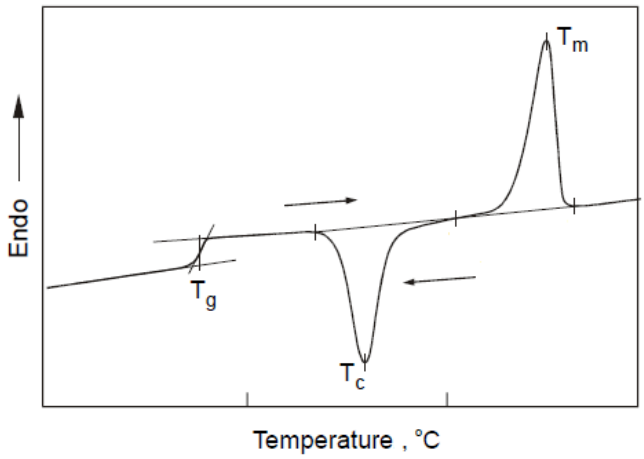

Fig. 24 Scheme of determination of the glass transition temperature, melting temperature and crystallization in DSC method.

The heating and cooling rate was 10°C/min and sample weight of 10 ± 0.2 mg. An indium standard was used to calibrate the temperature and the heat of fusion. The first cooling and second heating scans were used to determine the melting and crystallization peaks. The heat of fusion was determined by integration of the normalized area of melting endotherm. The glass transition temperature (T_g) for the polymer samples was taken as the midpoint of the change in heat capacity (ΔCp/*2*). The degree of crystallinity of the samples was calculated by the following equation: $x_c = \left(\Delta H_m / \Delta H_m^o\right)$; where ΔH_m^o is the enthalpy change of melting for a 100% crystalline sample (for PET: ΔH_m^0=140 J/g [319] and for PTT: ΔH_m^0=146 J/g [319] and ΔH_m is derived from melting peak area on DSC thermogram.

13.3. Determination of physical properties

The intrinsic viscosity [η] of the samples was determined at 30 °C in mixture phenol / 1,1,2,2-tetrachloroethane (60/40 by weight). The polymer solution had a concentration of 0.5 g/dl. The measurement was carried on a capillary Ubbelohde viscometer (type Ic, K = 0.03294). The following procedure was used to eliminate the influence of the nanofiller presence on measured [η] values. Nanocomposites samples were dissolved in mixture phenol/ phenol/1,1,2,2-tetrachloroethane (60/40 by weight), then filtered to separate nanofiller. The samples were precipitated by adding methanol and recovered by filtration. Finally, the precipitated solids were dried in vacuum at 60 °C for 24 hours. Through Mark-Houwink equation, that relates the limiting viscosity number with molecular weight, the Mv has been calculated using formula 2:

$$[\eta] = K \cdot M_v^{\alpha} \qquad (2)$$

where K and α are constants specific to the solvent and temperature. The viscosity average molecular weight (Mv) of neat PET and its composites was calculated using following constants: $K=3.72 \cdot 10^{-4}$ dl/g and α=0.73 [320], whereas for PTT and its nanocomposites: $K=5.36 \cdot 10^{-4}$ dl/g and α=0.69 accordingly to the literature [321].

Size-exclusion chromatography (SEC) was performed on a system equipped with a Waters 1515 Isocratic HPLC pump, a Waters 2414 refractive index detector working at 40 ^{o}C, a Waters 2707 autosampler, and a PSS PFG guard column followed by a 2PFG-linear-XL (7 mm, 8300 mm) columns in series at 40 ^{o}C. HFIP with potassium trifluoroacetate (3 g L^{-1}) was used as eluent at a flow rate of 0.8 mL min^{-1}. The molecular weights were calculated against poly(methyl methacrylate) standards (Polymer Laboratories, M_p = 580 Da to M_p = 7.1 x 10^6 Da).

The melt flow rate (MFR) was measured by using a melt indexer (CEAST, Italy) as weight of melt flow in grams per 10 min, at temperature of 205 ^{o}C, and at orifice diameter 2.095 mm and under 21.18 N load, according to ISO 1133 specification.

The density was measured at 23 ^{o}C on hydrostatic balance (Radwag WPE 600C, Poland), calibrated for standards with known density. Additionally, degree of crystallinity (Xc) was quantified based on the density measurements.

Weight % crystallinity was quantified using the formula:

$$Xc_w = \frac{\rho_c}{\rho}\frac{(\rho-\rho_a)}{(\rho_c-\rho_a)}\cdot 100\% \quad (3)$$

where: ρ- measured density of semicrystalline sample, ρ_a- density if the sample is completely amorphous, ρ_c- density if the sample is completely crystalline. For thermoplastic polyesters the following values of ρ_a and ρ_c were used: for neat PET and its composites: ρ_a=1.33 g/cm^3, ρ_c=1.40 g/cm^3 [319], while for neat PTT and its composites: ρ_a=1.299 g/cm^3, ρ_c=1.432 g/cm^3 [319].

13.4. Tensile properties

Tensile measurements were performed on Instron 5566 universal tensile testing frame, equipped with a 5 kN Instron load cell, an contact optical long travel extensometer and the Bluehill 2 software. Pneumatic 1 kN Instron side action grips were used for specimens clamping. The measurements were performed at room temperature on using a cross-head speed of 5 mm/min for thermoplastic polyesters (PET, PTT) and 100 mm/min for thermoplastic elastomers and a grip distance of 20 mm. The tensile properties were determined on injection moulded *dumbbell-shaped* bars (ISO 37 type 3). The Young's modulus, yield stress (elastic limit) and yield strain, stress and elongation at break of the nanocomposites were determined. The results are based on data collected from 6 specimens for each sample and the means value and standard deviations were calculated.

13.5. Electrical conductivity

Broad band dielectric spectroscopy

Circular gold electrodes (20 mm in diameter) were deposited by sputtering the metal onto both free surfaces of the sample film. The complex permittivity $\varepsilon^* = \varepsilon' - i\varepsilon''$, where ε' represents the permittivity and ε'' the dielectric loss, was measured as a function of frequency (10^{-1} Hz<F<10^6 Hz, being F the frequency of the applied electric field) and temperature (-150

^{o}C up to 150 ^{o}C) by using a Novocontrol broadband dielectric spectrometer. Temperature control was obtained by a nitrogen jet (QUATRO from Novocontrol) with a temperature error, during every single sweep in frequency, of 0.1 K. Electrical conductivity was derived by $\sigma(F) = \varepsilon_0 2\pi F\varepsilon''$ where ε_0 is the vacuum permittivity. The study was performed in cooperation with Instituto de Estructura de la Materia CSIC in Madrid, Spain.

13.6. Gas barrier properties

Oxygen permeability was measured using a Mocon-Ox-Tran 2/10 instrument (23°C and 0% humidity rate RH). Oxygen permeability was performed using 5 cm^2 samples of investigated polymer films in accordance with ASTM D3985-05 and ISO 15105-2 Standards. All film samples were additionally conditioned for 3h in the test chamber of OX-Tran apparatus in test parameters (23°C and 0% humidity rate RH). The measurement was automatically terminated when apparatus obtained stable subsequent results.

Gas permeability (according to DIN 53 380) is the amount of gas, reduced to standard conditions, which penetrates within 1 day by 1 m^2 of the film at a predetermined temperature and at the pressure differential. The gas permeability test method also describes the American standard ASTM D1434-82(2003) – Standard Test Method for Determining Gas Permeability.

Studies on composites based on poly (trimethylene terephthalate) have been made using the equipment to study gas barrier TotalPerm company ExtraSolution (Italy). The measurement was carried out in accordance with PN-EN ISO 4080:1998 / AC: 2000. Tests were performed on samples with a diameter of 10cm.

The film thickness was determined with the precision thickness gauge MG-401 (Elmetron, UK) with an accuracy of ±1 μm.

RESULT AND DISCUSION

14. Principle of preparation of polymer nanocomposites by *in situ* method

14.1. Kinetic of one shot polycondensation. Mass transfer and viscosity aspect

One of the objectives of this study was to establish the conditions for preparing the polymer composites containing carbon nanoparticles during *in situ* polymerization method, i.e. introducing a filler into the polymer during its synthesis. Scheme of the preparation of the composites is shown in Fig. 25.

Immediately before the beginning of the synthesis nanoparticles were dispersed in one of the substrates used in the reaction. In the case of composites based on both polyesters: PET and PTT, nanoparticles were stirred respectively in ethanediol or propanediol. Dispersion of nanofillers was prepared by dispersing the desired amount of EG, SWCNT or other form of carbon nanofiller used in the dissertation, in approximately 250-300 mL of glycol through ultrasonication for 15 min using laboratory homogenizer (Sonoplus HD 2200, with frequency of 20 kHz and 75% of power 200W) and subsequent intensive mixing for 15 min with high-speed stirrer (Ultra-Turax T25). Additionally, to improve the dispersion/exfoliation of graphene derivatives (EG, Graphene Ang etc.) in ED/PDO an ultra-power lower sonic bath (BANDELIN electronic GMbH & Co. KG, Sonorex Digitec, with frequency of 35kHz and power 140W) was applied for 8 hours. The use of vibration of laboratory homogenizer with ultrasound frequency was to break down the existing agglomerates of nanotubes or nanosheets, and in case of high speed shear forces to distribute nanoparticles in the entire volume of the system. As a result of intensive stirring, the temperature of the system rose, thereby reducing its viscosity and, consequently, facilitated the distribution. During the preparation of composites based on polyesters the obtained dispersion of nanoparticles, immediately after mixing, was introduced to the reactor together with other raw materials, wherein the synthesis of the polymer was carried out.

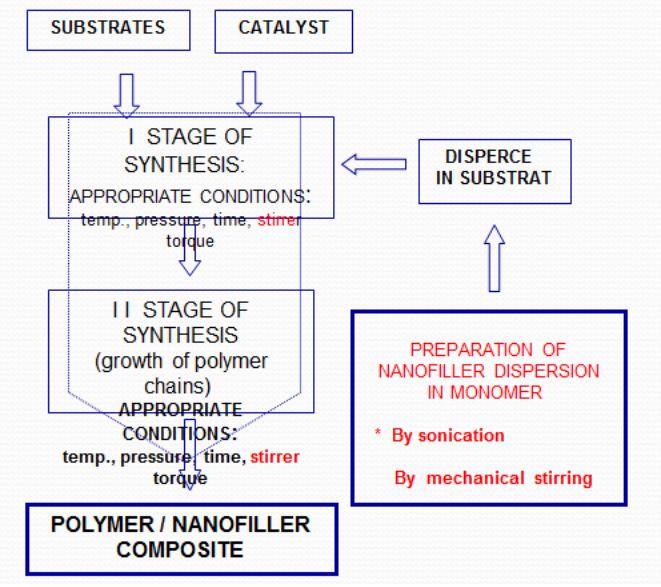

Fig. 25 Scheme of preparation procedure of polymer composites containing carbon nanofillers.

Within the framework of the research were prepared and tested 12 kinds of polymer composites, differing from one another the type of polymer matrix (PET, PTT, PTT-PTMO) and the type of nanofillers (EG, Graphene Ang, FLG, SWCNT) and their weight content in the polymer. For the comparative purpose (as a reference) were synthesized pure (unfilled) polymer samples. All received polymeric materials and their symbols used in the text are included in Table 7.

Table 7 Statement of composites based on thermoplastic polyesters and thermoplastic elastomers made and examined at work

Polymer matrix	Type of nanofiller	Wt % content of nanofiller	Name of the composite	comments
PET		0	PET	reference
	Single-walled carbon nanotubes (Cheaptubes)	0.025	PET/0.025 SWCNT	Dispersion in ED
		0.05	PET/0.05 SWCNT	
		0.1	PET/0.1 SWCNT	
		0.2	PET/0.2 SWCNT	
		0.4	PET/0.4 SWCNT	
	Expanded graphite EG (I)	0.025	PET/0.025 EG	Dispersion in ED
		0.05	PET/0.05 EG	
		0.075	PET/0.075 EG	
		0.1	PET/0.1 EG	
		0.2	PET/0.2 EG	
		0.4	PET/0.4 EG	
	Hybrid system of SWCNT+EG (I)	0.025+0.025	PET/0.025 EG+0.025 SWCNT	Dispersion in ED
		0.05+0.05	PET/0.05 EG+0.05 SWCNT	
		0.1+0.05	PET/0.1 EG+0.05 SWCNT	
PTT		0	PTT	reference
	Single-walled carbon nanotubes (High purity) (Grafen Co.)	0.025	PTT/0.025 SWCNT-KNT	Dispersion in PDO
		0.05	PTT/0.05 SWCNT-KNT	
		0.1	PTT/0.1 SWCNT-KNT	
		0.3	PTT/0.3 SWCNT-KNT	
		0.5	PTT/0.5 SWCNT-KNT	
	Expanded graphite EG (II)	0.1	PTT/0.1 EG	Dispersion in PDO
		0.3	PTT/0.3 EG	
		0.5	PTT/0.5 EG	
	Few-layer Graphene (FLG) (Strasbourg)	0.1	PTT/0.1 FLG (Strasbourg)	Dispersion in PDO
		0.3	PTT/0.3 FLG (Strasbourg)	
		0.5	PTT/0.5 FLG (Strasbourg)	
	Expanded graphite 500 μ (EG 500)	0.05	PTT/0.05 EG 500	Dispersion in PDO
		0.1	PTT/0.1 EG 500	
		0.3	PTT/0.3 EG 500	
		0.5	PTT/0.5 EG 500	
		1.0	PTT/1.0 EG 500	
	Graphene Angstron (<1nm)	0.1	PTT/0.1 G (1nm)	Dispersion in PDO
		0.3	PTT/0.3G (1nm)	
		0.5	PTT/0.5 G (1nm)	
		1.0	PTT/1.0 G (1nm)	
	Hybrid system of SWCNT+EG (II)	0.05+0.1	PTT/0.1EG+0.05SWCNT-KNT	Dispersion in PDO
		0.1+0.1	PTT/0.1EG+0.1SWCNT-KNT	
PTT-PTMO		0	PTT-PTMO	Reference
	Graphene Angstron (<1nm)	0.1	PTT-PTMO/0.1G	Dispersion in PDO
		0.3	PTT-PTMO/0.3 G	
		0.5	PTT-PTMO/0.5G	
		1.0	PTT-PTMO/1.0G	
	Single-walled	0.1	PTT-PTMO/0.1SWCNT-	Dispersion in PDO

carbon nanotubes (High purity) (Grafen Co.)	0.3	KNT PTT-PTMO/0.3SWCNT-KNT	
Hybrid system of SWCNT KNT+ Graphene Angstron (<1nm	0.1+0.3	PTT-PTMO/0.1SWCNT-KNT+0.3G	Dispersion in PDO
	0.3+0.1	PTT-PTMO/0.3SWCNT-KNT+0.1G	
	0.5+0.1	PTT-PTMO/0.5SWCNT-KNT+0.1G	

While working on the development of the conditions for receiving polymer nanocomposites by *in situ* an important issue was to investigate whether the presence of carbon nanotubes, graphene nanoplatelets and mixtures of both in the reaction mixture affects the course of the synthesis of the polymer. When developing the synthesis of nanocomposites based on polyester matrix earlier experience of the research group [3] on the use of this method for the preparation of nanocomposites with the participation of the CNT. The various stages of the preparation process of the composite have been analyzed, the technological aspects (such as the ability of the obtained composite extrusion of the reactor and its further processing) and the viscosity of the obtained composites.

In the case of syntheses of polyester and poly(ether-ester) block copolymer based composites), in the initial stage of the process (transesterification reaction) no phenomena has been observed indicating that the presence of of the carbon nanoparticles in the reaction mixture can disturb an ester exchange. The duration of the ester interchange, depended on the amount of substrates involved in the synthesis, and the intensity of the condensation of methanol were comparable during the preparation of filled and unfilled polymers. Observations for different polymer matrices (PET, PTT and PTT-*block*-PTMO are presented in Fig. 26 a-c. In any case, the amount of released methanol corresponds to the conversion level of 90 %.

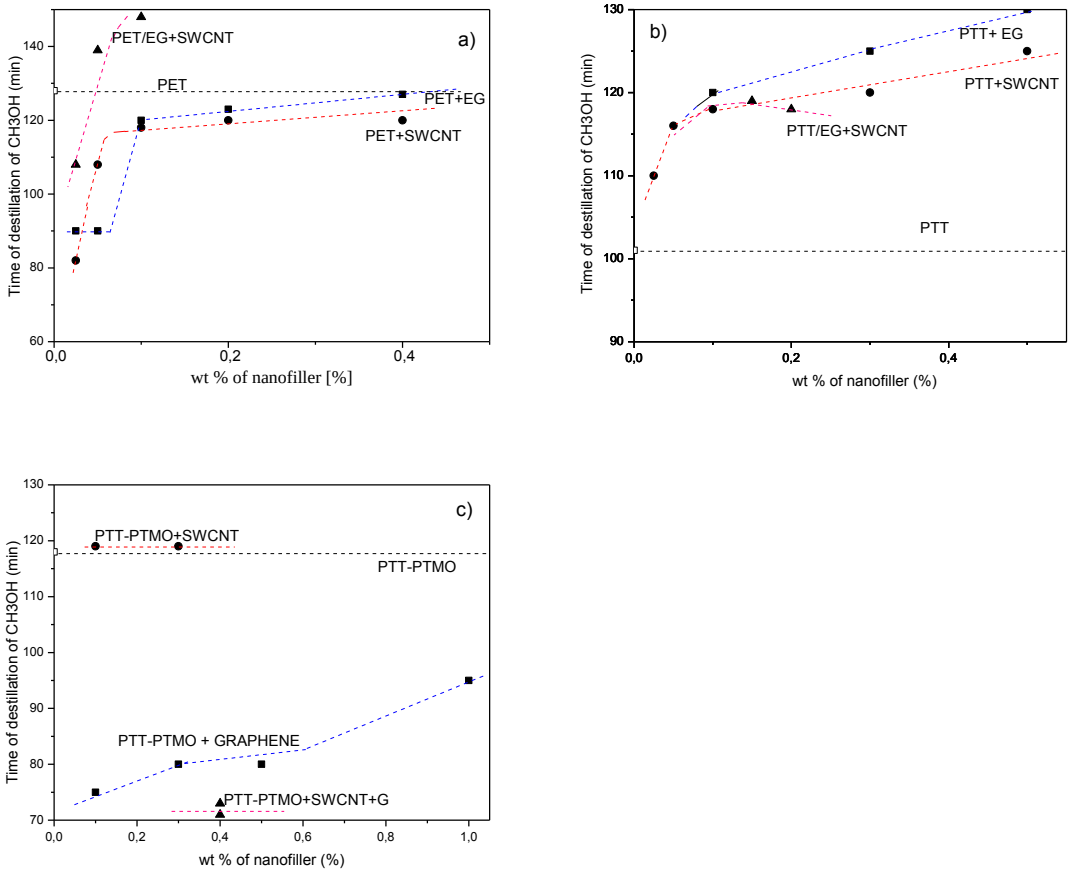

Fig. 26 The time required to condense the appropriate amount of methanol as a function of the wt % content of nanofiller a) for PET nanocomposites, b) PTT nanocomposites and c) PTT-PTMO nanocomposites.

The process of the second stage of the synthesis showed some differences depending on the type and concentration of carbon nanoparticles (CNT, EG, Graphene etc.), observed both for composites based on PET and PTT and PTT-PTMO block copolymer. These differences are related to an increase in viscosity of the reaction mixture. Observations were conducted by measuring the time of increase of the torque of the stirrer (a gradual increase in viscosity of the system), at a constant speed, since the first change was noted (indicating that the polymerization reaction proceeds) until it reaches a certain value at which the synthesis was terminated (0.35 a.u. at a speed of 40 rpm for PET; 0.28 a.u. at a speed of 20 rpm for PTT, 0.28 a.u. at a speed of 20 rpm for PTT-PTMO). In each case were preserved reproducible process conditions, i.e. comparable the temperature, pressure and stirring speed. For the composites synthesis, the time needed to achieve the required viscosity depended on the type and concentration of nanoparticles (Fig. 27).

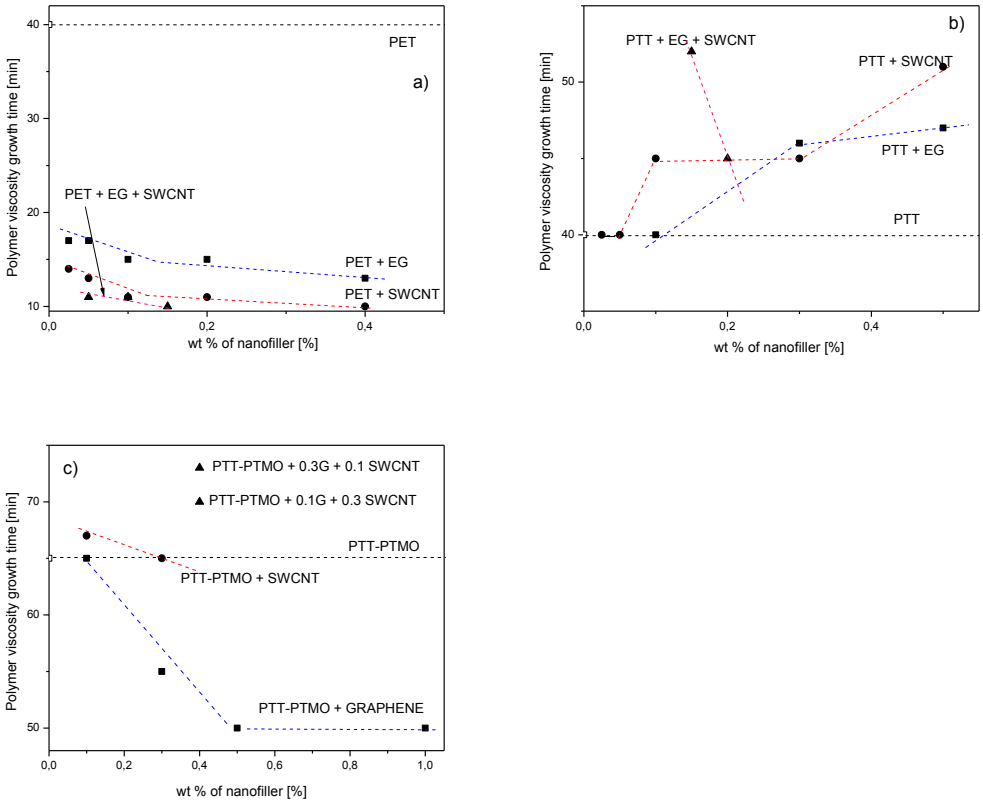

Fig. 27 Time dependence of the viscosity of the polymer growth (measured by the increase in torque stirrer to achieve an appropriate value at a given speed) from a) the type and concentration of carbon nanoparticles composites PET / CNT + EG, b) the type and concentration of carbon nanoparticles for composites PTT / CNT + EG c) the type and concentration of carbon nanoparticles for composites PTT-PTMO/CNT + G.

The presence of both types of nanofillers, both single-wall carbon nanotube, expanded graphite, as well as mixtures of both, resulted in a marked acceleration of PET polycondensation process, even at very low concentrations. Torque growth time decreased more than tripled in the case of nanotubes nanocomposites and graphene platelets, while almost four times decreased in the case of mixtures of two nanofillers. So effective decrease of the reaction time can suggest a strong catalytic activity in the case of poly (ethylene terephthalate) as a matrix.

The presence of various nanoparticles practically did not affect the process extension of the synthesis of poly(trimethylene terephthalate). At their smallest concentrations only slight elongation of reaction time was observed, however, the measurement error in estimating approximately ± 2 min. Therefore it can be assumed that the observed differences are within the measurement error. Increasing the concentration of single-wall carbon nanotubes in a mixture with expanded graphite gradually increased time of torque growth to about 12min for the highest concentration of nanofillers.

The slowdown of the polymerization reaction is more pronounced in the case of composites PTT-PTMO matrix containing both SWNT and graphene (and a mixture of SWCNT + G), even at very low concentrations. The cause of disturbance of the polymerization process may be that the presence of nanoparticles in the reaction mixture with a very high aspect ratio and dimensions slightly larger dimensions macromolecules limiting the mobility of the formed polymer chains. This hindered mobility leads to slow down the

merge of oligomeric particles into long macromolecules and consequently to extend the polymerization time. The presence of the carbon nanoparticles, especially carbon nanotubes (best seen in the synthesis of PET) which showed the highest surface area, decreased the ability of molten polymer to flow, which at certain concentrations pose some technical problems. There is a high probability that the polymer melt with nanotubes acquires thixotropic properties, which was not observed in the case of carbon nanoplatelets, as well as in case of a mixture of carbon nanotubes and nanoplatelets. This resulted in the need to increase the temperature of the melt, resulting in degradation of the polymer proceeded, and the resulting materials were subjected to further characterization. Preparation of composites with higher concentrations of nanofiller is possible by making modifications to the tooling design, taking into account the geometry of the flow paths of the resulting composite melt.
On the one hand, the presence of nanoparticles in the polymer melt impeded its flow, on the other hand, a sign of intrinsic viscosity [η] of nanocomposites showed a decrease in its value (the higher the concentration of the CNT, EG etc.), in comparison to values obtained for the polymers without filling (Tables 8,10,12 (with SWCNT), Tables 20, 22, 24 (with graphene derivatives) and Tables 35, 37, 39 with hybrid systems) and thus a lower molecular weight composite. This relationship is observed for each type of polymer used as a matrix for composites. It should be noted that the presence of carbon nanotubes and nanoplatelets in the reaction mixture increases the viscosity from the beginning of the synthesis, but this increase is small enough that there is not observed the resistance to mixing (i.e., higher torque). As a result, the torque, on the basis of which is controlled synthesis procedure, at various stages of the process is the same for both the synthesis of the polymer without the addition of nanofillers, and composite. This makes conducting polycondensation under the same conditions, and ending it with the same torque stirrer, resulting polymer without filling in reality will have a higher molecular weight (higher intrinsic viscosity) than that containing the nanoparticles, which may affect the physical properties of the obtained composites. The molecular weights calculated from measurements of [η] for composites based on thermoplastic polyesters (Tables 8, 10, 12 (with SWCNT) and Tables 20, 22, 24 (with graphene derivatives) are comparable or slightly lower than the molecular weight determined for the neat polyesters (PET, PTT) without filling. The increase of the molecular weight of the polymer matrix can be possible by using of post-polycondensation process in the solid state. It may therefore be a way to increase the molecular weight of the composite, but it needs to provide an appropriate apparatus for this purpose. Observations on the effect of the addition of nanofillers on the viscosity of the system, in addition to measuring the torque growth time, the intrinsic viscosity and the melt flow rate, also related to the determinated values of melt viscosity as a function of frequency using a rheometer ARES (Chapter 15.3, page 82 for SWCNTs and Chapter 16.3, page 106). In addition the changes in melt viscosity associated with the addition of carbon nanostructures in a poly(trimethylene terephthalate), and thermoplastic elastomer matrix for comparison, wherein the rigid segment consisted of PTT were studied. Results of this study are presented in the section on CNT contents on physical properties of polymer nanocomposites.

All observations made during the synthesis of nanocomposites with different types and concentrations of carbon nanoparticles and polymers are of great significance from the perspective of development and improvement of methods for *in situ* synthesis.

14.2. Dispersion and deagglomeration processes

As mentioned in the introduction, one of the difficulties in the technology of the polymeric nanocomposites based on the thermoplastic matrix is to obtain a homogenous dispersion of nanofiller. Developed in this dissertation the *in situ* polycondensation method, preceded by dispersing nanoparticles (nanotubes, nanoplatelets and mixtures of the two) in the liquid substrate, aims to provide a high uniformity of nanofillers in the entire volume of the material. The analysis presented below is the basis of the results of studies assessing the effectiveness of the method used in the context of the possibility of its application to polyesters and ester block copolymers and the structure of the resulting composite.

The main purpose of dispersing carbon nanotubes and graphene nanoplatelets in one of the substrates in the *in situ* polymerization method is to obtain as little agglomerated nanoparticles structure and ensure an uniform distribution throughout the volume of nanofiller reaction mixture. The use of two types of dispersants (high shear mixers and ultrasound), interacting directly on the nanotubes, and additionally in case of nanoplatelet an ultrasonic bath, was to dismantle and de-separate the existing aggregates and agglomerates of carbon nanotubes/nanoplatelets. The efficiency of their use is analyzed based on the state of dispersion of nanoparticles at different mixing times, using scanning and transmission microscopy. The main analysis indicates indirectly on uniform distribution of nanoparticles was dielectric spectroscopy method. With its use has been shown experimentally that the selected 8-hour working time of an ultrasonic bath influence on the formation of conduction paths. Additionally, the gas barrier properties analysis showed the dispersion a certain quality has been obtained.

Nanocomposites were analyzed in which the carbon nanoparticles (1D, 2D, 1D and 2 D) were suspended in a liquid substrate: in case of PET in 1,2-ethanediol, in case of PTT and PTT-b-PTMO in 1,3-propanediol. Nanofiller were introduced into a suitable glycol, then stirred for 15 min using a high speed stirrer (22 000 rpm) and for 15 min using ultrasonic agitator (30% power). During the dispersion, solution was cooled in ice-water (the temperature of the dispersion does not exceed 80 °C). While mixing the solution with the added carbon nanotubes and / or nanoplatelets with a high speed stirrer and ultrasonic, initial agglomerates are partially deagglomerated. Thus prepared dispersions of nanoparticles were used to obtain nanocomposites. It is expected that further separation of nanoparticles may occur during the synthesis of the matrix when forming the polymer chains are intercalated between individual nanotubes in a bundle and between the plates.

The use of shear forces and high energy oscillations for the separation of nanofiller particles and their uniform distribution in the polymer can be seen as a factor of damaging the surfaces of the nanotubes and their length causing shortening. Therefore, based on the experience of Institute of Materials Science and Engineering WUT in studies on polymer nanocomposites with carbon nanotubes, it has been shown, that in case of carbon nanotubes, to avoid significant damage during dispersing, only vibrations of the ultrasound frequency and the high-speed shear mixer were used, while in the case of graphene nanoplatelets suitable was to use ultra-low-power sonic bath. In fact, the effectiveness of dispersion strongly depends on both the method and process time. The usage of ultra-power lower sonic bath is rather effective in order to split the existing agglomerates of expanded graphite nanosheets,

and to distribute the additive in the entire volume of liquid substrate. For this purpose the synthesis with the participation of expanded graphite was prepared, in which the percolation threshold was set at 0.05 wt% in the nanocomposites of PET / EG using ultrasonic bath for 8 h [322]. Additionally, two synthesis have been prepared without using ultrasounds: PET/0.05 wt % of EG (previously it found to be the percolation threshold) and PET/0.075 wt % of EG (above percolation threshold). Both synthesis proved to be non-conductive, when ultrasonic bath was not applied (Fig. 28). The experiment clearly indicates the validity of the use of ultra-low power sonic bath by the time selected experimentally on the basis of own research in the Department of Polymer Materials. The use of ultrasonic waves for 8 h probably resulted in increase the interlayer distance (further exfoliation) and thus led to an even distribution of graphene nanoplatelets in the entire volume of the nanocomposite.

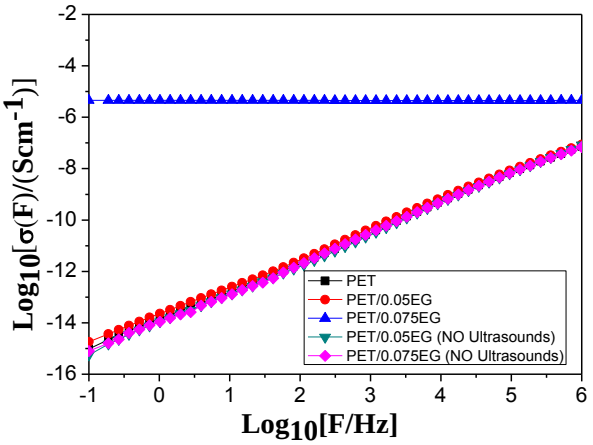

Fig. 28 Alternating current conductivity, σ(F) as a function of frequency (F) for PET/EG nanocomposites with different EG concentrations when ultra-low power sonic bath was applied and when it wasn't.

The above characteristics of the methods of dispersion preparation and presented below the analysis, that does not allow a quantitative assessment of dispersion quality of the carbon nanoparticles in the substrate, gives an overview of the validity of the use of this stage of preparation of the composite, the obtaining of a homogenous dispersion at this stage of the process, is crucial to the structure of obtained nanocomposites.

15. Polymer nanocomposites containing carbon nanotubes

15.1. Morphology of polymer matrices vs. nanofiller

Single-walled carbon nanotubes used in this study were characterized using scanning electron microscopy (SEM) and Raman spectroscopy. The purity of the samples was first characterized using SEM, which provided visual information of the ratio of SWCNTs to carbonaceous impurities. The SEM images of both types of carbon nanotubes are shown in Figure 29 (a and b for Cheaptubes and KNT 95 respectively). In this system, it was presumed that fiber-like areas correspond to bundled SWCNTs, while the other particles and lumps correspond to carbonaceous impurities. It can be clearly seen that SWCNT Cheaptubes are fully covered with carbonaceous impurities. On the other hand, SWCNT KNT 95 possessed

the highest purity, which is visibly seen from SEM analysis and is confirmed by Raman spectroscopy.

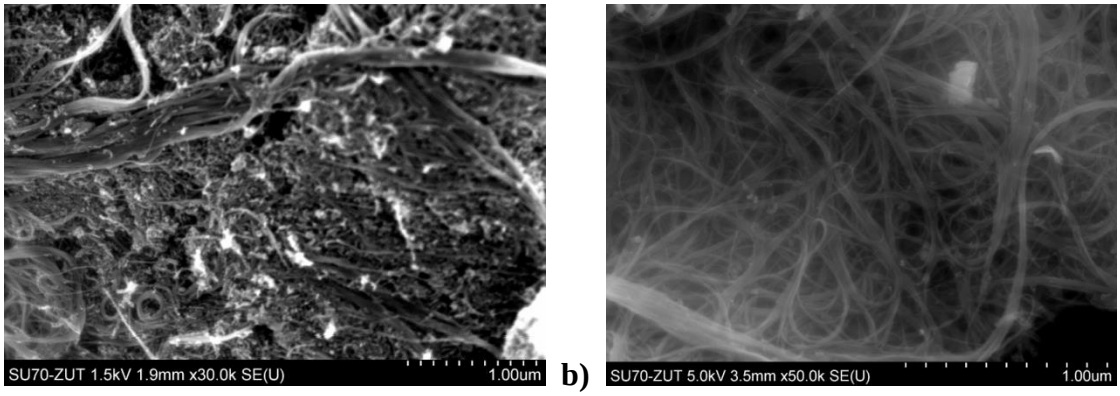

Fig. 29 SEM images of: a) SWCNT Cheaptubes, b) SWCNT KNT 95 (as received).

It is well known that the G-band of SWCNTs shows multipeaks around 1580 cm^{-1}. For purity evaluation using Raman spectroscopy, the G-band peak around 1593 cm^{-1}, which derives from the longitudinal optical (LO) phonons of semiconducting SWCNTs [323], was used for two reasons: first, the G-band intensity is less sensitive to excitation laser energy than the RBM intensity, because of a loose resonance condition due to the large phonon energy. Secondly, a recent theoretical study predicted that there is no significant diameter dependence of the G-band intensity for the LO phonon of semiconducting SWCNTs, while the RBM intensity is more sensitive to the diameter and chirality for SWCNTs with diameter of 0.8-2.0 nm [323]. The overtone of the D-band, the so-called G′-band, was also predicted to depend on the chirality [324]. Thus, the G-band around 1593 cm^{-1} is more appropriate than the other Raman modes for the comparison of purity of SWCNTs with different diameter distributions.

Raman spectra of the samples are presented in Figure 30 a. In the spectra, radial breathing modes (RBMs), the D-band, and the G-band were observed between 100-400 cm^{-1}, 1250-1350 cm^{-1}, and 1500-1600 cm^{-1}, respectively. For comparison purpose, normalized Raman spectra has been presented in Figure 30 b to observe carbonaceous impurities, such as graphitic and/or amorphous carbon particles, that SWCNT Cheaptubes contain in high amount. Because both the SWCNTs and carbonaceous impurities have the same π electron system, the carbonaceous impurities also exhibit a black color and absorb visible light similarly to the SWCNTs. However, their contribution to the G-band Raman intensity is significantly different. Actually, the Raman signal from SWCNTs in a raw soot is about 30 times higher than that of carbonaceous impurities due to a resonance effect. After normalizing the Raman shift the amount of carbonaceous impurities has been visibly seen in SWCNTs Cheaptubes. Thus, it is reasonable to suppose that carbonaceous impurities act as an optical absorber and any observed difference in the G-band intensity can be mainly attributed to a difference in the amount of carbonaceous impurities present. Because the absolute Raman intensity depends on the equipment and the specific measurement method, use of the G-band intensity to measure purity requires a common standard sample that gives a stable, uniform purity. As shown in Figures 29a and 29b the SWCNTs KNT 95 sample had extremely high purity and a highly stable G-band intensity.

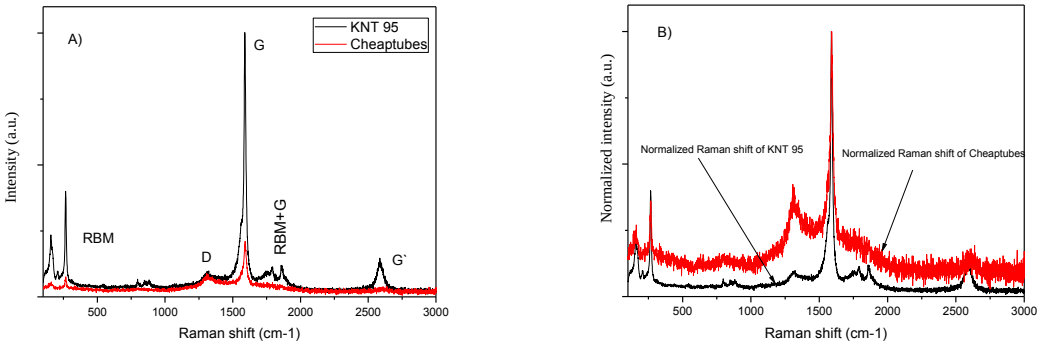

Fig. 30 Raman spectra of SWCNT KNT 95 and SWCNT Cheaptubes (laser excitation 785 nm) and normalized Raman spectra for both types of SWCNT.

Raman and SEM were used for purity evaluation and could be associated with the ratio of SWCNTs and carbonaceous impurities in a sample. These methods complement each other. Thus, it was concluded that it is better to combine Raman and SEM for SWCNT purity evaluation and to compare the results in accordance with their intended use.

As mentioned earlier the natural tendency of carbon nanostructures to agglomerate (due to van der Waals interactions) is an underlying reason of difficulties in preparation of composites based on thermoplastic matrices, which can be characterized by a high degree of homogeneity of the nanophase. Effectiveness of using of the *in situ* polycondensation method, preceded by dispersing the carbon nanotubes in the substrate, can be assessed qualitatively on the basis of an analysis structure using microscopic techniques. By taking into consideration the development of methods for the preparation of *in situ* polymer composites it was assumed that dispersing the carbon nanotubes in one of the substrates with the use of mechanical forces and vibrations of the ultrasonic frequency, and then carrying out the synthesis of the polymer matrix in the presence of the nanoparticles, allow to obtain uniform distribution in the mass, and increasing during the process of the polymer chains will intercalate between bundles of nanofibers, supporting their separation.

Analysis of the PET nanocomposites structure with the addition of single wall nanotubes shows a high degree of dispersion of nanoparticles in the matrix (Fig. 31).

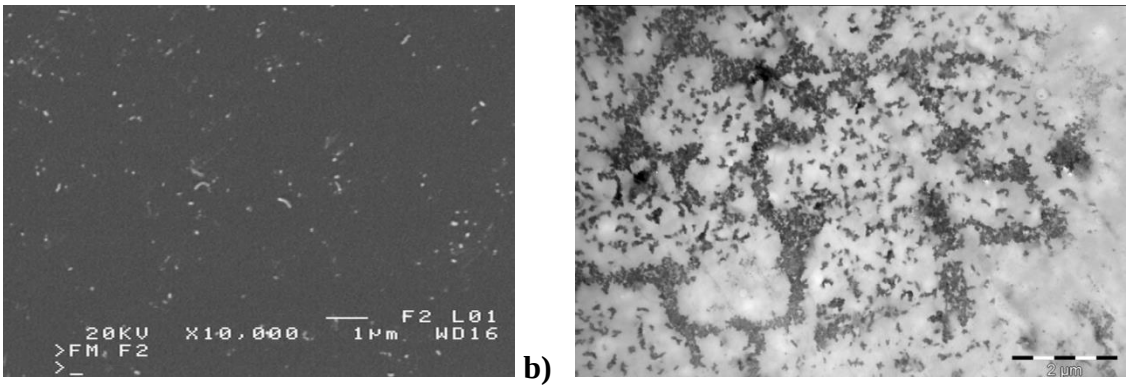

a) **b)**

Fig. 31 SEM (a) and TEM, x20.000 (b) images of PET/0.2 SWCNT.

At the observed fractures uniformly distributed nanoinclusions in the polymer can be distinguished. Further microscope analysis, especially by using a transmission microscope, indicates the presence of various forms of dispersion of carbon nanotubes, although all of the samples showed a crystalline structure. The use of lower magnification allowed to observe a rather homogeneous distribution of nanofiller, which confirms that in the case of poly(ethylene terephthalate) using *in situ* synthesis yield the desired effect, although the nanotubes still probably remain incompletely separated. However, in the thin films studied by TEM microscopy places where SWCNT bundles are arranged in a network are also visible. On SEM micrographs also can be observed the so called nanofibers "pulling" from the matrix even at the length of few micrometers, so that nanotubes appear to lie on the surface of the samples. On the basis of performed microscopic analysis is difficult to assess the degree of adhesion between the two phases of the composite, however, the surfaces of nanotubes forming a network are probably not coated with the polymer, and the degree of "pulling" them from a material suggests very weak interactions polymer – filler. Poor adhesion and the presence of various forms of dispersion, may also be explained by the purity of the carbon nanotubes used, as suggested above mentioned SEM and Raman analysis. The observed micrographs of SWCNT correspond to their quality (mainly purity) and this, in combination with their other properties thereof (e.g., electrical conductivity), should influence the resulting properties of the composite.

Morphology of PTT nanocomposites containing SWCNT was investigated by using SEM and TEM analysis. Figure 32 b shows SEM micrographs of fracture surfaces of PTT nanocomposites with nanotubes. As mentioned above, CNTs often tend to bundle together by van der Waals interaction between the individual nanotubes with high aspect ratio and large surface area and lead to some agglomerations, which prevent efficient load transfer to nanotube. Moreover, most of the nanotubes show pulling out and sliding at the surface of nanocomposite, suggesting a limitation of load transfer to nanotube. Individual nanotubes with some entanglements or bundles of CNTs, apparently pulled out from the matrix during fracturing are observed on the surface. SEM analysis of the fracture surfaces of PTT/SWCNT nanocomposites indicates rather homogenous distribution of carbon nanotubes in the PTT matrix. In the case of prepared composites in the observed TEM micrographs some nanoinclusions can be distinguished that are uniformly distributed in the polymer with small agglomerate. To identify the key mechanism for increasing mechanical properties micrograph analysis was performed using a scanning electron microscope (ULTRA 55 SEM) (Fig. 32 c and d). The images of the cracks visible in the polymer matrix clearly indicate evidence of fiber bridging and even some broken nanotubes were seen. These two SEM micrographs demonstrate the potential of carbon nanotubes to significantly improve the mechanical properties (eg. fatigue performance) of structural polymers that are widely used in engineering systems.

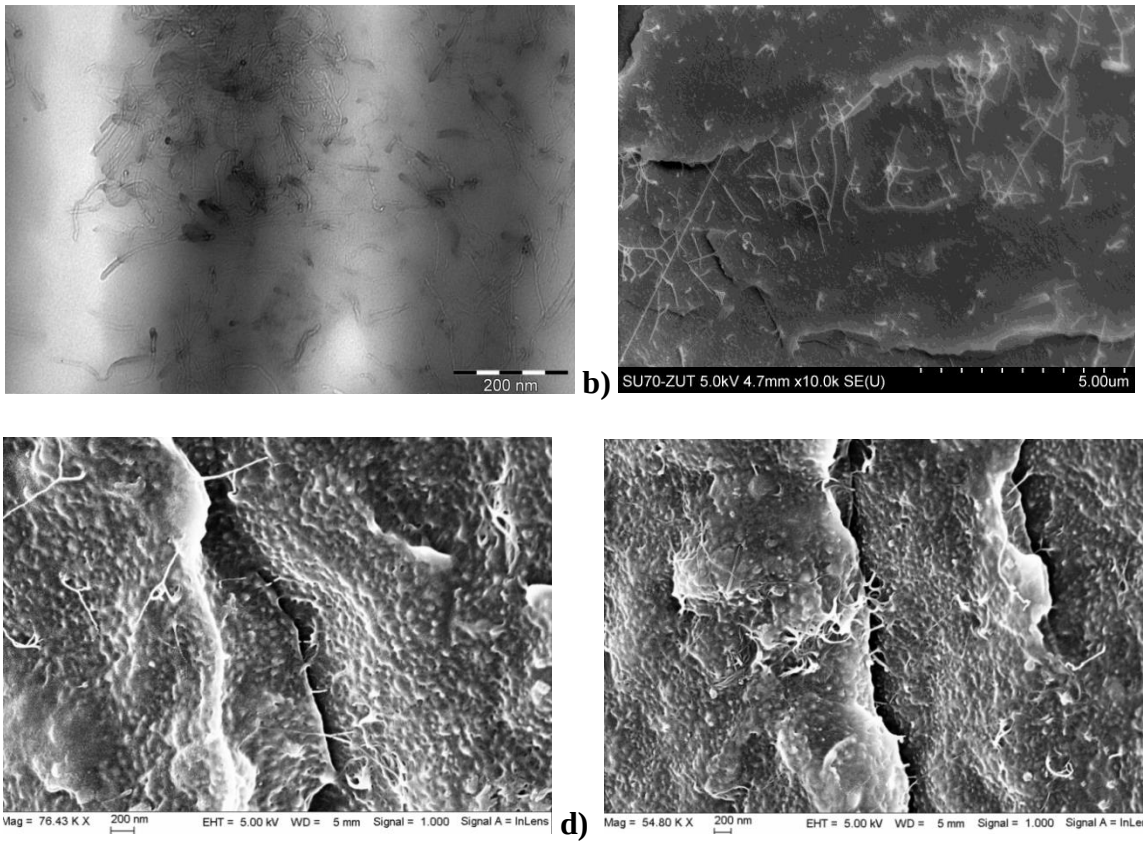

Fig. 32 TEM, x 200.000 (a) and SEM images of PTT/0.3 SWCNT nanocomposites (b). Additionally micrographs c and d from SEM ULTRA 55 was prepared to observe combination of some nanotubes that are bridging the crack and some tubes that are simply pulled out of the matrix.

SEM analysis of the fractures structure of composites based on PTT-PTMO (Fig. 33 a-d), revealed that the distribution of the SWCNT in polymer matrix has a rather high homogeneity. At the observed fractures single nanofibers uniformly distributed in the polymer can be distinguished. Considering the high propensity of the CNT (especially SWNTs) to clump together to form bundles, as mentioned in the theoretical part, the observed effect confirms the efficiency of mechanical mixing in combination with high-frequency vibration in eliminating existing agglomerates. There are no visible agglomerates, only at the highest concentration of nanotubes in the matrix there are locally small aggregates consisting of several entangled nanofibers (Fig 33 c). On the other hand, most of the nanotubes observed on the fracture surface were embedded in a polymer with both ends (Fig. 33 a, d). This suggests that during the preparation of brittle fracture of composite sample appears the "pulling" of the single nanofiber from polymer matrix. However, on micrograph 33 b nanotubes characterized by a distinct thickening are visible, most likely demonstrating the fact that their surface is covered with adsorbed polymer layer, which varies in thickness. In addition, observations of the surface morphology of the nanocomposite PTT-PTMO/0.3 wt % of SWCNT demonstrate a clear influence of nanotubes on crystallization. Sites with visible nanotubes at fracture surface exhibited significantly finer crystalline structure than is the case where the amount of nanotubes was lower. Fig 33 b shows the clear boundary confirming the existence of interactions between the nanofiller particles and the polymer, which had a significant impact on improving the mechanical properties of nanocomposites (an increase of Young's modulus of 40 MPa) (Table 19, page 91).

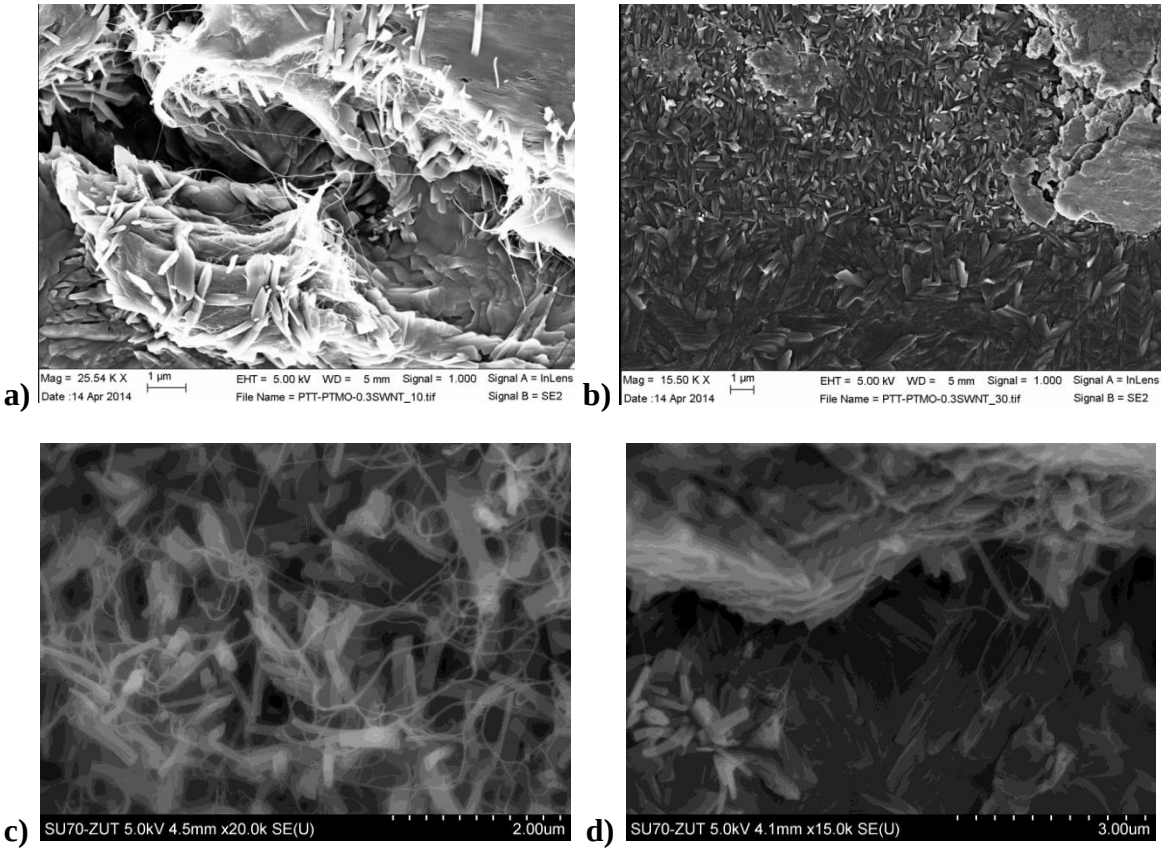

Fig. 33 SEM of PTT-PTMO/0.3 SWCNT nanocomposite.

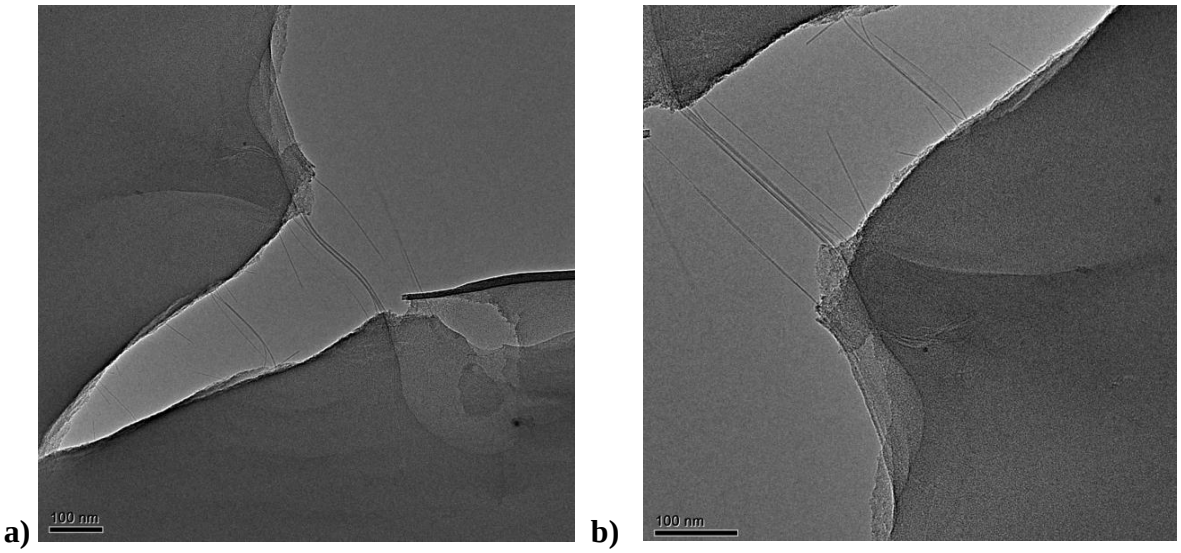

Fig. 34 TEM micrographs of PTT-PTMO/0.3 SWCNT nanocomposites.

The observations made by SEM analysis were supported by TEM, that provides information about the dispersion state of carbon nanotubes but also it helps to explain the improvement in mechanical properties of PTT-PTMO/SWCNTs nanocomposites. TEM images of the film section of the material showing SWCNTs protruding from the polymer matrix suggestive of strong adhesion between the nanotubes and the polymer matrix. However, some agglomerates of CNTs were also seen (Fig. 34 a). TEM micrographs show the

CNTs aligned perpendicular to the crack bridging the crack. Some broken and pulled out of matrix carbon nanotubes were also easily visible (Fig. 34 b).

On the basis of microscopic analysis, presented for the polyesters filled with carbon nanotubes, it can be concluded that the developed method of preparing composites containing carbon nanotubes yielding the desired results, i.e. composite materials are characterized by a high homogeneity of the nanoinclusions distribution regardless of the nanofiller structure (the presence of entanglements and agglomerates) before the process. This was confirmed both in the case of nanotubes with higher and lower purity. Providing a suitable process for the dispersion of nanoparticles in the substrate which is followed by a condensation polymerization process, it is possible to obtain materials in which a dispersed phase size of the precipitates is less than 100 nm. On this basis, materials prepared by *in situ* synthesis can be classified as polymer nanocomposites, and their physical properties due to the presence of carbon nanotubes are the subject of discussion in the following sections of PhD dissertation. The effectiveness of this method, although high, has a high relation with the chemical structure of the polymer, as evidenced by the higher degree of dispersion in PTT and slightly lower in the case of PET. Determination of this relationship, however, requires further study. This method is relatively simple to apply on an industrial scale and provides a wide choice of options in terms of both the polymer and the nanofiller.

15.2. Phase structure and percolation model confirmation

The use of carbon nanotubes to modify the electrical properties of polymers has attracted a considerable amount of research interest. Most polymeric materials are non-conductive and through dispersing a conductive reinforcement within the matrix, it is possible to form a conductive composite material. When a certain volume fraction of conductive materials is added to the polymer, electrical spanning clusters form and there is a drastic increase in the bulk electrical conductivity. This phenomenon is known as electrical percolation. The percolation threshold, the volume fraction at which the drastic increase in conductivity is observed, is sensitive to the reinforcement geometry of the conductive particle. The large aspect ratio and small size of carbon nanotubes can result in exceptionally low electrical percolation thresholds for nanotube/polymer composites. Larger aspect ratios result in a higher statistical probability of forming a conductive pathway within the matrix. As a consequence, the electrical properties of the polymer can be changed drastically without substantially changing the mechanical properties. The electrical properties of the nanocomposite are sensitive to the length of CNTs, dispersion and functional groups attached to the nanotubes.

In this dissertation thesis the effect of the addition of carbon nanotubes to the polyester PET and PTT and PTT-PTMO elastomer on their electrical conductivity has been discussed. Interesting from the point of view of their impact on the electrical conductivity seems to be the introduction of SWCNT to thermoplastic elastomer based on PTT (PTT-PTMO) to observe the difference in creating percolation paths in thermoplastic polyester (PTT) and in multiblock copolymer (PTT-PTMO), where PTT was a rigid segment.

Unfilled poly (ethylene terephthalate) has a conductivity of the order of $8.6 \cdot 10^{-17}$ S/cm, and a poly (trimethylene terephthalate) $1.4 \cdot 10^{-15}$ S/cm, so they are excellent insulators.

The use of *in situ* polycondensation method allows to obtain conductive nanocomposites filled with a relatively low loading (less than 0.5 wt %), which has been confirmed for the three types of polymer matrices. According to the classical theory of electrical percolation for composites insulator - metal showing, at a certain critical concentration of conductive phase ρ_c, the behavior close to the percolation threshold, there are the following relationships defined by Bergman and Imry [325]:

$$\sigma(F,\rho_c) \approx F^s \quad (4)$$

$$\varepsilon'(F,\rho_c) \approx F^{-y} \quad (5)$$

where: σ – electrical conductivity, S/cm; F – frequency, Hz; ε' – dielectric constant , s and y – exponents. Close to the percolation threshold the sum of the exponents is equal to unity. The dependence of conductivity and dielectric constant of the frequency is related to, inter alia, the phenomenon of polarization between the conductive beams in the studied phase of a mixture. [326]. For the composite PET/SWCNT with a concentration of less than 0.2 % the dependence of the conductivity σ in the entire range of the frequency F is a linear function and indicates on the non-conductive the nature of these systems (Fig. 35 a). However, in the case nanocomposites with nanofiller content of 0.4 wt % at low frequency, σ does not exhibit the above presented relationship up to a certain critical frequency value (0.1 Hz). The occurrence of plateau is characteristic for insulator - conductor transition at a threshold concentration of the conductive phase, in other words - the electrical percolation threshold. Above this concentration the electrical properties of the composite are dominated by the conductive paths existing in material, formed by the carbon nanotubes. The data shows that for the composite PET / SWCNT the threshold concentration of the conductive phase for which the electrical percolation threshold is observed is 0.4 wt %. From studies conducted on nanocomposites with SWCNT have been observed to have lower percolation threshold [51] [327] as compared to results obtained for PET/SWCNT. Electrical properties of the nanocomposites have been found to be strongly dependent on processing conditions (sintering temperature, sintering pressure, and dry mixing duration). Alignment of the nanotubes during the manufacturing process of nanocomposites has a significant effect on the electrical properties of the nanocomposite. From the SEM and Raman analysis the low purity of SWCNT Cheaptubes has been observed. Lots of impurities observed in SWCNT while added into polymer nanocomposite, affected the electrical conductivity, and low percolation threshold was obtained, whereas the greater improvement and much lower percolation threshold was expected.

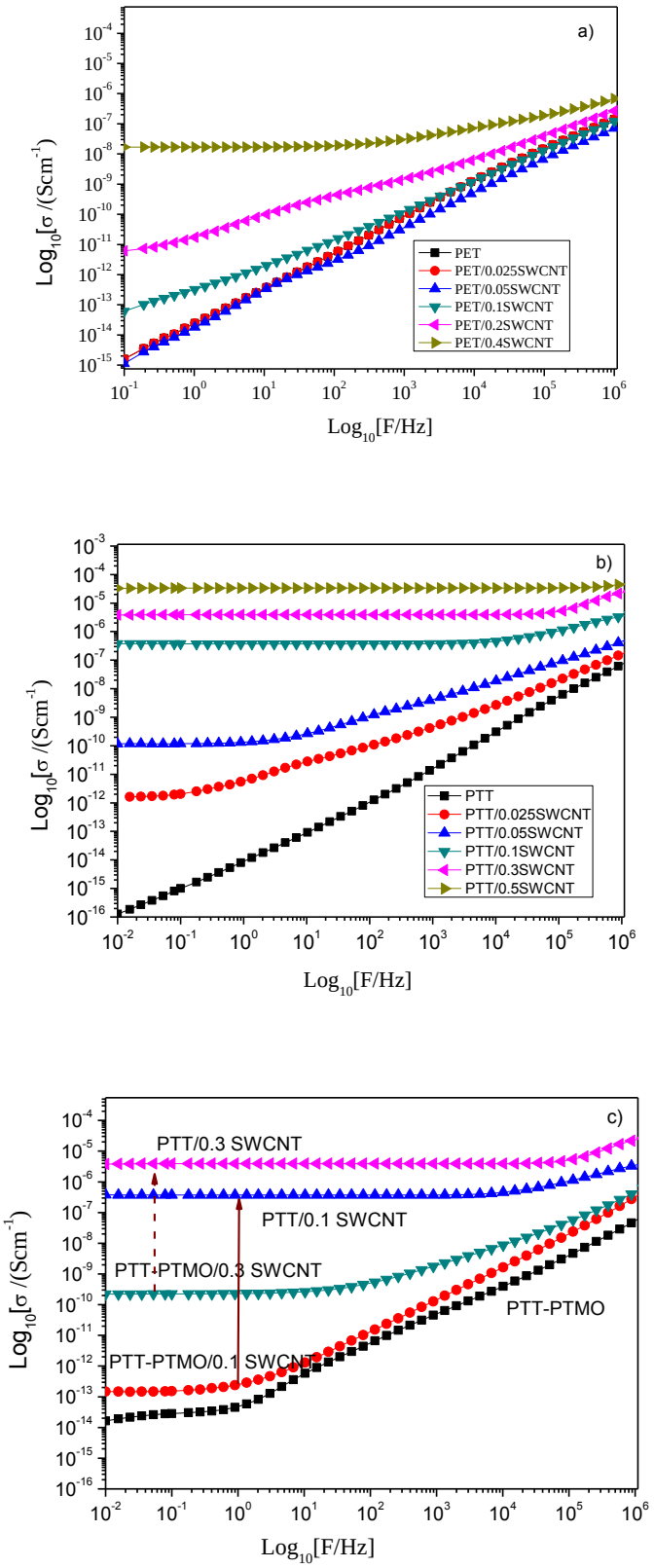

Fig. 35 Alternating current conductivity, σ(F) as a function of frequency (F) for a) PET/SWCNT nanocomposites, b) PTT/SWCNT nanocomposites and c) PTT-PTMO/SWCNT nanocomposites with different SWCNT concentrations. Presented here conductivity measurements for PET and PTT based composites were done for amorphous films.

The crystallization behaviour of polymers i.e. degree of crystallinity, crystallization temperature, size and shape of crystallites is a combined result of processing methods and conditions. Any change in this behavior will affect the electrical conductivity, mechanical and thermal properties, and even barrier properties (since permeation rates of polymer films strongly depends on crystallinity) of prepared composites. In case of electrically conductive nanoreinforecements, crystallization can alter the electrical conductivity and percolation threshold. Low percolation threshold is desirable in order to obtain low cost, good processability and satisfactory mechanical performance. There have been already published many studies on how various factors affect the electrical conductivity and percolation threshold [328] [329] [330]. Therefore, the electrical conductivity measurements of polymer nanocomposites based on PET and PTT were performed on amorphous samples. The influence of crystallinity on electrical conductivity and percolation threshold has been analyzed on the example of PET/EG nanocomposites, which will be later described in Chapter 6.1. Since for PTT-PTMO block copolymer it is impossible to prepare this amorphous film, the electrical conductivity measurements were examined for semicrystalline samples with a crystalline (PTT) phase content of about 16.9-18.0 % (according to DSC measurements, Table 11).

The results of electrical conductivity measurements of poly(trimethylene terephthalate) (Fig. 35 b) filled with high purity SWCNT purchased from Graphene Co., reported that for SWCNT/PTT nanocomposites percolation thresholds was below 0.1 wt% CNTs. To compare the electrical percolation threshold for MWCNT/PTT composites was found at an loading between 0.3 and 0.4 wt % of MWCNT [15]. A significant change in the properties of conductive composites based on polyesters is probably related to the previously described morphology, in particular the creation of the entangled nanotubes spatial structures, which play the role of the above-mentioned conductive paths. This effect is especially interesting in the context of further applications of the composite materials, even a very low content of SWCNT (0.05 wt%), increases the ability of PTT to conduct electrical current by six orders of magnitude and is sufficient to prevent the accumulation of electrostatic charge on the surface of the sample. This property can be used in the design and implementation of enclosures for electronic devices [326]. Whereas at the content of nanotubes at 0.3 wt %, composite has a conductivity of $1.6 \cdot 10^{-5}$ S/cm and is an excellent material for the manufacture of conductive polymer fibers. Low percolation thresholds of PTT/SWCNT nanocomposite indicate a very good dispersion of CNTs in the matrix while still preserving the carbon nanotube aspect ratio.

Studies of electrical conductivity have shown that the PTT-PTMO/SWCNT composites showed significantly lower electrical conductivity than when the polymer matrix was neat PTT (Fig. 35c). However unlike PTT, PTT-PTMO block copolymers show at low frequencies characteristic conducting behavior (the presence of a frequency independent component, $\sigma_{dc)}$ associated with the presence of PTMO. Such behavior may be due to ionic conductivity [331]. Even with the smallest loading of nanoparticles (0.1 wt % of SWCNT) a slight increase in conductivity for thermoplastic elastomers was observed, similarly as in case of 0.3 wt % of SWCNT. Comparing the nanocomposites with the same content of nanofiller (PTT/0.3 and PTT-PTMO/0.3) a marked decline of σ by about 4 orders of magnitude is observed, but on the other hand, the copolymer itself has higher conductivity than neat PTT.

A slight increase in electrical conductivity for prepared nanocomposites is due to the fact that thin films based on PTT-PTMO were semicrystalline with crystalline phase content of about 16.9 % (determined from DSC), whereas the values of electrical conductivity in case of PTT based composites were measured for thin amorphous films. However, in [322] for PET/EG nanocomposites it was proved that semicrystalline PET/EG nanocomposites have lower conductivity (about 2 orders of magnitude) if compared to amorphous samples, but the percolation threshold remained the same. Therefore taking into account the thermoplastic and elastic behavior of PTT-PTMO block copolymers arising from their multiphase structure, which is a consequence of the chemical nature and incompatibility of the two types of the contributing segments rigid and flexible built into polymer chains, the effect associated with this behavior on electrical conductivity might be observed. Although in each case the nanotubes were dispersed in the substrate forming a different phase, (DMT + PDO) forming the polyester hard phase, while PTMO the polyether soft phase, during the synthesis of the copolymer, occurred intermixing substrates with each other, and the phase separation in the polymer could have affected the location and separation of nanoparticles in the matrix.

15.3. Influence of CNT structure and their contents on physical properties of polymer nanocomposites

The obtained nanocomposites were characterized determining the intrinsic viscosity, density, weight degree of crystallinity determined from the density measurement (for PET, PTT), melt viscosity as a function of frequency (for PTT/CNT and PTT-PTMO/CNT), examining the effect of the presence of a CNT on their thermal stability in air and argon, and mechanical properties.

For PET based composites can be observed the initially increase in intrinsic viscosity [η] with an increase of CNT concentration (up to 0.05 wt %) in the composite, as compared with the value obtained without filling the polymer (Table 8), however the content of 0.1 wt% showed a gradual decline in the value of intrinsic viscosity, nanocomposites wherein with the highest concentration of carbon nanotubes were characterized by a significant decrease [η], compared to pure PET, which indicates that the resulting composites have lower molecular weights. Though lots of impurities on surface of SWCNTs, the interfacial bonding with the PET matrix supposed to be high enough to affect the intrinsic viscosity and molecular weight. However, it seems that these interactions are not strong enough to disperse the SWCNT as individual particles into the PET matrix, especially with higher loading of nanoparticles. Therefore, some fluctuations of intrinsic viscosity and molecular weight with the increasing content of carbon nanotubes were observed. The presence of CNT in the polymer melt hindered its flow and the introduction of a concentration higher than 0.5 wt % was not possible using the method of *in situ* due to the fact that the polymer extrusion from the reactor was impossible. This is the main problem in all nanocomposites, where nanoparticles, as a result of their high surface area, have substantially increased surface tension and thus easily create agglomerates. For all the nano-reinforcement contents considered, the experimental density measured for samples prepared by injection moulding is higher than the density of neat poly(ethylene terephthalate). This means that the added SWCNT partially occupies the free volume of the PET network, concluding that a densification of the polymer, determined

by an increase of its bulk density, is mainly associated to a loss in the free volume. The increase in weight degree of crystallinity determined from density measurement, especially in case of PET/0.4 wt % SWCNT, was four times higher than in pure PET. This increment of density could be also explained by the fact that the nanotubes can play a role of nucleation agent.

Table 8 Physical properties of PET/SWCNT composites

Sample	[η] dl/g	M_v x 10^4 g/mol	d g/cm^3	Xc_w (%)
PET	0.553	2.21	1.337	10.6
PET/0.025 SWCNT	0.606	2.51	1.342	17.5
PET/0.05 SWCNT	0.611	2.54	1.354	35.7
PET/0.1 SWCNT	0.571	2.31	1.348	26.8
PET/0.2 SWCNT	0.512	1.99	1.359	42.1
PET/0.4 SWCNT	0.517	2.02	1.361	45.7

M_v - viscosity average molecular weight; d-denstity measured at 23°C; Xc_w weight degree of crystallinity estimated from density measurement

Considering the known strong dependence of the PET crystallization rate on its molecular weight, an evaluation of the effect of SWCNTs on PET crystallization requires comparison at similar molecular weights. Since the fluctuations in intrinsic viscosities (or molecular weights) have been observed, also on the crystallization characteristics of *in situ* prepared PET/SWCNT nanocomposite samples similar effect has been suspected. The crystallization temperatures (T_c), the apparent melting temperatures (T_m) and the corresponding enthalpies (ΔH_c and ΔH_m) are also reported in Table 9. Fig. 36 shows the DSC cooling and heating (from the 2nd heating) scans of PET/SWCNT nanocomposite samples. During cooling from the melt, the SWCNT containing samples show crystallization exotherms earlier than neat PET, as also seen from the corresponding T_c values indicated in Table 9. It is found that the nanocomposite sample containing SWCNTs at a concentration as low as 0.05 wt% crystallizes 6 °C earlier than neat PET. The T_c values continue to increase with increasing SWCNT concentration. In other words, there is a saturation of the nucleant effect at low SWCNT concentrations, resulting in diminishing dependence on the increasing SWCNT induced nucleation, possibly because of the large surface area and good dispersion of SWNTs. The melting temperature and enthalpies of PET stay unaffected by SWCNTs (Fig. 36 b).

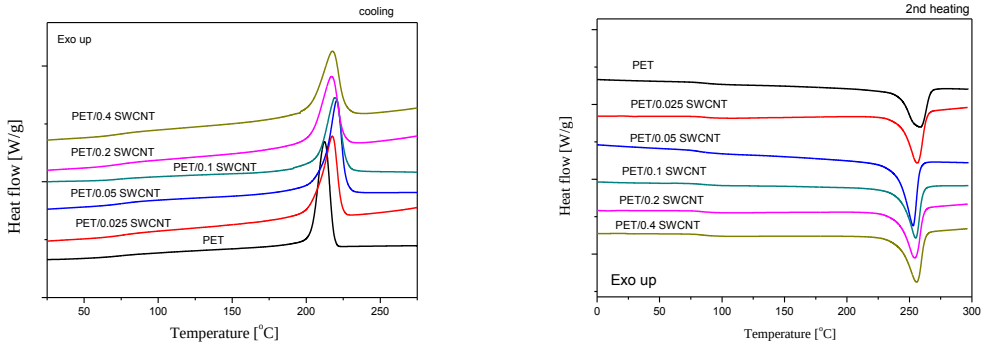

Fig. 36 DSC thermograms for PET and PET/SWCNT nanocomposites during the cooling and 2nd heating.

Table 9 Thermal properties of neat PET and PTT/SWCNT nanocomposites determined by DSC

Symbol	T_g °C	T_m °C	ΔHm J/g	T_c °C	ΔHc J/g	X_c %
PET	85	257	47.0	214	46.9	33.5
PET/0.025 SWCNT	83	253	52.7	217	52.7	37.6
PET/0.05 SWCNT	83	252	53.5	220	53.2	38.0
PET/0.1 SWCNT	84	255	47.1	219	47.0	33.6
PET/0.2 SWCNT	80	254	51.4	221	51.4	36.7
PET/0.4 SWCNT	80	255	50.8	222	51.0	36.4

T_g - glass transition temperature;-T_m - melting temperature; T_c - crystallization temperature ΔH_m, ΔH_c - enthalpy of melting and crystallization; x_c - mass fraction of crystallinity determined from DSC

The intrinsic viscosity measurements for PTT-based composites showed that the obtained composites have comparable values of molecular weights (38 500-39 600 g/mol) to neat PTT (38 400 g/mol, Table 10). This result demonstrates that the interconnected or network-like structures can be formed in PTT nanocomposites via the nanotube–nanotube or polymer–nanotube interactions in the presence of CNT, resulting in receiving PTT nanocomposites with enhanced properties. The addition of carbon nanotubes affected the density of the obtained nanocomposites. Density was determined for samples prepared by injection moulding. A significant increase in the weight degree of crystallinity determined from density measurement has been observed. The greatest impact was observed at the lowest (0.025 wt %) and the highest (0.5 wt %). In the first case it can be explained with the uniform distribution of nanotubes forming crystallization agents, the growth of which is not hindered in any manner. On the other hand, the increase in the degree of crystallinity along with the increasing content of nanotubes is due to the higher bulk density of CNT relative to the density of neat PTT of neat PTT. SWCNTs might also play a role of crystallization agents, which was also observed in case of PET based nanocomposites. Observations on the effect of carbon nanotubes on the structure of PTT were extended by using DSC.

Table 10 Physical properties of PTT/SWCNT KNT 95 nanocomposites

Sample	[η] dl/g	M_v x 10^4 g/mol	d, 23°C g/cm^3	Xc_w (%)
PTT	0.781	3.84	1.323	19.8
PTT/0.025 SWCNT	0.786	3.88	1.339	32.2
PTT/0.05 SWCNT	0.798	3.96	1.329	24.6
PTT/0.1 SWCNT	0.784	3.85	1.324	20.6
PTT/0.3 SWCNT	0.795	3.94	1.329	24.6
PTT/0.5 SWCNT	0.785	3.87	1.337	30.6

M_v viscosity average molar weight; d – density ; Xc_w weight degree of crystallinity estimated from density measurement

The effect of the presence of SWCNT in PTT matrix on the melting and crystallization processes was studied by DSC. Table 11 summarizes data obtained from heating and cooling DSC scans for PTT and PTT/SWCNTs nanocomposites which are presented in Figure 37. PTT/SWCNTs nanocomposites exhibit a negligible increase (1 °C) in the glass transition compared to neat PTT. Introduction of CNTs can separate the long polymer chain into shorter cooperatively rearranging (CRR) segments [332]. The shift of T_g toward higher temperatures can be a result of the lower mobility of these shorter CRR segments. Recently, for semicrystalline polymers such PTT, PET, PEEK [332] [333] [334], a three phase model consisting of crystalline, mobile amorphous phase (MAP) and rigid amorphous phase (RAP) was used to describe the structural formation of PTT at various conditions. The RAP exists at the interface of crystal and amorphous phase as a result of the immobilization of a polymer chain due to the crystal. In semicrystalline nanocomposites, the RAP fraction sometimes exists at the surface of nanofillers in the polymer nanocomposites material. Here, the melting temperature and degree of crystallinity of the PTT/SWCNTs nanocomposites (Table 11) were not significantly affected by the presence on the SWCNTs. The degree of crystallinity of nanocomposites increase very slightly around 1.4–3 %. Nanocomposites have narrower crystallization peaks than those of neat PTT, indicating the nucleation effect of the CNTs for the PTT matrix. In PTT/SWCNTs nanocomposites the crystallization peak temperature (T_c) increase by about 13-20 °C. The addition of nanofiller in polymer composites changes the thermal properties of the materials due to the formation of interfacial connections between the filler surfaces and polymer. The connections, which may be physical adsorption or chemical bonding, or a combination of both, restrict the mobility of the polymer chains. Here, the introduced high-purity SWCNT into PTT matrix are effective nucleating agent, giving similar effect as in case previously described PET/SWCNT nanocomposites. These can be a result of their high aspect ratio or their strong interactions with PTT chains. Comparison of the results obtained for PET and those studied here for PTT nanocomposites prepared by *in situ* polymerization seems to indicate that the preparation method in addition to the type of carbon nanotube can affect the crystallization behavior of polyesters.

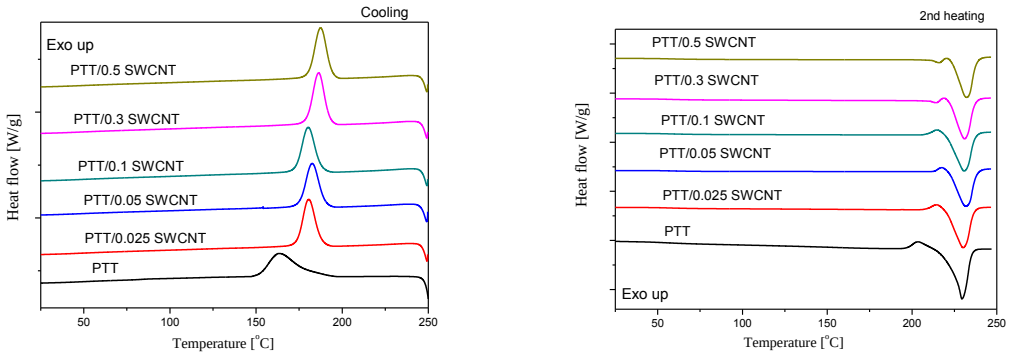

Fig. 37 DSC thermograms for PTT and PTT/SWCNT nanocomposites during the cooling and 2nd heating.

Table 11 Thermal properties of neat PTT and PTT/SWCNT nanocomposites determined by DSC

Symbol	T_g °C	T_m °C	ΔH_m J/g	T_c °C	ΔH_c J/g	X_c %
PTT	53	231	45.8	167	46.2	31.4
PTT/0.025 SWCNT	53	230	47.9	180	47.1	32.8
PTT/0.05 SWCNT	53	232	48.2	183	47.9	33.0
PTT/0.1 SWCNT	53	231	48.4	180	48.7	33.2
PTT/0.3 SWCNT	54	231	51.3	186	50.7	35.1
PTT/0.5 SWCNT	54	232	50.2	187	49.5	34.4

T_g - glass transition temperature;-T_m - melting temperature; T_c - crystallization temperature; ΔH_m, ΔH_c - enthalpy of melting and crystallization; x_c - mass fraction of crystallinity determined from DSC.

Multiblock copoly(ether-esters) (PEE) included in the group of thermoplastic elastomers, characterized by functional properties similar to vulcanized rubber, and a typical method for processing thermoplastics. These types of copolymers have the ability to phase micro- and nanoseparation and reproducible processing conditions, thereby obtaining a shape-memory properties and elastic recovery after deformation. Their specific characteristics are the result of the domain structure in a condensed state which consists of two phases: soft and hard. The amorphous phase is a homogenous mixture of PTMO-T with PTT segments that have not crystallize. Hard phase is formed by the crystallization of rigid segments and has a high melting point. In order to investigate the effect of CNTs on the properties and structure of the block copolymer a series composites based on PTT-PTMO was synthesized, for which the ratio of rigid PTT segments to the soft PTMO segments was 50:50 wt %, for comparison with PTT based nanocomposites. Both series of nanocomposites contained high purity nanotubes SWCNT KNT 95.

Table 12 summarizes the physical properties of the synthesized composites. The presence of nanotubes in the melt polymer hinders its flow (measurements using ARES rheometer shown below, Fig. 39 a) on the other hand, inherent viscosity determination of nanocomposites showed a comparable values to neat PTT-PTMO block copolymer suggesting

that molecular weight of copolymer in obtained nanocomposites are also comparable. The introduction of carbon nanotubes to the reaction mixture increased the viscosity from the beginning of the synthesis, however, the growth was so low that undetectable to the stirrer. As a result, the torque value by which the course of the synthesis was monitored at various stages of the process was the same as for the synthesis of both unfilled polymer and composite. This meant that polymerizing at the same conditions and finishing it with the same stirrer torque, the materials could be obtained with comparable molecular weight values. However, the carried out melt viscosity analysis with the selected composites showed that they have a higher melt viscosity than the polymer without filler (discussed in more details in the section on the influence on the rheological properties of the nanotubes, pages 82-83). A slight increase in the density of the obtained nanocomposites shows that the presence of nanoparticles in the polymer accelerates the formation of the crystalline phase, as confirmed by DSC studies.

Table 12 Physical properties of PTT-PTMO/SWCNT nanocomposites

Sample	SWCNT wt %	[η] dl/g	d g/cm^3
PTT-PTMO	0	1.30	1.172
PTT-PTMO/0.1 SWCNT	0.1	1.33^f	1.181
PTT-PTMO/0.3 SWCNT	0.3	1.34^f	1.176

[η] - intrinsic viscosity, f-measured after filtration of SWCNTs; d – density at 23 ^{o}C

In the multiblock ether-ester copolymers as a result of intermolecular interactions occurs phase separation. The consequence of this is that the resulting material has two characteristic temperatures: T_{g1} – corresponding to the glass transition temperature of amorphous PTMO-rich phase, and T_m – corresponding to the melting of the PTT crystalline phase. Figure 38 shows DSC thermograms for series of PTT-PTMO/SWCNT composites, the results for all composites are summarized in Table 13. The addition of single-wall carbon nanotubes do not affect the values of T_{g1}. In contrast, slight increase in T_m was observed in the case of the composite with 0.1 wt % content of SWCNT. However, due to the very low increase, we can say that the difference was within the margin of measurement error. However, their presence in the polymer affects the shift effects associated with crystallization (Fig. 38 a). This shift towards higher temperatures of 29-31 °C is significant and relevant to the processing of these materials. While the presence of nanoparticles in the polymer accelerates the formation of the crystalline phase, it does not significantly increase its content, which can be inferred from the melting enthalpy ΔH_m and designated on the basis of the degree of crystallinity of the tested composites. It proves that CNTs present in the melt as solid particles only promote nucleation. Observed, for the prepared composites based on PTT-PTMO, the elongation and reduction of the crystallization peak width compared with the thermogram of the unfilled copolymer, can provide a greater diversity in terms of crystallite size and generally rather their fine grain.

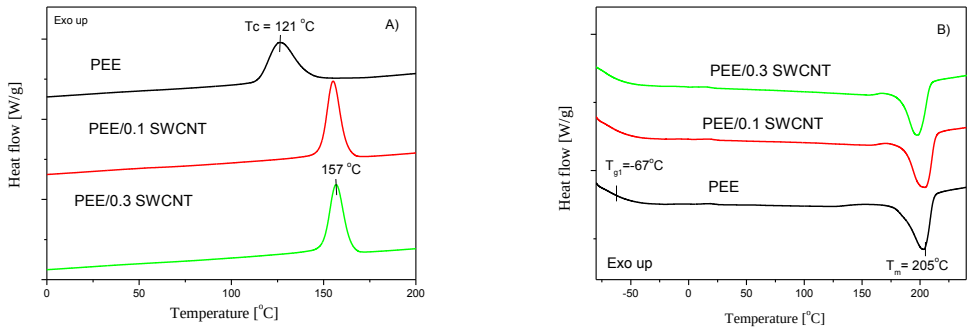

Fig. 38 DSC thermograms for PEE and PEE/SWCNT nanocomposites during the cooling (a) and 2nd heating (b).

Table 13 Thermal properties of neat PTT-PTMO and PTT-PTMO/SWCNT nanocomposites determined by DSC

Sample	T_{g1} °C	T_m °C	ΔH_m J/g	T_c °C	ΔH_c J/g	x_c %
PTT-PTMO	-67	205	25.8	126	26.2	17.7
PTT-PTMO/0.1 SWCNT	-67	205	26.3	155	27.2	18.0
PTT-PTMO/0.3 SWCNT	-67	204	24.7	157	25.7	17.4

T_{g1} - glass transition temperature of soft phase; T_m - melting temperature of polyester crystalline phase; T_c - crystallization temperature of polyester crystalline phase; ΔH_m, ΔH_c - enthalpy of melting and crystallization of polyester crystals, respectively; x_c - mass fraction of crystallinity.

Analysis of the effect of the addition of carbon nanotubes on the physical change in studied/obtained composites allows to formulate several conclusions, common to the all investigated materials. Namely, the presence of nanoparticles in the polymer melt accelerates the crystallization process and it is important, if refers it to the very small range of concentration and temperature shift changes of the matrix is not proportional to the concentration of nanofillers, i.e., no significant differences were observed for the following concentrations, even if the difference between them is multiple. Analysing the impact of CNTs on the increase in the amount of crystalline phase should also be remembered that investigated nanocomposites had comparable molecular weights to homopolymers, which affects the mobility of macromolecules and their alignment in the lamellae. Thus, in addition to the interactions of the nanoparticles, increase of crystallinity in the case of composite PET/SWCNT and PTT/SWCNT can also partly be due to this phenomenon. In the case of PTT-PTMO/SWCNT composites no significant effect of the presence of the nanotubes in the matrix on the degree of crystallinity was observed, which was comparable to the degree of elastomer crystallinity without nanofiller.

Influence of CNT loading on rheological properties of PTT and PTT-PTMO nanocomposites

The smaller the particle size of fillers smaller than micrometer, the more effect of Brownian motion of the particles is crucial. It is thought that the Brownian motion of CNT particles results in more outstanding viscoelastic rheological behavior than short fiber with micro-scale size. There are a few reports on rheological behavior of CNTs/polymer composites. Pötschke et al. [335] investigated rheological properties of the CNT/polycarbonate (PC) composites. It was found that viscosity increase of the nanocomposites filled with CNTs was much higher than viscosity changes of polymer composites filled with carbon fibers or CBs. The rheological behavior of aqueous dispersed CNTs was studied by Kinloch et al. [336] under consideration of the interaction between the nanotubes. It was reported that dispersion state of CNTs was highly sensitive to applied strain in the linear viscoelastic region and the storage and loss moduli were independent of frequency. It was shown that viscosity increased to the highest point when fibrous fillers such as carbon fibers were added and to the lowest point when spherical fillers were added. Agglomerates of the fillers caused higher viscosity [337] since the presence of agglomerates leads to higher filler loading. However, Mitchell et al. [110] examined the linear viscoelastic properties of nanocomposites prepared with pristine SWNTs and organically modified SWNTs in polystyrene (PS) matrix. It was found that the nanocomposites filled with functionalized CNTs had better dispersion of the CNTs and showed higher storage modulus and complex viscosity at low frequency.

As it was mentioned before, the rheological properties of polymer nanocomposites with carbon nanotubes depend on several major factors such as: characteristics of the filler loading, aspect ratio and dispersion, polymer molecular weight, and the interfacial interaction between the polymer and filler. It is necessary to understand the effect of CNTs dispersion and their quality (purity, length etc.) on various properties of the CNTs filled composites. Therefore, in this study, two different specimens with SWCNT (KNT 95) based on PTT (thermoplastic polyester) and PTT-PTMO (thermoplastic elastomer, where PTT was the rigid segment) were prepared.

It was observed, that at low frequencies, the fully relaxed polymer chains exhibit the typical Newtonian viscosity behavior (neat PTT and PTT-PTMO) but with the increasing concentration of CNT the low-frequency complex viscosity significantly increases with CNTs content, indicating that the relaxation of polymer chains in the nanocomposites is effectively restrained by the presence of CNT (Fig. 39). The increase in melt viscosity, could be attributed to increased CNT-polymer and CNT–CNT interactions. The researchers postulated that rheological properties are important for controlling material properties and their processing. Similar observations of the rheological behavior of CNT nanocomposites have also been reported using different polymer matrices, including nylon-6 [338], polyethylene [339] and polyester [340]. These results also indicate that using the *in situ* polycondensation method allowed to obtain polyester based nanocomposites displaying conductive properties at a relatively low filling rate (below 0.5 wt %). However, it needs to be noted that this method has certain limitations resulting from the fact that adding more nanotubes than 0.5 wt %

caused polymer viscosity to grow significantly, which made its extrusion from the reactor impossible and can brought about some difficulties in processing.

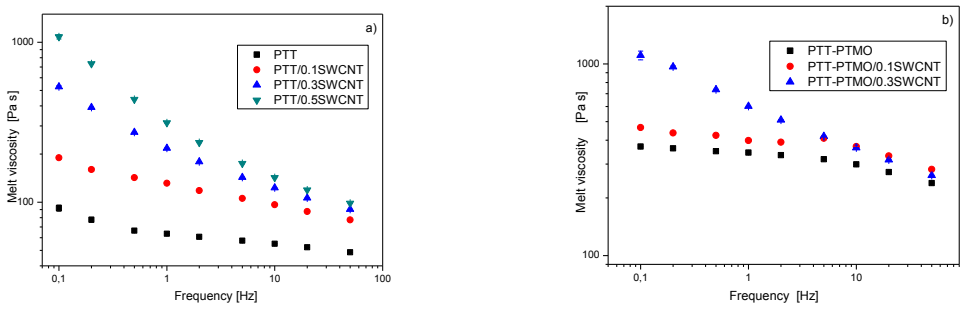

Fig. 39 Melt viscosity versus frequency for a) neat PTT and PTT/SWCNT nanocomposites at 250 °C and b) neat PTT-PTMO copolymer and PTT-PTMO/SWCNT nanocomposites at temperature of 220 °C.

Effect of carbon nanotubes on the thermal stability of the polyester composites (PET, PTT)

For most polymers, the introduction of nanofillers to the polymer matrix increases the thermal stability of both the oxidizing environment and in an atmosphere of inert gas. The effect of the addition of carbon nanotubes on the thermo-oxidative and thermal stability for PET composites containing SWCNT Cheaptubes and for PTT composites containing high purity SWCNT KNT 95 was analyzed, using the method of thermogravimetric analysis. The weight loss (TG) and the DTG (derivative TG) curves under air and argon atmosphere of all studied nanocomposites are shown on Figures 40-41. In Tables 14-15, temperatures corresponding to the 2 (5 for PTT), 20 and 50 % weight loss ($T_{2\%}$, $T_{10\%}$, $T_{50\%}$) and the temperature at maximum of weight loss rate at each step (peak on DTG curve) are presented.

The thermal degradations of aromatic polyesters PET and PTT have been studied extensively under a variety conditions [341]. As it can be seen on TGA curves (Fig. 40-41) the PET and PTT degradation process takes place in two steps in the air and in a single step in argon atmosphere. The study of the thermal decomposition kinetics of polyalkylene terephthalates [342] have shown that the first step of the decomposition of PET and PTT in both argon and air atmospheres is an overlapping of two decomposition processes. The first process is caused by degradation of the polymer chain implying an end group initiation mechanism affected by the molecular weight of polyester. The second degradation process is mainly caused by the thermal degradation of the products formed during the first decomposition process and it is not affected by the molecular weight (end groups) of polyester. Besides the first small weight-loss process (weight loss 2%) in argon for PTT is highly sensitive to molecular weight and the weight loss during this step decreased steadily with increasing molecular weight [343]. The second degradation step in air atmosphere in the temperature range 485-600 °C for PET and 450–600 °C for PTT, is due to the decomposition of some thermostable species formed during first degradation step. These may include decomposition of crosslinked carbonaceous structures and also carbon nanotubes. For nanocomposites, the temperature of the maximum weight loss rate (T_{DTG2}) at post-major/second weight loss step is shifted to higher temperatures.

For the unfilled poly(ethylene terephthalate), subjected to heating in an oxidizing atmosphere, the weight loss begins at 366 °C (Fig. 40, Table 14) and initially proceeds quite quickly, while SWCNT additive shifts the decomposition start temperature of 6 °C towards higher temperatures.

This effect can be determined that is practically within the limits of measurement error. In the case of carbon nanotubes in the PET matrix stabilization effect is greater at the higher concentration of CNTs. With further increase of temperature the degradation of all tested materials is of comparable rate and temperature of approximately 570 °C followed by practically all of their distribution (share of less than 1% ash).

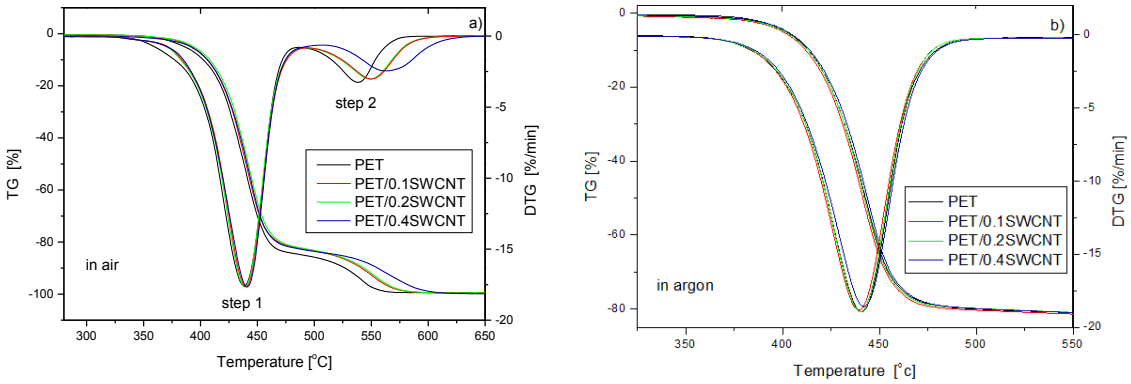

Fig. 40 Weight loss and derivative weight loss versus temperature for the PET/SWCNT nanocomposites in air (a) and in argon (b) at a heating rate of 10°C/min.

Table 14 Temperatures corresponding to 2,10 and 50% weight loss and the temperatures at maximum of weight loss rate for the nanocomposites obtained in air and argon atmosphere

Symbol	$T_{2\%}$. °C	$T_{10\%}$. °C	$T_{50\%}$. °C	T_{DTG1}, °C	T_{DTG2}. °C
Measurement carried out in an oxidizing atmosphere					
PET	366	402	438	440	539
PET/ 0.1 SWCNT	374	405	440	440	545
PET/ 0.2 SWCNT	372	406	440	440	549
PET/ 0.4 SWCNT	364	406	440	442	560
Measurement carried out in argon					
PET	387	413	442	441	-
PET/ 0.1 SWCNT	380	412	441	440	-
PET/ 0.2 SWCNT	383	413	442	441	-
PET/ 0.4 SWCNT	385	414	444	443	-

The presence of SWCNTs does not affect the degradation process of PTT. PTT and its nanocomposites show two degradation steps in air and one in argon atmosphere. The temperatures associated with 5 wt% and 10 wt% weight loss of neat PTT and PTT/0.5 SWCNT were 372 °C and 381 °C in air and 374 °C and 383 °C in argon.

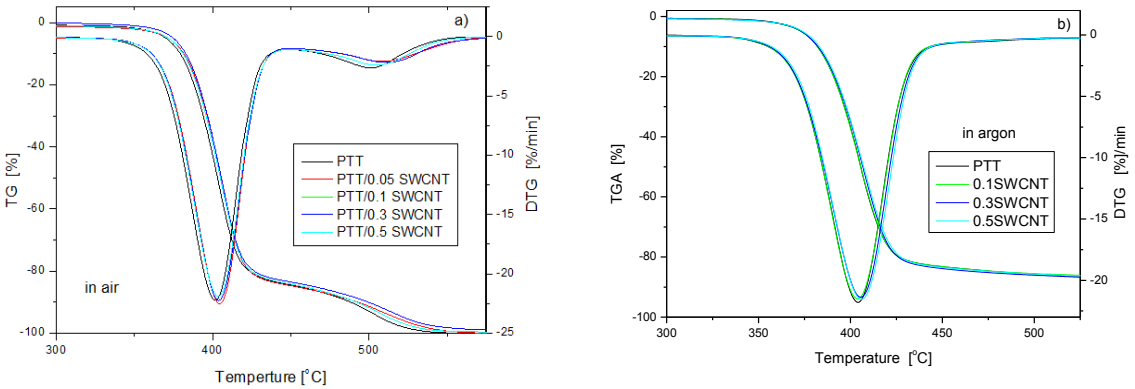

Fig. 41 Weight loss and derivative weight loss versus temperature for the PTT/SWCNT nanocomposites in air (a) and in argon (b) at a heating rate of 10°C/min.

Table 15 Temperatures corresponding to 5 and 10 % weight loss and the temperature at maximum of weight loss rate for the PTT/SWCNT nanocomposites obtained in air and argon atmosphere

Symbol	$T_{5\%}$. °C	$T_{10\%}$. °C	E_a, kJ/mol	T_{DTG1}, °C	T_{DTG2}. °C
Measurement carried out in an oxidizing atmosphere					
PTT	370	379	318.39	401	501
PTT/ 0.05SWCNT	372	382	323.87	404	508
PTT/ 0.1 SWCNT	372	381	314.90	402	500
PTT/ 0.3 SWCNT	374	383	318.01	404	511
PTT/ 0.5SWCNT	372	381	316.60	404	514
Measurement carried out in argon					
PTT	373	382	331.79	404	-
PTT/ 0.1 SWCNT	373	382	334.68	404	-
PTT/ 0.2 SWCNT	373	382	325.58	405	-
PTT/ 0.5 SWCNT	374	383	331.66	406	-

The temperature of maximum rate of weight loss (T_{DTG}, peak on DTG curve) was studied, to determine the thermal stability of the PTT/SWCNT composites in detail. The temperature of maximum rate of weight loss T_{DTG1} of neat PTT in air and in argon were 401 and 404 °C, respectively. In case of nanocomposites with highest concentration of SWCNT

the values of T_{DTG1} in air and argon were comparable to pure polymer. On the other hand, the increase of 13 ^{o}C in T_{DTG2} was observed when the concentration of SWCNT was 0.5 wt %.

Freeman-Carroll method can determine kinetic parameters for the thermal degradation of composites by using only one heating rate (equation 1, page 54). Activation energies determined by this method have not been changed in both air and argon atmosphere. Only PTT/0.05SWCNT showed a slight increase (5 kJ/mol) over the value obtained for neat PTT. The other nanocomposites with higher content of SWCNTs showed even an decrease in activation energy.

In general it can be concluded, that in both polyesters: poly(ethylene terephthalate) and poly(trimetylene terephthalate) addition of SWCNT didn't affect strongly the thermal stability of prepared nanocomposites. The observed small effect of the addition of carbon nanotubes to enhance the heat resistance of the polymer matrix may result from a number of phenomena: changes in the structure of the obtained composites, i.e. changes in the amount and quality of the crystal structure, changes in the polymer chain mobility and distribution of heat in the material. Since in both PTT and PET matrices no explicit effect on the degree of crystallinity and molecular weight was observed, therefore little effect on the thermal stability was obtained.

Effect of carbon nanotubes on the thermal stability of the thermoplastic elastomer nanocomposites (PTT-PTMO)

Introduction into the composite, filler with high thermal conductivity may facilitate heat distribution in the material and thereby improve its heat resistance. Moreover, carbon nanostructures as CNTs have electron affinities similar to those of fullerenes and they are therefore capable of acting as radical scavengers in free radical chain reactions, including polymerisation and the thermo-oxidative degradation of polymers [344]. Introduced into polymer matrix CNTs can be able to exhibit an antioxidant effect in these materials because their radical accepting capacity. The effect of the presence of SWCNT on the thermal and thermo-oxidative decomposition of obtained nanocomposites based on PTT-PTMO block copolymer has been investigated during heating in air and argon atmosphere. The weight loss (TG) and its derivative of weight loss (DTG) curves are shown in Fig. 42.

Analysis of the values of the characteristic temperatures of decomposition, including the temperature of 5 and 10% weight loss and the temperature at the maximum weight loss rate (T_{DTG}) of neat PTT and SWCNTs-filled nanocomposites (Table 16) showed that the presence of carbon nanotubes does not affect the thermal stability in an inert atmosphere (Fig. 42 b), regardless of CNTs content, whereas in oxidizing atmosphere an effect on thermo-oxidative stability of the polymer has been observed.

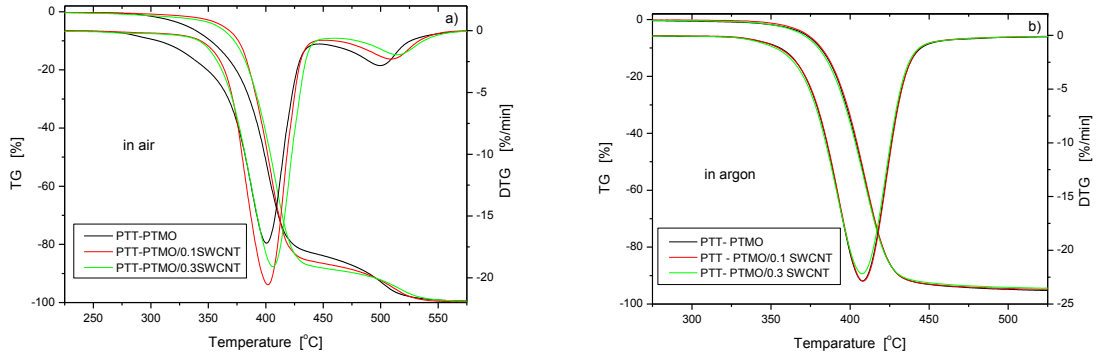

Fig. 42 Weight loss and derivative weight loss versus temperature for the PTT-PTMO/SWCNT nanocomposites in air (a) and in argon (b) at a heating rate of 10°C/min.

As a criterion for assessing the thermo-oxidative stability the temperature of 10% weight loss ($T_{10\%}$) has been assumed. In the initial decomposition stage the stabilizing effect of CNTs is noticeable, which presence shifts the decomposition process toward higher temperatures as compared to unfilled polymer. For composites containing 0.1 wt % of SWCNTs the shift of this temperature by 24 ^{o}C was observed, while at nanofiller content of 0.3 wt % by 20 ^{o}C. The smaller degree of improvement in case of nanocomposite with higher amount of nanoparticles may be due to their inhomogeneous distribution throughout the polymer matrix. In this PhD thesis only the influence of carbonaceous nanoparticles on thermal and thermo-oxidative degradation of PTT-PTMO was analyzed. However, the detailed mechanisms of thermal and thermo-oxidative degradation of copoly(ether-ester) were already published in [345].

Table 16 Temperatures corresponding to 5 and 10% weight loss and the temperature at maximum of weight loss rate for the PTT-PTMO/SWCNT nanocomposites obtained in an air and argon atmosphere

Symbol	$T_{5\%}$. ^{o}C	$T_{10\%}$. ^{o}C	T_{DTG1}, ^{o}C	T_{DTG2}. ^{o}C
Measurement carried out in an oxidizing atmosphere				
PTT-PTMO	331	352	400	499
PTT-PTMO/0.1SWCNT	363	376	402	510
PTT-PTMO/0.3SWCNT	358	372	406	515
Measurement carried out in argon				
PTT-PTMO	371	382	408	-
PTT-PTMO/0.1SWCNT	372	382	408	-
PTT-PTMO/0.3SWCNT	369	380	408	-

Testing the mechanical properties of polyester nanocomposites

Enhancement of mechanical properties is a general tendency for nanocomposites because the nanoadditives act as reinforcement and the degree of reinforcement is dependent on many factors, i.e the dispersion state and, above all, the quality of nanoadditives. For example, the mechanical properties improvement was observed for the polyacronitrile/ CNTs [346] composite fibers containing single wall carbon nanotubes (SWCNTs), double wall carbon nanotubes (DWNCTs) and multiwall carbon nanotubes (MWCNTs). In thermoplastic semicrystalline polymer nanocomposites, the presence of crystallinity in the polymer matrix makes it is difficult to elucidate the influence of nanotubes directly on the mechanical reinforcement mechanisms. In this PhD thesis, PET based composites containing CNTs Cheaptubes and PTT based composited containing SWCNT KNT 95 have been examined.

As it can be seen in Fig. 43 for composites with higher content of CNTs, the nature of stress-strain curve has been changed, from enhanced curve with yield stress for neat PET to curves with no yield stress for nanocomposites with higher content of CNTs characteristic for brittle materials. Yield stress remained at the very same level for all nanocomposites and neat PET. However, in case of brittle nanocomposites i.e. PET with carbon nanotubes' content higher than 0.05 wt % by the concept of σ_y instead of yield stress it will be understood by elastic limit. The observed slight differences in σ_y are within the measurement error. The agglomerates of the CNTs (showed on SEM micrographs in Fig. 31) reduce apparent volume fraction of the polymer matrix. However, as the CNTs loading increases, stress at break of the composites filled with CNTs firstly decreased to 33.9 MPa and then increased with an increasing content of SWCNTs up to ~68 MPa. Simultaneously with the increasing content of nanoparticles, strain at break drastically decreases (almost 100 times in comparison to neat PET). Moreover, an increase in Young's modulus was observed. PET based nanocomposites with 0.4 wt % of SWCNTs exhibited improvement in Young's modulus of 28 %. The cause of the observed improvement in mechanical properties of nanocomposites based on PET might be due to both: a nanoparticles addition themselves and their nucleating behavior (confirmed by density and DSC measurements, Tables 8 and 9).

Table 17 Tensile properties of PET/SWCNTs nanocomposites

Sample	E GPa	σ_y MPa	ε_y %	σ_b MPa	ε_b %
PET	2.08 ±0.14	68.8 ± 0.9	3.6 ± 0.2	38.1 ± 9.7	121.3 ± 12.4
PET/0.025 SWCNT	2.59±0.15	68.9 ± 2.2	3.4 ± 0.3	33.9 ± 1.9	72.4 ± 8.6
PET/0.05 SWCNT	2.57±0.13	68.9± 1.7	3.1 ± 0.5	66.6 ± 4.1	3.6 ± 0.6
PET/0.1 SWCNT	2.52 ±0.14	69.4 ± 1.5	3.2 ± 0.1	68.5 ± 4.3	3.3 ± 0.1
PET/0.2 SWCNT	2.42 ±0.19	70.5± .1.5	3.0 ± 0.1	69.4± .2.3	3.1 ± 0.1
PET/0.4 SWCNT	2.68 ±0.20	67.8 ± 3.3	2.6 ± 0.3	67.8 ± 3.1	2.8 ± 0.3

E – Young's modulus; σ_y - yield strength (elastic limit); ε_y – yield strain, σ_b (indicated with "x" in the figure), ε_b - stress and strain at break respectively

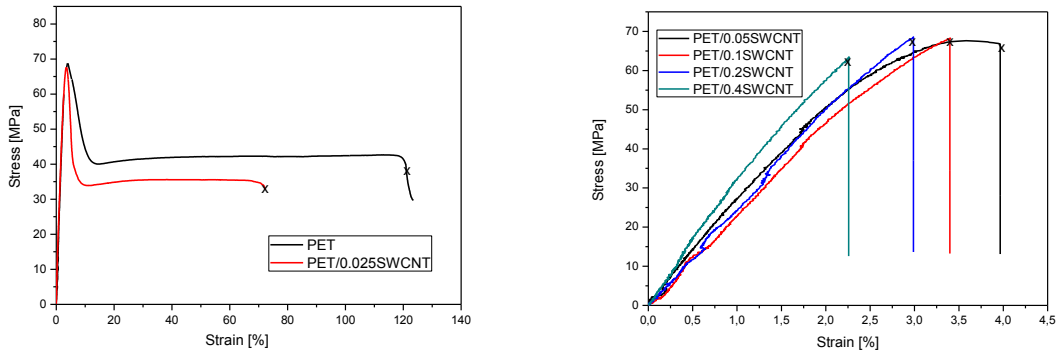

Fig. 43 Representative stress strain curves of PET/SWCNT nanocomposites.

The tensile properties of the synthesized PTT/SWCNTs nanocomposites are listed in Table 18 and representative stress-strain curves are shown in Figure 44. For the lowest concentration of carbon nanotubes, by means of 0.025 and 0.05 wt %, no effect on Young modulus has been observed. However, as the content of the SWCNTs increase to 0.5 wt%, the nanocomposites' tensile strength and Young's modulus increases. The highest increase was observed for PTT/0.1 SWCNT, perhaps due to the best dispersion state. However, further addition of SWCNTs (0.3 and 0.5 wt%) lowers Young's modulus, but their values are still higher than neat PTT. The values of elongation at break dramatically decrease in comparison to the neat PTT (similar effect as for PET/SWCNT composites). SEM analysis of PTT/SWCNT composites (Fig. 32, page 67) have shown that the CNTs are well distributed in the polymer matrix for all concentrations, note that the increase of CNT content does not lead to formation of visible agglomerates (except small entangled CNTs structures) in the bulk volume of the polymer. When two immiscible phases such PTT and SWCNTs meet, the interaction between them occurs at their interfaces. At the interface, the net internal force of each phase is not zero and will lead to the appearance of a tension called interfacial tension. Interfacial tension is somewhat similar to surface tension in that cohesive forces are also involved [347]. However, the main forces involved in interfacial tension are adhesive forces, i.e., tension between phases. The interphase in PTT nanocomposites is influenced by the Van der Waals forces between SWCNTs and PTT matrix. The increase of the tensile strength can be attributed to strong interphase interaction between the matrix and the CNTs. The lower values of tensile strength of nanocomposites with 0.3 and 0.5 wt % of CNTs compared with PTT/0.1 wt % could be explained by poorer dispersion state (Fig. 32 a -d). For many polymer/ CNTs nanocomposites a critical CNTs content in the matrix could be found when the CNTs reinforcement effect on randomly oriented polymer/ CNTs composites was studied. Below this content, the reinforcement effect for polymer/CNTs composites increases with increasing CNT content. Above this content, the strength of the polymer/ CNTs composites decreases, and in some cases, even lower than that of the polymer matrix. At higher CNTs content, the extent of improvement in mechanical properties might be limited by the high viscosity of the composite and by poor load transfer between CNTs and polymer matrix resulted from imperfect dispersion and not completely covered some surface of the CNTs by polymer matrix due to the large specific area of CNTs. As will be noted in many reports, most of randomly oriented polymer/CNTs composites show only a moderate or no strength

enhancement, especially for composites containing untreated CNTs, mainly attributed to poor load transfer between polymer matrix and CNTs.

To summarize the observation on the effect of SWCNT addition to two polyester matrices (PET and PTT), it can be noted that the high-purity CNTs (KNT 95) are more efficient than the lower purity CNTs Cheaptubes in transferring applied load.

Table 18 Tensile properties of PTT/SWCNTs nanocomposites

Sample	E GPa	σ_y MPa	ε_y %	σ_b MPa	ε_b %
PTT	2.36 ± 0.05	50.2 ± 9.5	3.6 ± 0.2	28.6 ± 9.7	178 ± 32.4
PTT/0.025 SWCNT KNT	2.36 ± 0.12	68.9 ± 5.5	1.4 ± 0.1	68.9 ±5.6	3.81 ± 0.1
PT/0.05 SWCNT KNT	2.38 ± 0.13	58.8 ± 9.2	1.3 ± 0.1	61.5 ± 5.3	2.64 ± 0.1
PTT/0.1 SWCNT KNT	2.63 ± 0.12	67.8 ± 6.7	1.1 ± 0.2	69.5 ± 6.3	2.75 ± 0.1
PTT/0.3 SWCNT KNT	2.52 ± 0.02	69.2 ± 6.9	1.1 ± 0.1	68.3 ± 6.5	2.83 ± 0.3
PTT/0.5 SWCNT KNT	2.46 ± 0.05	72.6 ± 7.5	1.2 ± 0.1	60.8 ± 9.2	2.49 ± 0.2

E – Young's modulus; σ_y - yield strength (elastic limit), ε_y – yield strain, σ_b (indicated with "x" in the figure),, ε_b - stress and strain at break respectively

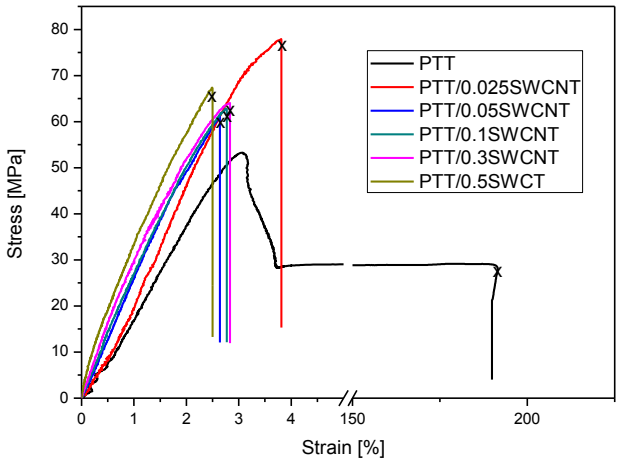

Fig. 44 Representative stress strain curves of PTT/SWCNT nanocomposites.

Testing the mechanical properties of nanocomposites based on thermoplastic elastomers

The addition of carbon nanotubes changes the stress-strain characteristics of PTT-PTMO, as illustrated in Figure 45. Enhancing effect of nanofiller manifests itself as increased strength of composites, but with increasing concentration of nanoparticles a gradual reduction in elongation, however within boundaries of measurement error, is observed (Table 19). As a result, composites exhibit higher stress at the same relative elongation (relative to the unfilled copolymer) and are destroyed when reaching higher values of strain (from the highest proportion of nanotubes at 0.3 wt %).

Table 19 Tensile properties of PTT-PTMO/SWCNTs nanocomposites

Sample	E MPa	σ_y MPa	ε_y %	σ_b MPa	ε_b %
PTT-PTMO	118 ± 1.5	13.6 ± 0.2	44.8 ± 0.9	20.3 ± 0.7	625 ± 12
PTT-PTMO/0.1 SWCNT	142 ± 3.9	14.2 ± 0.2	47.8 ± 0.8	20.7 ± 0.6	617 ± 24
PTT-PTMO/0.3 SWCNT	166 ± 2.5	14.1 ± 0.1	49.7 ± 0.5	19.9 ± 0.2	639 ± 13

E – tensile modulus; σ_y, ε_y – yield stress and strain respectively, σ_b, ε_b - stress and strain at break respectively

In block copolymers, the nanometric structure of segregated flexible and rigid segments is responsible for mechanical properties by means of: flexible segments of PTMO for the elastic properties, whereas rigid segments of PTT for an increase in strength. These semicrystalline thermoplastic elastomers can be treated as nanocomposites themselves as reported in [16]. The crystallization of PTT rigid segment sequences play a critical role in physical crosslinking formation and subsequently mechanical properties of these materials. The incorporation of carbon nanofillers to thermoplastic elastomers can change the macroscopic properties (for example tensile properties) due to the synergy between the nanoparticles and crystalline lamellae of polymer matrix. However, this factor is insufficient to obtain enhanced mechanical, good level of CNTs dispersion is also of great relevance. Here, the introduction of small amounts of CNTs didn't change the degree of crystallinity. Composites and neat PTT-PTMO block copolymer have comparable content of crystalline phase of 17 % (Table 12), so the enhancement in mechanical properties (modules increase) results from the addition of the carbon nanoparticles. As can be seen, an addition of a small amount of SWCNT to PTT-PTMO elastomer increases tension related to deformation, limiting the free length of chains which are located between physical nodes of the network / matrix (they create additional physical nodes). However, it is difficult to determine how the elasticity of nanocomposites is changed, because the permanent set wasn't examined here.

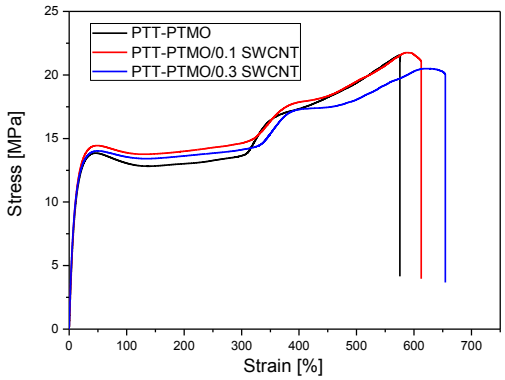

Fig. 45 Representative stress strain curves of PTT-PTMO/SWCNT composites.

16. Polymer nanocomposites containing graphene derivatives

16.1. Concept of graphene and expanded graphite used as nanofillers

In recent years, much attention was devoted to nanocomposites with lamellar nanofillers. The conformational structure and dynamic behaviour of polymer chains in a confined space formed by two plates of nanofiller mutually spaced by a distance less than the radius of the rotational motion of the chain fragments was studied in detail [348]. As lamellar fillers were used inter alia: montmorillonite, saponite and hectorite, however the most commonly used was montmorillonite. Polymer nanocomposites with montmorillonite (with a content <6 vol %) exhibited physical and thermal properties significantly better compared with the properties of the polymer itself, and also for certain properties of the composite properties superior to conventional mineral fillers. Improvement of these properties include increasing the modulus of elasticity, ultimate tensile strength, hardness, thermal conductivity, non- adhesion properties for paints and varnishes, as well as the reduction of linear expansion, and permeability to water vapor and oxygen, the effects of low temperatures on the impact strength [348] [349]. The discovery of graphene in 2004 as a new allotropic form of carbon (previously the existence of such structures provide theoretical models) caused increased interest on nanocomposites with its. The extremely mechanical properties of graphene: a high Young's modulus of about 1 ~ TPa, and tensile strength of 130 GPa [8], with a high aspect ratio and specific surface makes it with the carbon nanotubes a potentially attractive reinforcement material for polymers. The research conducted so far, in which graphene was the main point of interest, focused mainly on developing new methods of efficient synthesis and understanding the physicochemical properties of the material (with a strong emphasis on electrical conductivity) that this material could be used in various electronic circuits. Recent studies indicate that the production of large quantities of graphene is less expensive than the production of carbon nanotubes (CNT). The aim of this PhD thesis was to investigate the method of nanocomposites preparation based on thermoplastic polymers (PET, PTT, PTT-*block*-PTMO) with the participation of different varieties of graphene, differing form one another, inter alia, the size of the plate surface and the number of platelets, during polycondensation of matrix (*in situ*) and examine the impact of the content of different varieties of graphene on the physical properties of the material. For the preparation of nanocomposites have been used expanded graphite platelets with average sizes of 5, 50 and 500 μm, but also commercially available graphene (Graphene Angstron) with average dimension x & y of ~10 μm.

Expanded graphite (EG) can be obtained by exfoliating and reducing graphite oxide (GO) as the result of the expansion of the graphene sheets from loosely bonded graphene stacks. The differences in microstructures between these four different fillers can be clearly noted. EG I used in this work consists of worm-like agglomerates with a size of about 200 μm as revealed by SEM images (Fig. 46 a). As reported elsewhere, these worm-like particles consist on flattened balloon-like units made themselves of elementary graphite sheets [350]. Here relatively big stacks of densely packed EG particles are present. EG II observed at higher magnification showed completely different structure (Fig. 46 b). Graphene sheets were strongly connected to each other, which suggest that the expansion of graphene sheets in case

of EG II was smaller than in EG I. These observations will be confirmed by the electrical conductivity measurements of nanocomposites based on this two types of expanded graphite. To summarize, the high surface area and the prevalent pores in EG facilitate the processing and formation of *in situ* polymer/EG composites.

Fig 46 c shows the SEM photomicrographs of few layer graphene (FLG) provided by Institut de Chimie et Procédés pour l'Énergie, l'Environnement et la Santé (ICPEES). At magnification of 20k a lot of impurities were clearly observed. For FLG loose structure as in case of EG I and EGII is not observed. It also suggests that the interlayer distance between sheets was different than in case of above mentioned nanofillers.

Fig 46 d display the photomicrograph of the loose structures of graphene (Graphene <1nm) in successively larger magnification. Evidently, loose structures containing multi-pores in the graphene could be observed at this magnification. This micrograph also suggests the thickness of the graphene platelets layer is less than 100 nm.

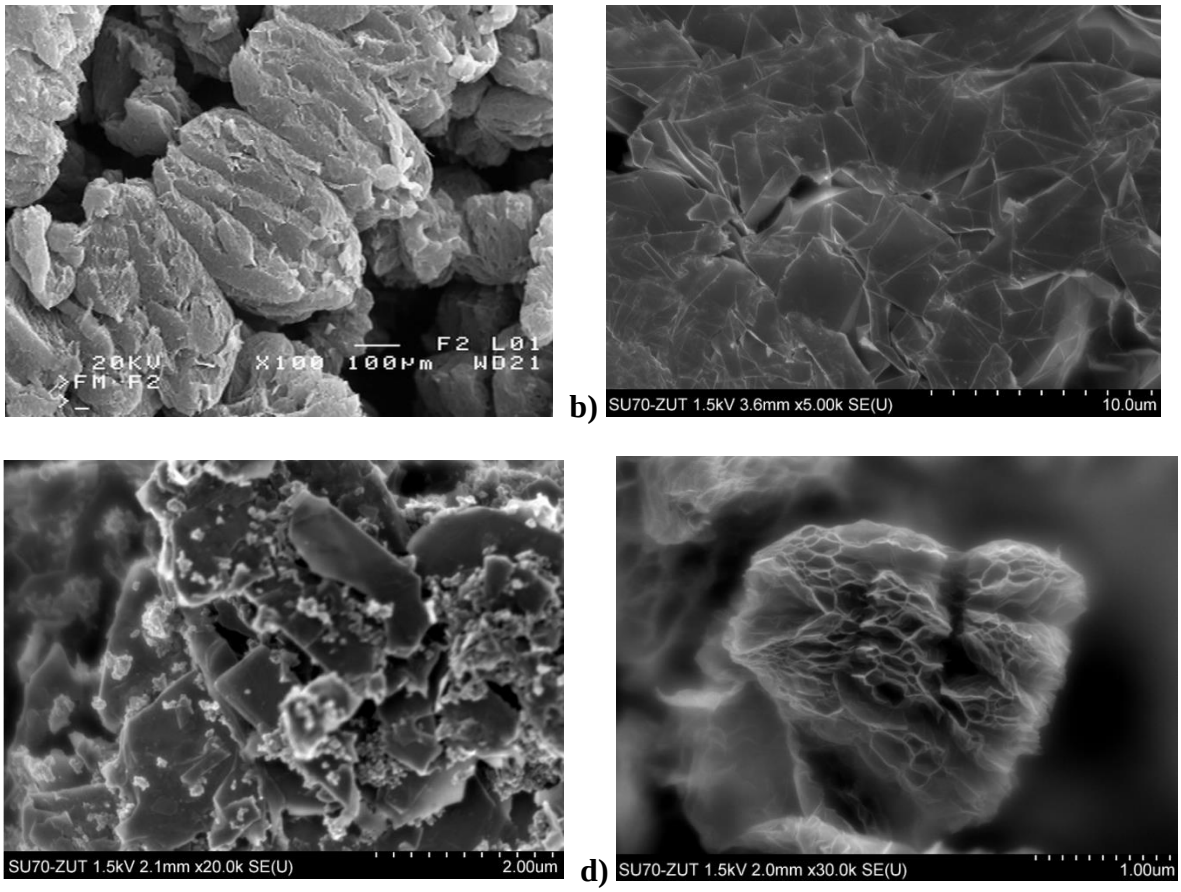

Fig. 46 SEM image of: a) expanded graphite (EG I), b) EG II, c) FLG, d) Graphene Angstron (<1nm).

This assumption can be corroborated by Raman Spectroscopy experiments. Fig. 47 compares the Raman spectra as a function of excitation energy of the EGI , EGII and Graphene Angstron (<1nm), three different types of graphene derivatives used to prepare nanocomposites intended to be used for measurements of electric properties. The well-known main groups of bands: the G band in the range of 1500–1600 cm^{-1}, as well as the D band in the range of 1200–1500 cm^{-1} is observed. The G band is related to the in-plane bond-tangential stretching motion of pairs of sp^2-C atoms of the E_{2g} phonons [351] [352] [353]and

[354]. The D band ("disordered" band) is the breathing mode of the sp^2-rings of the graphene layer that is related to a series of defects: bond–angle disorder, bond–length disorder, and hybridization [352] which are caused by heteroatom (hydrogen/oxygen) doping and structure defects caused by plasma treatment [351] [353] and [355]. The assignment of the D and G peaks is straightforward in the "molecular" picture of carbon materials. These bands are present in all poly-aromatic hydrocarbons.

EGII exhibits the characteristic bands of carbon-based materials namely the disorded-induced D-band, at ~1350 cm^{-1}, and the G-band at higher wave number values. The prominent D-band in EGII is consistent with the existence of a great amount of carboxylic or hydroxyl groups and amorphous carbon presents in the graphene surface. In contrast, EGI exhibits a decrease in the D-peak intensity as a consequence of the reduction process on GO that leads to EG, its conducting form. Nevertheless the less intense, although detectable, D-band indicates a residual amount of surface groups, which may be responsible for an enhanced interaction with the PET matrix. This effect suggests certain level of compatibility between the graphene surface and the PET matrix enabling an appropriate EG dispersion which facilitates the formation of a compact continuous network of EG particles throughout the PET matrix as observed by SEM (Fig. 51). The amount of residual groups and impurities in EGII also explains the properties of prepared nanocomposites (mainly lack of conductivity in case of PTT/EGII nanocomposites Fig. 50).

Raman spectra for Graphene Angstron has a typical two bands spectrum of disordered polycrystalline and noncrystalline graphitic carbons. The first one, at approximately 1360 cm^{-1}, exists only in defective carbons and is called "D-band", associated to disorder and edges of these crystals. The band at 1600 cm^{-1} can always be presented in vitreous carbon as a superposition of two components: G (1580 cm^{-1}) and D' (1620 cm^{-1}). The G-band is called "graphitic" and attributed to the graphite basal plane. On the other hand, the D' band is attributed to second first order zone boundary phonon. It is well seen that Graphene Angstron doesn't possess the typical Raman spectra observed for graphene or few layer graphene. This might explained the different SEM structure of nanofiller and no influence of graphene on rheology of both PTT and PTT-PTMO polymer matrices. Probably, lots of functional groups on the surface of Graphene Angstron provide better dispersion state (Fig. 55), improvement in mechanical properties (Fig. 64) with no conductivity in both (PTT/Graphene and PTT-PTMO/Graphene) (Fig. 50).

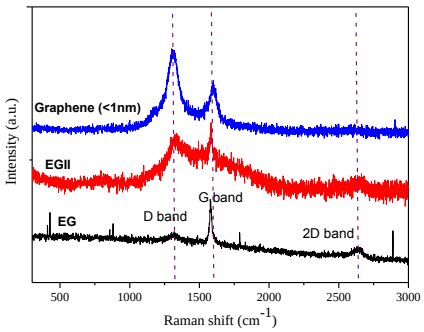

Fig. 47 Raman spectra of three types of graphenes used to prepare nanocomposites intended to be used for measurements of electric properties.

Expanded graphite (EG) is very attractive for its potential to increase the electrical conductivity of insulating polymers at very low concentration. In our case the electrical conductivity measurements of the samples were performed on nanocomposites with EGI, EGII and Graphene Angstron.

Since, poly(ethylene terephthalate) (PET) is a semicrystalline polymer, which has several properties such as good mechanical properties, chemical resistance, thermal stability, low melt viscosity, and spinnability, but may exist both as an amorphous (transparent) and as a semicrystalline polymer, the electrical conductivity of the PET based nanocomposites exhibited a distinct behavior depending on the cooling procedure. Fig. 48 shows the electrical conductivity for the nanocomposites with different amount of EG as a function of frequency for samples submitted to either fast cooling (FC, Fig.48 a) or slow cooling (SC, Fig. 48 b).

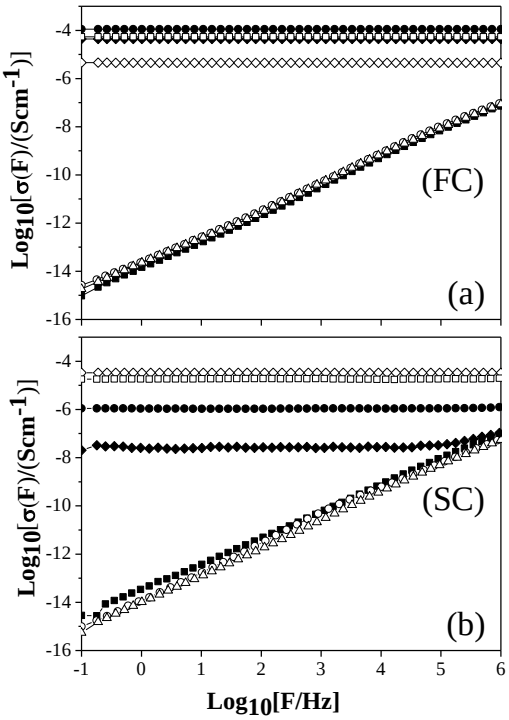

Fig. 48 (a) Alternating current conductivity, σ(F) as a function of frequency (F) for EG-PET nanocomposites with different EG concentrations: 0 (■), 0.025 (○), 0.05 (Δ) , 0.075 (◊), 0.1 (♦), 0.2 (●) and 0.4(□) wt%, (a) Fast cooling samples and (b) Slow cooling samples [322].

Nanocomposite films obtained in the process of fast cooling (amorphous films) showed higher conductivity than nanocomposites obtained in the slow cooling process (semicrystlline films), but the percolation threshold remained at the same value of 0.05 wt %. The degree of crystallinity of slow cooled samples determined from WAXS is presented in Table 20. The results displayed in Fig. 48 a have been taken with electrodes of 20 mm in diameter since it was observed that the reproducibility of the conductivity results was improved under these conditions. Probably the existence of a polymer passive layer in the surface of the nanocomposite films insulates the metal electrode from the conducting network. The probability of contacting the electrode with the network increases with the area of the electrode. In principle, the electrical conductivity of a material should follow a law as

$\sigma(F)= \sigma_{dc}+A\cdot F^s$ where the presence of a frequency independent component, σ_{dc}, is characteristic of a conducting behavior with a significant direct current (dc) conductivity. FC nanocomposites with EG content higher than 0.05 wt % exhibit an absence of frequency dependence indicating the presence of a σ_{dc} contribution significantly higher than that of the polymer matrix. For EG content lower than 0.05 wt % the conductivity follows a $\sigma(F)\sim F^s$ with s=1 what is characteristic of an insulating material with absence of σ_{dc} component in the measured frequency range. A qualitatively similar behavior is observed for the EG nanocomposites prepared by slow cooling (Fig. 48 b). Surprisingly the sample with 0.075 wt % of EG exhibited the higher conductivity. Surprisingly the sample with 0.075 wt % of EG exhibited the higher conductivity. This effect can be visualized in Fig. 49 which shows σ_{dc} values as a function of the EG concentration for both fast and slow cooled nanocomposites. For the sake of comparison a value of σ (F) taken at F= 0.1 Hz has been considered for the non-conducting samples. The most obvious feature is that FC nanocomposites exhibited significantly higher conductivity values than the slow cooled ones. In both cases, a characteristic percolative behavior was observed. Initially, for low concentrations, the conductivity remained at the same level as the insulating PET matrix. Initially, for low concentrations, the conductivity remained at the same level as the insulating PET matrix. At a certain critical concentration around 0.05 wt %, the conductivity started a sudden increase. The dc conductivity above the critical concentration of nanoadditive, σ_c, can be analyzed in terms of the percolation theory [356] by means of the standard scaling law given by $\sigma_{dc}\alpha(\Phi-\Phi_c)^t$, where t is a critical exponent. Although σ_c depends on the lattice in which particles are accommodated, the critical exponent t depends only on the dimensionality of the system [356]. This law can be applied upon considering both volume or weight % concentrations [87]. Theoretical calculations, supported by a great amount of experimental observations propose values of t between 1.6 and 2 for three-dimensional systems. The fitting of the percolation equation to the experimental data is represented in Fig. 49 by the continuous lines. For the SC series the 0.075 % wt EG sample was excluded from the fit. This analysis provides t values of around 1.7 and Φ_c = 0.05 for the fast cooled samples and of t = 3.5 and with Φ_c = 0.05 for the slow cooled nanocomposites, respectively. While the t-value for the FC nanocomposites was well within the expectations of the percolation theory, that one for the SC nanocomposites was much beyond. As mentioned before, the SC sample with 0.075 wt % of EG exhibited higher conductivity than the rest of the SC nanocomposites and has not been considered for the fitting. In a first approach we attribute this effect to the crystallinity of the nanocomposite which is for this sample of ≈ 12 % being lower than those of the rest SC samples. As a matter of fact the conductivity values for the 0.075 wt % sample are very close for both SC and FC. Percolative behavior in composite materials with high values of the critical exponents was frequently reported in the literature [357] [358] [359]. According to percolation theory the insulator-conductor transition occured at the critical concentration at which an infinite cluster of connected particles appeared. Two particles are usually considered to be connected when they are in physical contact. In this framework a homogeneous distribution of isotropic distribution is considered. Values of t-exponent higher than those expected by percolation theory were found in composite materials in which tunnelling conduction was present [359] or where anisotropy effects were significant [357]. In the later case, large apparent conductivity exponents should be associated to anisotropic conducting

heterogeneities in an insulating medium. In the present case, SC nanocomposites could present two sources of anisotropy induced effects. On the one hand, cooling was performed at such slow rate that crystallization of the PET matrix was possible (Table 21). On the other hand, the cooling was accomplished under a certain pressure. Considering the anisotropic nature of the EG nanoadditive (Table 21) one can suppose that the pressure could promote an orientation of the EG platelets imparting certain level of anisotropy unlike the case in which fast cooling at zero pressure was used. Accordingly, it was proposed that the semicrystalline matrix and/or the effect of pressure as the main reasons for the difference in the percolative behaviour between SC and FC PET/EG nanocomposites. Since the crystallinity of the SC samples varies with the concentration, the deviation of the 0.075 wt % EG sample from the percolative trend can be attributed to the low level of crystallinity of this sample which approach its value to that of the FC one.

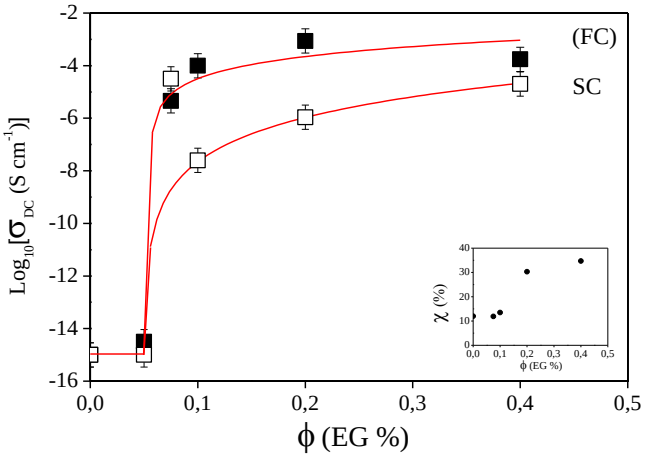

Fig. 49 Logarithm of the dc electrical conductivity versus nanoadditive weight concentration for the fast (FC, ■) and slow (SC, □) cooled nanocomposites. The continuous lines are the predictions of percolation theory [322].

The explanation of high conductivity of expanded graphite nanocomposites is: firstly, its two-dimensional nature should result in good connectivity and so a great choice of conductive paths for current to flow through and secondly, its planar nature should allow to pack really close, giving low porosity. The obtained here percolation thresholds for amorphous and semicrystalline PET/EG nanocomposites prepared by *in situ* polymerization are much lower than those presented previously for PET/graphene nanocomposites prepared by melt compounding [360] [361]. Li et al. [361] have shown that the electrical conduction paths of graphene sheets in PET/EG nanocomposites prepared by melt-compounding is formed at ~5 wt %.

Studies of the electrical conductivity showed that PTT/0.5 EG, PTT/0.5 Graphene Ang and PTT-PTMO/0.5 Graphene Ang nanocomposites do not conduct electricity; even with the highest concentration of nanoplatelet they remain insulators, since the values corresponding to the measured at room temperature electrical conductivity (Fig. 50) show its dependence on the frequency, which is typical insulators.

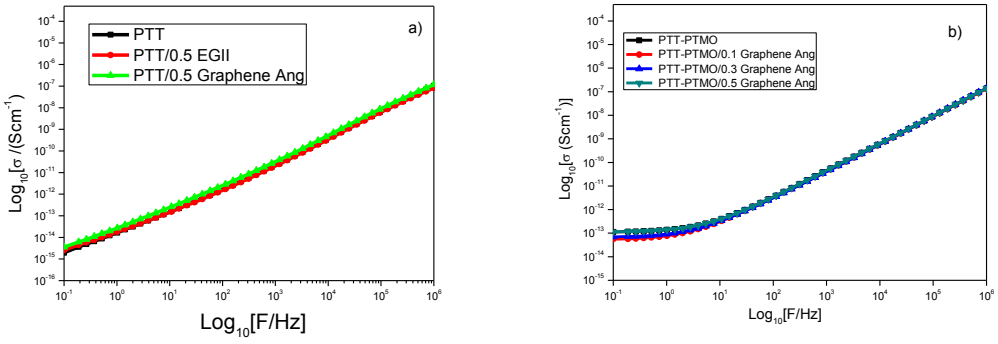

Fig. 50 Alternating current conductivity, σ(F) as a function of frequency (F) for PTT/EG and PTT/Graphene Ang nanocomposites (a) and PTT-PTMO/Graphene Ang nanocomposites (b).

While for the PET / EG composite the percolation threshold with the participation of graphene nanoplatelets of 0.05 wt % was observed. Based on analysis of SEM and Raman spectroscopy can be concluded that the lack of electrical conductivity in this case may be the result of the quality of the used graphene derivatives. Only EGI (added to PET), which Raman spectrum confirms the effectiveness of the method of thermal reduction, allowed to obtain conductive nanocomposites. In other cases, probably because of the numerous functional groups and impurities on the surface of EGII and the Graphene Ang, failed to receive the percolation threshold of less than 0.5 wt%. For this reason, hybrid nanocomposites with the participation of this three types of graphene derivatives were prepared to investigate how the combination of fillers with different shapes affect the properties of the starting material.

16.2. Morphology and phase structure

Morphology and phase structure of prepared nanocomposites based on thermoplastic polyesters (PET, PTT) and thermoplastic elastomers (PTT-PTMO) containing graphene derivatives were investigated by using SEM and DSC analysis. The measurements of physical properties (intrinsic viscosity, density etc.) of nanocomposites complimented further analysis of the influence of graphene derivatives on different matrices.

The dispersion of EG in ethanediol produced good exfoliation as shown in the SEM images (Fig. 51 b) where individual EG particles are clearly visualized embedded in the PET polymer matrix. It has been well documented that the effectiveness of nanoadditive dispersion strongly depends on both the method and the process time. As revealed by the SEM images, the use of a sonicator device seems to be rather effective in order to split the “as received” existing worm-like agglomerates into graphite sheets and to distribute them in the entire volume of ethanediol. SEM images also indicate that the expanded graphite nanosheets were encapsulated by the PET matrix. This suggests a strong interaction between graphene sheets and PET matrix. In order to further investigate the dispersion of expanded graphite in the PET matrix, TEM measurements were also performed. Fig. 51 a shows the microstructure of PET nanocomposites with 0.2 wt% of expanded graphite. The nanosheets appear to be completely embedded in the polyester matrix indicating an exfoliated structure. The high dispersion level of expanded graphite sheets can be attributed to a strong interaction between some residual polar groups on the surface of graphene and the polar groups of PET.

a) 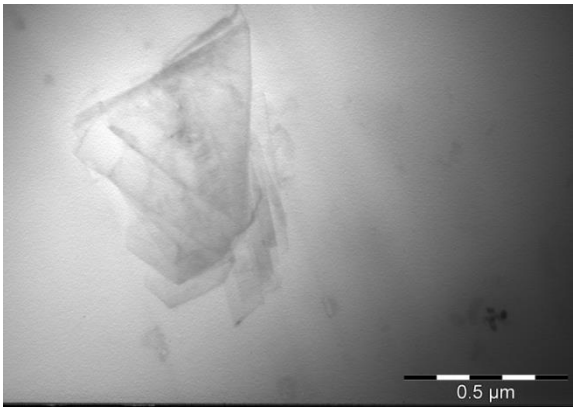

b) 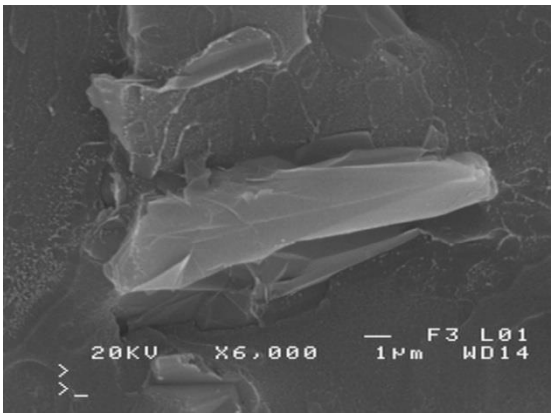

Fig. 51 TEM (x120.000) and SEM images of PET/0.1 wt % of EG I.

The molecular weight of polyesters and block copolymers during the synthesis were controlled by monitoring the maximum viscosity that can be obtained previous to the extrusion the polymers from the reactor. In our method, the maximum viscosity of the system was set to 14 Pa·s (at a constant temperature of 275 ^{o}C and at a stirrer speed of 40 min^{-1}). PET prepared by polymerization without EG had a number-average molecular weight of about 19500 g/mol. Chen et al. [362] reported that, in polymeric nanocomposites, the viscosity increases only after a certain range of volume fraction implying that at low volume fraction (less than 0.4 vol %), nanofluids have lower viscosity than corresponding base fluid, due to lubricating effect of nanoparticles. Accordingly, the molar weight of PET is expected to be dependent on the EG content in the reaction mixture. In Table 20, the values of intrinsic viscosities and molar weights of PET and PET/EG nanocomposites are presented. Both the intrinsic viscosities and molar weights of PET nanocomposites whit an EG content lower than 0.2 wt % were higher than those of neat PET. Thus, the results in Table 20 suggest that even though the viscosity of reaction mixture increased with EG content, for EG loadings below 0.2 wt % the viscosity was lower than the viscosity of reaction mixture without EG nanofiller, in agreement with Chen et al. observations [362]. The molecular weight of PET prepared in the presence of the highest studied EG content, 0.4 wt %, was 15600 g/mol. PET with this molar weight still exhibits suitable rheological properties for extrusion. For the sake of comparison let us remember that textile fibre-grade PET normally has a number-average molecular weight ranging from 15000 to 20000 g/mol, which corresponds to an intrinsic viscosity between 0.55 and 0.67 dl/g [319]. Moreover, it is worth to mention that the polydispersity values (M_w/M_n) remain at the same level as those of neat PET.

Table 20 Intrinsic viscosity and molecular weight of PET prepared in the presence of various EG loading. Last column includes mass crystallinity values, X_c, for the slow cooled (SC) samples as estimated by Wide Angle X-ray scattering

Sample	[η]	M_v x 10^4	M_w x 10^4	M_n x 10^4	M_w/M_n	X_c
	dl/g	g/mol	g/mol	g/mol		(%)
PET	0.553	2.22	4.69	1.95	2.41	12
PET/0.025 EG	0.601	2.48	5.28	2.40	2.21	-
PET/0.05 EG	0.556	2.23	4.95	2.03	2.44	-
PET/0.075 EG	0.548	2.19	4.56	1.88	2.43	11.9
PET/0.1 EG	0.550	2.19	-	-	-	13.5
PET/0.2 EG	0.513	1.99	4.17	1.69	2.47	30.3
PET/0.4 EG	0.501	1.93	3.85	1.56	2.47	34.7
PET[2]	0.450	1.67	2.98	1.15	2.60	-

M_v - viscosity average molecular weight ; M_w - weight average molecular weight; M_n - number average molecular weight; M_w/M_n dispersity; PET[2]- additionally synthesized neat PET with lower molecular weight

Nanofillers usually affect the ability to crystallize semi-crystalline polymers [363] [364] [365] [366] distributed in the polymer matrix nanoparticles assisted by nucleation and growth of crystallites. In the case of characterized in this work nanocomposites, there was no significant effect of nanoparticles on the physical transitions in PET or they were very small. Only for the highest content of EG in investigated nanocomposites based on PET it can be stated repeatedly the increase of crystallization temperature (T_c) and melting temperature (T_m) (Fig. 52). EG content does not significantly affect the degree of crystallinity of PET, which is between 34.4-36.1 (Table 21). This is due perhaps to the fact that the sizes of individual expanded graphite nanoplatelets were below the critical nucleation agents, as a result, may not constitute active centers of growth of crystallites. It also describes the lack of changes in the glass transition temperature (T_g) of semicrystalline PET regardless of the EG content

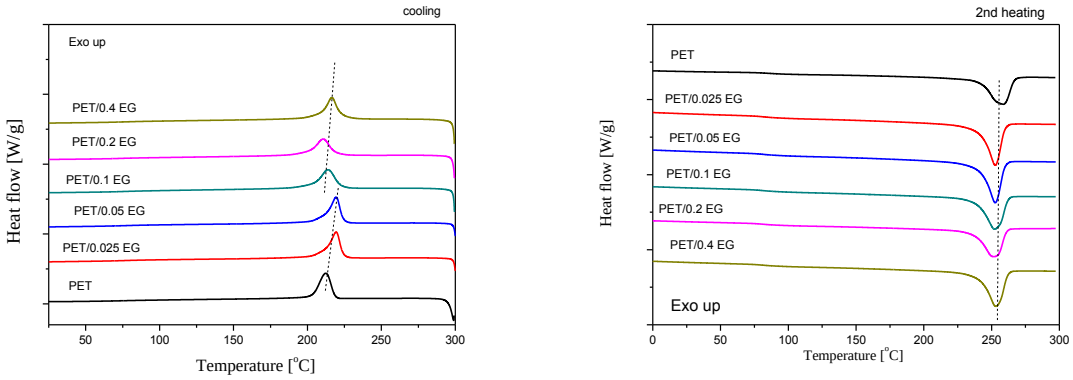

Fig. 52 DSC thermograms for PET and PET/EG nanocomposites during the cooling and 2nd heating.

Table 21 Thermal properties of neat PET and PET/EG nanocomposites determined by DSC

Symbol	T_g °C	T_m °C	ΔH_m J/g	T_c °C	ΔH_c J/g	X_c %
PET	85	257	47.0	214	46.9	33.5
PET/0.025 EG	83	251	49.4	207	48.8	35.3
PET/0.05 EG	83	253	49.4	210	49.1	36.1
PET/0.1 EG	83	252	50.5	214	49.8	36.0
PET/0.2 EG	83	252	48.2	217	47.5	34.4
PET/0.4 EG	83	253	50.1	217	49.5	35.8

T_g - glass transition temperature;-T_m - melting temperature; T_c – crystallization temperature; ΔH_m, ΔH_c - enthalpy of melting and crystallization; x_c - mass fraction of crystallinity determined from DSC

To confirm the morphological features of EG in the PTT matrix, SEM images of the fractured surfaces for the nanocomposite films were examined, as can be seen in 53 b. For further investigation, the TEM analysis was used to assess the degree of exfoliation of the expanded graphite platelets and the morphology of the nanocomposites (Fig. 53 a). From this micrograph, the more or less transparent graphene platelets providing a high degree of exfoliation of EG in a matrix has been observed. The fractured surface of PTT/EG composite film with 0.3 wt % EG also exhibits the smooth fractured surface without exhibiting any aggregates of graphene sheets. Nonetheless, it should be mentioned that the partial aggregates of graphene sheets in the nanocomposites (Fig. 53 b) with higher EG contents are not crystalline but disordered, as confirmed from density and DSC measurements of the nanocomposites in Tables 22 and 23. In addition, the accordion-like structures detected in the PTT/EG nanocomposites means that the graphene sheets of EG exist in a completely exfoliated and disordered state in the matrix of nanocomposites due to the high shear force generated during dispersion preparation followed by *in situ* polymerization. Direct evidence of the exfoliation of expanded graphite was provided by TEM analysis of PTT/0.3EG nanocomposites. The exfoliated morphology with clearly visible flakes (partially transparent) were observed. The flakes size supported from TEM was around $0.5x1\mu m^2$, which was probably due to the *in situ* procedure and dispersion process before polymerization, that causes wrapping and breaking of graphene sheets. It was observed that the expanded graphite sheets were dispersed homogeneously in PTT matrix. The occurrence of this exfoliation morphology may be attributed to the strong shear field in the mechanical stirrer and treatment of ultrasounds, and the strong interactions between EGII and PTT.

a) 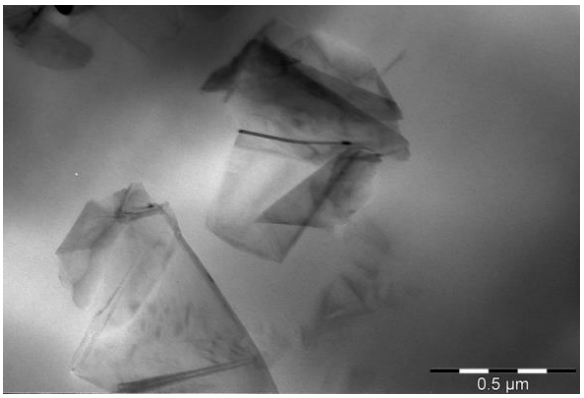

b) 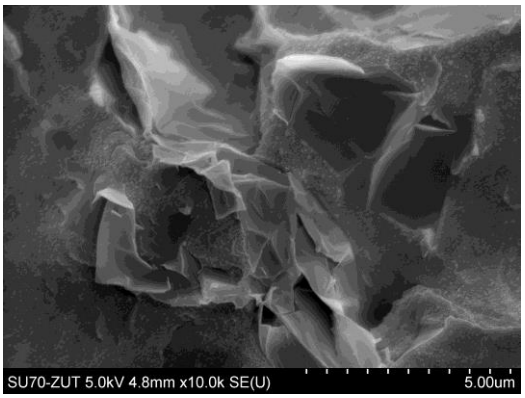

Fig. 53 TEM (x100.000) and SEM images of PTT/0.3 wt % of EG II.

Nanocomposites with concentrations of 0.1-0.5 wt % of EGII were prepared. Additionally, for comparison purposes, unmodified PTT was synthesized and characterized in the same manner as nanocomposites. In order to prepare high molecular weight polyesters, the polycondensation of these oligomers ensued at higher temperature, with the simultaneous application of high vacuum. The intrinsic viscosity of neat PTT was 0.781 dl/g. The presence of the expanded graphite in the polymerization mixture affected the reaction, leading to the decrease of intrinsic viscosity. As shown in Table 22, the intrinsic viscosity wasn't affected by the addition of EG. All obtained values of [η] are comparable to one another. Only the PTT/0.3EG exhibited slightly higher value of intrinsic viscosity to around 0.783 dl/g. As can be also seen in Table 22, the synthesized nanocomposite have also comparable molecular weights to the neat PTT, and only slight increase with the addition of 0.3 EG to $3.85 \cdot 10^4$ g/mol for PTT/0.5EG was observed. Even if the dumbbell shape samples were injection moulded to obtain amorphous samples, some crystallites have been formed, as it can be seen in increase of density. The prepared nanocomposites in comparison to the neat polymer showed slightly higher density due to the increase number of crystallites with an increasing content of nanosheets. Distinctive increase in weight degree of crystallinity was due to the nucleating influence of expanded graphite, also confirmed by DSC analysis, Table 23.

Table 22 Physical properties of PTT/EG nanocomposites

Sample	[η] dl/g	M_v x 10^4 g/mol	d g/cm^3	Xc_w %
PTT	0.781	3.84	1.323	19.8
PTT/0.1 EG	0.777	3.81	1.328	23.4
PTT/0.3 EG	0.783	3.85[f]	1.329	24.4
PTT/0.5 EG	0.778	3.82[f]	1.332	26.5

M_v - viscosity average molar weigh; f- measured after filtration of EG; d- density; Xc degree of crystallinity estimated from density measurement

Figure 54 shows DSC heating and cooling thermograms of neat PTT and PTT/EG nanocomposites with various EG contents. In the cooling thermograms of Figure 54 a the

melt-crystallization temperatures (T_m) of PTT/EG nanocomposites are shifted to higher temperatures, as the EG content in the nanocomposites increased up to 0.5 wt %. The melt-crystallization exothermic area (ΔH_m) also increased with increasing the EG content up to 0.5 wt %. Contrarily, in the heating thermograms of Figure 54 b, two thermal transitions are observed apparently with increasing temperature, i.e., the glass transition and melting. The glass transition temperatures (T_g) and melting temperatures (Tm) of PTT/EG nanocomposites remained practically unchanged, regardless of the EG content, as summarized in Table 23. These results indicate that the overall crystallization rates of PTT/EG nanocomposites become faster with the increasing content of EG content up to 0.5 wt %, which is due to the effective nucleating agent effect of the graphene nanosheets of EG for PTT matrix component.

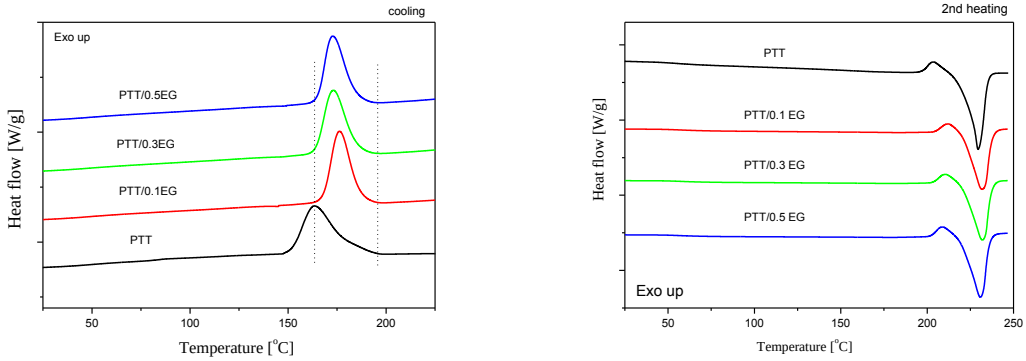

Fig. 54 DSC thermograms for PTT and PTT/EG nanocomposites during the cooling and 2nd heating.

Table 23 Thermal properties of neat PTT and PTT/EG nanocomposites determined by DSC

Sample	T_g °C	T_m °C	ΔH_m J/g	T_c °C	ΔH_c J/g	x_c %
PTT	53	231	45.8	167	46.2	31.4
PTT/0.1 EG	54	232	51.0	176	49.3	34.9
PTT/0.3 EG	54	231	47.7	173	46.9	32.7
PTT/0.5 EG	54	231	48.1	173	48.5	32.9

T_g - glass transition temperature;-T_m - melting temperature; T_c - crystallization temperature ΔH_m, ΔH_c - enthalpy of melting and crystallization; x_c - mass fraction of crystallinity determined from DSC.

The dispersion and orientation of graphene platelets within the thermoplastic elastomer was examined using SEM microscopy. In general, the surface of the cryuofracture injection molded specimens exhibited a high degree of graphene sheets alignment along the polymer. Figure 54a shows the SEM images for PTT-PTMO/0.3 wt % of Graphene Angstron, whose particle distribution morphology includes overall projection and microdomain. Due to the residual groups on the surface of graphene, after preparation process, it can be observed that the graphene platelets are covered by polymer matrix (Fig. 55 b).

The morphology of the ultramicrotomed nanocomposites was analyzed in detail using transmission electron microscope (TEM). Exfoliated graphene-based materials are often compliant, and when dispersed in a polymer matrix are typically not observed as rigid disks (flate platelets), but rather as bent or crumpled/wrinkled platelets. Moreover, graphene has been shown to 'scroll up' irreversibly when its polymer host is heated above its glass transition temperature (T_g) [345]. Compatibility between the polymer matrix and graphene platelets also can reportedly affect the platelets' conformation. In Fig. 55 c and d randomly oriented, exfoliated platelets was observed possibly due to restacking of the platelets. The processing technique by means of *in situ* polymerization could induce orientation of the dispersed platelets, which can be beneficial for reinforcement but may also raise the percolation threshold.

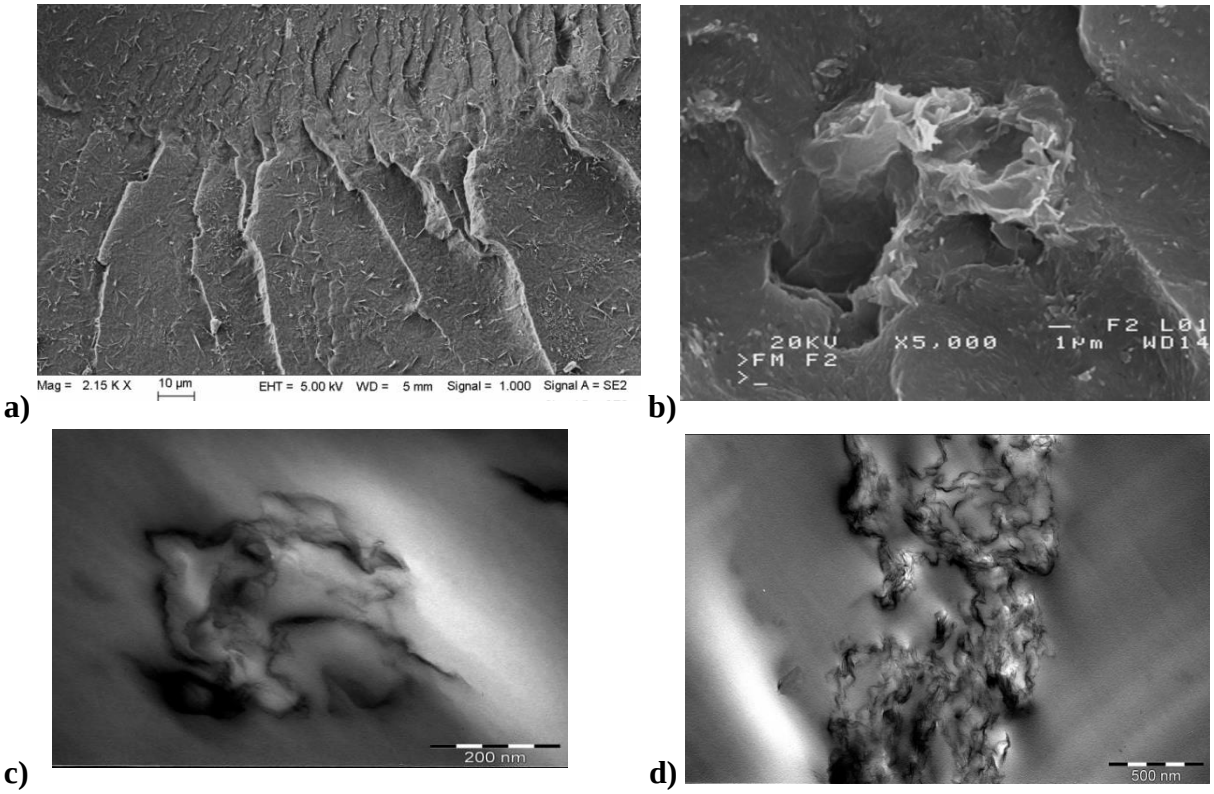

Fig. 55 SEM (a and b) and TEM (c-d, x75.000) images of PTT-PTMO/0.3wt % of Graphene Angstron.

The thermoplastic poly(ether-ester) segmented block copolymer, containing 50 wt % of PTT, as the rigid segment, and 50 wt % of PTMO as the flexible one, was used as polymer matrix. The nanocomposites containing from 0.1 to 1.0 wt % of graphene nanoplatelets (Graphene Angstron) were synthesised by a two-stage melt transesterification and polycondensation. The physical properties of the obtained nanocomposites are presented in Table 24. Values of [η] for copolymers in nanocomposites varied between 1.305 and 1.289 dl/g (from the lowest to the smallest concentration (Table 24), and are lower than the value obtained for the neat PTT-PTMO block copolymer (1.325 dl/g). As can be seen in Table 16, the obtained high values of [η] for matrix in nanocomposites show that the synthesized copolymers have high molecular weights and comparable to neat copolymer, which were confirmed by SEC analysis (Table 24). Only the slight increase in dispersity was observed for

the highest concentration of nanofiller (1.0 wt %). Nanocomposites in comparison to the neat copolymer have also slightly higher density due to the presence of nanofiller with higher density.

Table 24 Physical properties of PTT-PTMO/Graphene Ang nanocomposites

Sample	[η] dl/g	M_w g/mol	M_n g/mol	M_w/M_n	d g/cm^3
PTT-PTMO	1.325	102 066	56 773	1.797	1.174
PTT-PTMO/0.1 G	1.305	-	-	-	1.174
PTT-PTMO/0.3 G	1.327	-	-	-	1.175
PTT-PTMO/0.5 G	1.322	101 002	57 543	1.755	1.176
PTT-PTMO/1.0 G	1.289	100 849	54 249	1.859	1.177

M_w - weight average molecular weight; M_n - number average molecular weight; M_w/M_n dispersity; d - density

As mentioned earlier, the neat PTT–PTMO block copolymer has two phase morphology: a PTT crystalline phase and PTMO-rich amorphous phase. It was found in many semicrystalline systems that the addition of nano-additives have affected the crystalline structure and crystallization rate. The effect of Graphene (<1nm) on the thermal behaviour of the nanocomposites and neat PTT-PTMO block copolymer during heating and cooling is examined by DSC (Figure 56, Table 25). As can be seen from the Table 25, the glass transition temperature (T_g), corresponding to the amorphous soft PTMO-rich phase, and the meting point (T_m) derived from the crystallized rigid PTT segments (T_m) are not affected by the presence of graphene nanoplatalets in polymer matrix. Degrees of crystallinity of the nanocomposites are comparable to the neat PTT-PTMO block copolymer, with only slight decrease with the highest concentration of nanofiller. However, the crystallization traces in Fig. 54a indicate that graphene worked as a nucleation agent for the crystallization of PTT segments. At the same cooling rate, the nanocomposites have higher crystallization temperatures (Fig. 56 a, Table 25) with the increase of nanoplatelets content than neat PTT-PTMO copolymer. Crystallization rate of a polymer is determined by the nucleation rate and mobility of polymer chains. The introduction of nanoscale platelets produces a hindrance on the molecular chains movement, which will reduce the tendency for molecular chains to be crystallized, though the confined molecular chains may be well ordered in the lamellar space. Hence, in our system only increase of crystallization rate was observed, but degree of crystallinity is not affected by the presence of the graphene sheets. Similar effect was previously observed for PTT-PTMO and PTT nanocomposites after introduction of carbon nanotubes

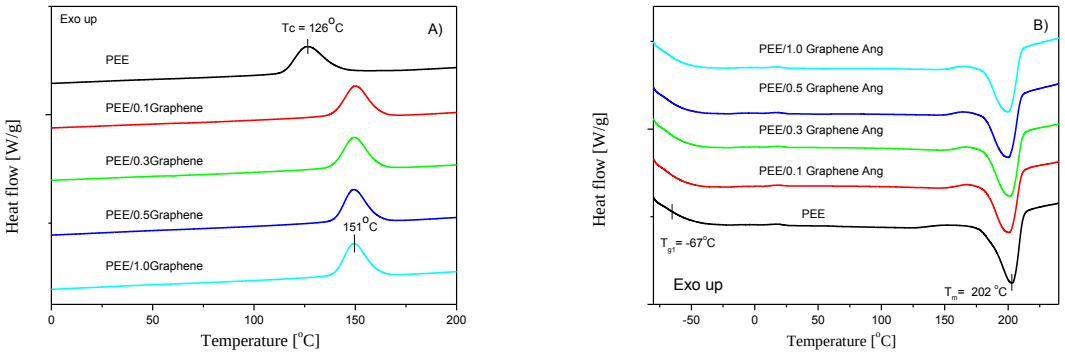

Fig. 56. DSC thermograms obtained during cooling (A) and 2nd heating (B) for PTT-PTMO/Graphene Ang nanocomposites.

Table 25 Thermal properties of neat PTT-PTMO and PTT-PTMO/Graphene Angstron nanocomposites determined by DSC

Sample	T_g °C	T_m °C	ΔH_m J/g	T_c °C	ΔH_c J/g	x_c %
PTT-PTMO	-67	206	25.8	126	26.2	17.7
PTT-PTMO/0.1 G	-67	204	24.9	149	25.1	17.1
PTT-PTMO/0.3 G	-67	205	25.6	149	25.2	17.5
PTT-PTMO/0.5 G	-67	203	24.3	148	22.7	16.6
PTT-PTMO/1.0 G	-67	203	24.1	151	23.6	16.5

T_g - glass transition temperature of polyether-rich soft phase;-T_m - melting temperature of polyester crystalline phase; T_c - crystallization temperature of polyester crystalline phase; ΔH_m, ΔH_c - enthalpy of melting and crystallization of polyester crystals, respectively; x_c - mass fraction of crystallinity.

16.3. Rheology and processing

It is known that rheological properties of nanocomposites containing layered nanofillers are related to the degree of exfoliation of nanofiller in polymer matrix and also to the level of interfacial interaction between the nanofiller surface and polymer chains [367]. Usually, in nanocomposites the increase of melt viscosity is observed with increasing of nanofiller content due to nanofiller–polymer interactions. The dependence of melt viscosity of neat PTT and neat PTT-PTMO block copolymer and nanocomposites with graphene (Graphene Angstron <1nm) based on this two matrices measured at different frequencies is presented in Fig. 57 (a and b). In case of PTT, with an increase of frequency, the melt viscosity of neat PTT and nanocomposites decreases. However, the addition of graphene platelets caused the increase of melt viscosity in the function of frequency. The increase wasn't as significant as in case PTT/SWCNT nanocomposites, but still we can observe the influence of graphene platelets on melt viscosity. However, the nanocomposite with 1.0 wt %

of graphene exhibited melt viscosity low enough that it could be easily extruded from the reactor and in the case of PTT / SWCNT nanocomposites, introducing more than 0.5 wt % of nanotubes resulted in such high increase in the melt viscosity that it could not be extruded from the reactor. As the filler loading increases, interaction between the graphene sheets and the polymer matrix becomes larger due to the high aspect ratio of the nanofiller and causes an increase in melt viscosity.

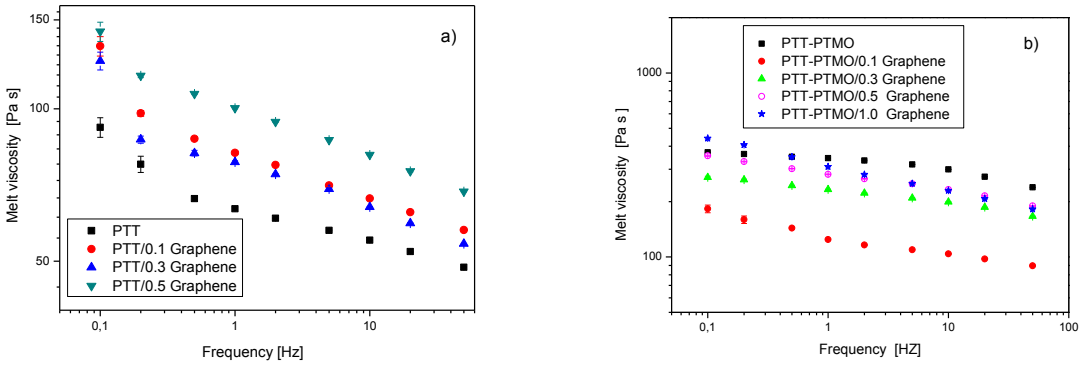

Fig. 57 Melt viscosity versus frequency for a) neat PTT and PTT/Graphene Ang nanocomposites at 250 °C and b) neat PTT-PTMO copolymer and PTT-PTMO/Graphene Ang nanocomposites at temperature of 220 °C.

Whereas, with an increase of frequency, the melt viscosity of neat PTT-PTMO copolymer and nanocomposites decreases. In comparison to the neat PTT-PTMO copolymer, the melt viscosity of nanocomposites at low graphene loading (<0.3 wt %) is slightly reduced, and then increases at the highest graphene loading (1.0 wt %). However, the molecular weights of matrices in nanocomposites (Table 24) were comparable to the molecular weight of neat polymer. It is not clear what mechanism causes the reduction of melt viscosity in the nanocomposites with low graphene loading. One possibility is acting of graphene sheets as plasticizer, increasing the free volume and therefore decreasing the melt viscosity [368]. Whereas at higher graphene loading, the polymer–graphene and graphene-graphene interactions are predominate and causes increase the melt bulk viscosity. The possible mechanisms of selective adsorption [369], excluded free volume [370] and ball-bearing effect [371] are also reported in literature to explain the decrease in melt viscosity when nanofillers are introduced to the polymer matrix. Another possible explanation for observed melt viscosity changes with graphene loading can result from lubricant behaviour of graphite [372]. The graphene layers coupled by week van der Waals-like bonds can easily slide past each other. At low graphene content, few layer graphene in the studied composites can act as lubricant reducing melt viscosity.

16.4. Barrier properties

Barrier materials possess the ability to restrict the passage of gases and vapors through their boundaries. Plastic films and sheeting, coatings and many others types of materials are constructed to achieve economic and efficient barrier layer. Polymeric materials dominates the barrier materials used in packaging industry, and are ranging from window films to clothing, due to their superior properties and low cost. Polymeric packaging materials are

used to surround a package completely, securing contents from gases and vapors, moisture, and other effects from the outside environment, while providing pleasant and decorative appearance. Atmospheric gases and water vapor if allowed to permeate in and out of a package can alter the color, taste and nutritional content of the package good.

Since poly(ethylene terephthalate) (PET) has found a variety of application as fiber, bottles, films etc. because of its low cost and high performance, many studies have been already reported to develop nanocomposites based on PET with improved gas barrier properties that are required for beverages and food packaging. The reduction in gas permeability of PET nanocomposite depends on its crystallinity and nanofiller loading levels. The relationship between the crystallinity and the oxygen permeability of PET, as well as the filler model, which follows a standard, predictable pattern, and dependent upon filler loading levels have been extensively studied [373] [374] [375]. As mentioned in introduction [Chapter 4.2, page 35] graphene and its derivatives has attracted strong scientific and technological interest also in the area of gas barrier materials. Introduction of graphene or graphene derivatives can be a new way to improve PET barrier properties. Graphene derivatives with different flake size, different sheets amount etc. that can significantly reduce gas permeation through a polymer nanocomposites compared to the neat polymer matrix. A percolating network of platelets can create a 'tortuous path' which inhibits molecular diffusion through the matrix, thus resulting in significantly reduced permeability.

In this work, for the obtained PET/EGI nanocomposites via *in situ* polycondensation the oxygen permeability was studied. Neat PET films with various thicknesses where measured in the same conditions. Table 26 lists the oxygen transmission rate (OTR) data for neat PET and PET/EG nanocomposites. The study was carried out on thin amorphous films (with controlled samples' thickness) obtained in the same way as films for testing electrical conductivity (described in Chapter 16.1, pages 93-96), where the degree of crystallinity was measured through WAXS as reported in [322]. For comparison purpose, in first lines of table 26 are presented the already reported OTR values for amorphous and crystalline PET films. It has been seen that the permeability of oxygen decreased with an increase of the graphene nanoplatalets content, if the sample thickness is comparable. The 0.025 wt % composition showed a reduction of about 22 %, but 0.2 wt % reduced permeability about 71 % if compared to neat PET. However in case of the highest content of expanded graphite sheets (0.4 wt %) the slight decrease in OTR was observed. Graphene nanoplatelts themselves are impervious to oxygen, providing barrier resistance. The volume occupied by the EG sheets and amount of nanoparticles has influenced the actual three-dimensional arrangement and dispersion. With the increasing concentrations of nanoplatelets, permeability increase indicating there was sufficient platelets arrangement to provide resistance to permeability and the torturous path required. The permeability depends on the aspect ratio and dispersion of graphene nanosheets. Since the dispersion of EG ranged from exfoliation and agglomeration of nanoplatelets at 0.4 wt % loading, the decrease in oxygen permeability can be observed. The change in oxygen permeability of nanocomposites was controlled by the EG content, nanostructure and sample thickness, since it was observed that the degree of crystallinity and sample thickness play a critical role in enhancement of gas barrier properties of nanocomposites.

Table 26 Oxygen transmission rate of neat PET and PET/EG nanocomposite films

Sample	EGI Wt %	Thickness µm	O_2 transmission rate (OTR) $cm^3/m^2 \cdot 24h$	Reference
PET amorphous		180	857	[376]
PET amorphous		200	21.25	[377]
PET oriented crystlline ϕ_c =0.22		200	9.67	[377]
PET oriented crystlline ϕ_c =0.16		200	19.37	[377]
		88	**81.34**	
PET	**-**	**151**	**48.6**	
		339	**40.67**	
PET/0.025 EGI	0.025	155	37.7	
PET/0.05 EGI	0.05	172	33.9	
PET/0.1 EGI	0.1	156	29.5	
PET/0.2 EGI	0.2	156	14.2	
PET/0.4 EGI	0.4	150	28.1	

[a]Measured at 23 °C and 0% relative humidity; ϕ_c – volume fraction of crystallinity;

Moreover, in this work carbon dioxide and oxygen barrier properties for PTT nanocomposites were studied. Poly(trimetylene terephthalate) is recently commercialized polyester that combines the advantageous properties of polyesters and polyamides with main application field in textile industry. Owing to unique properties such as excellent elastic recovery, high thermal and chemical resistance and dyeability, PTT is now a potential competitor of PBT and PET in textile, packing and engineering thermoplastic markets. PTT is an important candidate for being compounded with various nanoparticles to further broaden its utility [15]. Poly(trimetylene terephthalate) (PTT)/graphene derivatives nanocomposites have been synthesized via *in situ* polymerization, with several different types of graphene derivatives which resulted in exfoliated or intercalated morphology. Table 27 summarizes the carbon dioxide and oxygen permeability of these PTT/graphene derivatives films as a function of volume fraction of filler and nanofiller type. The permeability strongly depends on the morphology of the nanocomposites.

Table 27 Carbon dioxide and oxygen permeability of PTT and PTT/graphene derivatives nanocomposite films

Sample	Wt %	Nanofiller type	CO_2 transmission rate $cm^3/m^2 \cdot 24h$	O_2 transmission rate $cm^3/m^2 \cdot 24h$
PTT	**0**	**-**	**649.6**	**74.3**
PTT/0.05 EG500	0.05	EG 500 µm	35.5	-
PTT/0.1 EG500	0.1	EG 500 µm	105.4	-
PTT/0.3 EG500	0.3	EG 500 µm	254.3	-
PTT/1.0 EG500	1.0	EG 500 µm	101.0	24.7
PTT/0.1 EGII	0.1	EG II	36.2	58.9
PTT/0.3 EGII	0.3	EG II	48.6	39.6
PTT/0.5 EGII	0.5	EG II	44.5	44.8
PTT/0.1 G Ang	0.1	Grafen 1nm	34.53	0.5
PTT/0.3 G Ang	0.3	Grafen 1nm	128.6	0.2
PTT/0.5 G Ang	0.5	Grafen 1nm	368.2	22.3
PTT/1.0 G Ang	1.0	Grafen 1nm	378.6	-

PTT/0.1 FLG	0.1	FLG	28.6	13.7
PTT/0.3 FLG	0.3	FLG	36.7	2.3
PTT/0.5 FLG	0.5	FLG	44.6	2.1

For all nanocomposites based on PTT, significant enhancement in CO_2 and O_2 impermeability has been observed, where four different types of graphenes were used with an average dimension of x & y were as follows: EG500 ~500 μm, EGII from SAS ~50 μm, Graphene from Angstron Materials ~10 μm, and FLG ~ 2 μm. Neat PTT and its nanocomposites exhibited better barrier properties in relation to oxygen than to carbon dioxide. In case of nanocomposites based on PTT with expanded graphite with the largest flakes' size i.e. 500 μm, the lowest CO_2 transmission rate was obtained for the lowest concentration of nanosheets (0.05 wt %). With and increasing content of EG500 an increase in CO_2TR was observed. However, PTT/1.0 EG500 exhibited almost the same value of permeability to carbon dioxide as PTT with as low concentration as 0.1 wt % of EG500. It was due to dispersion quality in case of nanocomposites based on nanofiller with large surface flakes in case of lower concentration. However, an improvement in case of PTT/1.0EG500 was probably due to the large surface area of nanoflakes that were added in large amount. The lower concentration of nanoparticles enables to uniformly disperse nanoplatelets in whole volume of polymer matrix. EGII with flake size of ~50 μm exhibited a strong improvement in CO_2 transmission rate but with an increasing content of this nanofiller, perhaps due to poorer quality of dispersion, a slight decrease in barrier permeability was seen. On the other hand, EGII gave also an enhanced in O2 barrier property, but in this case the lowest OTR was observed for nanocomposite with 0.3 wt % of EGII. An addition of graphene derivatives with smaller flakes' size (FLG, Graphene Angstron) allowed to obtain even better improvement in both CO_2 and O_2 transmission rates. In case of PTT/Graphene Angstron nanocomposites almost a total impermeability to oxygen (0.5 and 0.2 $cm^3/m^2 \cdot 24h$ for 0.1 and 0.3 wt % of nanoplatalets respectively) was observed. Whereas, the lowest CO_2 transmission rate was observed for PTT based nanocomposites with the lowest concentration of Graphene Angstron i.e. 0.1 wt %. An increasing content of this nanofiller showed a decrease in carbon dioxide permeability. Note that for few layer graphene based nanocomposites CO_2TR exhibited the lowest values. Furthermore, the oxygen barrier properties were also at the lowest level. More than 35-folds improvement in O_2 transmission rate was observed for PTT/0.5FLG in comparison to neat PTT.

It can be suggested that an addition of all graphene derivatives used in this PhD thesis enables to obtain nanocomposites that are impermeable to gases like oxygen and carbon dioxide. The smaller concentration in case of nanoflakes with large surface area was a critical factor to obtain proper dispersion that constitute a barrier to the diffusion of the CO_2 and O_2 molecules. However, the greater improvement in barrier properties was achieved for nanocomposites based on nanoplateletes with smaller surface area. Graphene Angstron allows to obtain nanocomposites based on PTT that were almost completely impermeable to O_2 molecules. The diffusion mechanism is not possible when nanosheets were homogenously dispersed, since they create the tortuous paths to gases. In all cases graphene platelets really do act as a barrier to the diffusion paths.

16.5. Influence of graphene on thermal and tensile properties

Effect of graphene derivatives on the thermal stability of the polyester composites (PET, PTT)

The mechanism of the improvement of thermal stability in polymer nanocomposites is not fully understood yet. It is usually well accepted that the improved thermal stability for polymer–graphene nanosheets nanocomposites is mainly due to the formation of char which hinders the out-diffusion of the volatile decomposition products, as a direct result of the decrease in permeability, usually observed in exfoliated nanocomposites**.** In the existing literature [378] [379] [380] it was found that the addition of expanded graphite into the polymer matrix (PVC, PLA) improves the thermal stability in both oxidizing and in an antioxidant atmosphere due to the activity of graphene. Another example of antioxidant activity of graphene, are nanocomposites based on polypropylene and reduced graphene oxide (rGO). Yang et al. [381] have shown that rGO can serve as a promising and multifunctional nanofiller in the preparation of polymeric composites with excellent performance and good thermal stability.

In this work the influence of graphene nanoplatelets on thermal and thermo-oxidative stability of nanocomposites based on PET and PTT measured by thermogravimetric method has been observed. The obtained results are described below, presented in Figures 58 (for PET) and 59 (for PTT) and all data are summarized in Table 28 (for PET) and Table 29 (for PTT).

The studies of graphene influence on thermal and thermo-oxidative stability of PET showed that even so small amount as 0.025 wt % of EG affected the thermo-oxidative resistance of nanocomposite (Fig. 58). Obviously, in an inert atmosphere in the process of degradation occurred at approximately 20°C higher than in an oxidizing atmosphere. The nanocomposite containing 0.1 wt% of graphene nanosheets exhibit the highest temperature of 5 % mass loss in an inert atmosphere. However, the differences between the temperatures corresponding to 5 and 10 weight loss and the temperature of maximum rate of weight loss for obtained PET/EG nanocomposites and unmodified PET at 3 to 5^{o}C are within the measurement error. The values of activation energy (E_a) of thermal decomposition for the PET/EG nanocomposites are higher or comparable-(excluding sample containing 0.05 wt % of EG) to the value determined for neat PET, for both, when the measurement was carried out in an oxidizing atmosphere and in argon. The values of E_a for the measurement carried out in air ranged between 247-268 kJ/mol, while for the measurement carried out in argon these values were in the range 304-318 kJ/mol. The results of research carried out in an oxidizing atmosphere and in argon are presented in Table 28.

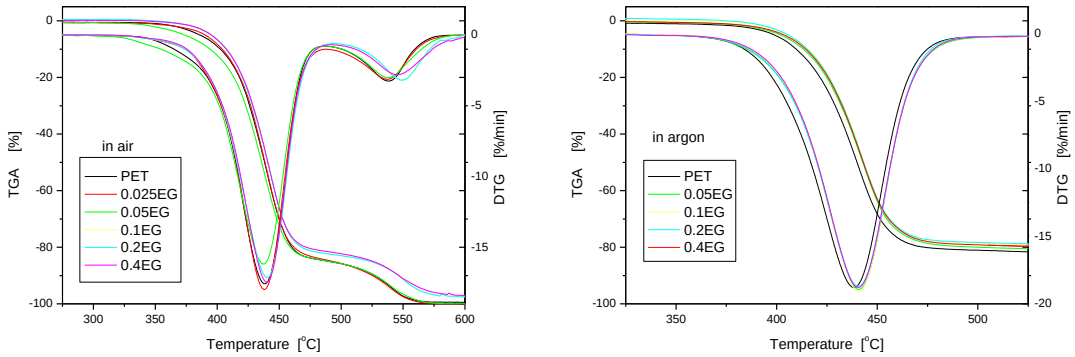

Fig. 58 Weight loss and derivative weight loss versus temperature for the PET/EGI nanocomposites in air (a) and in argon (b) at a heating rate of 10°C/min.

Table 28 Temperatures corresponding to 5 and 10% of weight loss, activation energy and the temperature at maximum of weight loss rate for the nanocomposites obtained in air and argon atmosphere

Symbol	$T_{5\%}$. °C	$T_{10\%}$. °C	T_{DTG1},°C	E_a. kJ/mol	T_{DTG2}. °C
Measurement carried out in an oxidizing atmosphere					
PET	386	402	438	256.42	538
PET/0.025 EG	390	404	438	267.67	537
PET/0.05 EG	372	394	438	226.78	538
PET/ 0.1 EG	382	408	438	247.02	544
PET/ 0.2 EG	381	407	439	255.25	541
PET/ 0.4 EG	381	407	440	268.34	546
Measurement carried out in argon					
PET	399	410	438	287.6	-
PET/0.05 EG	402	413	441	313.6	-
PET/ 0.1 EG	402	413	441	315.8	-
PET/ 0.2 EG	406	415	441	304.9	-
PET/ 0.4 EG	406	415	441	317.7	-

In an oxidizing and inert atmosphere in the thermal degradation process PET/EG nanocomposites showed improved thermal stability. In an inert atmosphere the degradation process does not depend on the participation of EG. It can therefore be assumed that the mechanism of thermo-oxidative stability of PET by graphene sheets is related to the annihilation of free radicals by carbon planes [382] [383]. Probable mechanism of thermal

degradation of PET is the free radical reaction. This phenomenon of improving the stability has also been observed for composites with carbon nanotubes. So it can be assumed that the mechanism of increasing the stability of PET is due to the transfer of free radicals on the carbon planes and its deactivation. Expanded graphite therefore fulfills the role of antioxidant operating at higher temperatures.

The influence of expanded graphite (EGII) on thermal stability of PTT based nanocomposites has been presented in Fig. 59 and in Table 29. As can be seen in Fig. 59 the degradation of neat PTT and PTT/EG nanocomposites followed the same mechanism as previously described for PTT/SWCNTs. Typical thermo-oxidative degradation temperatures of 5 and 10% weight loss in air atmosphere were summarized in Table 29. Overall, the thermo-oxidative degradation temperatures of the neat PTT and PTT/EG nanocomposites in oxygen atmosphere were found to be similar to the corresponding degradation temperatures under the argon gas condition. Furthermore, it should be mentioned that the thermo-oxidative degradation temperatures of nanocomposites in air atmosphere in comparison with the neat PTT are also close to that in argon atmosphere. For the nanocomposite with 0.5 wt % of EG, the thermo-oxidative degradation temperatures corresponding to 5 % and 10 % weight loss are 373 and 381 °C, respectively, are only 2 °C higher than those of neat PTT. However, at the very same time the increase in activation energy of thermo-oxidative degradation determined for first stage was observed. It is believed that the enhancement in the thermal stability of PTT/EG nanocomposites under the oxygen athmosphere might be attributed to the barrier effect of graphene sheets of EG, well dispersed in the PTT matrix, to the volatile decomposed products as well as the oxygen permeating through the nanocomposites. The other explanation for this enhancement might be due to the same mechanism of annihilation of free radicals previously observed and described for PET/EG nanocomposites

TGA curves of neat PTT and its nanocomposites with different EG content under the argon atmosphere are shown in Fig 59 b. Generally, graphene sheets of EG exhibits very high thermal stability with only little weight loss up to 800 °C [384]. However, all nanocomposites show thermal degradation at lower or similar temperatures as neat PTT. Thermal degradation temperatures at 5% and 10% weight loss are given in Table 29. It was found that thermal stability of the nanocomposites examined in argon atmosphere was only slightly enhanced by the incorporation of EG, compared with the neat PTT. For instance, the thermal degradation temperatures for 5% and 10% weight loss of the neat PTT are 373 and 382 °C, while for the nanocomposite with 0.5 wt % EG, they slightly increase to 375 and 383 °C, respectively.

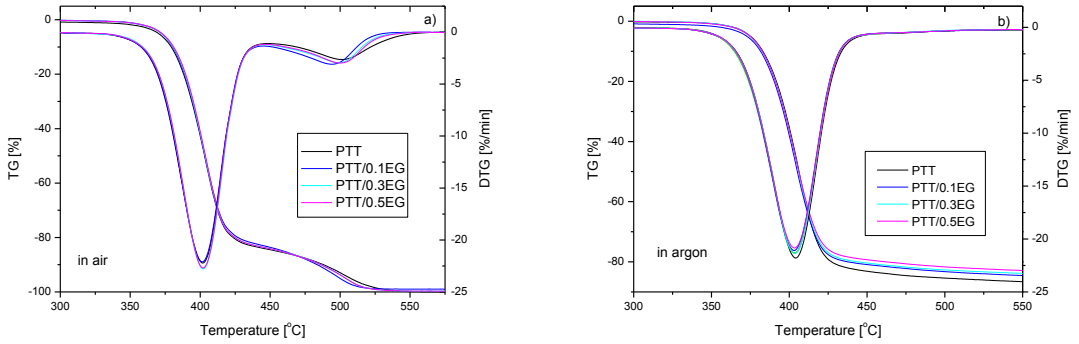

Fig. 59 Weight loss and derivative weight loss versus temperature for the PTT/EGII nanocomposites in air (a) and in argon (b) at a heating rate of 10°C/min.

Table 29 Temperatures corresponding to 5 and 10 % weight loss. activation energy and the temperature at maximum of weight loss rate for the PTT/EG nanocomposites obtained in air and argon atmosphere

Symbol	$T_{5\%}$. °C	$T_{10\%}$. °C	E_a. kJ/mol	T_{DTG1}, °C	T_{DTG2}. °C
Measurement carried out in an oxidizing atmosphere					
PTT	370	379	318.39	401	501
PTT/ 0.1 EG	372	381	323.76	401	494
PTT/ 0.3 EG	373	382	325.72	402	500
PTT/ 0.5 EG	373	381	329.01	402	500
Measurement carried out in argon					
PTT	373	382	331.79	404	-
PTT/ 0.1 EG	373	382	343.47	403	-
PTT/ 0.3 EG	374	382	344.71	404	-
PTT/ 0.5 EG	375	383	337.59	403	-

Effect of graphene on the thermal stability of composites based on the thermoplastic elastomer (PTT-PTMO)

In Table 30 are presented the results for the PTT-PTMO/Graphene Angstron nanocomposites and neat PTT-PTMO block copolymer. Figure 60 shows TGA and DTG curves of prepared nanocomposites with various graphene contents. Mechanisms of thermal and thermo-oxidative degradation of copoly(ether-ester) have been widely discussed in the literature [345], [385]. Destruction of copoly(ether-ester) begins with the flexible segment PTMO. Oxygen mainly affects the carbon atom located in the α position relative to the ether oxygen atom in ether [345]. Detailed studies have been done for PBT-PTMO copolymers, however, for the PTT-PTMO, the mechanism is identical, differing only in decay fragments. The thermal decomposition process of poly(1,4-tetraoksymethylene) (PTMO) chains has a

radical nature and in the initial stage of PTMO chain decomposition is observed the secretion of tetrahydrofurane (THF) aldehydes and low-boiling and volatile alkenes. At temperature 200 ^{o}C occurs the thermal oxidation of PTMO segment with releasing volatile substances. The studies of the effect of graphene content on thermal decomposition of PTT-PTMO nanocomposites proved, that in oxidized atmosphere the thermal degradation process proceeds in two steps and starts at 322 ^{o}C (with 0.1 wt % of graphene) and at 357 ^{o}C (with 0.3 wt % of graphene), whereas in inert atmosphere proceeds in only one step starts at 366 ^{o}C (with 0.1 wt % of graphene) and at 374 ^{o}C (with 0.3 wt % of graphene). Thermal degradation profiles of PTT-PTMO nanocomposites displayed that thermal stability of the nanocomposites was improved with the increase of graphene sheets content up to 1.0 wt %. For the quantitative comparison of thermal stabilities between pure and PTT-PTMO /Graphene composites, the thermal degradation temperatures of 5% and 10% weight losses ($T_{5\%}$ and $T_{10\%}$) were evaluated from the TGA thermograms (Fig. 60) and summarized in Table 30. The $T_{5\%}$ and $T_{10\%}$ of PTT-PTMO block copolymer were determined to be about 331 °C and 352 °C, respectively. In cases of PTT-PTMO/graphene composites the thermal degradation temperatures increased with the increasing of graphene nanoplatalets content. For instance, the $T_{5\%}$ of the PTT-PTMO nanocomposite with 0.3 wt % Graphene Angstron was 357 °C, which is 26 ^{o}C higher than that of PTT-PTMO copolymer. Furthermore, PTT-PTMO nanocomposite with even higher graphene content of 1.0 wt %, where poorer dispersion was found, has higher thermal degradation temperatures than PTT-PTMO copolymer by 23^{o}C. This improved thermal stability of PTT-PTMO/Graphene Angstron nanocomposites is believed to originate from the fact that graphene nanoplatelets, which were dispersed homogeneously in the PTT-PTMO matrix, annihilate free radicals generated during thermal decomposition of polymer matrix in nanocomposite, and thus retarding thermal degradation of the nanocomposites.

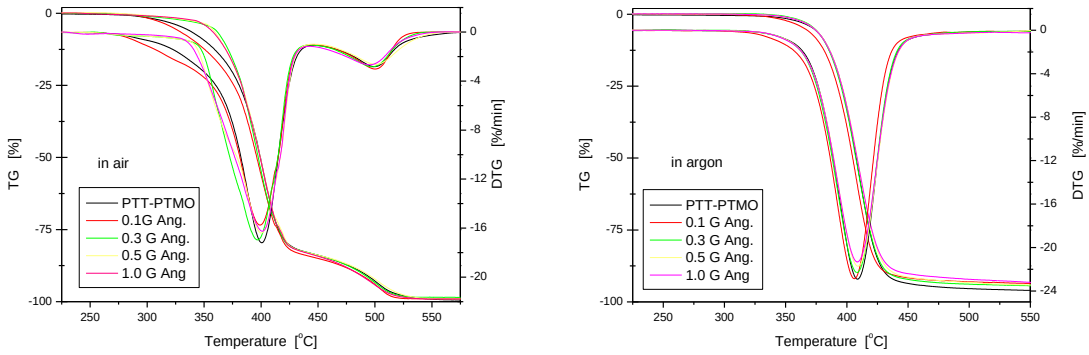

Fig. 60 Weight loss and derivative weight loss versus temperature for the PTT-PTMO/Graphene Ang nanocomposites in air (a) and in argon (b) at a heating rate of 10°C/min.

Table 30 Temperatures corresponding to 5 and 10% weight loss, activation energy and the temperature at maximum of weight loss rate for the PTT-PTMO/Graphene Angstron nanocomposites obtained in air and argon atmosphere

Symbol	$T_{5\%}$. °C	$T_{10\%}$. °C	Ea, kJ/mol	T_{DTG1}, °C	T_{DTG2}. °C
Measurement carried out in an oxidizing atmosphere					
PTT-PTMO	331	352	-	400	499
PTT-PTMO/0.1 G	322	342	-	398	500
PTT-PTMO/0.3 G	357	368	-	397	499
PTT-PTMO/0.5 G	356	365	-	400	501
PTT-PTMO/1.0 G	354	365	-	401	495
PTT-PTMO	371	382	296.4	408	-
PTT-PTMO/0.1 G	366	383	288.9	406	-
PTT-PTMO/0.3 G	374	382	283.1	408	-
PTT-PTMO/0.5 G	373	383	277.6	409	-
PTT-PTMO/1.0 G	373	383	277.7	408	-

Testing the mechanical properties of polyester nanocomposites

The results of uniaxial tensile testing of the obtained PET/EG nanocomposites are presented in Table 31. Figure 61 shows the representative stress–strain curves for neat PET and nanocomposite samples. It was found that the Young's modulus of PET/EG nanocomposites increased noticeably with the EG content. The lowest values of Young's modulus were obtained for 0.025 and 0.2 wt % of EG, however, they were still higher than those obtained for neat PET. The greatest improvement in mechanical strength was obtained for the nanocomposite with the highest concentration of nanoplatalets i.e. 0.4 wt % , as can be seen in Table 31. Since there was only slight increase in degree of crystallinity (DSC measurements, Table 21) and graphene nanoplatelets were dispersed homogeneously in whole volume of polymer matrix (SEM, Fig. 51) it can be concluded that expanded graphite nanosheets acted as the effective mechanical reinforcing nanoparticles.

Table 31 Tensile properties of PET/EG nanocomposites

Sample	E GPa	σ_y MPa	ε_y %	σ_b MPa	ε_b %
PET	2.08 ±0.14	68.8 ± 0.9	3.6 ± 0.2	38.1 ± 9.7	121.3 ± 12.4
PET/0.025 EG	2.15 ± 0.08	74.0 ± 2.9	1.4 ± 0.1	37.1 ± 7.9	268 ± 20.7
PET/0.05 EG	2.46 ± 0.10	70.6 ± 2.9	1.3 ± 0.1	37.3 ± 5.6	116 ± 20.4
PET/0.075 EG	2.41 ± 0.08	69.3 ± 8.7	1.1 ± 0.2	67.8 ± 1.2	47.8 ± 2.9
PET/0.1 EG	2.54 ± 0.05	65.0 ± 5.2	1.1 ± 0.1	65.9 ± 8.3	21.4 ± 3.2
PET/0.2 EG	2.27 ± 0.11	63.7 ± 1.8	1.2 ± 0.1	61.2 ± 3.1	4.1 ± 0.7
PET/0.4 EG	2.67 ± 0.10	62.0 ± 2.9	1.1 ± 0.1	60.8 ± 2.3	3.6 ± 0.3

E–Young's modulus;σ_y-yield strength (elastic limit);ε_y – yield strain, σ_b,ε_b-stress and strain at break respectively

The yield stress of neat PET was measured to be 68.8 MPa, as can be seen in Table 31. For PET/EG nanocomposites, the yield stress increased initially to be 74 MPa at 0.025 wt % EG, and slightly decreased at higher EG contents. It should be noted that the stress at break values of PET/EG nanocomposites with higher concentration of EG are within the measurement error if compared to neat PET. Overall, it is reasonable to conclude that the noticeable improvement of mechanical properties for PET/EG nanocomposites is owing to the reinforcing effect of graphene nanoplatelets dispersed homogeneously in the PET matrix. For PET/EG composites, the strain at break decreased with increasing the expanded graphite content. This large decrease in strain at break of PET/EG nanocomposite can be explained of the hardening effect of graphite nanoplatelets in the PET matrix.

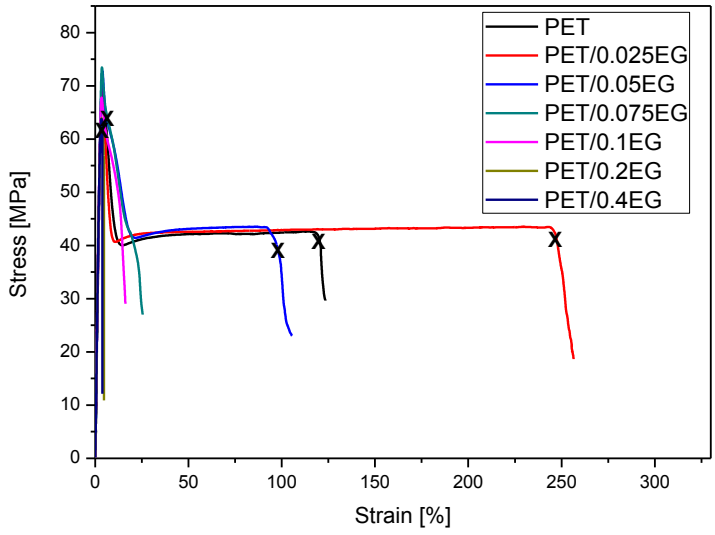

Fig. 61 Representative stress strain curves of PET/EG nanocomposites.

The mechanical behavior of the prepared PTT/EGII nanocomposites is displayed in Figure 62 by representative stress–strain curves and in Table 32 that summarizes the obtained results. As expected, an increase in Young's modulus was observed for all nanocomposite systems investigated. The highest increase was obtained in PTT/0.3EG, probable due to the best dispersion quality in this system. More interesting is the comparison of the strain at break for the different systems, as shown in Table 32.While PTT without nanofiller presents typical stress-stain behavior for semicrystalline polyesters, a clear embrittlement at graphene nanoplatelets concentrations as low as 0.1 wt % that do not preserve the ductile nature of the polymer matrix, was observed. Only a limited enhancement in yield stress can be noticed in Table 32 and it was only observed for the lowest concentration of graphene sheets. The fundamental concept of nanocomposites is based on the high aspect ratios and large interfaces provided by the nanofillers and hence a substantial reinforcement achieved at small loadings. However, the peculiarity of nanofillers to have very high specific surface areas and small dimensions simultaneously leads to a preference for agglomeration in micrometric stacks or bundles due to van der Waals interactions, ionic interaction, and/or hydrogen bonds. Another important issue in nanocomposites is the variation of properties of the polymer matrix induced by nanofillers. In fact, semicrystalline polymers, like PTT, can be relevantly affected in their

crystalline structure as well as in their total crystallinity, as a consequence of the presence of fillers (Tables 22 and 23) and that can result in differences in observed mechanical properties. For comparison purposes, a series of PTT/Graphene Angstron nanocomposites was prepared.

Table 32 Tensile properties of PTT/EG nanocomposites

Sample	E GPa	σ_y MPa	ε_y %	σ_b MPa	ε_b %
PTT	2.36 ± 0.05	53.2 ± 9.5	1.42 ± 0.3	28.6 ± 9.7	178 ± 32.4
PTT/0.1 EG	2.37 ± 0.12	49.3 ± 4.5	1.46 ± 0.1	47.2 ± 6.7	1.89 ± 0.3
PTT/0.3 EG	2.67 ± 0.13	48.6 ± 5.3	0.95 ± 0.2	46.3 ± 5.5	2.28 ± 0.2
PTT/0.5 EG	2.56 ± 0.15	45.3 ± 7.9	0.83 ± 0.4	45.4 ± 7.8	2.09 ± 0.4

E – Young's modulus; σ_y - yield strength (elastic limit); ε_y – yield strain, σ_b, ε_b - stress and strain at break respectively

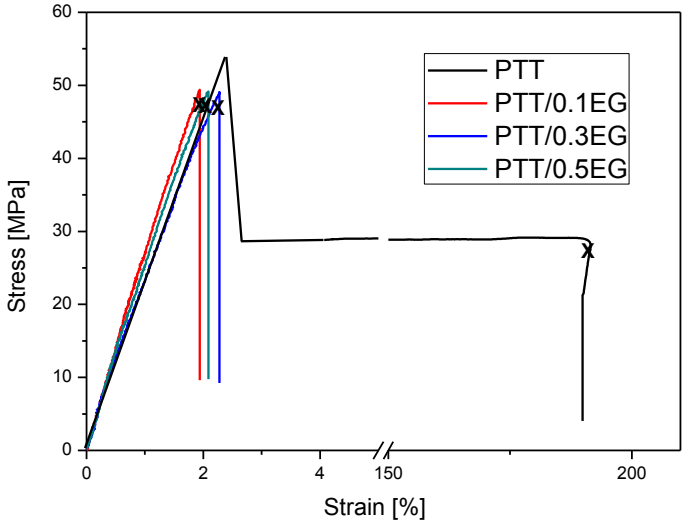

Fig. 62 Representative stress strain curves of PTT/EG nanocomposites.

Representative stress–strain curves and their key tensile property dependence on graphene concentration are shown in Fig. 63 and Table 33. With an increasing content of graphene an obvious increase in yield stress was observed. Only specimen with the highest loading of graphene (1.0 wt %) showed the increase in modulus. However, considerable increase in elongation at break for samples with 0.05 and 0.1 wt % of Graphene Ang but with an increasing loading of nanosheets (higher than 0.01 wt %) a strong decrease was observed. This remarkable effect of graphene at small concentration is related to better dispersion of nanoplatelets and stronger interfacial interaction between the PTT and Graphene Ang. The results of this research underline the promising characteristic of Graphene Angstron, as reinforcement for thermoplastic polymers at lower concentration of nanofiller. Even better results are expected for PTT-PTMO block copolymer containing 50 wt % of PTT rigid segments due to the change between polymer-nanoparticle interactions. Stronger interaction will lead to a dramatic decrease in aggregation, improved dispersion and homogeneity.

Table 33 Tensile properties of PTT/Graphene Ang 1nm nanocomposites

Sample	E GPa	σ_y MPa	ε_y %	σ_b MPa	ε_b %
PTT	2.36 ± 0.05	50.2 ± 9.5	1.42 ± 0.3	28.6 ± 9.7	178 ± 32.4
PTT/0.05 Graphene	2.33 ±0.07	56.5 ± 4.5	0.99 ± 0.1	47.9 ± 3.9	355 ± 23.6
PTT/0.1 Graphene	2.32 ±0.05	55.2 ± 2.4	1.00 ± 0.1	29.6 ± 2.8	255 ± 11.4
PTT/0.3 Graphene	2.26 ± 0.10	55.1 ± 2.2	0.96 ± 0.1	32.1 ± 3.1	43.2 ± 4.1
PTT/0.5 Graphene	2.17 ±0.11	55.1 ± 2.1	0.96 ± 0.1	44.9 ± 3.6	23.2 ± 2.4
PTT/1.0 Graphene	2.42 ± 0.06	59.9 ± 5.2	0.83 ± 0.1	59.9 ± 5.3	2.2 ± 0.1

E – Young's modulus; σ_y - yield strength (elastic limit); ε_y – yield strain, σ_b, ε_b - stress and strain at break respectively

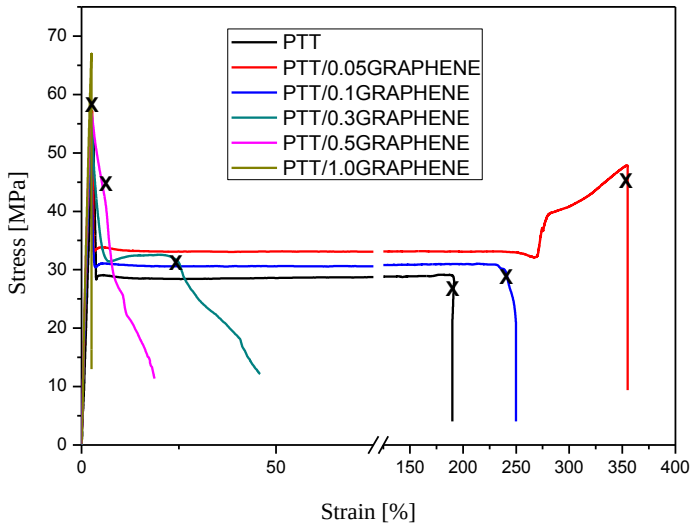

Fig. 63 Representative stress strain curves of PTT/Graphene Ang nanocomposites.

Testing the mechanical properties of nanocomposites based on multiblock copolymer

The tensile properties of PTT-PTMO/Graphene nanocomposites are presented in Table 34 and representative stress-strain curves are shown in Fig. 64. The tensile modulus increases gradually from 118 to 151 MPa with increasing Graphene Angstron content from 0 to 1.0 wt%. The presence of graphene platelets lead to increase also the nanocomposites yield stress and σ(100%) ("modulus at 100%") but yield elongation did not change significantly when compared to the neat PTT-PTMO copolymer, only slight increase was observed. For nanocomposites with 0.1, 0.3 and 0.5 wt % of graphene, the values of elongation at break are higher or comparable to the neat PTT-PTMO copolymer. Only in case of PTT-PTMO/1.0 wt % of graphene a significant decrease in strain at break was observed. As mentioned above, nanocomposites have comparable values of degree of crystallinity (Table 25) with neat PTT-PTMO copolymer. This can indicate that increase of modulus, stress at 100% and yield stress is attributed to the presence of highly exfoliated or intercalated graphene structures and the good interfacial bonding between the graphene sheets and the matrix.

Table 34 Tensile properties of PTT-PTMO/Graphene nanocomposites.

Sample	E MPa	σ(100%) MPa	σ_y MPa	ε_y %	σ_b MPa	ε_b %
PTT-PTMO	118.3 ± 1.5	12.69 ± 0.06	13.6 ± 0.2	44.8 ± 0.9	20.3 ± 0.7	625 ± 12
PTT-PTMO /0.1 G	123.0 ±1.3	12.79 ± 0.06	13.4 ± 0.2	50.4 ± 1.3	20.3 ± 0.1	594 ± 12
PTT-PTMO /0.3 G	131.7 ±4.1	13.10 ± 0.05	13.7 ± 0.1	49.6 ± 0.1	19.8 ± 0.2	594 ± 14
PTT-PTMO /0.5 G	133.0 ±1.7	13.22 ± 0.04	13.7 ± 0.1	48.7 ± 0.1	18.2 ± 0.3	625 ± 23
PTT-PTMO /1.0 G	151.8 ±1.6	13.81 ± 0.03	14.5 ± 0.1	44.8 ± 0.2	13.9 ± 0.1	319 ± 53

E – tensile modulus; σ(100%) – stress at strain of 100%; σ_y, ε_y – yield stress and strain respectively, σ_b, ε_b - stress and strain at break respectively

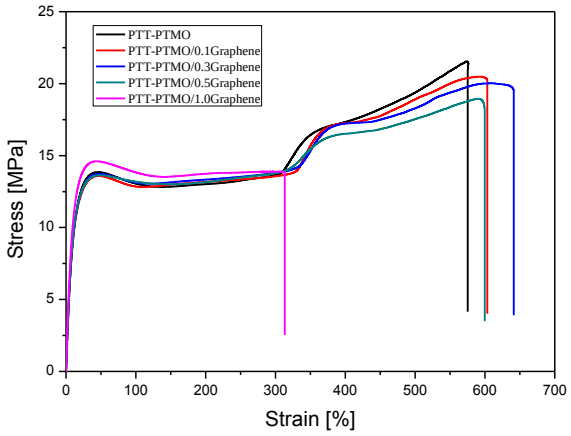

Fig. 64 Representative stress strain curves of PTT-PTMO/Graphene Ang nanocomposites.

17. Hybrid carbon nanofillers/polymer nanocomposites

Research on polymer nanocomposites has exploded over the last few years. The prospect of a new materials technology that can perform as a low-cost alternative to high-performance composites for applications ranging from automotive to food packaging to tissue engineering has become irresistible to researchers around the world.

This PhD thesis is part of a larger project on the development of conducting composites with enhanced mechanical properties based on different polymer matrices (thermoplastic polyesters and thermoplastic elastomers) and hybrid composition of carbon nanotubes and graphene nanoplatelets (i.e expanded graphite, graphene, few layer graphene etc.). The introduction of layered nanofillers (such as graphene nanoplatelets, with one dimension in the order of the nanometer range) or fibrous nanofillers (such as carbon nanotubes, with two dimensions in the order of the nanometer scale) has opened a new area of research. The improvements of properties using such nanofillers are really important, even if not completely understood. Polymer-based nanocomposites, and especially polymer graphene nanoplatelets and/or carbon nanotube nanocomposites, represent a radical alternative to conventionally filled polymers. Because of the dispersion of nanometer-size sheets and/or tubes, these nanocomposites exhibit markedly improved properties when compared with unfilled polymers or conventional microcomposites.

In this thesis, thermoplastic polyester-based (PET, PTT) and elastomer-based (PTT-PTMO block copolymer) nanocomposites containing hybrid fillers of CNTs and graphene

derivatives were developed, aiming at enhancing the electrical conductivity of composites with balanced mechanical properties and lowering the cost of the final product. The electrical and mechanical properties of the nanocomposites were evaluated and favorably compared with those of neat polymer matrices and those containing either CNTs or graphene nanoplatelets alone.

17.1. Morphology of polymer matrix vs. hybrid 1D/2D type of carbon nanoparticles

The distribution of the nanofillers in the polymer matrices (PET, PTT and PTT-PTMO) and their mutual interactions were studied using imaging techniques, scanning electron microscopy (SEM) and transmission electron microscopy (TEM).

Nanofiller dispersion is a well-known challenge since CNT and graphene nanoplatelets have an inherent tendency to agglomerate and good dispersion is an important factor for mechanical reinforcement and creation electrical percolation paths. The main reasons behind agglomeration is the van der Waals attraction and the large surface areas of the nanofillers [386], for graphene nanosheets additional π-π bonding also accounts for the stacking of the individual sheets. All nanofillers (1D- nanotubes and 2D- graphene derivatives) were mixed using procedures as written before for single nanofiller and followed by mixing together for another 30 min (15 min with speed stirrer and 15 min with ultrasounds) to avoid agglomeration before synthesis process.

In Fig. 65 a and c a good distribution of the graphene sheets with agglomerates of carbon nanotubes were observed. Both SEM and TEM analysis confirmed that expanded graphite was well dispersed, but nanotubes due to lots of impurities were entangled with one another and create aggregates. The morphology of fractured surfaces depicts the intimate contact and high embedding with polymer matrices, indicating good interfacial bonding between nanoplatelets and PET matrix. Interestingly, some of the nanoplatelets dispersed almost as a monolayer as indicated in figure 65 c (almost completely transparent nanosheets). In general, nanoplatelets can be easily attracted to each other due to their very high specific surface area and high surface energy. From the cryo-fractured surface (Fig. 65 a) and ultramicrotomed films (Fig. 65 c) it can be seen that the nanoplatelets are well dispersed as thin nanoplatelets. It indicates that the employed mechanical stirring plus the ultrasonic treatment approach was proven to be an effective approach to obtain composites with well-dispersed nanoplatelets in the PET polymer matrix. Importantly, the whole process of preparation the dispersion is carried out just before polymerization reaction, which made the processing simple and effective. In another way, one can say that, during dispersion process, the PET molecules could more sufficiently intercalate galleries of nanoplatelets during *in situ* polymerization, and as the intercalation process proceeds further, the exfoliated graphene sheets might be further delaminated and exfoliated, which would allow more polymer molecules to enter and enlarge the space between them. However, the agglomeration of SWCNT was observed. The agglomerates of SWCNT disturbed the good connection between graphene nanoplatelets. This might be an explanation of efficiency of using high speed stirrer and ultrasounds. However, in case of PET hybrids agglomerates of SWCNT caused that prepared nanocomposites weren't conductive (chapter 17.3, pages 134-136) even with the

concentration of 0.1 wt % of EG, wherein in the nanocomposites, based on PET with EG only, the percolation threshold was obtained at 0.05 wt %.

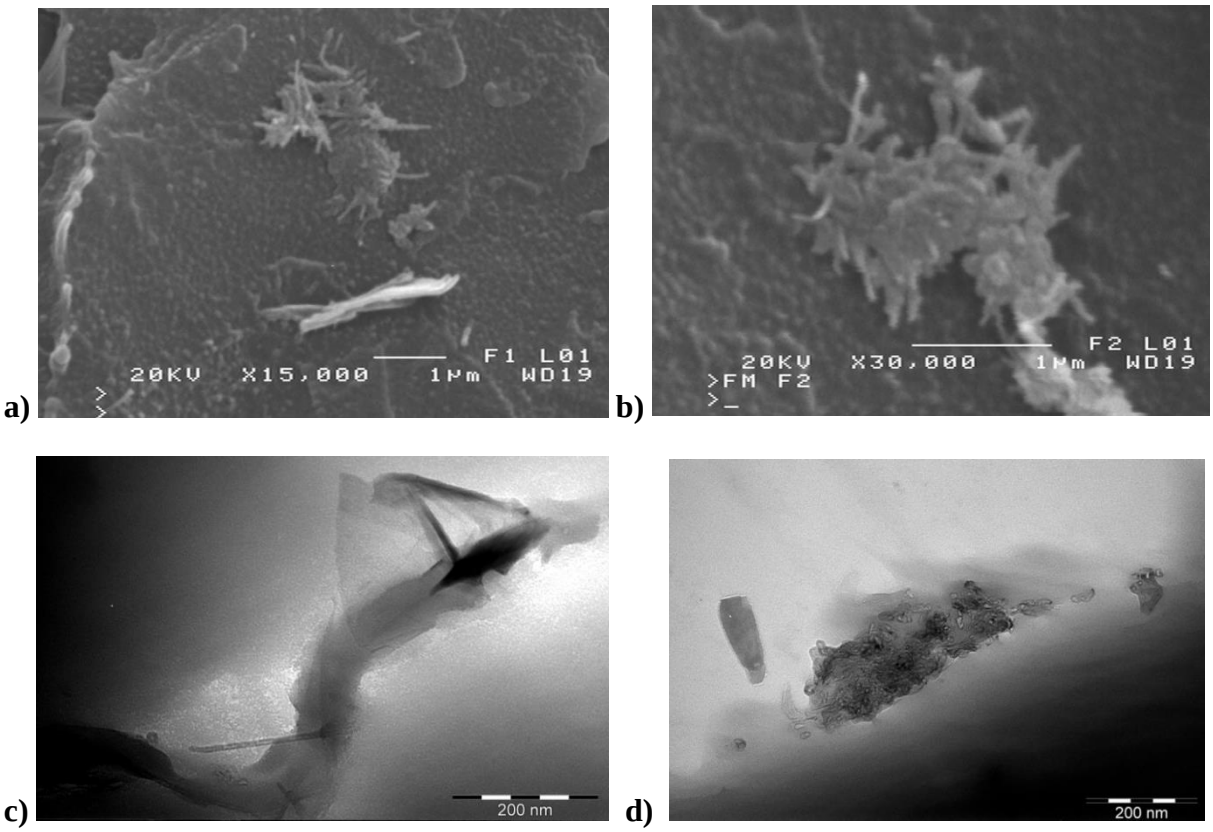

Fig. 65 Scanning and transmission electron micrographs of PET/0.1EG+0.05SWCNT nanocomposite: a) SEM with visible agglomerate of carbon nanotubes; b) SEM of zoomed in agglomerate of SWCNT in polymer matrix; c) TEM at 250 000x and d) TEM at 200 000x.

SEM and TEM were used to visually evaluate the degree of exfoliation and the amount of aggregation of nanofillers in poly(trimetylene terephthalate) matrix. TEM analysis tends to support the findings from SEM but also shows that the SWCNT nanoparticles are well dispersed on the nanoscale in all systems. The efficiency of the hybrid system in modifying the properties of the matrix polymer is primarily determined by the degree of its dispersion in the polymer matrix. The aggregated EG morphology can be characterized with SEM. Because of the difference in scattering density between the nanofiller and PTT, nanoplatelets aggregates can be easily imaged in SEM. However at the same time well-dispersed carbon nanotubes are clearly visible. More direct evidence of the formation of a true nanocomposite is provided by TEM of an ultramicrotomed section. Figure 66 a shows micrograph of PTT hybrid containing different 0.1EG+0.05SWCNT. The dark regions in the photograph are the thicker agglomerates of expanded graphite (less expanded), and the brighter regions show the better dispersed sheets. TEM photography proves that some graphene layers were dispersed homogeneously into the matrix polymer, however mostly clusters or agglomerated particles were detected. This will be cross-checked by ultimate strength and initial modulus in the tensile property section. The SEM and TEM micrographs in Fig. 66 for the hybrid nanocomposite with 0.1EG and 0.05SWCNT KNT 95 indicates that

electrical conducting networks were formed by well-dispersed carbon nanotubes. Incorporation of 0.1 wt % of EG did not make much change in the morphology and electrical conductivity (Fig. 75 b), with some isolated graphene sheets (Fig. 66 a). There was no improvement in electrical conductivity in hybrid system because SWCNT were the main contributor for the formation of network.

.

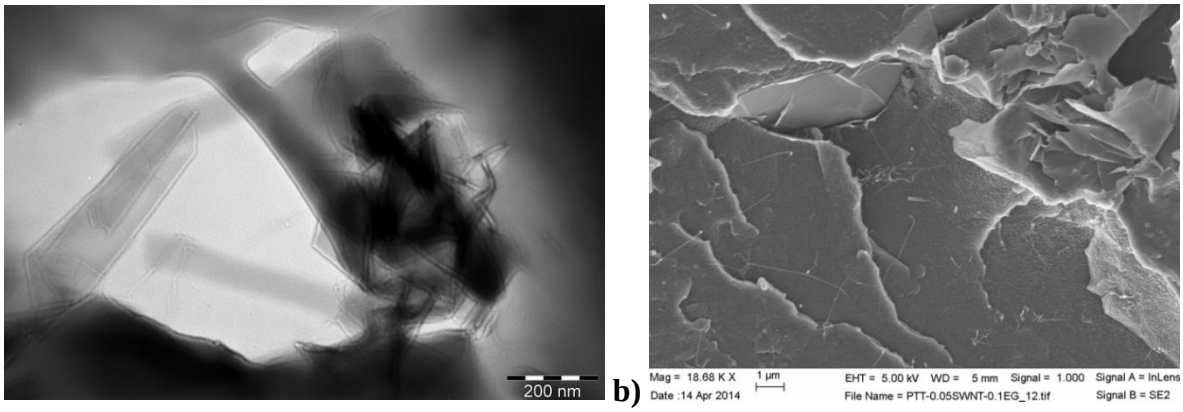

Fig. 66 Transmission electron micrograph at 150 000x (a) and scanning electron micrograph (b) of PTT/0.1EG+0.5SWCNT nanocomposites.

As it was mentioned before, the strong intertube attraction between carbon nanotubes is one of the main problems to overcome making the dispersion of CNTs in polymer matrices challenging and hence limit its effective use as nanofiller in polymer matrix. Many approaches to overcome the affinity of the tubes result in excessive modification or even damage to the unique morphology of the CNTs. An efficient alternative to tailor the polymer/CNT interface while preserving the integrity of the tubes is mixing carbon nanotubes together with the nanofiller with different shape (plate-like shape). In Fig. 67 we observe a good distribution of the CNT on the surface of the graphene platelets which should together act as a stronger reinforcing agent for the polymer causing synergistic effects in electrical conductivity and mechanical properties. The uniformly dispersed bright dots and lines are attributed to the ends of the broken PTT-PTMO-wrapped SWCNTs/Graphene clearly observed due to their high electrical conductivity. For use in the CNT, graphene nanoplatelets mixture samples were hitched to the CNTwalls to facilitate better attachment to the defect sites and residual oxide groups on the Graphene Angstron surface and also to the elastomer matrix. The dual-filler strategy appears to yield a more efficient dispersion of SWCNT+Graphene-PTT-PTMO. The formation of conducting networks (chapter 17.3, page 134-139) and dispersion state in the composites with hybrid CNT - graphene particles was further confirmed by transmission microscopy.

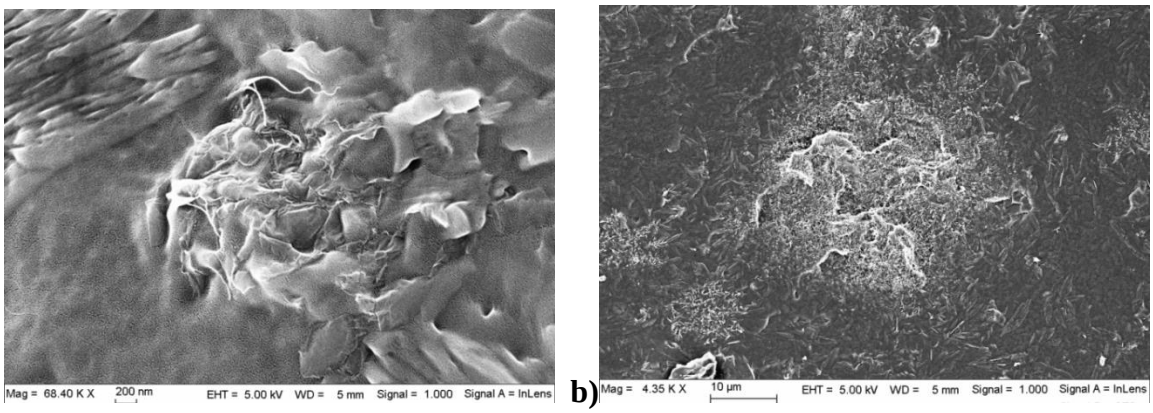

Fig. 67 SEM micrographs of PTT-PTMO/0.1SWCNT+0.3Graphene hybrid nanocomposites.

The TEM images in Figure 67 (with two different magnifications) present the real distribution of conducting fillers in the respective nanocomposites. They may shed some insight into the mechanisms behind the synergy in enhancing the conductivity of nanocomposites due to the hybrid fillers of CNT and graphene platelets. In Fig 68 a there were both randomly dispersed individual CNTs and a round CNT agglomerate but also well-dispersed graphene sheets. In some places carbon nanotubes and graphene plates seemed to connected to one another. It is better seen in Fig. 68 b, were the dispersion of both nanofiller was even better and only nanotubes "hitched" to graphene planes were observed. This should be the reason why the hybrid nanocomposites filled non-conductive Graphene Angstron and SWCNT achieved enhanced electrical conductivity (chapter 17.3, page 134-139) in comparison to PTT-PTMO composite with 0.1 wt % of SWCNT.

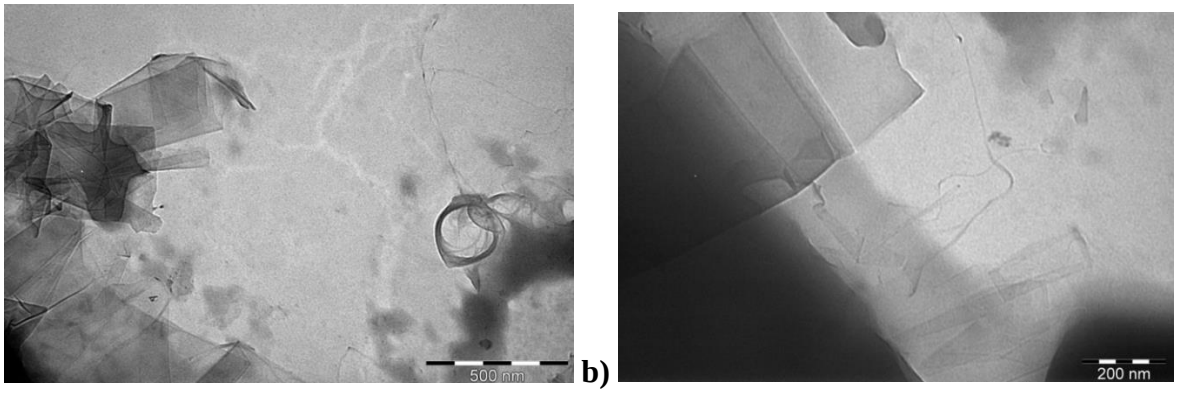

Fig. 68 Transmission electron microscopy (TEM) micrographs of PTT-PTMO/0.1SWCNT+0.3Graphene Ang nanocomposites at a) 100 000x and b) 150 000x.

The SEM images of the PTT-PTMO/0.3SWCNT+0.1 Graphene Angstron are shown in Fig. 69. Both the SWCNTs and Graphene Angstron show fairly good distribution in Fig. 69 c and d. The graphene nanosheets in Figure 69 appear to show better dispersion than those in the PTT-PTMO/Graphene in Figure 54. This indicates that co-addition of SWCNT improves the dispersion of graphene nanoplatelets, which agrees with the electrical conductivity results that exhibit conductivity improvement by the coaddition of SWCNT. However, because of the van der Waals interactions, the as-reduced graphene sheets tend to form irreversible agglomerates and even restack to form graphite (Fig. 69 b). Additionally, the SEM image of PTT-PTMO/SWCNT+Graphene in Figure 69 (c and d) show that the SWCNTs and graphene

nanoplatelets form some kind of network structure. The SWCNTs appear to a have good affinity for Graphene Angstron. This kind of conductive network formation due to graphene nanosheets may explain the good electrical conductivity results from PTT-PTMO/0.3SWCNT+0.1Graphene Angstron (chapter 17.3, pages 134-139).

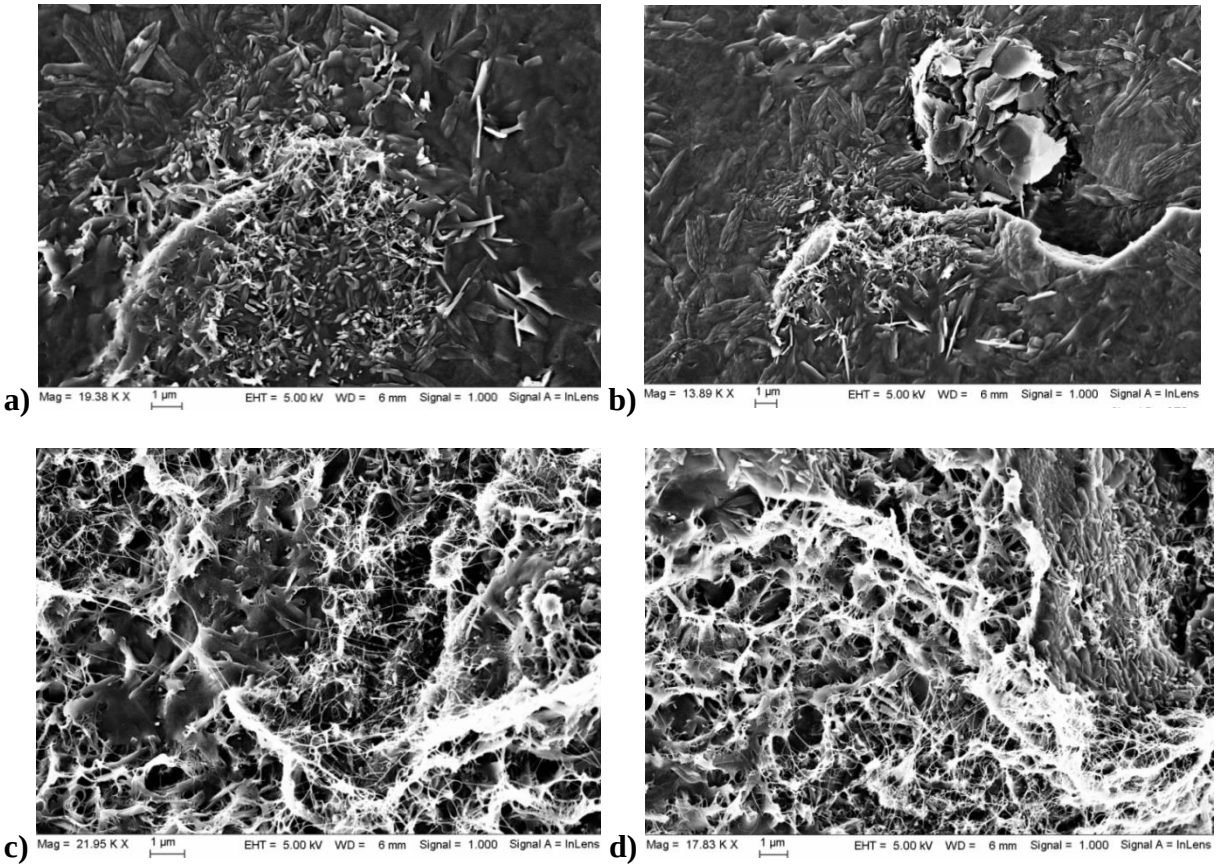

Fig. 69 SEM micrographs of PTT-PTMO/0.3SWCNT+0.1Graphene hybrid nanocomposites.

To examine exactly the dispersion of the SWCNT/graphene in the polymer hybrids, TEM studies were carried out. A TEM allows a qualitative understanding of the internal structure through direct observation. Typical TEM photographs for hybrids with 0.3 wt % of SWCNT and 0.1 wt % of Graphene Angstron are shown in Fig. 70 a (lower magnification) and 70 b. Fig. 70 a shows that both nanofillers were well dispersed in polymer matrix, although some parts of agglomerated layers still exist. To observe the agglomerated structures of 1D+2D hybrid system the TEM micrograph were done at higher magnification. Here agglomerates of CNTs strongly connected to agglomerates of graphene nanoplatelets were seen. However, also some single nanotubes were observed. Interestingly, with the concentration of 0.1SWCNT+0.3 graphene sheets more homogenously dispersion was observed. On the other hand, the "pull-out" mechanism of SWCNTs has been observed in Fig 69 c and d. Carbon nanotubes counteracted the break of polymer matrix, which is clearly seen at higher magnification. In this case, higher concentration of SWCNT:Graphene (3:1) seemed to create more agglomerates than in case of SWCNT:Graphene (1:3). However, a few studies suggest that CNT agglomeration could favor the formation of a percolating network [86] [92] [387]. As observed from these figures, agglomeration promotes CNT-to-CNT and CNT-

Graphene interactions through surface contact (or tunneling) and hence it should increase the electrical conductivity of the composite, as it will be further discussed.

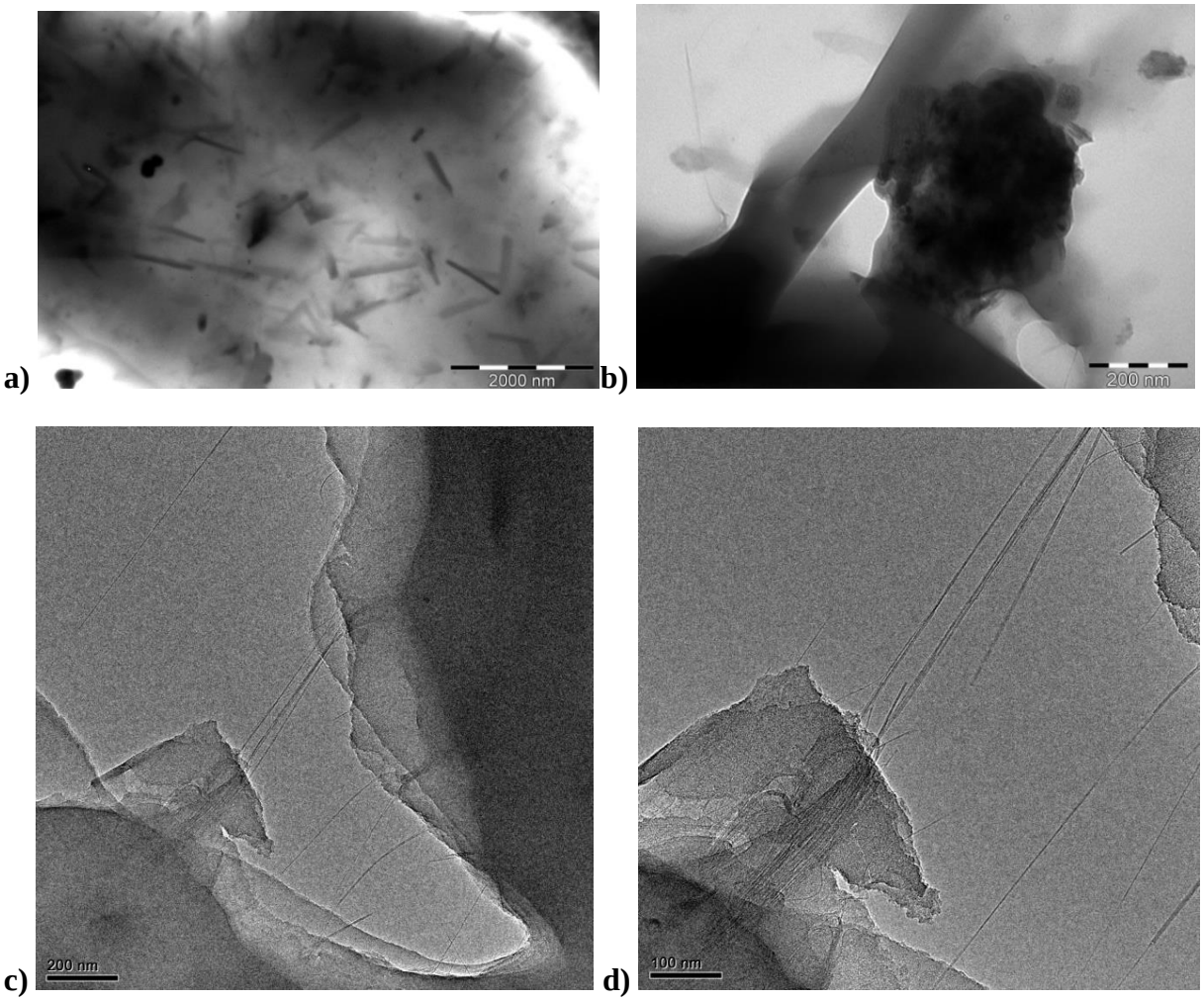

Fig. 70 Transmission electron microscopy (TEM) micrographs of PTT-PTMO/0.3SWCNT+0.1Graphene Ang nanocomposites at a) 25 000x , b) and c) 150 000x and d) 175 000x.

17.2. New concept of phase structure

A new generation of hybrid nanostructured materials signifies an emerging field in the frontier between materials science, life science, and nanotechnology. The development of polymer nanocomposites has been a significant area of research and has evolved significantly over the last two decades owing to the ability of nanoscale reinforcements to create remarkable property enhancements at relatively low filler concentrations, compared to conventional composites. The growth of different types of nanomaterials starting from nanoclays, cellulose nanowhiskers, carbon nanofibers, carbon nanotubes (CNTs), graphenes, nano-oxides like nanosilica, nanoalumina, titanium dioxide etc. has led to the development of composites with extremely attractive macroscopic properties– multifunctional in most circumstances depending on their inherent characteristics. Excellent electrical, thermal, mechanical, optical, fire-retardant, barrier, anti-bacterial and scratch resistant properties of these composites have been reported and the results are only getting better with time.

Carbon based nanomaterials are highly attractive due to their ability to transition an insulating polymer matrix to a conductive composite, in addition to the proven advantage in achieving excellent structural properties. CNTs stand out among the other carbon based fillers like carbon fibers or carbon nanofibers which require higher filler loading fractions to exhibit similar levels of electrical conductivity. Graphene tipped to be a strong competitor for the CNTs on the other hand is still in its infancy, and large production volumes of these materials is still challenging. Interesting from this point of view is to prepare the mixture of both types of this carbon nanofiller. The potential of CNT/graphene derivatives as fillers for multifaceted product development in polymer matrices certainly tilts the tide in its favour compared to its competitors. Due to the renowned challenge involved with dispersing the hybrid system of CNT/graphene derivatives in thermoplastic matrices for good macroscopic properties of the composites, thermoplastic composites with nanofillers is the main focus of attention in this chapter of PhD thesis. The influence of 2D+1D carbon nanofillers on three different polymer matrices i.e. PET, PTT and PTT-PTMO has been investigated.

The physical properties of PET/SWCNT+EGI nanocomposites i.e. intrinsic viscosity, density and weight degree of crystallinity estimated from density measurements are presented in Table 35, which shows that there was almost no influence on intrinsic viscosity (average viscosity molecular weight) with the amount of hybrid nanofiller system as compared to that of the neat PET. Moreover, the glass-transition temperatures of PET/SWCNT+EG (Table 36) increased slightly with the amount of both nanofiller if compared to "single" nanocomposites, and showed no change if compared to pure PET. No increase in the glass-transition temperature of PET/SWCNT+EG could be a result of two factors: a molecular weight of PET and in the nanocomposites remains at the very same value and there was no retardation on the PET molecule main-chain motion by the hybrid system. However, the density measured at 23 ^{o}C increased with the increasing content of SWCNT/EG. The lower crystallinity seen in the hybrid nanocomposite in comparison to PET/0.1EG and PET/0.05SWCNT, may be due to the hindrance of PET chain mobility in the presence of two types of carbon nanostructures which resulted in more thinner crystallites. More information about the influence of EG and CNTs in comparison to CNTs+EG can be obtained from DSC measurement (Fig. 71, Table 36).

Table 35 Physical properties of PET/SWCNT Cheaptubes + EGI nanocomposites

Sample	[η] dl/g	M_v x 10^4 g/mol	d g/cm^3	Xc_w %
PET	0.553	2.21	1.337	10.6
PET/0.05 EG	0.556	2.23	1.338	11.7
PET/0.1 EG	0.550	2.19	1.346	24.2
PET/0.05 SWCNT+0.05EG	0.560	2.25	1.345	22.1
PET/0.05 SWCNT+0.1EG	0.550	2.19	1.343	22.1
PET/0.05 SWCNT	0.611	2.54	1.354	35.7

M_v - viscosity average molecular weight ; d - density measured at 23 ^{o}C, Xc_w weight degree of crystallinity estimated from density measurement

The non-isothermal melt crystallization of neat PET and its nanocomposites at low SWCNT-EG contents was studied using DSC to investigate the effect of the presence and concentration of hybrid system of nanofillers on the crystallization of PET. Table 36 summarizes the data derived from the DSC cooling curves from the melt of neat PET and its nanocomposites at the rate of 10 ^{o}C/min.

The neat PET shows a crystallization peak temperature 214 ^{o}C with a crystallization enthalpy (ΔHc) of around 46.9 J/g. The Tm values shifts to lower values with the addition of EG only and SWCNT only and increased slightly with an addition of both carbon nanofillers but still remaining Tm values below Tm of neat PET (Fig 71). Considering a value of 140 J/g for the melting enthalpy of 100% crystalline PET, the degree of crystallinity for neat PET, and PET with 0.05 and 0.1 of EG, 0.05 of SWCNT and 0.05+0.05 and 0.05+0.1 of SWCNT+EG nanocomposites was determined to be 33.5, 35.3, 36, 38, and 35.8 for both hybrid nanocomposites, respectively. The result obtained for the highest concentration suggested that the addition of hybrid system caused no appreciable change in the Tm and x_c that remained comparable to nanocomposites with SWCNT and EG only. This implies that the addition of SWCNT together with EG cancels out the reported nucleating effect of SWCNT on PET crystallization. All these data suggest that neither SWCNTs nor EG exert a nucleating effect on PET in the nanocomposites. In particular, the presence of the SWCNT-EG may in fact impede the diffusion and rearrangement of the long polymer chains due to the interaction between both components (i.e. SWCNTs and EG) and the PET matrix, thereby delaying the overall crystallization process. Such imperfections in crystalline structure may also explain the lower melting points observed for the nanocomposites.

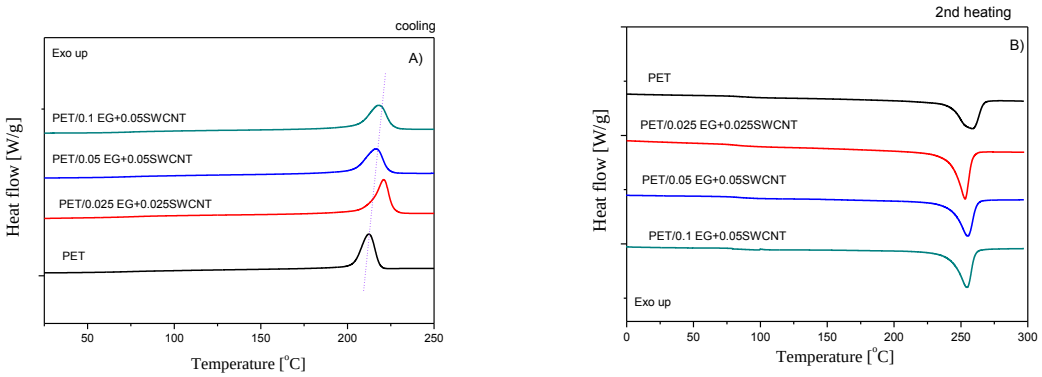

Fig. 71 DSC thermograms for PET and PET/SWCNT+EGI nanocomposites during the cooling and 2nd heating

Table 36 Thermal properties of neat PET and PET/SWCNT+EG nanocomposites determined by DSC

Symbol	T_g	ΔCp	T_m	ΔH_m	T_c	ΔH_c	X_c
	°C	J/g°C	°C	J/g	°C	J/g	%
PET	85	0.13	257	47	214	46.9	33.5
PET/0.05 EG	83	0.17	253	49.4	210	49.1	35.3
PET/0.1 EG	83	0.15	252	50.5	214	49.8	36.0
PET/0.05 SWCNT+0.05EG	85	0.13	255	50.2	216	49.9	35.8
PET/0.05 SWCNT+0.1EG	85	0.13	256	50.1	218	49.3	35.8
PET/0.05 SWCNT	83	0.18	252	53.5	220	53.2	38.0

T_g - glass transition temperature;-T_m - melting temperature; T_c - crystallization temperature ΔH_m, ΔH_c - enthalpy of melting and crystallization; x_c - mass fraction of crystallinity determined from DSC

Table 37 presents the intrinsic viscosity and density of PTT based nanocomposites with SWCNT only, EG only and with hybrid mixture of both of this nanofillers. For PTT/EG nanocomposites the decrease in [η] was observed. On the other hand, the addition of SWCNT to PTT matrix caused increase in [η], and thus causing an increase in molecular weight. There was no significant effect of the addition of carbon nanoparticles on molecular weights of prepared nanocomposites which are within the range of 38 100 and 39 600 g/mol and they are comparable to the molecular weight obtained for neat PTT i.e 38 400 g/mol. In both cases, it was observed that carbon nanotubes determined both morphology and conductivity, without apparent effect agglomerates of EG.

Table 37 Physical properties of PTT/SWCNT KNT 95 + EGII nanocomposites

Sample	[η]	M_v x 10^4	d	Xc_w
	dl/g	g/mol	g/cm^3	%
PTT	0.781	3.84	1.323	19.8
PTT/0.1 EG	0.777	3.81	1.328	23.4
PTT/0.05SWCNT+0.1 EG	0.782	3.85	1.322	18.9
PTT/ 0.1SWCNT+0.1 EG	0.789	3.90	1.313	12.2
PTT/0.05 SWCNT	0.798	3.96	1.329	24.6
PTT/0.1 SWCNT	0.784	3.85	1.324	20.6

M_v - viscosity average molar weight ; d – density; Xc_w weight degree of crystallinity estimated from density measurement

On the other hand, the density for both hybrid nanocomposites decreased with the increasing content of SWCNT. At the same time the weight degree of crystallinity strongly decreased if compared to neat PTT but also to "single" nanocomposites. These results indicated that the incorporation of appropriate amount of SWCNT/EG nanoparticles had strong effects on the degree of crystallinity of PTT. The effect of the presence of SWCNTs on non-isothermal crystallization behaviour of PTT nanocomposites observed here, is in contrast to the results reported in literature for PTT composites containing MWCNT [15], where the presence of MWCNT decrease crystallization rate of PTT in composites.

Figures 72 a and b show the DSC traces during cooling and 2nd heating for neat PTT and PTT/SWCNT+EGII hybrid nanocomposites. Furthermore, the glass transition temperature (T_g) data helps in understanding the effects of hybrid system of particles on the movement of polymer chains. DSC showed no influence in the glass transition temperature (T_g) of the nanocomposite prepared by *in situ* polymerization as compared to neat polymer and nanocomposites with "single" nanofillers (Table 38). At low concentration of nanofillers no influence on T_g and Tm has been observed. Furthermore, the degree of crystallinity also hasn't changed much with the addition of nanoparticles. Composites exhibited the values of x_c 1.4-2 % higher than neat PTT. In contrast, a significant effect was observed on the rate of crystallization. The results for PTT/SWCNT+EGII nanocomposites are listed in Table 38. The DSC thermograms recorded during the cooling of the samples from melt with a constant cooling rate showed a prominent crystallization exothermic peak. The crystallization temperatures T_c and the ΔHc values for PTT/SWCNT+EGII nanocomposites are higher than those of neat PTT in both two compositions. The PTT/0.1SWCNT+0.1EG exhibited the highest Tc value (184^{o}C) of the prepared nanocomposites. Changes in the crystallization peak width and the heat of crystallization (ΔHc) are related to the overall crystallization rate and the extent of crystallization, respectively. The Tc peak widths for both hybrid nanocomposites are narrower than that of neat PTT. On the other hand, the values of H_c for hybrid nanocomposites are larger than that of PTT (36.2 J/g), however they slightly decrease with increase in the SWCNT content.

From these results, it can be concluded that 0.1SWCNT+0.1EGII exhibits a strong heterophase nucleation effect on PTT crystallization due to its enormous surface area of both carbon nanofillers. The crystallization rate of PTT may be accelerated by the addition of this two nanofillers of 0.1 wt % SWCNT and 0.1 wt % of EG where the acceleration efficiency probably reaches a maximum at this level. In both systems (0.1+0.05 and 0.1+0.1), EGII together with SWCNT is an effective nucleating agent due to the high surface area of graphene platelets and their chemical affinity for the polymer, which induce a nucleation and lamellar ordering effect.

Figure 72 b depicts the heating runs of neat PTT and PTT/SWCNT+EGII hybrid nanocomposites. There is an endothermic melting peak on all of the heating scans. The values of melting parameters (T_m and ΔH_m) are summarized in Table 38. The T_m values are nearly unchanged, regardless of hybrid system loading. The melting temperatures and melting peak width are related to the lower thermal stability and the distribution of crystallites, respectively. The temperature of melting is not significantly affected, regardless of hybrid nanofillers loading. A clear decrease in melting peak width is found in the nanocomposites with respect to neat PTT. In other words, the distribution of crystallites of PTT in PTT/SWCNT+EGII

nanocomposites is narrower and higher (about 1.4-2%) than that of neat PTT. The values of ΔH_m for all nanocomposites are negligible larger (46.9-48.7 J/g) than that of PTT (45.8 J/g). However, they decrease with increasing content of SWCNT in hybrid system. This reveals that the degree of crystallinity of PTT slight increases with the addition of carbon nanotubes together with expanded graphite but at the same time decrease with the increasing content of SWCNT KNT 95.

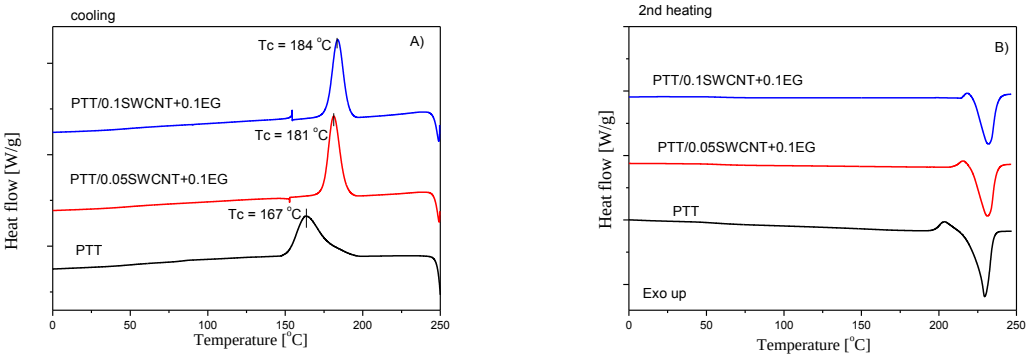

Fig. 72 DSC thermograms for PTT and PTT/SWCNT+EGII nanocomposites during the cooling and 2nd heating.

Table 38 Thermal properties of neat PTT and PTT/SWCNT+EG nanocomposites determined by DSC

Symbol	T_g °C	T_m °C	ΔH_m J/g	T_c °C	ΔH_c J/g	X_c %
PTT	53	231	45.8	167	46.2	31.4
PTT/0.1 EG	53	230	47.9	180	47.1	32.8
PTT/0.05SWCNT+0.1 EG	53	231	48.7	181	47.9	33.4
PTT/ 0.1SWCNT+0.1 EG	53	232	46.9	184	46.8	32.1
PTT/0.05 SWCNT	53	232	48.2	183	47.9	33.0
PTT/0.1 SWCNT	53	231	48.4	180	48.7	33.2

T_g - glass transition temperature;-T_m - melting temperature; T_c - crystallization temperature ΔH_m, ΔH_c - enthalpy of melting and crystallization; x_c - mass fraction of crystallinity determined from DSC.

To compare the results already described for hybrid nanocomposites based on PTT, the series of hybrid nanocomposites based on multiblock poly(ether-ester) copolymer with PTT as a rigid segment were synthesized via *in situ* polymerization. The synthesized PTT have viscosity average molecular weight (M_v) of 38 400 g/mol. The Mark–Houwink constant are not known for PTT– PTMO copolymers, therefore values of [η] were used for comparison purpose. The measured values of intrinsic viscosity for PTT-PTMO copolymer

(1.325 dl/g) and PTT-PTMO hybrid nanocomposites (1.299-1.322) dl/g for three hybrids with increasing content of SWCNT) suggest that molecular weights of the polymers under study should be reasonable high. The presented in Table 39 values of intrinsic viscosity, melt viscosity and density are dependent on the sample composition. The value of [η] slightly decreased with addition of nanofillers, but with the increasing content of SWCNT and graphene platelets, this value increased.

In Fig 73., it is clearly seen that the addition of SWCNTs strongly affected the melt viscosity of PTT-PTMO nanocomposites. On the other hand, no such behavior is observed when graphene nanoplatelets were added to the polymer (Fig. 57). Since the addition of nanotubes greater effect on the viscosity of the composition, if compared to the hybrid nanocomposite PTT-PTMO/0.1SWCNT+0.3Graphene with the same amount of SWCNTs (0.1 wt%), even slight increase was observed. The same observations were done for the nanocomposite with 0.3 wt % of SWCNTs. It can be concluded, that in case of PTT-PTMO hybrid nanocomposites, the mixture of both nanofiller stronger affected the melt viscosity of the polymer than when only graphene and nanotubes were added.

Density of PTT-PTMO hybrid nanocomposites slightly increased with addition of nanofillers. Since the obtained hybrid nanocomposites showed density values compared with those for the nanocomposites with nanotubes only, we may conclude that the greater impact of the density has, in this case, the addition of carbon nanotubes.

Table 39 Intrinsic viscosity, density and melt viscosity of PTT-PTMO/SWCNT+Graphene Ang nanocomposites

Sample	Nanofiller Wt %	[η] dl/g	d g/cm^3	Melt viscosity^M Pa s
PTT-PTMO	0	1.325	1.174	340.02 ± 0.76
PTT-PTMO/0.1 G	0.1	1.315	1.174	124.38 ± 0.93
PTT-PTMO/0.3 G	0.3	1.327	1.175	232.66 ± 0.84
PTT-PTMO/0.1 SWCNT+0.3 G	0.1+0.3	1.299	1.173	428.76 ± 1.22
PTT-PTMO/0.3 SWCNT+0.1 G	0.3+0.1	1.319	1.177	648.65 ± 1.31
PTT-PTMO/0.5 SWCNT+0.1 G	0.5+0.1	1.322	1.176	-
PTT-PTMO/0.1 SWCNT	0.1	1.325	1.181	398.52 ± 1.08
PTT-PTMO/0.3 SWCNT	0.3	1.324	1.176	602.11 ± 1.60

[η]- intrinsic viscosity, d – density; η- melt viscosity measured at 220^{o}C at 1Hz

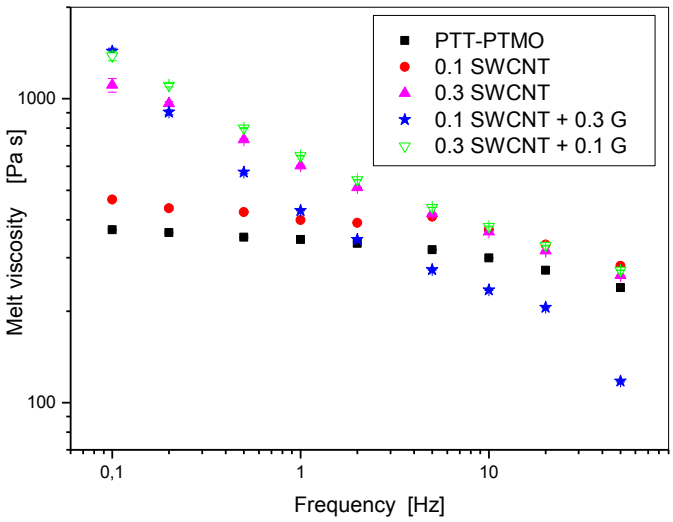

Fig. 73 Melt viscosity versus frequency for neat PTT-PTMO and PTT-PTMO/SWCNTs+Graphene Ang nanocomposites at temperature of 220 ^{o}C.

Due to intermolecular interactions between rigid and flexible segments of various chemical structure in multiblock poly(ether-ester) copolymers, a microphase separation occurred. The separation proceeds with the formation of a soft (PTMO-rich) phase and a hard semicrystalline polyester (PTT) phase with characteristic temperatures T_g and T_m, respectively. Such a structure was confirmed DSC (Fig. 74 a and b). Since the size of domains of the hard phase (few nm, [316]) is comparable to the size of SWCNTs and graphene nanoplateltes, used to obtain hybrid nanocomposites, from DSC studies, it is really hard to explain the influence of hybrid nanofillers on the microstructure of the resulting nanocomposites. The glass transition temperatures (T_g) of nanocomposites were not affected by the incorporation of SWCNTs together with graphene nanoplatalets. Both nanofillers, despite good interactions with the polymer matrix (SEM, chapter 17.1, pages 123-126) showed no effect on the mobility of the polymer chains of (PTMO-rich) phase. In contrast, the crystallization process was affected more in the nanocomposites. The crystallization temperature dramatically increased with increasing content of both, SWCNT and graphene nanofillers. The highest shift toward higher T_c temperature was observed for PTT-PTMO/0.5SWCNT+0.1Graphene, as high as 45 ^{o}C. However, the stronger influence seems to occur for to the presence of carbon nanotubes in PTT-PTMO matrix. It is well seen for hybrid naocomposites, where with increasing loading of SWCNT (from 0.1 to 0.5) the increase in T_c was observed. However, all values of ΔH_c were comparable to neat PTT-PTMO block copolymer. In addition, the melting temperature remains unchanged for all nanocomposites. It can be also concluded from the obtained results that the composition of SWCNT:Graphene of 5:1 accelerated the rate of crystallization perhaps due to many more crystallization agents. It is clearly seen that with an increasing content of CNTs the Tc value also increased. The degree of crystallinity estimated from DSC seemed to confirmed the values of density (Table 38). The addition of nanofillers caused changes in both degree of crystallinity and density,

firstly slightly decrease but with increasing loading of both nanofillers increased in comparison to neat PTT-PTMO.

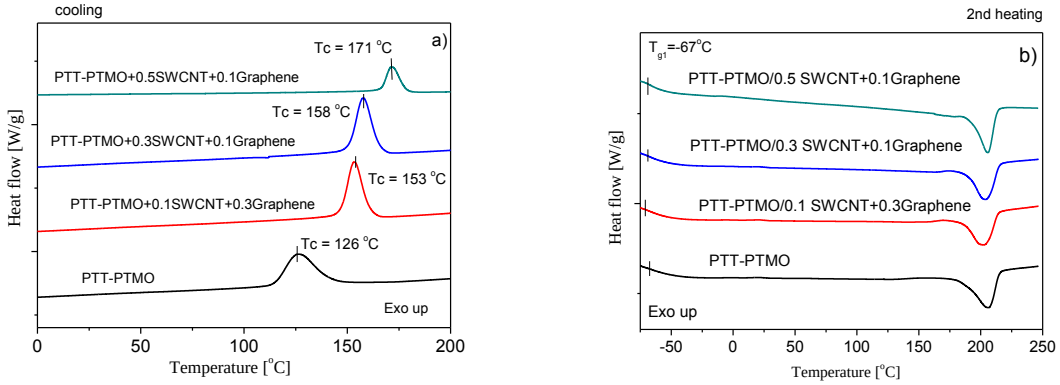

Fig. 74 DSC thermograms for PTT-PTMO and PTT-PTMO/SWCNT+Graphene Ang nanocomposites during the cooling and 2nd heating.

Table 40 Thermal properties of neat PTT-PTMO and PTT-PTMO/SWCNT+Graphene Angstron nanocomposites determined by DSC

Sample	T_g °C	T_m °C	ΔH_m J/g	T_c °C	ΔH_c J/g	x_c %
PTT-PTMO	-67	206	25.8	126	26.2	17.7
PTT-PTMO/0.1 G	-67	204	24.9	149	25.1	17.1
PTT-PTMO/0.3 G	-67	205	25.6	149	25.2	17.5
PTT-PTMO /0.1SWCNT+0.3G	-67	203	24.8	153	25.1	16.9
PTT-PTMO /0.3SWCNT+0.1G	-67	204	26.5	158	26.1	18.2
PTT-PTMO /0.5SWCNT+0.1G	-67	206	27.8	171	28.1	19.0
PTT-PTMO /0.1SWCNT	-67	208	26.3	155	27.2	18.0
PTT-PTMO /0.3SWCNT	-67	204	24.7	157	25.7	16.9

T_g - glass transition temperature of soft phase;-T_m - melting temperature of polyester crystalline phase; T_c - crystallization temperature of polyester crystalline phase; ΔH_m, ΔH_c - enthalpy of melting and crystallization of polyester crystals, respectively; x_c - mass fraction of crystallinity.

17.3. Influence of hybrid system of electrical conductivity

Though significant progress has been made in developing nanocomposites with different polymer matrices and nanofillers with different shapes (also aspect ratio), a general understanding has yet to be emerged. For example, what allows nanocomposites to be both stiffer and tougher than conventional composites, without sacrificing other properties? How

does the nanofiller interact with polymer matrix that makes it conducting? Why do they display better thermal stability versus unfilled polymers? How can we utilize specific molecular interactions to control structure and morphology? A major challenge to further development of nanocomposites is the lack of even simple structure–property models.

Electrical conductivity is an important attribute brought about by the inclusion of nanofillers onto the insulating polymer matrix. The conductivity is largely influenced by factors like dispersion, loading amount and importantly the electrical resistance of the polymer-nanofiller interface. Furthermore, the electrical conductivity of the nanofiller itself plays critical role to obtain electrically conductive polymer nanocomposites.

Hybrid composites have lately attracted the attention of researchers with different mixtures of different types of nanofillers being tried out. It is still an open question to completely understand the synergistic effect brought about by the combinations. Improvement in electrical conductivity have been reported but the ratio of the nanofiller mixture is an important factor governing the creation of percolation path in the entire volume of polymer matrix.

In this part of my work the influence of 1D and 2D mixture of nanofillers on electrical conductivity of hybrid nanocomposites was investigated. The properties of the hybrid nanocomposites with different combinations of CNT/graphene derivatives contents for three polymer matrices: PET, PTT and PTT-PTMO with total filler content of 0.4 wt.% are compared with those of the nanocomposite containing nanofillers alone. Fig. 75 a plots the electrical conductivities of PET/SWCNT Cheaptubes+EGI nanocomposites, showing that the electrical conducting samples weren't obtained. The results of conductivity for hybrid with the concentration of 0.1 wt % of EG and 0.05 wt % of SWCNT exhibited typically insulating behavior. The combination of this both nanofillers was selected based on previous results obtained for PET/EG and PET/SWCNT nanocomposites. In case of PET/EG nanocomposites, percolation threshold as low as 0.05 wt % (Fig. 48, page 96) of nanofiller was obtained.

Based on this results three hybrids were synthesized with various amounts of nanofillers. The schematic explanation of those mechanisms is presented in Figures 76-78. The electrical network created by graphene sheets at 0.1 wt % of EG in PET was destroyed by even small amounts of agglomerates of carbon nanotubes, clearly seen on SEM and TEM micrographs (Fig 65, page 122). This might explain the good dispersion of this two nanofillers in entire volume of polymer. However, carbon nanotubes with lots of impurities (confirmed by Raman and SEM analysis, see pages 65-67) strongly affected the percolation paths of graphene sheets.

On the other hand, Fig. 75 b plots the alternating current conductivity, $\sigma(F)$ as a function of frequency (F) of PTT/SWCNT KNT 95+EGII nanocomposites. In case of PTT/0.5SWCNT+0.1EG conductivity increases abruptly at a critical filler concentration, i.e. the percolation threshold, at which a continuous conducting network of fillers is formed. However if compared to PTT/0.05SWCNT, no influence of EGII was observed. The similar observations were done for the hybrid with 0.1 wt % of SWCNT and 0.1 wt % of EGII. A high electrical conductivity along tube axis, a high aspect ratio and the one-dimensional reinforcement of SWCNT are mainly responsible for the above observations. TEM and SEM analysis of hybrid nanocomposites (Fig. 65, page 122) have shown that graphene bundles were observed together with well dispersed carbon nanotubes. By comparing the electrical

conductivity of polymer hybrid nanocomposites (0.05 wt % of SWCNT+0.1 wt % of EG) with the conductivity of PTT/0.05SWCNT it was concluded that SWCNTs were much more efficient in forming the electrical conducting network than graphene nanoplatelets. SWCNTs formed such a perfect conducting network that even agglomerates of graphene sheets could not destroy it. However, the much higher cost of producing of CNTs with high conductivity (called "metallic") is a major drawback, severely limiting its applications as a conductive filler. Therefore, the research on hybrid systems consisted of carbon nanotubes and graphene nanoplatelets in poly(trimetylene terephthalate) is continued. For comparative purpose, hybrid nanofillers system consisted of SWCNT KNT 95 and Graphene Angstron was used PTMO-PTMO block copolymer matrix, where PTT was used as rigid segment.

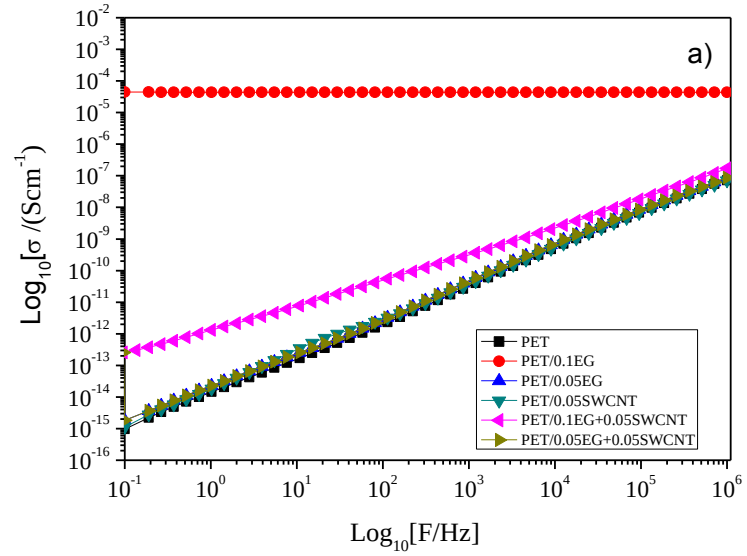

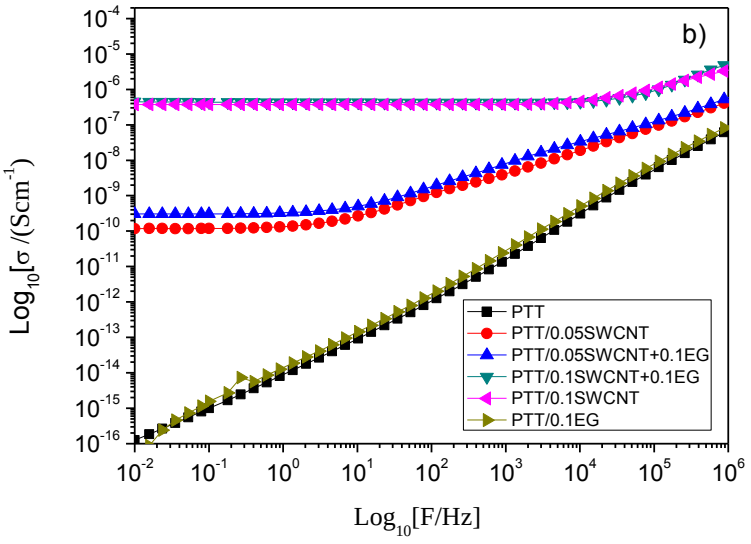

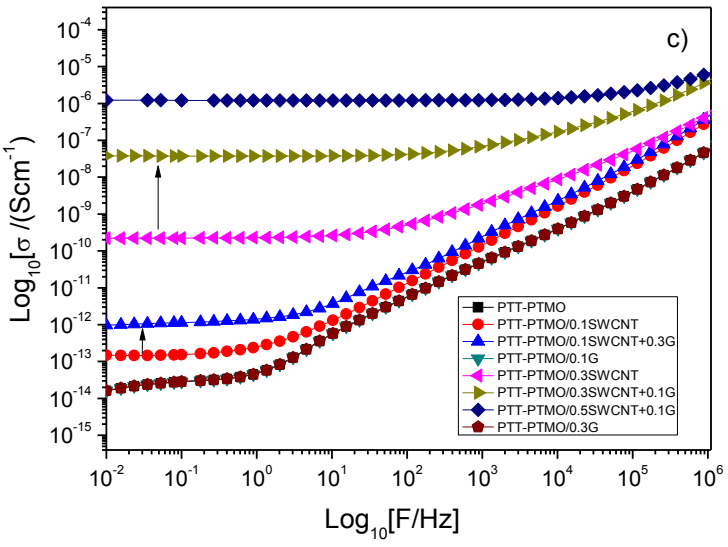

Fig. 75 Alternating current conductivity, σ(F) as a function of frequency (F) for a) PET/SWCNT+EGI; b) PTT/SWCNT+EGII and c) PTT-PTMO/SWCNT+Graphene Ang nanocomposites.

Fig. 75 c shows the alternating current conductivity, σ(F) as a function of frequency (F) for PTT-PTMO/SWCNT KNT 95+Graphene Angstron hybrid nanocomposites. Because, conducting networks have already been formed by 0.3 wt % SWCNT alone (the percolation threshold of SWCNT, page 73), 0.1 wt % Graphene Ang can provide multiple electron pathways through a synergy between the SWCNT and Graphene. Once the filler content exceeds the percolation threshold, agglomerates can even better improve the electrical conductivity than well-dispersed CNTs. With the increasing content of SWCNT to Graphene as 5:1 we observe the typical flat plot, where no dependency of σ in the function of frequency is seen. The hybrid PTT-PTMO/0.5SWCNT+0.1Graphene exhibited the behavior typical for semiconducting samples with the conductivity of 10^{-6} S/cm. Probable explanation of enhancing the electrical conductivity of PTT-PTMO/SWCNT by Graphene Ang, which proved to be non-conductive, was that carbon nanotubes were hitched to the residual functionalized groups on the surface of graphene. Since these groups were “deactivated” by carbon nanotubes, the free movement of electrical charge was observed in case of PTT-PTMO hybrid nanocomposites. The schematic mechanism explaining the synergetic effect of SWCNT and Graphene Ang is presented in Fig.79.

According to the observation and discussion above, the following mechanisms were proposed to explain the electrical percolation behavior observed for three types of polymer matrices: PET, PTT and PTT-PTMO.

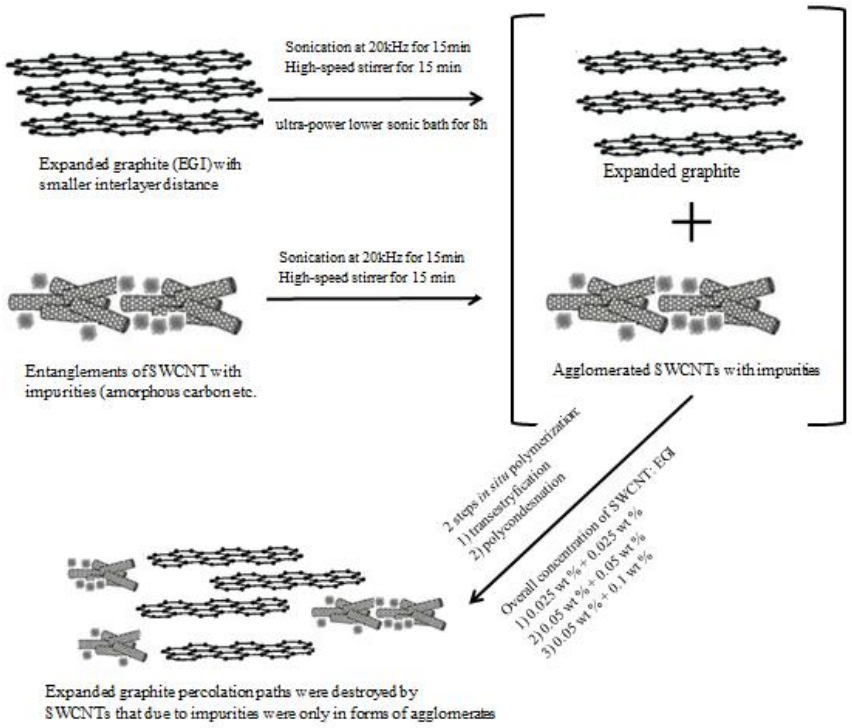

Fig. 76 Proposed mechanism to explain the electrical conductivity in PET based nanocomposites.

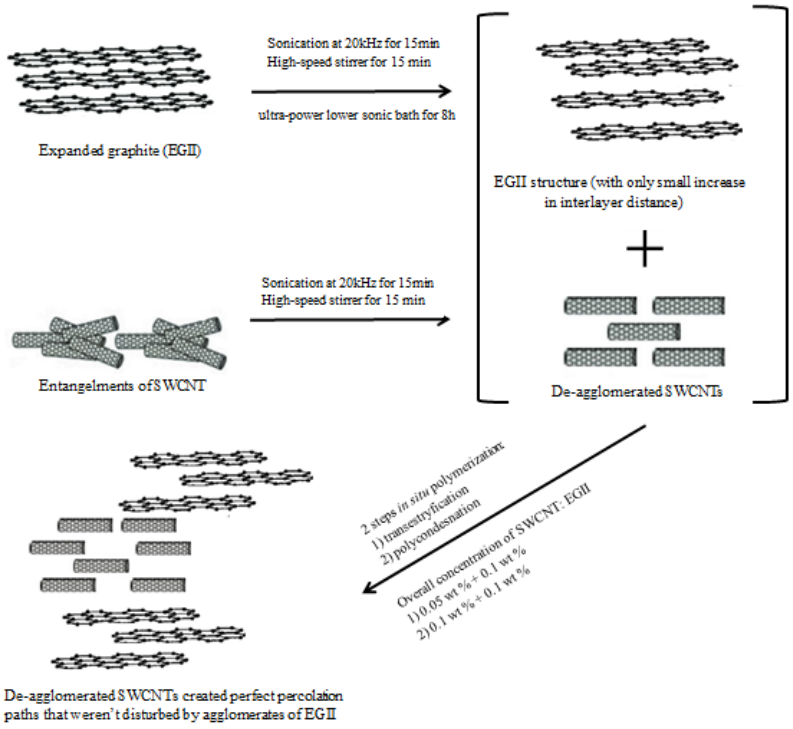

Fig. 77 Proposed mechanism to explain the electrical conductivity in PTT based nanocomposites.

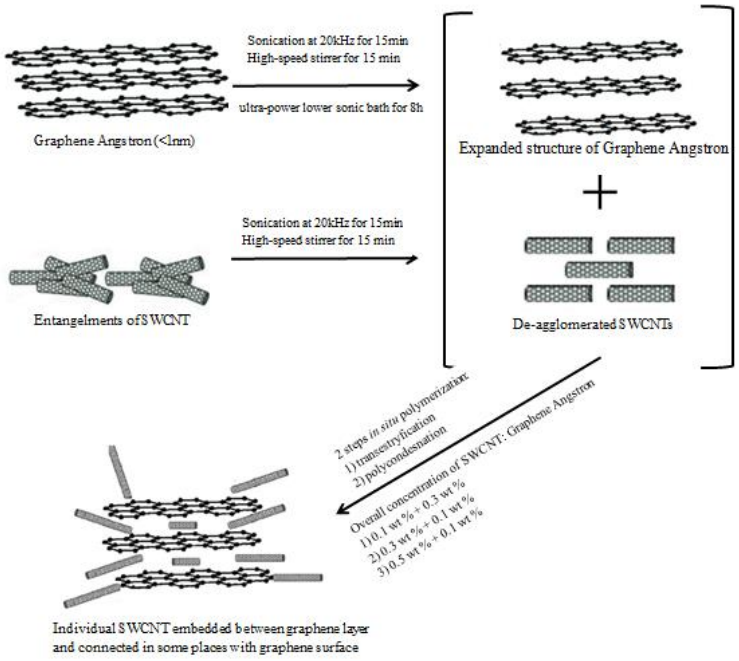

Fig. 78 Proposed scheme of the mechanism that explains the electrical conductivity in PTT-PTMO based nanocomposites.

17.4. Other physical properties of hybrid nanocomposites

Effect of hybrid nanofillers on the thermal stability of the polyester composites (PET, PTT)

In general, the thermal stability of the polymer nanocomposites plays a crucial role in determining their processing and applicability because it affects the final properties of the polymer nanocomposites, such as its upper usage temperature limit and dimensional stability.

The thermal and thermo-oxidative stability of PET nanocomposites containing dispersed in the hybrid system (SWCNT+EG) was studied by using the thermogravimertic analysis. Fig. 79 present weight loss and derivative weight loss versus temperature for the neat PET and PET/SWCNT+EG nanocomposites in air (a) and in argon (b) atmosphere. The TGA and DTG curves are shown in temperatures range from 250 to 600 ^{o}C and in air and from 300 to 550 ^{o}C in argon, because below this temperature ranges no changes on TGA and DTG curves have been observed. Since the onset of the thermal degradation of the nanocomposites wasn't affected by addition of as low as 0.05 wt % of SWCNT (page 84), only the influence of expanded graphite was observed in case of prepared hybrids. The differences between the temperatures corresponding to 5 and 10 % weight loss and the temperature of maximum rate of weight loss for obtained PET/SWCNT+EG hybrid nanocomposites and unmodified PET are within the measurement error. The value of activation energy (Ea) for the PET/ SWCNT+EG nanocomposites increase with increasing content of nanofiller, both when the measurement was carried out in an oxidizing atmosphere and in argon. However, these values are still lower than for pure PET. The values of Ea for the measurement carried out in air ranged between 227-256 kJ/mol, while for the

measurement carried out in argon these values were in the range 300-318 kJ/mol. The results of research carried out in an oxidizing atmosphere and in argon are presented in Table 41. The enhancement in the thermal properties is due to the presence of the EG nanolayers, which acted as barriers to minimize the permeability of volatile degradation products out from the material, hasn't been observed in case of combination of two nanofillers.

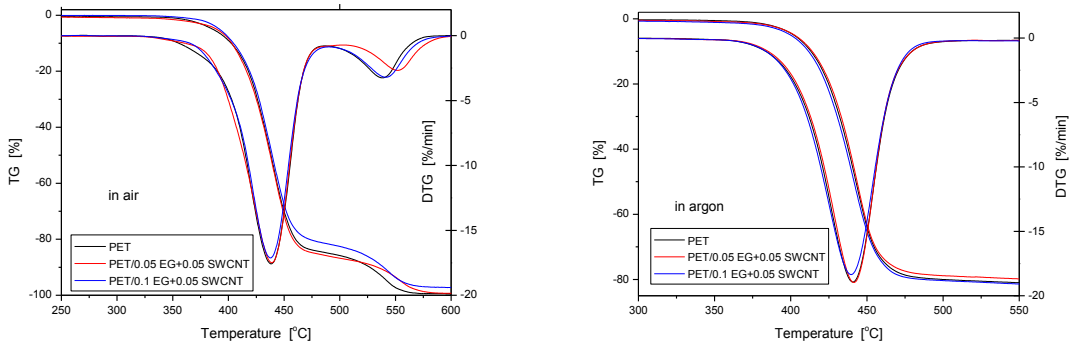

Fig. 79 Weight loss and derivative weight loss versus temperature for the PET/SWCNT+EG nanocomposites in air (a) and in argon (b) at a heating rate of 10°C/min.

Table 41 Temperatures corresponding to 5 and 10% of weight loss, activation energy and the temperature corresponding to a maximum weight loss rate for the PET/SWCT+EG nanocomposites obtained in air and argon atmosphere

Symbol	$T_{5\%}$. °C	$T_{10\%}$. °C	T_{DTG1}. °C	T_{DTG2}. °C	E_a, kJ/mol
Measurement carried out in an oxidizing atmosphere					
PET	386	402	438	538	256.4
PET/0.05EG	373	394	438	538	226.78
PET/ 0.1 EG	396	408	439	544	247.0
PET/0.05 SWCNT+0.05EG	386	403	439	552	227.3
PET/0.05 SWCNT+0.1EG	390	403	438	542	256.1
Measurement carried out in argon					
PET	399	410	438	-	287.6
PET/0.05EG	402	414	441	-	313.6
PET/ 0.1 EG	406	415	441	-	315.8
PET/0.05 SWCNT+0.05EG	402	413	441	-	318.0
PET/0.05 SWCNT+0.1EG	400	412	440	-	300.4

The TGA and DTG curves of neat PTT and PTT/SWCNT+EGII nanocomposites are shown in Figure 80 and temperatures corresponding to 5 and 10 % of weight loss, activation energy of thermal decomposition and the maximum temperature of the mass loss rate are summarized in Table 42. As it can be seen, similarly to nanocomposites with single nanofillers i.e. SWCNTs or EGII (chapter 15.3, page 85 and chapter 16.5, page 114, respectively), hybrid nanocomposites show similar thermal stability to pristine polymer, and also temperatures corresponding to a maximum of weight loss (T_{DTG1}) didn't shifted to higher values with increasing content of nanofillers.

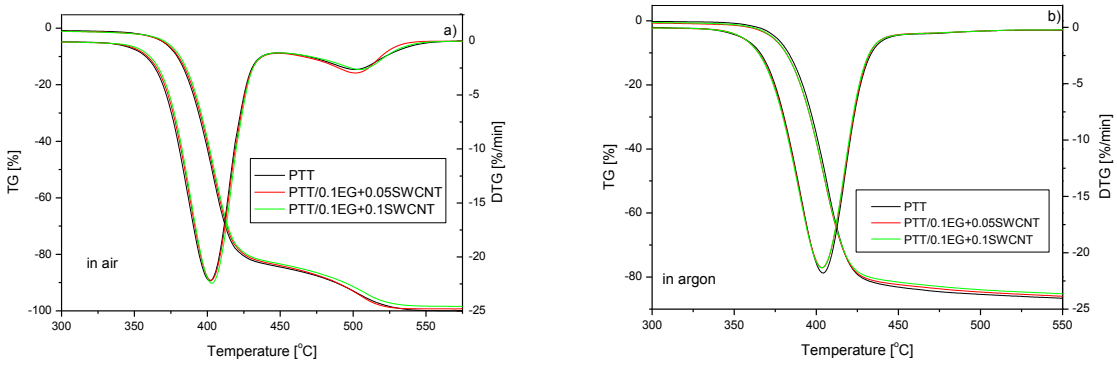

Fig. 80 Weight loss and derivative weight loss versus temperature for the PTT/SWCNT+EGII nanocomposites in air (a) and in argon (b) at a heating rate of 10°C/min.

Table 42 Temperatures corresponding to 5 and 10 % weight loss, activation energy and the temperature at maximum of weight loss rate for the PTT/SWCNT+EGII nanocomposites obtained in air and argon atmosphere

Symbol	$T_{5\%}$. °C	$T_{10\%}$. °C	E_a. kJ/mol	T_{DTG1}. °C	T_{DTG2}. °C
Measurement carried out in an oxidizing atmosphere					
PTT	370	379	318.39	401	501
PTT/0.1 EG+0.05SWCNT	371	380	327.86	402	502
PTT/0.1 EG+0.1SWCNT	372	381	329.25	403	505
Measurement carried out in argon					
PTT	373	382	331.79	404	-
PTT/0.1 EG+0.05SWCNT	373	382	341.92	403	-
PTT/0.1 EG+0.1SWCNT	373	382	339.15	403	-

Since the similar behaviour was already described for PTT/SWCNTs and PTT/EGII, no effect on thermal stability in an oxidizing and inert atmosphere for hybrid nanocomposites has been expected. Only in case of activation energies of thermal decomposition a slightly

increase was observed. It can be concluded that the minimum energy that must be input to the system to cause the decomposition process is bigger in case of nanocomposites than in neat PTT. No improvement of thermal stability of hybrid nanocomposites, with homogenous dispersion of nanofillers, might be caused by too small amount of both SWCNTs and graphene nanosheets to observe any effect.

Effect of hybrid nanofillers on the thermal stability of the elastomer composites (PTT-PTMO)

Thermogravimetric analysis (TGA) was also used to analyze the effect of the hybrid system of nanofillers (1D+2D) dispersed in PTT-PTMO block copolymer matrix on their thermal and thermo-oxidative stability. The obtained results are summarized in Table 43 and in Fig. 81 the TGA curves of PTT-PTMO/hybrid nanoparticles nanocomposites in air and an inert (argon) atmosphere were presented. No improvement in thermal stability has been observed in an inert atmosphere, as compared to the neat PTT-PTMO block copolymer, but also to previously described PTT-PTMO/SWCNT and PTT-PTMO/Graphene nanocomposites. Even a slight decrease in temperatures of 5 and 10 % weight loss ($T_{5\%}$, $T_{10\%}$) and was observed. However in an oxidizing atmosphere for all hybrid nanocomposites the noticeable stabilizing effect of nanofillers has been found. When comparing the temperature of 5 % weight loss for neat PTT-PTMO block copolymer and the hybrids composites, a significant improvement of 24 ^{o}C toward higher temperatures was observed. It is interesting to note that the addition of carbon nanofillers with different shapes and aspect ratios greatly improves the thermo-oxidative stability of this thermoplastic elastomer. Apparently the thermal stability improvement does not seem to depend upon particular shape of nanofiller, since for SWCNTs and graphene nanosheets individually and for the mixture of both the same observations were made. Apparently, both nanoparticles (carbon nanotubes and graphene nanoplatelets) affect the thermal stability of polymers following the same manner. Besides, all the curves shown in Figure 81 are close to each other. Thus, morphology difference in PTT-PTMO/SWCNT+Graphene nanocomposites does not appear to make an appreciable difference in the thermal stability of the nanocomposites. The possible explanation for such behavior is because CNTs have high electron affinities similar to graphene nanosheets; as such they have been proposed to acts as scavengers of free radicals. By incorporating CNTs and/or graphene nanoplatelets in polymers the thermal stability of polymers should be enhanced.

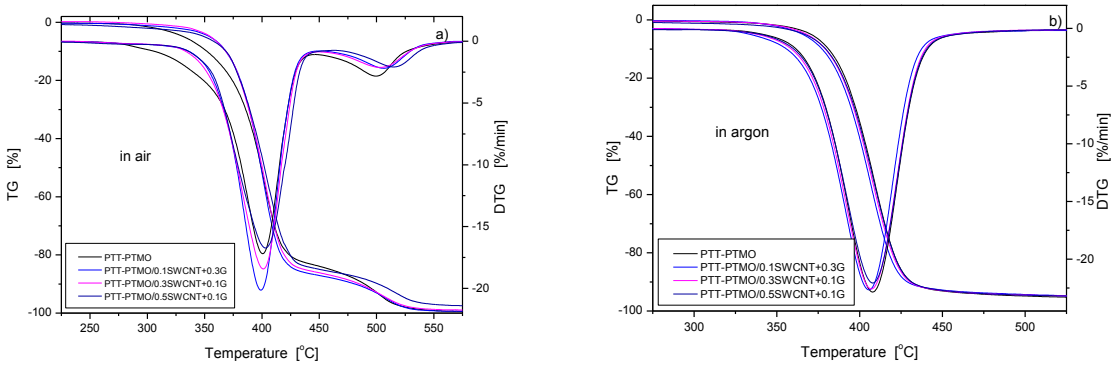

Fig. 81 Weight loss and derivative weight loss versus temperature for the PTT-PTMO/SWCNT+Graphene Angstron nanocomposites in air (a) and in argon (b) at a heating rate of 10°C/min.

Table 43 Temperatures corresponding to 5 and 10 % weight loss, activation energy and the temperature at maximum of weight loss rate for the PTT-PTMO/SWCNT+Graphene Angstron nanocomposites obtained in air and argon atmosphere

Symbol	$T_{5\%}$. °C	$T_{10\%}$. °C	T_{DTG1}, °C	T_{DTG2}. °C
Measurement carried out in an oxidizing atmosphere				
PTT-PTMO	331	352	400	499
PTT-PTMO/0.1 SWCNT+0.1G	355	368	399	507
PTT-PTMO/0.3SWCNT+0.3G	355	358	401	504
PTT-PTMO/0.5SWCNT+0.3G	350	369	403	515
Measurement carried out in argon				
PTT-PTMO	374	382	408	-
PTT-PTMO/0.1 SWCNT+0.1G	366	377	406	-
PTT-PTMO/0.3SWCNT+0.3G	368	379	407	-
PTT-PTMO/0.5SWCNT+0.3G	367	380	409	-

Mechanical properties of polyester hybrid nanocomposites

It is well known that the modulus of the fiber or particulate reinforced composites is dependent mainly on the moduli and volume fractions of composites constitutes. Because CNT and graphene platelets have similar moduli approximately 1 TPa within the elastic limit, the CNT/graphene derivatives nanocomposites should have a similar modulus as far as the total filler content are the same. Fig. 82 are typical stress–strain curves for the dumbbell shape samples of PET/hybrid nanocomposites prepared in this work. From these curves, we have measured the Young's modulus, E, yield stress σ_y, and strain ε_y, tensile strength, σ_b, and the strain at break (ductility), ε_b. These parameters are shown as a function of nanofillers content

in Table 44. The nanotube-only nanocomposites with higher concentration of nanotubes (0.05 wt %) had modulus strength and ductility values of: E = 2.57 GPa, σ_b = 66.6 MPa and ε_b = 2.6%. On the other hand expanded graphite-only nanocomposite with 0.1 wt % of EG exhibited modulus strength and ductility values of: E = 2.54 GPa, σ_b = 65.9 MPa and higher than nanotubes ε_b = 21.4%. However, more interestingly, when expanded graphite is added to the nanotubes to form a hybrid, both stiffness and strength were comparable to the values obtained when only nanotubes or graphene plataletes were added i.e 2.50 GPa and 63.1 MPa, respectively for PET/0.05SWCNT+0.1EG. These values are close to values of neat poly(ethylene terephthalate) which is a tough and ductile material. As both nanofillers were added as the mixture to neat PET matrix, the modulus and strength tend to fall off, if compared to nanocomposites based on one of those carbon nanofillers, and only in case of hybrid composition with 0.05SWCNT and 0.1EG. It has been proposed that nanotubes relax under applied stress by the motion of inter-tube or inter-bundle junctions, while graphene planes moving relative to each other by improving ductility of hybrid nanocomposites (when an addition of EG was lower than 0.05). It is also possible that the addition of small quantities of expanded graphite impedes the deformation of the network and hinders junction motion. This would mean greater stress would be required to cause a given amount of junction motion resulting in an increased modulus. In addition it is likely that stress would build at the jammed junctions. Thus, failure would tend to occur at higher stresses and lower strains resulting in increased strengths and reduced ductility, as observed

Table 44 Tensile properties of PET/SWCNTs+EGI hybrid nanocomposites

Sample	E GPa	σ_y MPa	ε_y %	σ_b MPa	ε_b %
PET	2.08 ±0.14	68.8 ± 0.9	3.6 ± 0.2	38.1 ± 9.7	121.3 ± 12.4
PET/0.025 SWCNT	2.59±0.15	68.9 ± 2.2	3.4 ± 0.3	33.9 ± 1.9	72.4 ± 8.6
PET/0.05 SWCNT	2.57±0.13	68.9± 1.7	3.1 ± 0.5	66.6 ± 4.1	2.6 ± 0.6
PET/0.025 SWCNT+0.025 EG	2.31±0.2	74.2 ± 2.5	1.3 ± 0.1	41.3 ± 4.5	71.2 ± 7.3
PET/0.05 SWCNT+0.05 EG	2.03±0.3	69.5 ± 3.5	1.3 ± 0.1	60.7 ± 5.3	12.3 ± 0.9
PET/0.05 SWCNT+0.01 EG	2.50±0.40	73.9 ± 0.8	1.3 ± 0.1	68.1± 8.2	3.6 ± 0.3
PET/0.025 EG	2.15 ± 0.08	74.0 ± 2.9	1.4 ± 0.1	37.1 ± 7.9	268 ± 20.7
PET/0.05 EG	2.46 ± 0.10	70.6 ± 2.9	1.3 ± 0.1	37.3 ± 5.6	116 ± 20.4
PET/0.1 EG	2.54 ± 0.05	65.0 ± 5.2	1.1 ± 0.1	65.9 ± 8.3	21.4 ± 3.2

E – Young's modulus; σ_y - yield strength (elastic limit); ε_y – yield strain, σ_b, ε_b - stress and strain at break respectively

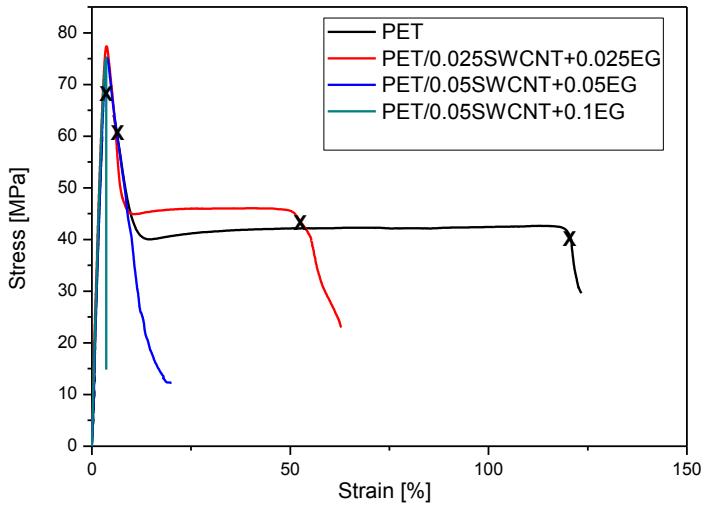

Fig. 82 Representative stress strain curves of PET/SWCNT+ EGI nanocomposites.

Mechanical properties were analyzed also for the SWCNT KNT 95 + EGII reinforced PTT hybrid composites are shown in Figure 83. Here the stress is plotted against strain for all investigated samples. The values for the Young's modulus, E, yield stress (elastic limit) σ_y, and strain ε_y, tensile strength, σ_b, and the strain at break (ductility), ε_b are additionally summarized in Table 45. All "single" nanocomposites exhibited moduli values similar to the neat PTT. These values are similar to values previously reported for PTT/MWCNT-COOH nanocomposites prepared in our lab [15]. With an addition of EG of 0.1 wt % to nanotubes of 0.05 wt %, an increase in the Young's modulus from 2.38 to 2.44 MPa is observable. However, the increase of amount of CNT to 0.1 wt % in the mixture with EG causes then the decrease in modulus. Probable it was due to the dispersion state in case of nanocomposite with lower amount of nanofillers. The elongation at break seems to be nearly constant for all „single" nanocomposites, but in comparison to pure PET this value dramatically decreased. Only slight increase in ductility for hybrid nanocomposites was observed. It is caused by an immobilization of the polymer chains and plays a significant role when a CNT network is formed. Poorer results observed for PTT with 0.1SWCNT+0.1EG supposed to be that with a higher CNT loading the homogeneous dispersion of the tubes is getting more difficult resulting in the existence of agglomerates which are not dispersed. Probably cracks are originated at such CNT agglomerates which behave as stress concentrators. Here, in dependence of the aspect ratio and the orientation of the single platelets crystallization at smaller strains that does not appear for the unfilled samples, has been observed. Similar effects could occur with CNT as reinforcing filler, if during the stress/strain measurements, an orientation of the tubes takes place. Such behavior could explain the increase of the stress especially at low strain compared to pure PTT, where the addition of both types of nanofillers induced crystallization resulting in decrease in ductility. However, since a combination of different types of filler are applied, a clear statement seems to be difficult. Here further investigations are necessary.

Table 45 Tensile properties of PTT/SWCNTs+EG hybrid nanocomposites

Sample	E GPa	σ_y MPa	ε_y %	σ_b MPa	ε_b %
PTT	2.36 ± 0.05	50.2 ± 9.5	1.42 ± 0.3	28.6 ± 9.7	178 ± 32.4
PTT/0.025 SWCNT KNT	2.36 ± 0.12	68.9 ± 5.5	1.38 ± 0.1	68.9 ±5.6	3.81 ± 0.1
PTT/0.05 SWCNT KNT	2.38 ± 0.13	58.8 ± 9.2	1.11 ± 0.1	61.5 ± 5.3	2.64 ± 0.1
PTT/0.1EG+0.05SWCNT-KNT	2.44 ± 0.07	57.1 ± 1.3	1.25 ± 0.1	45.1 ± 3.4	16.3 ± 0.1
PTT/0.1EG+0.1SWCNT-KNT	2.29 ± 0.05	59.4 ± 3.2	1.30 ± 0.2	52.3 ± 2.3	11.2 ± 0.2
PTT/0.1EG	2.37 ± 0.12	72.3 ± 4.5	1.46 ± 0.1	47.2 ± 6.7	1.89 ± 0.3

E – Young's modulus; σ_y - yield strength (elastic limit); ε_y – yield strain, σ_b, ε_b - stress and strain at break respectively

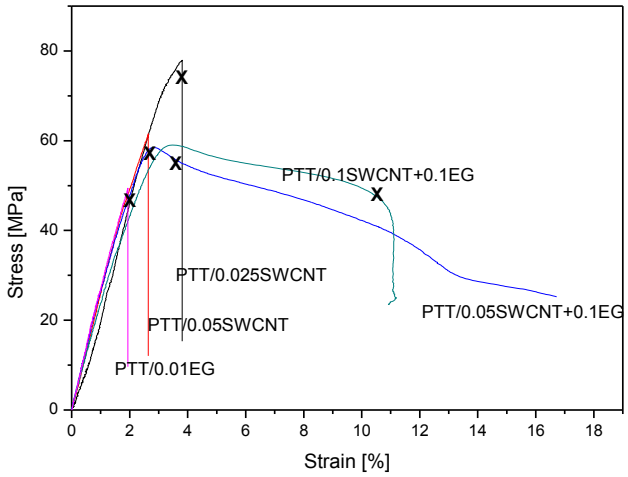

Fig. 83 Representative stress strain curves of PTT/SWCNT KNT + EGII nanocomposites.

Mechanical properties of hybrid nanocomposites based on multiblock copolymer

The tensile properties of the PTT-PTMO/SWCNT+graphene hybrid nanocomposites were examined. Fig. 84 shows typical stress–strain curves for PTT-PTMO block copolymers. To make the plots more understandable, the obtained data are presented in two separate figures, in which the results obtained for the hybrid nanocomposites were compared to those obtained for graphene (a) and carbon nanotubes (b). As summarized in Table 46, there was a clear tendency that the tensile modulus increases and elongation decreases with an increase hybrid system content. In case of an addition of hybrid system of carbon nanofiilers the similar effect has been observed, as previously observed and described for PTT-PTMO/SWCNT (Chapter , page). Carbon nanofillers (SWCNT and Graphene) added in small amount to PTT-PTMO elastomer increases tension related to deformation, limiting the free length of chains which are located between physical nodes of the network / matrix (they create additional physical nodes). However, this effect was much stronger when two nanofillers were used. For pristine PTT-PTMO the tensile modulus was 118 MPa. With the incorporation up to 0.3 wt % of Graphene, the tensile modulus decreased to ca. 131 MPa, which is ca. 11 % higher than that of the neat PTT-PTMO block copolymer. However, in case of PTT-PTMO/SWCNT the significant increase up to 162 MPa. The increase in the modulus was accompanied with decrease in the elongation at break for nanocomposites with

graphene and with 0.1 wt % of SWCNT. Only slight increase in ε_b for PTT-PTMO/0.3SWCNT to 639 % was observed. Addition of hybrid system further increased the modulus to 149 MPa, 178 MPa and 212 MPa, for 0.1SWCNT+0.3G, 0.3SWCNT+0.1G and 0.5SWCNT+0.1G respectively. Hybrid nanocomposite with the concentration of 0.5 wt % of nanotubes and 0.1 wt % of graphene achieved modulus value, which is ca. 68 % higher than the pristine elastomer. Thus the tensile measurements revealed that the effect of hybrid nanofillers system is more pronounced on the tensile modulus. The pronounced increase in the tensile modulus reflects the reinforcement effect attained by the dispersion of the nanotubes and graphene platelets into PTT-PTMO matrix. Calorimetric studies for obtained PTT-PTMO/hybrid nanocomposites (Table 40) showed only small differences in the polymer melt enthalpy and negligible increase in degree of crystallinity. Therefore, the observed here improvement in the tensile properties at low nanofillers' loading cannot be due to a change in crystallinity and is more likely caused by the presence of SWCNTs and graphene nanoplatelets next to PTT hard domains dispersed in PTMO-rich soft phase. Similar results has been also previously observed for PTT-PTMO nanocomposites with graphene oxide (GO) [388] and montmorillonite (MMT) [389]. Elongation at break, on the other hand, decreased significantly for PTT-PTMO/0.5SWCNT+0.1Graphene. At the same time, an increase in the permanent set accompanying to the deformation of 100% was observed, by means of limited, in only small extent, reversible deformation range. The synergistic toughening mechanisms of combination of SWCNT and graphene has been observed for PTT-PTMO block copolymer. This strong effect has been previously observed in described system in enhancement of electrical conductivity (Fig.75 c).

Table 46 Tensile properties of PTT-PTMO/SWCNT + Graphene Ang nanocomposites

Sample	E MPa	$\sigma_{(100\%)}$ MPa	σ_y MPa	ε_y %	σ_b MPa	ε_b %
PTT-PTMO	118.3 ± 1.5	12.7 ± 0.1	13.6 ± 0.2	44.8 ± 0.9	20.3 ± 0.7	625 ± 12
PTT-PTMO/0.1 G	123.0 ± 1.3	12.8 ± 0.1	13.4 ± 0.2	50.4 ± 1.3	20.3 ± 0.1	594 ± 12
PTT-PTMO/0.3 G	131.7 ± 4.1	13.1 ± 0.1	13.7 ± 0.1	49.6 ± 0.1	19.8 ± 0.2	594 ± 14
PTT-PTMO/0.1 SWCNT+0.3 G	149.2 ± 2.7	13.6 ± 0.1	14.0 ± 0.1	49.8 ± 0.8	19.2 ± 0.3	634 ± 29
PTT-PTMO/0.3 SWCNT+0.1 G	178.3 ± 6.9	13.9 ± 0.1	14.4 ± 0.1	48.1 ± 1.1	20.4 ± 0.2	642 ± 21
PTT-PTMO/0.5 SWCNT+0.1 G	212.2 ± 6.5	14.1 ± 0.1	14.6 ±0.9	47.6 ± 1.2	18.5 ± 1.2	542 ± 59
PTT-PTMO/0.1 SWCNT	145.1 ± 3.9	13.6 ± 0.3	14.2 ± 0.2	47.8 ± 0.8	20.7 ± 0.6	617 ± 24
PTT-PTMO/0.3 SWCNT	162.5 ± 2.5	13.7 ± 0.1	14.1 ± 0.1	49.7 ± 0.5	19.9 ± 0.2	639 ± 13

E – tensile modulus; $\sigma_{(100\%)}$ – stress at strain of 100%; σ_y, ε_y – yield stress and strain respectively, σ_b, ε_b - stress and strain at break respectively

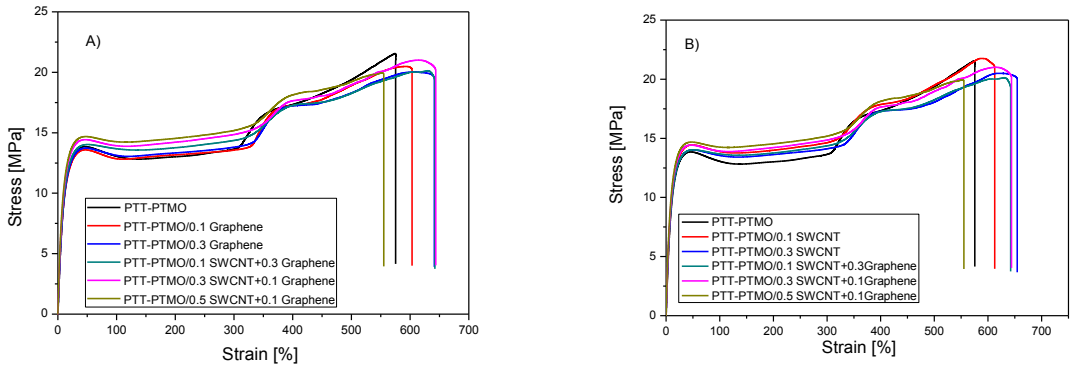

Fig. 84 Representative stress strain curves of PTT-PTMO/SWCNT + Graphene Ang hybrid nanocomposites a) in comparison to PTT-PTMO/Graphene Ang and b) in comparison to PTT-PTMO/SWCNT nanocomposites.

18. Summary and conclusions

Within the framework of the present dissertation thesis, the research experiments were conducted on the preparation and characterization of polymer composites containing carbon nanotubes, graphene derivatives and hybrid systems of both CNTs/graphene derivatives, in which condensation polymers constituted the matrix. Polymer nanocomposites, including polymer hybrid nanocomposites, are a relatively new group of engineering materials with promising, yet not fully known, physical properties, requiring the use of appropriate methods of production due to the size and properties of the dispersed phase. The use of *in situ* synthesis allowed to obtain composites with a high degree of homogeneity, which is a key issue for further industrial applications, while the analysis of the properties of obtained materials showed effect of the addition of carbon nanotubes and graphene derivatives on their structure, physical transitions, thermal stability, mechanical strength and electrical conductivity. The knowledge gained in the course of preparation of this PhD thesis is important from the cognitive point of view and contributes to the development of this new group of composite materials.

General conclusions drawn based on the results presented in the dissertation are as follows:

1. Using *in situ* synthesis, i.e. the introduction of carbon nanofillers into polymer during its synthesis, preceded by dispersing nanoparticles in a liquid substrate with the use of mechanical and ultrasounds treatment, while in the case of graphene nanoplatelets additionally ultra-low-power sonic bath, allows to obtain nanocomposites in which the dispersed phase is characterized by homogeneous dispersion in the entire volume of the system. The validity of the use of ultra-low power sonic bath for 8h was confirmed for nanocomposites based on PET. The use of ultrasonic waves probably resulted in increase the interlayer distance (further exfoliation) and thus led to an even distribution of graphene nanoplatelets in the entire volume of the nanocomposite. The effectiveness of the *in situ* method was confirmed as applied to thermoplastic polyesters: poly(ethylene terephthalate) and poly(trimethylene terephthalate) and thermoplastic elastomer based on PTT (PTT-*block*-PTMO), obtained by condensation polymerization, and the different structures/forms of carbon nanoparticles.
2. The obtained nanocomposites may be processed by conventional methods for thermoplastics, which was confirmed using the injection molding method, while preserving the ease of forming characteristic for the polymers constituting the matrix. This gives the wide possibilities of the use of nanocomposites in terms of design, forming complicated workpieces, profiles, etc.
3. Introduction to polymers (PET, PTT, PTT-PTMO), single walled carbon nanotubes and graphene derivatives allows to obtain composites with improved or new physical/utility features with respect to the properties of the matrix, expanding their functional character. The observed improvement in properties, however moderate, if compared to the expectations resulting from exceptional physical properties of carbon nanotubes. Only in the case of hybrid nanocomposites based on PTT-block-PTMO the synergic effect was observed in both mechanical and electrical properties. Probable explanation of enhancing the electrical conductivity and

mechanical strength of PTT-PTMO/SWCNT by Graphene Ang, which proved to be non-conductive, was that carbon nanotubes were hitched to the residual functionalized groups on the surface of graphene. Since these groups were "deactivated" by carbon nanotubes, the free movement of electrical charge was observed in case of PTT-PTMO hybrid nanocomposites.

4. The effect of the interaction between the polymer and the dispersed phase in the nanocomposites is not uniform and depends on both the chemical structure and properties of the matrix, as well as the structure of carbon nanofillers; does not allow to formulate clear conclusions and requires individual analysis for each surveyed polymer system.

Characteristics of the physical properties of the obtained polymer nanocomposites proved that the addition of both carbon nanotubes and graphene derivatives with a concentration of not higher than 0.6 wt % to condensation polymers allows to obtain lightweight composite materials, exhibiting enhanced thermal stability, improved mechanical properties and electrical conductivity. These features come together with the requirements of modern materials for various industries and are the result of the phenomena occurring in the polymer in the presence of carbon nanofillers of different shapes (1D and 2D) and the interaction between the two phases.

Analysis of the effect of the addition of carbon nanoparticles on the properties of PET, PTT and PTT-PTMO allowed to draft the specific conclusions:

- the presence of CNTs and graphene nanosheets in the melt polymer during cooling significantly speed up the crystallization process, regardless of the type of nanoparticles, while significantly in terms of polymer matrix; so in case of PET a slight effect (3-7 ^{o}C) was observed, in PTT matrix this effect was even more visible (15-20 ^{o}C), while the greatest differences were observed for thermoplastic elastomers (20-30 ^{o}C), wherein for PTT-PTMO/0.5SWCNT+0.1G hybrid nanocomposite the shift of the crystallization peak up to 45 ^{o}C was recorded; however, there was no effect on the glass transition temperature, which allows to extend the temperature range of formation of the crystalline phase, and has a technological significance; the structure of the forming phase and its quality are related to type of nanofillers (1D, 2D or the mixture of both) and the „sensitivity" of the matrix on their presence (i.e. PET); in general, addition of both nanofillers increased the degree of crystallinity, and the differences in its quality are seen at the melting endotherms;
- the introduction of carbon nanoparticles into polymer matrices has not significantly affected the thermal stability of obtained nanocomposites at inert atmopshere; however, the addition of SWCNT and graphene derivatives individually and in the mixture of both effects in enhancement of thermo-oxidative stability, both in thermoplastic polyesters (PET, PTT) and thermoplastic elastomers (PTT-PTMO); the addition of both carbon nanotubes, graphene, and mixtures of both imply an increase of thermal stability of nanocomposites, as can be seen by shifting the beginning of the chemical decomposition temperature of up to 20-25 ^{o}C for composites based on the used matrices even at the lowest concentrations of nanoparticles;

- the presence of the nanoparticles results in a moderate increase in the mechanical properties, including tensile strength; this is particularly evident in the case of polyesters, where there is an increase of the Young's modulus with a definite deterioration of flexibility; increasing the maximum stress and elongation at break during the stretching is particularly evident in nanocomposites based on thermoplastic elastomers wherein the values obtained for strength parameters do not depend on the type of nanoparticles; for composites based on thermoplastic polyesters the mechanical strength remains at the level of the matrix;
- for nanocomposites based on thermoplastic elastomers in case of mechanical properties the synergic hybrid effect has been observed; the addition of carbon nanotubes together with graphene nanosheets caused the strength increase of 68 % for the highest concentration of nanofillers;
- graphene nanoplatelets (EGI, EGII, EG50, EG500, FLG, Graphene Angstron) found to be impervious to oxygen and carbon dioxide, providing barrier resistance. PET based nanocomposites with 0.025 wt % of EGI showed a reduction in oxygen permeability of about 22 %, but the addition of 0.2 wt % of EG reduced permeability about 71 % if compared to neat PET. The change in oxygen permeability of PET based nanocomposites was controlled by the nanosheets content, nanostructure and sample thickness, since it was observed that the degree of crystallinity and sample thickness play a critical role in barrier properties enhancement of nanocomposites. The smaller concentration in case of PTT based nanocomposites with nanoflakes with large surface area (~500 μm) was a critical factor to obtain proper dispersion that constitute a barrier to the diffusion of the CO_2 and O_2 molecules. However, the greater improvement in barrier properties was achieved for nanocomposites based on nanoplateletes with smaller surface area i.e. EGII (~50 μm), Graphene Angstron (~10 μm) and FLG (~2 μm). Graphene Angstron allows to obtain nanocomposites that were almost completely impermeable to O_2 molecules. The diffusion mechanism was not possible when nanosheets were homogenously dispersed, since they create the tortuous paths to gases. In all cases graphene platelets really do act as a barrier to the diffusion paths.
- nanocomposites based on PET, PTT and PTT-PTMO with carbon nanotubes showed the percolation threshold of 0.4, 0.05 and 0.3 wt % respectively; on the other hand the addition of graphene nanoplatalets, only in case of nanocomposites based on PET allowed to obtain conductive polymers with percolation threshold of 0.05 wt %;
- hybrid nanocomposites based on thermoplastic polyesters didn't demonstrate the synergic effect in case of electrical conductivity; in PET matrix, low-purity SWCNTs disturbed the percolation paths formed by nanoplatelets of EG, whereas in case of PTT, nanosheets of EG didn't affect the electrical conductivity received via paths forms by carbon nanotubes of high-purity;
- as with mechanical properties, also in case of electrical conductivity, hybrid nanocomposites based on PTT-PTMO with an addition of SWCNTs+Graphene allowed to observe the synergic hybrid effect, where non-conducting (2D) nanofiller improved the conductivity in the mixture with one-dimensional (1D) nanofiller; for all

hybrid systems the schematic models showing the probable explanation for the presence or absence of a positive hybrid effect has been proposed.

Implementation of this PhD thesis has brought a lot of new information about obtaining and characterization of polymer hybrid nanocomposites, however it also revealed some scarcities of those materials, which at this stage are not entirely understandable, including lack of correlation between the materials structure and their mechanical properties and lack of significant correlations between the change of a given parameter and the increase in concentration of nanoparticles. One of the possible explanations, that has been already mentioned several times in this thesis, is the molecular weight of polymer matrix, which can affect a number of properties of the final nanocomposite. The means for eliminating this phenomenon in the course of further research is the application of the third stage of the synthesis process – post-polycondensation in the solid state (a separate reactor required).

The acquired knowledge indicates the potential of a new group of materials, which are polymer hybrid nanocomposites and might be useful or their further development. Determination of the conditions of obtaining hybrid nanocomposites during synthesis of polymer matrix is the basis to develop new technologies for receiving those materials in pilot-scale and in industrial scale. Among the potential applications of the designed composite materials based on thermoplastic polyesters, particularly interesting seems to be the possibility of spinning high-modulus electro-conductive fibers. Moreover, the observed positive hybrid effect in the case of thermoplastic elastomers will allow lowering the final price of the finished product (suitable selection of properties at the optimum price), which can be characterized by good electrical conductivity with, at the same time, improved mechanical properties.

References

1. Kurzydłowski K., Lewandowska M. Nanomateriały inżynierskie konstrukcyjne i funkcjonalne. Wydawnictwo Naukowe PWN, 2011 (copyright 2010).
2. Królikowski W., Rosłaniec Z. Nanokompozyty polimerowe. Kompozyty (Composites), 2004, 4, 3-16.
3. Kwiatkowska M., Broza G., Męcfel J. Sterzyński T., Rosłaniec Z. Otrzymywanie i charakterystyka nanokompozytów polimerowych PBT/nanorurki węglowe. Kompozyty (Composites), 2005, 5, 99-105.
4. Kim H., Abdala A.A., Macosko C.W., Graphene/Polymer Nanocomposites. Macromolecules, 2010, 43, 6515-6530.
5. Slonczewski J.C., Weiss P.R. Band structure of graphite. Phys Rev, 1958, 109, 272.
6. Zhang Y., Tan Y.W., Stormer H.L., Kim P. Experimental Observation of the Quantum Hall Effect and Berry's Phase in Graphene. Nature, 2005, 438, 201-204.
7. Novoselov K.S., Geim A.K., Morozov S.V., Jiang D., Zhang Y., Dubonos S.V., Grigorieva I.V., Firsov A.A. Electric field effect in atomically thin carbon films. Science, 2004, 306, 666-669.
8. Lee C., Wei X., Kysar J.W., Hone J. Measurement of the elastic properties and intrinsic strength of monolayer graphene. Science, 2008, 321, 385–388.
9. Balandin A.A., Ghosh S., Bao W., Calizo I., Teweldebrhan D., Miao F., Lau C.N. Superior thermal conductivity of single-layer graphene. Nano Lett, 2008, 8, 902-907.
10. Bunch J.S., Verbridge S.S., Alden J.S., van der Zande A.M., Parpia J.M., Craighead H.G., McEuen P.L. Impermeable Atomic Membranes from Graphene Sheets. Nano Lett, 2008, 8, 2458–2462.
11. Hernandez Y., Nicolosi V., Lotya M., Blighe F.M., Sun Z., De S., McGovern I.T., Holland B., Byrne M., Gun'Ko Y.K., Boland J. J., Niraj P., Duesberg G., Krishnamurthy S., Goodhue R., Hutchison J., Scardaci V., Ferrari A.C.,Coleman J.N. High-yield production of graphene by liquid-phase exfoliation of graphite. Nature Nanotechnology, 2008, 3, 563-568.
12. Chen X., Jintong Xia J., Peng J., Li W., Xie S. Carbon-nanotube metal-matrix composites prepared by electroless plating. Composites Sci Technol, 2000, 60, 301-306.
13. H., Gleiter. Nanostructured materials: basic concepts and microstructure. Acta Mater, 2000, 48, 1-29.
14. Ning J., Zhang J., Pan Y., Guo J. Fabrication and physical properties of SiO2 matrix composites reinforced by carbon nanotubes. Mater Sci Eng, 2004, A357(1-2), 392 – 396.
15. Szymczyk A., Roslaniec Z., Zenker M, Garcia-Gutierez M.C., Hernandez J.J., Rueda D.R., Nogales A., Ezquerra T.A. Preparation and characterization of nanocomposites based on COOH functionalized multi-walled carbon nanotubes and on poly(trimetylene terephthalate. eXPRESS Polym Lett Vol 2011, 5, 11, 977-995.
16. Szymczyk A., Poly(trimethylene terephthalate-block-tetramethylene oxide) elastomer/single-walled carbon nanotubes nanocomposites: Synthesis, structure, and properties. Journal of Applied Polymer Science 2012, 126, 796-807.
17. Lv C., Xue Q., Xia D., Ma M., Xie J., Chen H., Effect of Chemisorption on the Interfacial Bonding Characteristics of Graphene−Polymer Composites. J Phys Chem C 2010, 114, 6588–6594.

18. Das B., Eswar Prasad K.E., Ramamurty U., Rao C.N.R. Nano-indentation studies on polymer matrix composites reinforced by few layer graphene. Nanotechnology 2009, 20, 25705-09.
19. Prasad K.E., Das B., Maitra U, Ramamurty U., Rao C.N.R. Extraordinary synergy in the mechanical properties of polymer matrix composites reinforced with two nanocarbons. Procedings of the National Academy of Science USA, 2009, 106, 13186-89.
20. Stoeberl U., Wurstbauer U., Wegscheider W., Weiss D., Eroms D. Morphology and flexibility of graphene and few-layer graphene on varrious substrates. J Appl Phys Lett, 2008, 93, 051906-10.
21. Shao Q., Liu G., Teweldebrhan D., Balandin A.A. High-temperature quenching of electrical resistance in graphene interconnects. Appl Phys Lett, 2008, 92, 2108-112.
22. Wei T., Song L., Zheng C., Wang K., Yan J., Shao B., Fan Z.J. The synergy of a three filler combination in the conductivity of epoxy composites. Mater Lett, 2010, 64, 2376-2379.
23. S., Iijima. Helical microtubules of graphitic carbon. Nature, 1991, 354, 56-58.
24. Cooper C.A., Young R.J., Halsall M. Investigation into the deformation of carbon nanotubes and their composites through the use of Raman spectroscopy. Composites Part A, 2001, 32A, 401-411.
25. Gao G., Cagin T., Goddard III W.A. Energetics, structure, mechanical and vibrational properties of single-walled carbon nanotubes. Nanotechnology, 1998, 9, 184-191.
26. Wong E.W., Sheehan P.E., Lieber C.M. Nanobeam mechanics: Elasticity, strength, and toughness of nanorods and nanotubes. Science, 1997, 277, 1971−1975.
27. J.P., Lu. Elastic properties of carbon nanotubes and nanoropes. Phys Rev Lett 1997, 79, 1297−1300.
28. Dumitrica T., Hua M., Yakobson B.I. Symmetry-, time-, and -dependent strength of carbon nanotubes. Proc. Nat. Acad. Sci. U. S. A., 2006, 103, 6105−6109.
29. Moniruzzaman M., Winey K. I., Polymer nanocomposites containing carbon nanotubes: Review. Macromolecules 2006, 39, 5194-5205.
30. Awasthi K., Srivastava A., Srivastava O.N. Synthesis of Carbon Nanotubes. J Nanosci Nanotechnol, 2005, 5, 1616-1636.
31. M., Monthioux. Filling single-wall carbon nanotubes. Carbon, 2002, 40, 1809-1823.
32. Aqel A., Kholoud M.M., El-Nour A., Ammar R.A.A., Al-Warthan A. Carbon nanotubes, science and technology part (I) structure, synthesis and characterization. Arabian Journal of Chemistry 2012, 5, 1-23.
33. Thostenson E.T., Zhifeng R., Chou T-W. Advances in the science and technology of carbon nanotubes and their composites: a review. Compos Sci Technol, 2001, 61, 1899-1912.
34. Dyke C.A., Tour J.M. Feature Article: Covalent Functionalization of Single-Walled Carbon Nanotubes for Materials Applications. J Phys Chem A, 2004, 108, 11151-11159.
35. Dresselhaus M.S., Dresselhaus G., Saito R. Physics of carbon nanotubes. Carbon, 1995, 33, 883–891.
36. Ebbesen T.W., Ajayan P.M. Large-scale synthesis of carbon nanotubes. Nature, 1992, 358, 220–221.
37. Terrones M. Science and Technology of the twenty-First Century: Synthesis, Properties and Applications of Carbon Nanotubes,. Annu Rev Mater Res, 2003, 33, 419–501.

38. Guo T., Nikoleav P., Rinzler A.G., Tomanek D., Colbert D.T., Smalley R.E. Self-Assembly of Tubular Fullerenes. J Phys Chem1995, 99, 10694–97.
39. Hsu W.K., Hare J.P., Terrones M., Kroto H.W., Walton D.R.M., Harris P.J.F. Condensed phase nanotubes. Nature, 1995, 377, 687.
40. Laplaze D., Bernier P., Maser W.K., Flamant G., Guillard T., Loiseau A. Carbon nanotubes: The solar approach. Carbon, 1998,36, 685–88.
41. Niyogi S., Hamon M.A., Hu H., Zhao B., Bhowmik P., Sen R., Itkis M.E., Haddon R.C. Chemistry of single-walled carbon nanotubes. Acc Chem Res, 2002, 35, 1105-1113.
42. Star A., Stoddart J.F., Steuerman D., Diehl M., Boukai A., Wong E.W., Yang X., Chung S.W., Choi H., Heath J R. Preparation and Properties of Polymer-Wrapped Single-Walled Carbon Nanotubes. Angew Chem Int Ed, 2001, 40, 1721-1725.
43. Star A., Liu Y., Grant K., Ridvan L., Stoddart J.F., Steuerman D.W., Diehl M.R., Boukai A., Heath J.R. Noncovalent Side-Wall Functionalization of Single-Walled Carbon Nanotubes. Macromolecules, 2003, 36, 553-560.
44. Ajayan P.M., Stephan O., Colliex C., Trauth D. Aligned carbon nanotube arrays formed by cutting a polymer resin-nanotube composite. Science, 1994, 265, 1212-14.
45. Badaire S., Poulin P., Maugey M., Zakri C. In Situ Measurements of Nanotube Dimensions in Suspensions by Depolarized Dynamic Light Scattering. Langmuir, 2004, 20, 10367-10370.
46. Barrau S., Demont P., Perez E., Peigney A., Laurent C., Lacabanne C. Effect of Palmitic Acid on the Electrical Conductivity of Carbon Nanotubes−Epoxy Resin Composites. Macromolecules, 2003, 36, 9678-9680.
47. Bryning M.B., Milkie D.E., Islam M.F., Kikkawa J.M., Yodh A.G. Thermal conductivity and interfacial resistance in single-wall carbon nanotube epoxy composites. Appl. Phys. Lett. 2005, 87, 161909-1-161909-3.
48. Sundararajan P.R., Singh S., Moniruzzaman M. Surfactant induced crystallization of Polycarbonate. Macromolecules, 2004, 37, 10208-10211.
49. Zhu J., Kim J., Peng H., Margrave J.L., Khabashesku V.N., Barrera E.V. Improving the Dispersion and Integration of Single-Walled Carbon Nanotubes in Epoxy Composites through Functionalization. Nano Lett, 2003, 3, 1107-1113.
50. Nogales A., Broza G., Roslaniec Z., Schulte K., Sics I., Hsiao B.S., Sanz A., Garcia-Gutierrez M.C., Rueda D.R., Domingo C., Ezquerra T.A. Low percolation threshold in nanocomposites based on oxidized single wall carbon nanotubes and poly(butylene terephthalate). Macromolecules, 2004, 37, 7669-7672.
51. Hernández J.J, García-Gutiérrez M.C., Nogales A., Rueda D.R., Kwiatkowska M., Szymczyk A., Roslaniec Z., Concheso A., Guinea I., Ezquerra T.A. Influence of preparation procedure on the conductivity and transparency of SWCNT-polymer nanocomposites. Compo Sci Technol 2009, 69, 1867–1872.
52. Jia Z.J., Wang Z.J., Xu C.L., Liang J., Wei B.Q., Wu D.H., Zhu S.W. Study on poly(methyl methacrylate)/carbon nanotube composites. Mater Sci Eng A Struct, 1999, 271(1/2), 395-400.
53. Park C., Ounaies Z., Watson K.A., Crooks R.E., Smith Jr. J., Lowther S.E., Connell J.W., Siochi E.J., Harrison J.S., St. Clair T.L. Dispersion of single wall carbon nanotubes by in situ polymerization under sonication. Chem Phys Lett, 2002, 364(3-4), 303-308.

54. Velasco-Santos C., Martínez-Hernández A.L., Fisher F.T, Ruoff R., Castaño V.M. Improvement of thermal and mechanical properties of carbon nanotube composites through chemical functionalization. Chem Mater, 2003, 15(23), 4470-4475.
55. Jang J., Bae J., Yoon S.H. A study on the effect of surface treatment of carbon nanotubes for liquid crystalline epoxide–carbon nanotube composites. J Mater Chem, 2003,13, 676-681.
56. Wiśniewska E. Pabin-Szafko B., Huczko A. Nanofibres and Nanotubes in Radical Polymerisation. FIBRES & TEXTILES in Eastern Europe, 2009, 17 (76), 23-25.
57. Pabin-Szafko B. Wisniewska E., Szafko J. Carbon nanotubes and fullerene in the solution polymerisation of acrylonitrile. Europ Polym J, 2006, 42, 1516-1520.
58. Xia H., Wang Q., Li K., Hu G.H. Preparation of polypropylene/carbon nanotube composite powder with a solid-state mechanochemical pulverization process. J Appl Polym Sci, 2004, 93(1), 378-386.
59. Kasimatis K.G., Nowell J.A., Dykes L.M., Burghardt W.R., Thillalyan R., Brinson L.C., Andrews R., Torkelson J.M. Morphology, thermal, and rheological behavior of nylon 11/multi-walled carbon nanotube nanocomposites prepared by melt compounding. PMSE Prepr, 2005, 92, 255-256.
60. Regev O., ElKati P.N.B., Loos J., Koning C.E. Preparation of conductive nanotube-polymer composites using latex technology. Adv Mater, 2004, 16(3), 248-251.
61. Dufresne A., Paillet M., Putaux J.L., Canet R., Carmona F., Delhaes P., Cui S. Processing and characterization of carbon nanotubes/poly(styrene-co-butyl acrylate) nanocomposites. J Mater Sci, 2002, 37, 3915-3923.
62. Vigolo B., Penicaud A., Coulon C., Sauder C., Pailler R., Journet C., Bernier P., Poulin P. Macroscopic fibers and ribbons of oriented carbon nanotubes. Science, 2000, 290, 1331-1334.
63. Raravikar N.R., Schadler L.S., Vijayaraghavan A., Zhao Y., Wei B., Ajayan P.M. Synthesis and characterization of thickness-aligned carbon nanotube-polymer composite films. Chem Mater, 2005, 17, 974-983.
64. Feng W., Bai X.D., Lian Y. Q., Liang J., Wang X.G., Yoshino K. Well-aligned polyaniline/carbon-nanotube composite films grown by in-situ aniline polymerization. Carbon, 2003, 41, 1551-1557.
65. Kimura T., Ago H., Tobita M., Ohshima S., Kyotani M., Yumura M. Polymer composites of carbon nanotubes aligned by a magnetic field. Adv Mater, 2002, 14, 1380-1383.
66. Jin L., Bower C., Zhou O. Alignment of carbon nanotubes in a polymer matrix by mechanical stretching. Appl Phys Lett, 1998, 73, 1197-1199.
67. Safadi B., Andrews R., Grulke E.A. Multiwalled carbon nanotube polymer composites: Synthesis and characterization of thin films. J Appl Polym Sci, 2002, 84, 2660-2669.
68. Haggenmueller R., Zhou W., Fischer J.E., Winey K.I. Production and characterization of polymer nanocomposites with highly aligned single-walled carbon nanotubes. J Nanosci Nanotechnol, 2003, 3, 105-110.
69. Ge Jason J., Hou H., Li Q., Graham Matthew J., Greiner A., Reneker Darrell H., Harris Frank W., Cheng Stephen Z.D. Assembly of Well-Aligned Multiwalled Carbon Nanotubes in Confined Polyacrylonitrile Environments: Electrospun Composite Nanofiber Sheets. J Am Chem Soc, 2004, 126(48), 15754-15761.

70. Hou H., Ge J.J., Zeng J., Li Q., Reneker D.H., Greiner A., Cheng S.Z.D. Electrospun Polyacrylonitrile Nanofibers Containing a High Concentration of Well-Aligned Multiwall Carbon Nanotubes. Chem Mater, 2005, 17(5), 967-973.
71. Agarwal B.D., Broutman L.G. Analysis and Performance of Fiber Composites. Wiley: New York, 1980.
72. P.K., Mallick. Fiber-Reinforced Composites, Marcel Dekker: New York, 1993.
73. Qian D., Dickey E.C. Load transfer and deformation mechanisms in carbon nanotube polystyrene composites. Appl Phys Lett 2000, 76, 2868–70.
74. Ma P.C., Siddiqui N.A., Marom G., Kim J.K. Dispersion and functionalization of carbon nanotubes for polymer-based nanocomposites: A review. Composites: Part A, 2010, 41, 1345-1367.
75. Desai A.V., Haque M.A. Mechanics of the interface for carbon nanotube polymer composites. Thin-Walled Struct, 2005, 43, 1787–803.
76. Ma P.C., Kim J.K., Tang B.Z. Effects of silane functionalization on the properties of carbon nanotubes/epoxy nanocomposites. Compos Sci Technol, 2007, 67, 2965–72.
77. Frankland S.J.V., Caglar A., Brenner D.W., Griebel M. Molecular simulation of the influence of chemical cross-links on the shear strenght of carbon-polymer interfaces. J Phys Chem B, 2002, 106, 3046-3048.
78. Geng H., Rosen R., Zheng B., Shimoda H., Fleming L., Liu J., Zhou O. Fabrication and Properties of Composites of Poly(ethylene oxide) and Functionalized Carbon Nanotubes. Adv Mater, 2002, 14, 1387-1390.
79. Wu H.P., Wu X.J., Ge M.Y., Zhang G.Q., Wang Y.W., Jiang J. Properties investigation on isotropical conductive adhesives filled with silver coated carbon nanotubes. Comp Sci Technol 2007, 67(6), 1182–1186.
80. Grossiord N., Loos J., Regev O., Koning C.E. Toolbox for dispersing carbon nanotubes into polymers to get conductive nanocomposites. Chem Mater, 2006, 18, 1089–99.
81. Li C., Thostenson E.T., Chou T.W. Sensors and actuators based on carbon nanotubes and their composites: review. Comp Sci Technol, 2008, 68(6), 1227–1249.
82. Aneli J.N., Khananasvili L.M., Zaikov G.E. Structuring and conductivity of polymer composites. New York: Nova Science Publishers; 1998. p. 1–100.
83. Sham M.L., Li J., Ma P.C., Kim J.K. Cleaning and functionalizaton of polymer surfaces and nanoscale carbon fillers by UV/ozone treatment: a review. J Compos Mater, 2009, 43, 1537–64.
84. Maiti S., Shrivastava N.K., Suin S., Khatua B.B. A strategy of achieving low percolation threshold and high electrical conductivity in melt-blended polycarbonate (PC)/ multiwall carbon nanotube (MWCNT) nanocomposites: Electrical and thermo-mechanical properties. eXPRESS Polymer Letters 2013, 7(6), 505–518.
85. Bauhofer W., Kovacs J.Z. A review and analysis of electrical percolation in carbon nanotube polymer composites. Compos Sci Technol, 2009, 69, 1486–98.
86. Li J., Ma P.C., Chow W.S., To C.K., Tang B.Z., Kim J.K. Correlations between percolation threshold, dispersion state and aspect ratio of carbon nanotube. Adv Funct Mater, 2007, 17, 3207–15.
87. Sandler J.K.W., Kirk J.E., Kinloch I.A., Shaffer M.S.P., Windle A.H. Ultra-low electrical percolation threshold in carbon nanotube-epoxy composites. Polymer, 2003, 44, 5893–9.

88. Martin C.A., Sandler J.K.W., Windle A.H., Schwarz M.K., Bauhofer W., Schulte K., Shaffer M.S.P. Electric field-induced aligned multi-wall carbon nanotube networks in epoxy composites. Polymer, 2005, 46, 877–86.
89. Bryning M.B., Islam M.F., Kikkawa J.M., Yodh A.G. Very low conductivity threshold in bulk isotropic single-walled carbon. Adv Mater, 2005, 17, 1186-1191.
90. Du F., Fischer J.E.,Winey K.I. Coagulation method for preparing single-walled carbon nanotube/poly(methyl methacrylate) composites and their modulus, electrical conductivity, and thermal stability. J Polym Sci Part B Polym Phys, 2003, 41, 3333-3338.
91. Haggenmueller R., Gommans H.H., Rinzler A.G., Fischer J.E., Winey K.I. Aligned single-wall carbon nanotubes in composites by melt processing methods. Chem Phys Lett, 2000, 330, 219-225.
92. Martin C.A., Sandler J.K.W., Shaffer M.S.P., Schwarz M.K., Bauhofer W., Schulte K., Windle A.H. Formation of percolating networks in multi-wall carbon-nanotube-epoxy composites. Compos Sci Technol, 2004, 64, 2309-2316.
93. Du F., Fischer J.E., Winey K.I. Effect of nanotube alignment on percolation conductivity in carbon nanotube / polymer composites. Phys ReV B Condens Matter, 2005, 72, 121404/1-121404/4.
94. Ma P.C., Tang B.Z., Kim J.K. Effect of CNT decoration with silver nanoparticles on electrical conductivity of CNT–polymer composites. Carbon, 2008, 46, 1497–505.
95. Li S., Qin Y., Shi J., Guo Z.X., Li Y., Zhu D. Electrical Properties of Soluble Carbon Nanotube/Polymer Composite Films. Chem Mater, 2005, 17(1), 130-135.
96. Ramanathan T., Liu H., Brinson L.C. Functionalized SWNT/polymer nanocomposites for dramatic property improvement. J Polym Sci Part B Polym Phys, 2005, 43(17), 2269-2279.
97. Tamburri E., Orlanducci S., Terranova M.L., Valentini F., Palleschi G., Curulli A., Brunetti F., Passeri D., Alippi A., Rossi M. Modulation of electrical properties in single-walled carbon nanotube/conducting polymer composites. Carbon, 2005, 43, 1213-1221.
98. Valentini L., Armentano I., Puglia, D., Kenny J.M. Dynamics of amine functionalized nanotubes/epoxy composites by dielectric relaxation spectroscopy. Carbon, 2004, 42, 323-329.
99. Moisala A., Li Q., Kinloch I.A., Windle A.H. Thermal and electrical conductivity ofsingle- and multi-walled carbon nanotube-epoxy composites. Compos Sci Technol, 2006, 66, 1285–8.
100. Buldum A., Lu J.P. Contact resistance between carbon nanotubes. Phys Rev B, 2001, 63, 161403-1–3-4.
101. Stadermann M., Papadakis S.J., Falvo M.R., Novak J., Snow E., Fu Q., Liu J., Fridman Y., Boland J.J., Superfine R., Washburn S. Nanoscale study of conduction through carbon nanotube networks. Phys Rev B, 2004, 69, 201402-1–2-3.
102. Liu C., Zhang J., He J., Hu G. Gelation in carbon nanotube/polymer composites. Polymer, 2003, 44, 7529–32.
103. Du F., Scogna R.C., Zhou W., Brand S., Fischer J.E., Winey K.I. Nanotube networks in polymer nanocomposites: rheology and electrical conductivity. Macromolecules, 2004,37, 9048–55.
104. Fan Z., Advani S.G. Rheology of multiwall carbon nanotube suspensions. J Rheol, 2007, 1, 585–604.

105. Abbasi S., Carreau P.J., Derdouri A., Moan M. Rheological properties and percolation in suspensions of multiwalled carbon nanotubes in polycarbonate. Rheol Acta, 2009, 48, 943–59.
106. Sandler J. Shaffer M.S.P., Lam Y.-M., Windle A., Werner P., Altstädt V., Nastalczyk J., Broza G., Schulte K., Keun C.-A. Carbon-Nanofibre-Filled Thermoplastic Composites. MRS 2001 Fall Meeting, Boston MA, USA (2001).
107. Poetschke P., Abdel-Goad M., Alig I., Dudkin S., Lellinger D. Rheological and dielectrical characterization of melt mixed polycarbonate-multiwalled carbon nanotube composites. Polymer, 2004, 45, 8863-8870.
108. Bose S. Bhattacharyya A.R., Kulkarni A.R., Pötschke P. Electrical, rheological and morphological studies in co-continuous blends of polyamide 6 and acrylonitrile–butadiene–styrene with multiwall carbon nanotubes prepared by melt blending. Compos Sci Technol, 2009, 69, 65-72.
109. Siddiqui N.A., Khan S.U., Ma P.C., Li C.Y., Kim J.K. Manufacturing and characterization of carbon fibre/epoxy composite prepregs containing carbon nanotubes. Compo Part A Appl Sci Manuf, 2011, 42(10), 1412-1420.
110. Mitchell C.A. Bahr J.L., Arepalli S, Tour J.M., Krishnamoorti R. Dispersion of functionalized carbon nanotubes in polystyrene. Macromolecules, 2002,35, 8825–8830.
111. Ma P.C., Mo S.Y., Tang B.Z., Kim J.K. Dispersion, interfacial interaction and reagglomeration of functionalized carbon nanotubes in epoxy composites. Carbon, 2010, 48, 1824–34.
112. Phillpot S.R., McGaughey A.J.H. Introduction to thermal transport. Mater Today, 2005, 8,18–20.
113. Biercuk M.J., Llaguno M.C., Radosavljevic M., Hyun J.K., Johnson A.T., Fischer J.E. Carbon nanotube composites for thermal management. Appl Phys Lett, 2002, 80, 2767–9.
114. Evseeva L.E., Tanaeva S.A. Thermal conductivity of micro-and nanostructural epoxy composites at low temperatures. Mech Compos Mater, 2008, 44, 87–92.
115. Guthy C., Du F., Brand S., Winey K.I., Fischer J.E. Thermal conductivity of singlewalled carbon nanotube/PMMA composites. J Heat Trans, 2007,129, 1096–9.
116. Shenogin S., Xue L.P., Ozisik R., Keblinski P., Cahill D.G. Role of thermal boundary resistance on the heat flow in carbon-nanotube composites. J Appl Phys, 2004;95:8136–44.
117. Gojny F.H., Wichmann M.H.G, Fiedler B., Kinloch I.A., Bauhofer W., Windle A.H., Schulte K. Evaluation and identification of electrical and thermal conduction mechanisms in carbon nanotube/epoxy composites. Polymer, 2006, 47(6), 2036–45.
118. Probst O., Moore E.M., Resasco D.E., Grady B.P. Nucleation of polyvinyl alcohol crystallization by single-walled carbon nanotubes. Polymer, 2004, 45(13), 4437-4443.
119. Anand K.A., Agarwal U.S., Joseph R. Carbon nanotubes induced crystallization of poly(ethylene terephthalate). Polymer, 2006, 47(11), 3976-3980.
120. Valentini L., Biagiotti J., Kenny J.M., Santucci S. You have full text access to this content. J Appl Polym Sci, 2003, 87(4), 708-713.
121. Bhattacharyya A.R., Sreekumar T.V., Liu T., Kumar S., Ericson L.M., Hauge R.H. Crystallization and orientation studies in polypropylene/single wall carbon nanotube composite. Polymer, 2003, 44(8), 2373-2377.

122. Kashiwagi T., Grulke E., Hilding J., Harris R., Awad W., Douglas J. Thermal degradation and flammability properties of poly(propylene)/carbon nanotube composites. Macromol Rapid Commun, 2002, 232, 761–5.
123. Kashiwagi T., Du F., Douglas J.F., Winey K.I., Harris R.H., Shields J.R. Nanoparticle networks reduce the flammability of polymer nanocomposites. Nat Mater, 2005, 4, 928–33.
124. Kashiwagi T., Du F., Winey K.I., Groth K.M., Shields J.R., Bellayer S.P., Kim H., Douglas J.F. Flammability properties of polymer nanocomposites with single-walled carbon nanotubes: effects of nanotube dispersion and concentration. Polymer, 2005, 46, 471–81.
125. Schartel B., Pötschke P., Knoll P.U., Abdel-Goad M. Fire behavior of polyamide 6/multiwall carbon nanotube nanocomposites. Eur Polym J, 2005, 41, 1061–70.
126. Li J., Wong P.S., Kim J.K. Hybrid nanocomposites containing carbon nanotubes and graphite nanoplatelets. Mater Sci Eng A, 2008, 483–484, 660–3.
127. Bokobza L., Rahmani M., Belin C., Bruneel J., Bounia N.E.E. Blends of carbon blacks and multiwall carbon nanotubes as reinforcing fillers for hydrocarbon rubbers. J Polym Sci B, 2008, 46, 1939–51.
128. Fan Z.J., Wang Y., Luo G.H., Li Z.F., Wei F. The synergetic effect of carbon nanotubes and carbon black in a rubber system. New Carbon Mater, 2008, 23, 149–53.
129. Sun Y., Bao H.D., Guo Z.X., Yu J. Modeling of the electrical percolation of mixed carbon fillers in polymer-based composites. Macromolecules, 2009, 42, 459–63.
130. Fim F., Guterres J.M., Basso N.R.S., Galland G.B. Polyethylene/graphite nanocomposites obtained by in situ polymerization. J Polym Sci A, 2010, 48(3), 692-698.
131. Viculis L.M., Mack J.J., Mayer O.M., Hahn H.T., Kaner R B. Intercalation and exfoliation routes to graphite nanoplatelets. J Mater Chem, 2005, 15, 974–978.
132. Yakovlev A.V., Finaenov A.I., Zabud'kov S.L., Yakoleva E.V. Thermally expanded graphite: Synthesis, Properties and Prospects for Use. Russ J Appl Chem, 2006, 79(11), 1741-1751.
133. Li J., Lin H., Zhao W., Chen G. You have full text access to this content. J Appl Polym Sci, 2008, 109(3), 1377-1380.
134. Fan H., Wang L., Zhao K., Li N., Shi Z., Ge Z., Jin Z. Fabrication, mechanical properties, and biocompatibility of graphene-reinforced chitosan composites. Biomacromolecules, 2010, 11(9), 2345-2351.
135. Ramanathan T., Stankovich S., Dikin D.A., Liu H., Shen H., Nguyen S.T., Brinson L.C. Graphitic nanofillers in PMMA nanocomposites—An investigation of particle size and dispersion and their influence on nanocomposite properties. J Polym Sci Part B Polym Phys, 2007, 45(15), 2097-3112.
136. Park S., Ruoff R.S. Chemical methods for the production of graphenes. Nature Nanotechnol, 2009, 4, 217–224.
137. Geim A.K., Novoselov K.S. The rise of graphene. Nature Mater, 2007, 6, 183–191.
138. Wang X., You H., Liu F., Li M., Wan L., Li S., Li Q., Xu Y., Tian R., Yu Z., Xiang D., Cheng J. Large-Scale Synthesis of Few-Layered Graphene using CVD. J Chem Vapor Deposition, 2009, 15(1-3), 53–56.
139. Wang Y., Chen X., Zhong Y., Zhu F., Loh K.P. Large area, continuous, few-layer graphene as anodes in organic photovoltaic devices. Appl Phys Lett, 2009, 95, 063302/1–063302/3.

140. S.J., Chae and Güneş F., Kim K.K., Kim E.S., Han G.H., Kim S M., Shin H.J., Yoon S.M., Choi J.Y., Park M.H., Yang C.W., Pribat D., Lee Y.H. Synthesis of Large-Area Graphene Layers on Poly-Nickel Substrate by Chemical Vapor Deposition: Wrinkle Formation. Adv Mater, 2009, 21(22), 2328–2333.
141. Li X., Cai W., An J., Kim S., Nah J., Yang D., Piner R., Velamakanni A., Jung I., Tutuc E., Banerjee S.K., Colombo L., Ruoff R.S. Large-Area Synthesis of High-Quality and Uniform Graphene Films on Copper Foils. Science, 2009, 324, 1312–1314.
142. Li N., Wang Z., Zhao K., Shi Z., Gu Z., Xu S. Large scale synthesis of N-doped multi-layered graphene sheets by simple arc-discharge method. Carbon, 2010, 48, 255–259.
143. Karmakar S., Kulkarni N.V., Nawale A.B., Lalla N.P., Mishra R., Sathe V.G., Bhoraskar S.V., Das A.K. A novel approach towards selective bulk synthesis of few-layer graphenes in electric arc. J Phys D Appl Phys, 2009, 42, 115201/1–115201/14.
144. Rollings E., Gweon G.H., Zhou S.Y., Mun B.S., McChesney J.L., Hussain B.S., Fedorov A.V., First P.N., de Heer W.A., Lanzar A. Synthesis and characterization of atomically thin graphite films on a silicon carbide substrate. J Phys Chem Solids, 2006, 67, 2172–2177.
145. Alexander M., Oleg P. Density functional study of graphene overlayers on SiC. Phys Status Solidi B, 2008, 245, 1425–1435.
146. Sutter P.W., Flege J.I., Sutter E.A. Epitaxial graphene on ruthenium. Nature Mater, 2008, 7, 406–411.
147. Sprinkle M., Soukiassian P., de Heer W.A., Berger C., Conrad E.H. Epitaxial graphene: The material for graphene electronics. Phys Status Solidi RRL, 2009, 3, A91–A94.
148. Yannick C., Wim K. Growing graphene sheets from reactions with methyl redicals: A quantum chemical study. Chem Phys Chem, 2006, 7, 1770–1778.
149. Yang X., Dou X., Rouhanipou A., Zhi L., Rader Hans J., Mullen K. Two-Dimensional Graphene Nanoribbons. J Am Chem Soc, 2008, 130(13), 4216–7.
150. Zhi L., Muellen K. A bottom-up approach from molecular nanographenes to unconventional carbon materials. J Mater Chem, 2008, 18, 1472–1484.
151. Kim C.D., Min B.K., Jung W.S. Preparation of graphene sheets by the reduction of carbon monoxide. Carbon, 2009, 47, 1610–1612.
152. Kosynkin D.V., Higginbotham A.L., Sinitskii A., Lomeda J.R., Dimiev A., Price B.K., Tour J.M. Longitudinal unzipping of carbon nanotubes to form graphene nanoribbons. Nature, 2009, 458, 872–876.
153. A., Hirsch. Unzipping carbon nanotubes: A peeling method for formation of graphene nanoribbons. Angew Chem Int Ed, 2009, 48, 6594–6596.
154. Worsley K.A., Ramesh P., Mandal S.K., Niyogi S., Itkis M. E., Haddon R.C. Soluble graphene derived from graphite fluoride. Chem Phys Lett, 2007, 445, 51–56.
155. K.E., Carr. Intercalation and oxidation effects on graphite of a mixture of sulphuric and nitric acids. Carbon, 1970, 8, 155–166.
156. Chen G., Wu D., Weng W., Wu C. Exfoliation of graphite flake and its nanocomposites. Carbon, 2003, 41, 619–621.
157. Lee J.H., Shin D.W., Makotchenko V.G., Nazarov A.S., Fedorov V.E., Kim Y.H., Choi J.Y., Kim J.M., Yoo J.B. One-step exfoliation synthesis of easily soluble graphite and transparent conducting graphene sheets. Adv Mater, 2009, 21, 4383–4387.

158. Celzard A., Mareche J.F., Furdin G. Surface area of compressed expanded graphite. Carbon, 2002, 40, 2713– 2718.
159. H., Fukushima. Graphite nanoreinforcements in polymer nanocomposites. Ph.D. Thesis, Michigan State University, 2003.
160. Kalaitzidou K., Fukushima H., Drzal L.T. A new compounding method for exfoliated graphite-polypropylene nanocomposites with enhabced flexural properties and lower percolation threshold. Compos Sci Technol, 2007, 67, 2045–2051.
161. Bourlinos A.B., Georgakilas V., Zboril R., Steriotis T.A., Stubos A. Liquid-phase exfoliation of graphite towards solubilized graphenes. Small, 2009, 5, 1841–1845.
162. Liu N., Luo F., Wu H., Liu Y., Zhang C., Chen J. One-step ionic-liquid-assisted electrochemical synthesis o ionic-liquid-functionalized graphene sheets directly from graphite. Adv Funct Mater, 2008, 18, 1518–1525.
163. Behabtu N., Lomeda J.R., Green M.J., Higginbotham A.L., Sinitskii A., Kosynkin D.V., Tsentalovich D., Parra-Vasquez A.N.G., Schmidt J., Kesselman E., Cohen Y., Talmon Y., Tour J.M., Pasquali M. Spontanous high-concentration dispersions and liquid crystals of graphene. Nature Nanotechnol, 2010, 5, 406–411.
164. B.C., Brodie. On the atomic weight of graphite. Philos Trans R Soc London, 1859, 149, 249–259.
165. L., Staudenmaier. Preparation of graphitic acid. Ber Dtsch Chem Ges, 1898, 31, 1481–87.
166. He H., Klinowski J., Forster M., Lerf A. A new structural model for graphite oxide. Chem Phys Lett, 1998, 287, 53–56.
167. Li J.L., Kudin K.N., McAllister M. J., Prud'homme, R. K., Aksay, I. A., Car R. Oxygen-driven unzipping of graphitic materials. Phys Rev Lett, 2006, 96, 176101/1–176101/ 4.
168. Stankovich S., Dikin D.A., Piner R.D., Kohlhaas K.A., Kleinhammes A., Jia Y., Wu Y., Nguyen S.T., Ruoff R.S. Synthesis of graphene-based nanosheets via chemical reduction of exfoliated graphite oxide. Carbon, 2007, 45, 1558–1565.
169. Wang G., Shen X., Wang B., Yao J., Park J. Synthesis and characterisation of hydrophilic and organophilic graphene nanosheets. Carbon, 2009, 47, 1359–1364.
170. Stankovich S., Piner R.D., Chen X., Wu N., Nguyen S.T., Ruoff R.S. Stable aqueous dispersions of graphitic nanoplatelets via reduction of exfoliated graphite oxide in the presence of poly(sodium-4-styrenesulfonate). J Mater Chem, 2006, 16, 155–158.
171. Lomeda J.R., Doyle C.D., Kosynkin D.V., Hwang W.F., Tour J.M. Diazonium Functionalization of Surfactant-Wrapped Chemically Converted Graphene Sheets. J Am Chem Soc, 2008, 130(48), 16201–16206.
172. Wang H., Robinson J.T., Li X., Dai H. Solvothermal Reduction of Chemically Exfoliated Graphene Sheets. J Am Chem Soc, 2009, 131(29), 9910–9911.
173. Stankovich S., Dikin D.A., Dommett G.H.B., Kohlhaas K.M., Zimney E.J., Stach E.A., Piner R.D., Nguyen S.T., Ruoff R.S. Graphene-based composite materials. Nature, 2006, 442, 282–286.
174. Wang G., Yang J., Park J., Gou X., Wang B., Liu H., Yao J. Facile synthesis and characterization of graphene nanosheets. J Phys Chem C, 2008, 112, 8192–8195.

175. Schniepp H.C., Li J.L., McAllister M.J., Sai H., Herrera- Alonso M., Adamson D.H., Prud'homme R.K., Car R., Saville D.A., Aksay I.A. Functionalized single graphene sheets derived from splitting graphite oxide. J Phys Chem B, 2006, 110, 8535–8539.
176. Du X., Skachko I., Barker A., Andrei E.Y. Approaching ballistic transport in suspended graphene. Nature Nanotechnol, 2008, 3, 491–495.
177. Prud'homme R.K., Aksay I.A., Adamson D., Abdala A.A. Thermally exfoliated graphite oxide. U.S. Patent 20070092432, 2007.
178. McAllister M.J., Li J.L., Adamson D.H., Schniepp H.C., Abdala A.A., Liu J., Herrera-Alonso M., Milius D.L., Car R., Prud'homme R.K., Aksay I.A. Single Sheet Functionalized Graphene by Oxidation and Thermal Expansion of Graphite. Chem Mater, 2007, 19(18), 4396– 4404.
179. Steurer P., Wissert R., Thomann R., Muelhaupt R. Functionalized Graphenes and Thermoplastic Nanocomposites Based upon Expanded Graphite Oxide. Macromol Rapid Commun, 2009, 30, 316–327.
180. Aksay I.A., Milius D.L., Korkut S., Prud'homme R.K. Functionalized graphene sheets having high carbon to oxygen ratios. W.O. Patent 2009/134492 A2, 2009.
181. Verdejo R., Bernal M.M., Romasanta L.J., Lopez-Manchado M.A. Graphene Filled Polymer Nanocom posites. J Mater Chem, 2011, 21(10), 3301-3310.
182. Huang X., Qi X., Boey F., Zhang H. Graphene- Based Composites. Chemical Society Reviews, 2012, 41(2), 666-686.
183. Kuilla T., Bhadra S., Yao D., Kim N.H., Bose S., Lee J.H. Recent Advances in Graphene Based Polymer Composites. Progress in Polymer Science, 2010, 35(11), 1350-1375.
184. Jinhong Y., Huang X., Wu C., Jiang P. Permittivity, Thermal Conductivity and Thermal Stability of Poly (Vinylidene Fluoride)/Graphene Nanocomposites. IEEE Transactions on Dielectrics and Electrical Insulation, 2011, 18(2),478-484.
185. Chen Y, Qi Y., Tai Z., Yan X., Zhu F., Xue Q. Preparation, Mechanical Properties and Biocompatibility of Graphene Oxide/Ultrahigh Molecular Weight Polyethylene Composites. Europ PolymJ,l 2012, 48(6), 1026-1033.
186. Zhao X., Zhang Q., Chen D. Enhanced Mechanical Properties of Graphene-Based Poly (Vinyl Alcohol) Composites. Macromolecules, 2010, 43(5), 2357-2363.
187. Layek R.K, Samanta S., Nandi A.K. The Physical Properties of Sulfonated Graphene/Poly (Vinyl Alcohol) Composites. Carbon, 2012, 50(3), 815-827.
188. Zhang H.B., Zhang W.G., Yan Q., Jiang Z.G., Yu Z.Z. The Effect of Surface Chemistry of Graphene on Rheological and Electrical Properties of Polymethylmethacrylate Composites. Carbon, 2012, 50(14), 5117-5125.
189. Kim H., Miura Y., Macosko C.W. Graphene/Poly urethane Nanocomposites for Improved Gas Barrier and Electrical Conductivity. Chemistry of Materials, 2010, 22(11), 3441-3450.
190. Ren P.G., Yan D.X., Chen T., Zeng B.Q., Li Z.M. Improved Properties of Highly Oriented Graphene/ Polymer Nanocomposites. J Appl Polym Sci, 2011, 121(6), 3167-3174.
191. Goncalves G., Marques P.A.A., Barros-Timmons A., Bdkin I., Singh M.K., Emani N., Gracio J. Graphene Oxide Modified with PMMA via ATRP as a Reinforcement Filler. J Mater Chem, 2010, 20(44), 9927- 9934.

192. Singh V., Joung D., Zhai L., Das S., Khondaker S.I., Seal S. Graphene Based Materials: Past, Present and Future. Progress in Materials Science, 2011, 56(8), 1178-1271.
193. Pei S., Cheng H.M. The Reduction of Graphene Oxide. Carbon, 2012, 50(9), 3210-3228.
194. An X., Simmons T., Shah R., Wolfe C., Lewis K.M., Washington M., Nayak S.K., Talapatra S., Kar S. Stable Aqueous Dispersions of Noncova- lently Functionalized Graphene from Graphite and Their Multifunctional High-Performance Applications. Nano Lett, 2010, 10(11), 4295-4301.
195. Ansari S., Kelarakis A., Estevez L., Giannelis E.P. Oriented Arrays of Graphene in a Polymer Matrix by in situ Reduction of Graphite Oxide Nanosheets. Small, 2010, 6(2), 205-209.
196. Wei T., Luo G., Fan Z., Zheng C., Yan J., Yao C., Li W., Zhang C. Preparation of Graphene Nanosheet/ Polymer Composites Using in Situ Reduction-Extractive Dispersion. Carbon, 2009, 47(9), 2296- 2299.
197. Park S., Suk J.W., An J., Oh J., Lee S., Lee W., Potts J.R., Byun J.H., Ruoff R.S. The Effect of Concentration of Graphene Nanoplatelets on Mechanical and Electrical Properties of Reduced Graphene Oxide Papers. Carbon, 2012, 50(12), 4573-4578.
198. Beckert F., Friedrich C., Thomann R, Mülhaupt R. Sulfur-Functionalized Graphenes as Macro-Chain-Transfer and RAFT Agents for Producing Graphene Polymer Brushes and Polystyrene Nanocomposites. Macromolecules, 2012, 45(17), 7783-7090.
199. Song P., Cao Z., Cai Y., Zhao L., Fang Z., Fu S. Fabrication of Exfoliated Graphene-Based Polypropylene Nanocomposites with Enhanced Mechanical and Thermal Properties. Polymer, 2011, 52(18), 4001-4010.
200. El Achaby M., Arrakhiz F.A., Vaudreuil S., Qaiss A.K., Bousmina M., Fassi-Fehri O. Mechanical, Thermal, and Rheological Properties of Graphene-Based Polypropylene Nanocomposites Prepared by Melt Mixing. Polym Compos, 2012, 33(5), 733-744.
201. El Achaby A., Arrakhiz F.Z., Vaudreuil S., Essassi E.M., Qaiss A., Bousmina M. Preparation and Characterization of Melt-Blended Graphene Nanosheets-Poly (Vinylidene Fluoride) Nanocomposites with Enhanced Properties. J Appl Polym Sci, 2012, 127(6), 4697-4707.
202. Bao C., Song L., Xing J., Guo Y., Hu Y. Preparation of Graphene by Pressurized Oxidation and Multiplex Reduction and Its Polymer Nanocomposites by Masterbatch-Based Melt Blending. J Mater Chem, 2012, 22(13), 6088-6096.
203. Kim H., Kobayashi S., AbdurRahim M.A., Zhang M.J., Khusainova A., Hillmyer M.A., Abdala A.A., Macosko C.W. Graphene/Polyethylene Nanocomposites: Effect of Polyethylene Functionalization and Blending Methods. Polymer, 2011, 52(8), 1837-1846.
204. Potts J.R., Lee S.H., Alam T.M., An J., Stoller M.D., Piner R.D., Ruoff R.S. Thermomechanical Properties of Chemically Modified Graphene/Poly (Methyl Methacrylate) Composites Made by in situ Polymerization. Carbon, 2011, 49(8), 2615-2623.
205. Zhang F., Peng X., Yan W., Peng Z., Shen Y. Non- isothermal Crystallization Kinetics of in situ Nylon 6/Graphene Composites by Differential Scanning Calorimetry. J Polym Sci Part B Polym Phys, 2011, 49(19), 1381-1388.
206. Wang X., Hu J., Song L., Yang H., Xing W., Lu H. In Situ Polymerization of Graphene Nanosheets and Polyurethane with Enhanced Mechanical and Thermal Properties. J Mater Chem, 2011, 21(12), 4222-4227.

207. Fabbri P., Bassoli E., Bon S.B., Valentini L. Preparation and Characterization of Poly (Butylene Terephthalate)/Graphene Composites by in-Situ Polymerization of Cyclic Butylene Terephthalate. Polymer, 2012, 53(4), 897-902.
208. Mo Z.L., Xie T.T., Zhang J.X., Zhao Y.X., Guo R.B. Synthesis and Characterization of NanoGs-PPy/ Epoxy Nanocomposites by In Situ Polymerization. Synthesis and Reactivity in Inorganic, Metal-Organic, and Nano-Metal Chemistry, 2012, 42(8), 1172- 1176.
209. Chatterjee S., Wang J.W., Kuo W.S., Tai N.H., Salzmann C., Li W.L., Hollertz R., Nuesch F.A., Chu B.T.T. Mechanical Reinforcement and Thermal Conductivity in Expanded Graphene Nanoplatelets Reinforced Epoxy Composites. Chem Phys Lett, 2012, 531, 6-10.
210. Huang Y.F., Lin C.W. Facile Synthesis and Morphology Control of Graphene Oxide/Polyaniline Nanocomposites via in-Situ Polymerization Process. Polymer 2012, 53(13), 2574-2582.
211. Fim F.D.C., Basso N.R.S., Graebin A.P., Azambuja D.S., Galland G.B. Thermal, Electrical, and Mechanical Properties of Polyethylene-Graphene Nanocomposites Obtained by in situ Polymerization. J Appl Polym Sci, 2012, 128(5), 2630-2637.
212. Zaman I., Kuan H.C., Meng Q., Michelmore A., Kawashima N., Pitt T., Zhang L., Gouda S., Luong L., Ma J. A Facile Approach to Chemically Modified Graphene and Its Polymer Nanocomposites. Adv Function Mater, 2012, 22(13), 2735-2743.
213. Yang S.Y., Lin W.N., Huang Y.L., Tien H.W., Wang J.Y., Ma C.C.M., Li S.M., Wang Y.S. Synergetic effects of graphene platelets and carbon nanotubes on the mechanical and thermal properties of epoxy composites. Carbon, 2011, 49(3), 793–803.
214. El Achaby M., Qaiss A. Processing and Properties of Polyethylene Reinforced by Graphene Nanosheets and Carbon Nanotubes. Materials & Design, 2013, 44, 81-89.
215. Du J., Cheng H.M. The Fabrication, Properties, and Uses of Graphene/Polymer Composites. Macromolecular Chem Phys, 2012, 213(10-11), 1060-1077.
216. Suk J.W., Piner R.D., An J., Ruoff R.S. Mechanical Properties of Monolayer Graphene Oxide. ACS Nano, 2010, 4(11), 6557-6564.
217. Rafiee M.A., Rafiee J., Srivastava I., Wang Z., Song H., Yu Z.Z., Koratkar N. Fracture and Fatigue in Graphene Nanocomposites. Small, 2010, 6(2), 179- 183.
218. El Achaby M., Arrakhiz F.Z., Vaudreuil S., Essassil E.M., Quiss A. Piezoelectric β-polymorph Formation and Properties Enhancement in Graphene Oxide—PVDF Nanocomposite Films. Appl Surface Sci, 2012, 258(19), 7668-7677.
219. Jiang L., Shen X.P.,Wu J.L. , Shen X.L. Preparation and Characterization of Graphene/Poly (Vinyl Alcohol) Nanocomposites. J Appl Polym Sci, 2010, 118(1), 275-279.
220. Yang Y., Tu Y, Li L., Shang S., Tao X.M. Well-Dispersed Chitosan/Graphene Oxide Nanocomposites. ACS Applied Materials & Interfaces, 2010, 2(6), 1707-1713.
221. Ramanathan T., Abdala A.A., Stankovich S., Dikin D.A., Herrera-Alonso M., Piner R.D.,Adamson D.H., Schniepp H.C., Chen X., Ruoff R.S., Nguyen S.T., Aksay I.A., Prud'Homme R.K., Brinson L.C. Functionalized Graphene Sheets for Polymer Nanocomposites. Nat Nanotechnol, 2008, 3, 327-31.
222. Cai D., Jin J., Yusoh K., Rafiq R., Song M. High Performance Polyurethane/Functionalized Graphene Nanocomposites with Improved Mechanical and Thermal Properties. Compo Sci Technol, 2012, 72(6), 702-707.

223. Huang X., Yin Z., Wu S., Qi X., He Q., Zhang Q., Yan Q., Boey F., Zhang H. Graphene-Based Materials: Synthesis, Characterization, Properties, and Applications. Small, 2011, 7(14), 1876-1902.
224. Rafiee M.A., Rafiee J., Wang Z., Song H., Yu Z.Z., Koratkar N. Enhanced Mechanical Properties of Nanocomposites at Low Graphene Content. ACS Nano, 2012, 3(12), 3884-3890.
225. Zandiatashbar A., Picu C.R., Koratkar N. Control of Epoxy Creep Using Graphene. Small, 2012, 8(11), 1676-1682.
226. Zhang W., Srivastava I., Zhu Y.F., Picu C.R., Koratkar N.A. Heterogeneity in Epoxy Nanocomposites Initiates Crazing: Significant Improvements in Fatigue Resistance and Toughening. Small, 2009, 5(12), 1403-1407.
227. Kim K.H Oh Y., Islam M.F. Graphene Coating Makes Carbon Nanotube Aerogels Superelastic and Resistant to Fatigue. Nature Nanotechnology, 2012, 7(9), 562-566.
228. Jiang X., Drzal L.T. Multifunctional High Density Polyethylene Nanocomposites Produced by Incorporation of Exfoliated Graphite Nanoplatelets 1: Morphology and Mechanical Properties. Polym Compos, 2010, 31(6), 1091-1098.
229. Galpaya D., Wang M., Liu M., Motta N., Waclawik E., Yan C. Recent advances in fabrication and characterization of graphene-polymer nanocomposites. Graphene, 2012,1, 30-49.
230. Teng C.C., Ma C.C.M., Lu C.H., Yang S.Y., Lee S.H., Hsiao M.C., Yen M.Y., Chiou K.C., Lee T.M. Thermal Conductivity and Structure of Non-Covalent Functionalized Graphene/Epoxy Composites. Carbon, 2011, 49(15), 5107-5116.
231. Zandiatashbar A., Picu R.C., Koratkar N. Mechanical Behavior of Epoxy-Graphene Platelets Nanocomposites. J Engineer Mater Technol, 2012, 134(3), 031011-031016.
232. Zaman I., Phan T.T., Kuan H.C., Meng Q., La L.T.B., Luong L., Youssf O., Ma J. Epoxy/Graphene Platelets Nanocomposites with Two Levels of Interface Strength. Polymer, 2011, 52(7), 1603-1611.
233. Miller S.G., Bauer J.L., Maryanski M.J., Heinmann P.J., Barlow J.P., Gosau J.M., Allred R.E. Characterization of Epoxy Functionalized Graphite Nanoparticles and the Physical Properties of Epoxy Matrix Nanocomposites. Compos Sci Technol, 2010, 70(7), 1120-1125.
234. Rafiee M.A., Lu W., Thomas A.V., Zandiatashbar A., Rafiee J., Tour J.M., Koratkar N.A. Graphene Nanoribbon Composites. ACS Nano, 2010, 4(12), 7415-7420.
235. Bortz D.R., Heras E.G., Martin-Gullon I. Impressive Fatigue Life and Fracture Toughness Improvements in Graphene Oxide/Epoxy Composites. Macromolecules, 2011, 45(1), 238-245.
236. Layek R.K, Samanta S., Nandi A.K. The Physical Properties of Sulfonated Graphene/Poly (Vinyl Alcohol) Composites. Carbon, 2012, 50(3), 815-827.
237. Bao Q.L. Zhang H., Yang J.X., Wang S., Tong D.Y., Jose R., Ramakrishna S., Lim C.T., Loh K.P. Graphene-Polymer Nanofiber Membrane for Ultrafast Photonics. Adv Funct Mater 2010, 20, 782-91.
238. Potts J.R., Dreyer D.R., Bielawski C.W, Ruoff R.S. Graphene-Based Polymer Nanocomposites. Polymer, 2011, 52(1), 5-25.
239. Shen Y., Jing T., Ren W., Zhang J., Jiang Z.G., Yu Z.Z., Dasari A. Chemical and Thermal Reduction of Graphene Oxide and Its Electrically Conductive Polylactic Acid Nanocomposites. Compos Sci Technol, 2012, 72(12), 1430-1435.

240. Liang J., Wang Y., Huang Y., Ma Y., Liu Z., Cai J., Zhang C., Gao H., Chen Y. Electromagnetic Interference Shielding of Graphene/Epoxy Composites. Carbon, 2009, 47(3), 922-925.
241. Pham V.H., Dang T.T., Hur S.H., Kim E.J. Chung J.S. Highly Conductive Poly (Methyl Methacrylate) (PMMA)-Reduced Graphene Oxide Composite Prepared by Self-Assembly of PMMA Latex and Graphene Oxide through Electrostatic Interaction. ACS Appl Mater Interface, 2012, 4(5), 2630-2636.
242. Yang Y.K., He C.E., Peng R.G., Baji A., Du X.S., Huang Y.L., Lie X.L., Mai Y.W. Non-Covalently Modified Graphene Sheets by Imidazolium Ionic Liquids for Multifunctional Polymer Nanocomposites. J Mater Chem, 2012, 22(12), 5666-5675.
243. Tang H., Ehlert G.J., Lin Y., Sodano H.A. Highly Efficient Synthesis of Graphene Nanocomposites. Nano Letters, 2011, 12(1), 84-90.
244. Harish C., SreeHarsha V.S., Santhosh C., Rajendran R., Saranya M., Vanchinathan T.M., Govardhan K., Grace A.N. Synthesis of Polyaniline/Graphene Nanocomposites and Its Optical, Electrical and Electrochemical Properties. Adv Sci Eng Med, 2013, 5(2), 140-148.
245. Ansari S., Giannelis E.P. Functionalized Graphene Sheet—Poly (Vinylidene Fluoride) Conductive Nanocomposites. J Polym Sci Part B Polym Physics, 2009, 47(9), 888-897.
246. Ghosh S., Calizo I., Teweldebrhan D., Pokatilov E.P., Nika D.L., Balandin A.A., Bao W., Miao F., Lau C.N. Extremely high thermal conductivity of graphene: Prospects forthermal management applications in nanoelectronic circuits. Appl Phys Lett 2008, 92, 151911.
247. Seol J.H., Jo I., Moore A.L., Lindsay L., Aitken Z.H., Pettes M.T., Li X., Yao Z., Huang R., Broido D., Mingo N., Ruoff R.S., Shi L. Two-dimensional phonon transport in supported graphene. Science, 2010, 328, 213-6.
248. Yu A., Ramesh P., Sun X., Bekyarova E., Itkis M.E., Haddon R.C. Enhanced Thermal Conductivity in a Hybrid Graphite Nanoplatelet - Carbon Nanotube Filler for Epoxy Composites. Adv Mater, 2008, 20(28), 4740-7744.
249. Lin W., Zhang R., Wong C.P. Modeling of Thermal Conductivity of Graphite Nanosheet Composites. J Electron Mater, 2010, 39(3), 268-72.
250. Kim P., Shi L., Majumdar A., McEuen P.L. Thermal transport measurements of individual multiwalled nanotubes. Phys Rev Lett, 2001, 87(21), 215502-6.
251. Pop E., Mann D., Wang Q., Goodson K., Dai H. Thermal Conductance of an Individual Single-Wall Carbon Nanotube above Room Temperature. Nano Lett, 2006, 6, 96.
252. Hone J., Whitney M., Piskoti C., Zettl A. Thermal conductivity of single-walled carbon nanotubes. Phys Rev B, 1999, 59(4), R2514-17.
253. Kalaitzidou K., Fukushima H., Drzal L.T. Multifunctional polypropylene composites produced by incorporation of exfoliated graphite nanoplatelets. Carbon, 2007, 45, 1446-52.
254. Veca L.M., Meziani M.J., Wang W., Wang X., Lu F., Zhang P., Lin Y., Fee R., Connell J.W., Sun Y.P. Carbon Nanosheets for Polymeric Nanocomposites with High Thermal Conductivity. Adv Mater, 2009, 21, 2088-92.
255. Ghose S., Watson K.A., Working D.C., Connell J.W., Smith Jr J.G., Sun Y.P. Thermal conductivity of ethylene vinyl acetate copolymer/nanofiller blends. Compos Sci Technol, 2008, 68, 1843-53.

256. Ganguli S., Roy A.K., Anderson D.P. Improved thermal conductivity for chemically functionalized exfoliated graphite/epoxy composites. Carbon, 2008, 46, 806-17.
257. Yu A., Ramesh P., Itkis M.E., Bekyarova E., Haddon R.C. Graphite Nanoplatelet-Epoxy Composite Thermal Interface Materials. J Phys Chem C, 2007, 111(21), 7565-9.
258. Wang S.R., Tambraparni M., Qiu J.J., Tipton J., Dean D. Thermal Expansion of Graphene Composites. Macromolecules, 2009, 42, 5251-5.
259. Heo S., Cho S.Y., Kim do H., Choi Y., Park H.H., Jin H.J. Improved Thermal Properties of Graphene Oxide-Incorporated Poly (Methyl Methacrylate) Microspheres. J Nanosci Nanotechnol, 2012, 12(7), 5990-5994.
260. King J.A., Via M.D., Morrison F.A., Wiese K.R., Beach E.A., Cieslinski M.J., Bogucki G.R. Characterization of Exfoliated Graphite Nanoplatelets/Polycarbonate Composites: Electrical and Thermal Conductivity, and Tensile, Flexural, and Rheological Properties. J Comp Mater, 2012, 46(9), 1029-1039.
261. Kim I.H., Jeong Y.G. Polylactide/exfoliated graphite nanocomposites with enhanced thermal stability, mechanical modulus, and electrical conductivity. J Polym Sci Part B Polym Phys, 2010, 48, 850-8.
262. Kim S., Do I., Drzal L.T. Thermal stability and dynamic mechanical behavior of exfoliated graphite nanoplatelets - LLDPE nanocomposites. Polym Compos, 2010, 31(5), 755-61.
263. Xu Z., Gao C. In situ Polymerization Approach to Graphene-Reinforced Nylon-6 Composites. Macromolecules, 2010, 43, 6716-23.
264. Zhang W.L., Park B.J., Choi H.J. Colloidal graphene oxide/polyaniline nanocomposite and its electrorheology. Chem Commun, 2010, 46(30), 5596-8.
265. Yan D. Xu L., Chen C., Tang J., Ji X., Li Z. Enhanced Mechanical and Thermal Properties of Rigid Polyurethane Foam Composites Containing Graphene Nanosheets and Carbon Nanotubes. Polymer International, 2012, 61(7), 1107-1114.
266. Leszczynska A., Njuguna J., Pielichowski K., Banerjee J.R. Polymer/montmorillonite nanocomposites with improved thermal properties: Part I. Factors influencing thermal stability and mechanisms of thermal stability improvement. Thermochim Acta, 2007, 453(2), 75-96.
267. Yang X., Li L., Shang S., Tao X. Well-dispersed chitosan/graphene oxide nanocomposites. ACS Appl Mater Interfaces, 2010, 2(6), 1707-13.
268. Xu Y.X., Hong W.J., Bai H., Li C., Shi G.Q. Strong and ductile poly(vinyl alcohol)/graphene oxide composite films with a layered structure. Carbon, 2009, 47, 3538-43.
269. Zhan Y. Yang X., Gou H., Yang J., Meng F., Liu X. Cross-Linkable Nitrile Functionalized Graphene Oxide/Poly (Arylene Ether Nitrile) Nanocomposite Films with High Mechanical Strength and Thermal Stability. J Mater Chem, 2012, 22(12), 5602-5608.
270. Gedler G., Antunes M., Realinho V., Velasco J.I. Thermal Stability of Polycarbonate-Graphene Nano-composite Foams. Polymer Degr Stab, 2012, 97(8), 1297-1304.
271. Patole A.S, Patole S.P., Kang H., Yoo J.B., Kim T.H., Ahn J.H. A Facile Approach to the Fabrication of Graphene/Polystyrene Nanocomposite by in Situ Microemulsion Polymerization. J Colloid Interface Sci, 2010, 350(2), 530-537.

272. Mounet N., Marzari N. First-principles determination of the structural, vibrational and thermodynamic properties of diamond, graphite, and derivatives. Phys Rev B Condens Matter Mater Phys, 2005, 71, 205214.
273. Fasolino A., Los J.H., Katsnelson M.I. Intrinsic ripples in graphene. Nat Mater, 2007, 6, 858-61.
274. Paul D.R., Robeson L.M. Polymer nanotechnology: Nanocomposites. Polymer, 2008, 49, 3187-204.
275. Solomon M.J., Almusallam A.S., Seefeldt K.F., Somwangthanaroj A., Varadan P. Rheology of Polypropylene/Clay Hybrid Materials. Macromolecules, 2001,34, 1864-72.
276. Wagener R., Reisinger T.J.G. A rheological method to compare the degree of exfoliation of nanocomposites. Polymer, 2003, 44(24), 7513-8.
277. Zhang Q., Fang F., Zhao X., Li Y., Zhu M., Chen D. Use of dynamic rheological behavior to estimate the dispersion of carbon nanotubes in carbon nanotube/polymer composites. J Phys Chem B, 2008, 112(40), 12606-11.
278. Vermant J., Ceccia S., Dolgovskij M.K., Maffettone P.L., Macosko C.W. Quantifying dispersion of layered nanocomposites via melt rheology. J Rheol, 2007, 51, 429-50.
279. Kim H., Macosko C.W. Processing-property relationships of polycarbonate/graphene composites. Polymer, 2009, 50(15), 3797-809.
280. —. Kim H., Macosko C.W., Morphology and Properties of Polyester/Exfoliated Graphite Nanocomposites. Macromolecules, 2008, 41, 3317-27.
281. Pramoda K.P., Linh N.T.T., Tang P.S., Tjiu W.C., Goh S.H., He C.B. Thermo-mechanical properties of poly(vinylidene fluoride) modified graphite/poly(methyl methacrylate) nanocomposites. Compos Sci Technol, 2010, 70, 578-83.
282. Jang B.Z., Zhamu A. Processing of nanographene platelets (NGPs) and NGP nanocomposites: a review. J Mater Sci, 2008, 43, 5092-101.
283. Fang M., Zhang Z., Li J., Zhang H., Lu H., Yang Y. Constructing hierarchically structured interphases for strong and tough epoxy nanocomposites by amine-rich graphene surfaces. J Mater Chem, 2010, 20, 9635-43.
284. Compton O.C. Kim S., Pierre C., Torkelson J.M., Nguyen S.B.T. Crumpled Graphene Nanosheets as Highly Effective Barrier Property Enhancers. Adv Mater, 2010, 22, 4759-63.
285. Sumfleth J. Adroher X., Schulte K. Synergistic effects in network formation and electrical properties of hybrid epoxy nanocomposites containing multi-wall carbon nanotubes and carbon black. J Mater Sci, 2009, 44(12), 3241–7.
286. Li C., Li Z., Zhu H., Wang K., Wei J., Li X., Sun P., Zhang H., Wu D. Graphene Nano-'Patches' on a Carbon Nanotube Network for Highly Transparent/Conductive Thin Film Applications. The Journal of Physical Chemistry C, 2010, 114(33),14008-14012.
287. Patole A.S., Patole S.P., Jung S.Y., Yoo J.B., An J.H., Kim T.K. Self Assembled Graphene/Carbon Nanotube/Polystyrene Hybrid Nanocomposite by in Situ Microemulsion Polymerization. Europ Polym J, 2012, 48(2),252-259.
288. Zhang C., Liu T. A Review on Hybridization Modification of Graphene and Its Polymer Nanocomposites. Chinese Sci Bull, 2012, 57(23), 3010-3021.
289. Kumar S., Sun L.L., Caceres S., Li B., Wood W., Perugini A., Maquire R.G., Zhong W.H. Dynamic Synergy of Graphitic Nano- platelets and Multi-Walled Carbon Nanotubes in Polyetherimide Nanocomposites. Nanotechnology, 2010,21,105701-105709.

290. Ma P.C., Liu M.Y., Zhang H.,Wang S.Q., Wang R., Wang K. , Wong Y.K., Tang B.Z., Hong S.H., Paik K.W, Kim J.K. Enhanced electrical conductivity of nanocomposites containing hybrid fillers of carbon nanotubes and carbon black. ACS Applied Mater Interfaces, 2009, 1(5),1090-96.
291. Tang Y., Gou J. Synergetic effect on electrical conductivity of few-layer graphene/multi-walled carbon nanotube paper. Mater Lett, 2010, 64, 2513-2516.
292. Wei T., Song L., Zheng C., Wang K., Yan J., Shao B, Fan Z.J. The synergy of a three filler combination in the conductivity of epoxy composites. Mater Lett, 2010, 64, 2376-79.
293. Wang Y., Shi Z., Huang Y., Ma Y., Wang C., Chen M., Chen Y. Supercapacitor Devices Based on Graphene Materials. J Phys Chem C, 2009, 113, 13103–13107.
294. Liang J., Xu Y., Huang Y., Zhang L., Wang Y., Ma Y., Li F., Guo T., Chen Y. Infrared-triggered Actuators from Graphene-based Nanocomposites. J Phys Chem C, 2009, 113, 9921–9927.
295. Wang X. Zhi L.J., Mullen K. Transparent, Conductive Graphene Electrodes for Dye-sensitized Solar Cells. Nano Lett, 2008, 8, 323–327.
296. Yoo E. Kim J., Hosono E., Zhou H., Kudo T., Honma I. Large Reversible Li Storage of Graphene Nanosheet Families for Use in Rechargeable Lithium Ion Batteries. Nano Lett, 2008, 8, 2277–2282.
297. Vivekchand S.R.C., Rout C.S., Subrahmanyam K.S., Ovindaraj A., Rao C.N.R. Graphene-Based Electrochemical Supercapacitors. J Chem Sci, 2008, 120, 9–13.
298. Wang X., Zhi L.J., Tsao N., Tomovic Z., Li J.L., Mullen K. Transparent Carbon Films as Electrodes in Organic Solar Cells. Angew Chem Int Ed, 2008, 47, 2990–2992.
299. Eda G., Chhowalla M. Graphene-Based Composite Thin Films for Electronics. Nano Lett, 2009, 9, 814–818.
300. Fan Z.J, Yan Y., Zhi L.J., Zhang Q., Wei T., Feng J., Zhang M.L., Qian W.Z., Wei F. A three-dimensional carbon nanotube/graphene sandwich and its application as electrode in supercapacitors. Adv Mater, 2010, 22 (33), 3723-3728.
301. Yu D., Nagelli E., Du F., Dai L. Metal-free carbon nanomaterials become more active than metal catalysts. J Phys Chem Lett, 2010, 1, 2165.
302. Tung V.C Chen L.M., Allen M.J., Wassei J.K, Nelson K., Kaner R.B, Yang Y. Low-Temperature solution processing of graphene & carbon nanotube hybrid material for high-performance transparent conductors. Nano Lett, 2009, 9, 1949-1955.
303. Kim Y.K, Min D.H. Durable Large-Area Thin Films of Graphene/Carbon Nanotube Double Layers as a Transparent Electrode. Langmuir, 2009,25(19), 11302-11306.
304. Xin G., Hwang W., Kim N., Cho S.M, Chae H. A graphene sheet exfoliated with microwave irradiation and interlinked by carbon nanotubes for high-performance transparent flexible electrodes. Nanotechnology, 2010, 21, 405201.
305. Lu X., Dou H., Gao B., Yuan C., Yang S., Hao L., Shen L., Zhang X. A flexible graphene/multiwalled carbon nanotube film as a high performance electrode material for supercapacitors. Electrochimica Acta, 2011, 56(14), 5115–5121.
306. Yan J., Wei T., Shao B., Fan Z., Qian W., Zhang M., Wei F. Preparation of a Graphene Nanosheet/Polyaniline Composite with High Specific Capacitance. Carbon, 2009, 48, 487–493.

307. Yan J. Fan Z., Wei T., Qian W., Zhang M., Wei F. Preparation of Exfoliated Graphite Containing Manganese Oxides with High Electrochemical Capacitance by Microwave Irradiation. Carbon, 2009, 47, 3371–3374.
308. Yu D., Dai L. Self-assembles graphene/carbon nanotube hybrid films for supercapacitors. J Phys Chem Lett, 2010, 1, 467–470.
309. Fan Z.Yan J., Zhi L., Zhang Q., Wei T., Feng J., Zhang M., Qian W., Wei F. A Three-Dimensional Carbon Nanotube/Graphene Sandwich and Its Application as Electrode in Supercapacitors. Adv Mater, 2010, 22(33), 3723–3728.
310. Wu C., Huang X., Wu X., Xie L., Yang Ke., Jiang P. Graphene oxide-encapsulated carbon nanotube hybrids for high dielectric performance nanocomposites with enhanced energy storage density. Nanoscale, 2013,5, 3847-3855.
311. Jha N., Jafri R.I., Rajalakshmil N., Ramaprahbu S. Graphene-multi walled carbon nanotube hybrid electrocatalyst support material for direct methanol fuel cell. International J Hydrogen Energy, 2011, 36(12), 7284–7290.
312. Spitalsky Z., Danko M., Mosnacek J. Preparation of functionalized graphene sheets. Current Oragan Chem, 2011, 15, 1133-1150.
313. Janowska I., Vignerona F., Begin D., Ersen O., Bernhard P., Romero T., Ledoux M.J., Pham-Huu C. Mechanical thinning to make few-layer graphene from pencil lead. Carbon, 2012, 50(8), 3106-3110. pp. 3092-3116.
314. Gabrielse W., Soliman M., Dijkstra K. Microstructure and phase behavior of block copoly(ether-ester) thermoplastic elastomers. Macromolecules, 2001, 34, 1685-1693.
315. Schmalz H., Abetz V., Lange R., Soliman M. New thermoplastic elastomers by incorporation of nonpolar soft segment in PBT-based copolymers. Macromolecules, 2001, 34,795–800.
316. Szymczyk A., Senderek E., Nastalczyk J., Roslaniec Z. New multiblock poly(ether-ester)s based on poly(trimetylene terephthalate) as rigid segment. Eur Polym J, 2008, 44, 436-43.
317. Szymczyk A., Nastalczyk J., Sablong R.J., Roslaniec Z. The influence soft segment length on structure and properties of poly(trimetylene terephthalate)-block-poly(tetramethylene oxide) segmented random copolymers. Polym Adv Technol, 2011, 21, 72-83.
318. Freeman E.S., Carroll B. The application of thermoanalytical technique to reaction kinetics: The thermogravimetric evaluation of the kinetics of the decomposition of calcium oxalate monohydrate. J Phys Chem, 1958, 62, 4, 394-397.
319. Scheirs J., Long T. E. Modern Polyesters. Wiley&Sons Ltd., 2003, ISBN: 978-0-471-49856-8.
320. Samperi F. Puglisi C., Alicata R., Montaudo G. Thermal degradation of poly(butylene terephthalate) at the processing temperature. Polym Degrad Stab, 2004, 83(3),11-17.
321. Chuah H. H., Lin-Vien D., Soni U. Poly(trimethylene terephthalate) molecular weight and Mark–Houwink equation. Polymer, 2001, 42, 7137–7139.
322. Paszkiewicz S., Szymczyk A., Spitalsky Z., Soccio M., Mosnacek J., Ezquerra T.A., Roslaniec Z. Electrical conductivity of PET/expanded graphite nanocomposites prepared by in situ polymerization. J Polym Sci Polym Phys, 2012, 50, 1645-1652.

323. Popov V.N, Lambin P. Resonant Raman intensity of the totally symmetric phonons of single-walled carbon nanotubes. Phys Rev B, 2006,73(16), 165425-11.
324. Kim K.K., Park J.S., Kim S.J., Geng H.Z., An K.H., Yang C.M., Sato K., Saito R., Lee Y.H. Dependence of Raman spectra G′ band intensity on metallicity of single-wall carbon nanotubes. Phys Rev B, 2007, 76, 205426-8.
325. Bergman D.J. Imry Y. Critical Behavior of the Complex Dielectric Constant near the Percolation Threshold of a Heterogeneous Material. Phys Rev Lett, 1977, 39, 1222.
326. G.W., Ehrenstein. Polymeric Materials. Structure, Properties, Application. Hanser, Monachium 2001.
327. Grunlan J.C., Mehrabi A.R., Bannon M.V., Bahr J.L. Water-based single-walled-nanotubefilled polymer composite with an exceptionally low percolation threshold. Adv Mater, 2004, 16,150–153.
328. Banerjee P. Mandal B.M. Conducting polyaniline nanoparticle blends with extremely low percolation thresholds. Macromolecules, 1995, 28, 3940–3943.
329. Kalaitzidou K. Fukushima H., Askeland P., Drzal L.T. The nucleating effect of exfoliated graphite nanoplatelets and their influence on the crystal structure and electrical conductivity of polypropylene nanocomposites. J Mater Sci, 2008, 43, 2895-2907.
330. Jing X. Zhao W., Lan L. The effect of particle size on electric conducting percolation threshold in polymer/conducting particle composites. J Mater Sci Lett, 2000, 19(5), 377-379.
331. Watanabe M. Nagaoka K., Kanba M., Shinohara I. Ionic conductivity of polymeric solid electrolytes based on (polypropoylene oxide) and poly(tetramathylene oxide). Polym J, 1982, 14(11), 877-886.
332. Hong P.D., Chuang W.T., Yeh W.J., Lin T.L. Effect of rigid amorphous phase on glass transition behaviorof poly(trimethylene terephthalate). Polymer, 2002, 43, 6879–6886.
333. B., Wundrelich. Reversible crystallization and the rigid–amorphous phase in semicrystalline macromolecules. Progress in Polymer Science, 2003, 28, 383–450.
334. Ma Q., Cebe P. Phase structure of electrospun poly (trimethylene terephthalate) composite nanofibers containing carbon nanotubes. J Therl Anal Calor, 2010, 102, 425–434.
335. Pötschke P., Fornes T.D., Pau D.R.l. Rheological behavior of multiwalled carbon nanotube/polycarbonate composites. Polymer, 2002, 43,3247–3255.
336. Kinloch I.A., Roberts S.A, Windle A.H. A rheological study of concentrated aqueous nanotube dispersions. Polymer, 2002, 43,7483–7491.
337. A.V., Shenoy. Rheology of filled polymer systems. Kluwer Academic Publishers, Dordrecht (1999).
338. Wang M., Wang W., Liu T., Zhang W.D. Melt rheological properties of nylon-6/ multi-walles carbon nanotube composites. Compos Sci Technol, 2008,68, 2498-2502.
339. McNally T., Potschke P., Halley P., Murphy M., Martin D., Bell S.E.J., Brennan G.P., Bein D., Lemoine P., Quinn J.P. Polyethylene multiwalled carbon nanotube composites. Polymer, 2005, 46, 8222-8232.
340. Kayatin M.J., Davis V.A. Viscoelasticity and Shear Stability of Single-Walled Carbon Nanotube/Unsaturated Polyester Resin Dispersions. Macromolecules, 2009,42, 6624-6632.
341. Kelsey D.R. Kiibler K.S., Tutunjian P.N. Thermal stability of poly(trimethylene terephthalate). Polymer, 2005, 46(21), 8937-8946.

342. Wang X-S. Li X-G., Yan D. Thermal decomposition kinetics of poly(trimethylene terephthalate). Polym Degrad Stabil, 2000, 69(3), 361–372.
343. —. High-resolution thermogravimetric analysis of poly(trimethylene terephthalate) with different molecular weights. Polym Test, 2001, 20(5), 491–502.
344. Zeynalov E.B. Friedrich J.F. Antioxidative activity of carbon nanotube and nanofiber. The Open Materials Science Journal, 2008, 2,28-34.
345. Szymczyk A., Rosłaniec Z. Degradacja i stabilizacja termoplastycznych elastomerów. Polimery, 2006, 51, 627-642.
346. Chae H.G., Liu J., Kumar S. Carbon nanotubes-enabled materials. Carbon nanotubes properties and applications (ed.: O'Connell M. J.) CRC Press Taylor and Francis Group Boca Raton, 213–253 (2006).
347. Kopczynska A., Ehrenstein G. W. Polymeric surfaces and their true surface tension in solids and melts. J Mater Edu, 2007, 29, 325–340.
348. J. Gołębiewski. Nanokompozyty polimerowe. Struktura, metody wytwarzania i właściwości. Przemysł Chemiczny, 2004, 83(1), 15-20.
349. Pinnavaia T.J, Beall G.W. Polymer Clay nanocomposites. Chichester: Wiley Series in Polymer Science, 1997, 207-225.
350. Celzard A., Mareche J.F., Furdin G. Modelling of exfoliated graphite. Progress in Materials Science, 2005,50(1), 93-179.
351. A.C., Ferrari. Raman spectroscopy of graphene and graphite: disorder, electron–phonon coupling, doping and nonadiabatic effects. Solid State Commun, 2007, 143, 47–57.
352. Ferrari A.C., Robertson J. Interpretation of Raman spectra of disordered and amorphous carbon. Phys Rev B, 2000, 61,14095–14107.
353. Pimenta M.A., Dresselhaus G., Dresselhaus M.S.,Cancado L.G., Jorio A., Saito R. Studying disorder in graphite-based systems by Raman spectroscopy. Phys Chem Chem Phys, 2007, 9, 1276–1291.
354. Tuinstra F., Koenig J.L. Raman spectrum of graphite. J Chem Phys, 1970, 53,1126–1130.
355. Allen M.J., Fowler J.D., Tung V.C., Yang Y., Weiller B.H, Kaner R.B. Temperature dependent Raman spectroscopy of chemically derived graphene. Appl Phys Lett, 2008, 93,193119–193123.
356. D. Stauffer. Introduction to Percolation Theory; Taylor & Francis. London, 1987.
357. Carmona F. Prudhon P., Barreau F. Percolation in short fibres epoxy resin composites: Conductivity behavior and finite size effects near threshold. Solid State Communications, 1984, 51(4), 255-257.
358. Quivy A. Deltour R., Jansen A.G.M., Wyder P. Transport phenomena in polymer-graphite composite materials. Phys Rev B, 1989, 39, 1026.
359. Ezquerra T.A. Kulescza M.. Cruz C.S., Balta-Calleja F.J. Charge transport in polyethylene–graphite composite materials. Adv Mater,1990, 2(12), 597-600.
360. Zhang H-B. Zheng W-G., Yan Q., Yang Y., Wang J-W., Lu Z-H., Ji G-Y., Yu Z-Z. Electrically conductive polyethylene terephthalate/graphene nanocomposites prepared by melt compounding. Polymer, 2010, 51(5), 1191-1196.

361. Li M. Jeong Y.G. Poly(ethylene terephthalate)/exfoliated graphite nanocomposites with improved thermal stability, mechanical and electrical properties. Compos Part A, 2011, 42(5), 560-566.
362. Chen L., Xie H., Li Y., Yu W. Nanofluids containing carbon nanotubes treated by mechanochemical reaction. Thermochimica Acta, 2008, 477, 21-24.
363. Krikorian V., Kochan D.J. Crystallization Behavior of Poly(l-lactic acid) Nanocomposites: Nucleation and Growth Probed by Infrared Spectroscopy. Macromolecules, 2005, 38, 6520-6527.
364. Hu X., An H., Li Z., Yang L. Origin of Carbon Nanotubes Induced Poly(l-Lactide) Crystallization: Surface Induced Conformational Order. Macromolecules, 2009, 42(8), 3215-3218.
365. Zhang J., Tsuji H., Noda I., Ozaki Y. Structural Changes and Crystallization Dynamics of Poly(l-lactide) during the Cold-Crystallization Process Investigated by Infrared and Two-Dimensional Infrared Correlation Spectroscopy. Macromolecules, 2004, 37, 6433-6439.
366. Zhang J., Duan Y., Sato H., Tsuji H., Noda I., Yan S.K., Ozaki Y. Crystal Modifications and Thermal Behavior of Poly(l-lactic acid) Revealed by Infrared Spectroscopy. Macromolecules, 2005, 38, 8012-8021.
367. S.S, Ray. Rheology of polymer/layered silicate nanocomposites. J Ind Eng Chem, 2006, 12, 811-842.
368. Roberts C., Cosgrove T., Schmidt R.G., Gordon G.V. Diffusion of poly(dimethylsiloxane) mixtures with silicate nanoparticles. Macromolecules, 2001, 34, 538-543.
369. Jain S., Goossens J.G.P., Peters G.W.M., Van Duin M., Lemstra P.J. Strong decrease in viscosity of nanoparticle-filled polymer melts through selective adsorption. Soft Matter, 2008, 4, 1848-1854.
370. Mackay M.E., Dao T.T., Tuteja A., Ho D.L., Van Horn B., Kim H.C., Hawker C.J. Nanoscale effects leading to non-Einstein-like decrease in viscosity. Nature Materials 2003;2:762-766.
371. Xie X.L. Liu Q.X., Li R.K.Y., Zhou X.P., Zhang Q.X., Yu Z.Z., Mai Y.W. Rheological and mechanical properties of PVC/CaCO3 nanocomposites prepared by in situ polymerization. Polymer, 2004, 45, 6665-6673.
372. You Y.L., Li D.X., Deng X., Li W.L., Xie Y. Effect of solid lubricants on tribological behavior of glass fiber reinforced polyamide 6. Polym Comp, 2013, 34, 1783-93.
373. Hu Y.S. Liu R.Y.F., Zhang L.Q., Rogunova M., Schiraldi D.A., Nazarenko S., Hiltner A., Baer E. Oxygen Transport and Free Volume in Cold-Crystallized and Melt-Crystallized Poly(ethylene naphthalate). Macromolecules, 2002, 35(19), 7326-7337.
374. Hu Y.S. Schiraldi D.A., Hiltner A., Baer E. Structural Model for Oxygen Permeability of a Liquid Crystalline Polymer. Macromolecules, 2003, 36(10), 3606-3615.
375. Liu R.Y.F. Hu Y.S., Hibbs, M.R., Collard D.M., Schiraldi D.A., Hiltner A., Baer E. Improving oxygen barrier properties of poly(ethylene terephthalate) by incorporating isophthalate. I. Effect of orientation. J Appl Polym Sci, 2005, 98(4), 1615-1628.
376. Choi W.J, Kim H.J, Yoon K.H., Kwon O.H, Hwang C.I. Preparation and barrier property of poly(ethylene terephthalate)/clay nanocomposite using clay-supported catalyst. J Appl Polym Sci, 2006,100(4),4875-4879.

377. Liu R.Y., Hu Y.S., Hibbs M.R., Collard D.M., Schiraldi D.A., Hiltner A., Baer E. Improving oxygen barrier properties of poly(ethylene terephthalate). J Appl Polym Sci, 2005, 98(4), 1615-1628.
378. Abdala M., Dean D., Robinson P., Nyairo E. Cure behavior of epoxy/MWCNT nanocomposites: The effect of nanotube surface modification. Polymer, 2008, 49(15),3310-3317.
379. Vadukumpully S., Jinu P., Narahari M., Suresh V. Flexible conductive graphene/poly(vinyl chloride) composite thin films with high mechanical strength and thermal stability. Carbon, 2011,49(1), 198-205.
380. Tang X., Li W., Yu Z., Rafiee M.A., Rafiee J., Yavari F., Koratkar N. Enhanced thermal stability in graphene oxide covalently functionalized with 2-amino-4,6-didodecylamino-1,3,5-triazine. Carbon, 2011, 49(4), 1258-1265.
381. Yang J. Huang Y., Lv Y., Zhao P., Yang Q., Li G. The intrinsic thermal-oxidative stabilization effect of chemically reduced graphene oxide on polypropylene. J Mater Chem A, 2013, 1, 11184-11191.
382. Martin-Gullon I., Esperanza M., Font R. Kinetic model for the pyrolysis and combustion of poly(ethylene terephthalate) (PET). J Anal Appl Pyrol, 2001, 58–59, 635–650.
383. Paszkiewicz S. Roslaniec Z., Szymczyk A., Spitalsky Z., Mosnacek J. Morphology and thermal properties of expanded graphite (EG)/Poly(ethylene terephthalate) (PET) nanocomposites. Chemik, 2012, 66(1), 26-30.
384. Kim I.H., Jeong Y.G. Polylactide/exfoliated graphite nanocomposites with enhanced thermal stability, mechanical modulus, and electrical conductivity. J Polym Sci Part B Polym Phys, 2010, 48(8), 850–858.
385. Fakirov S. Roslaniec Z. Handbook of Condensation Thermoplastic Elastomers. Chapter 3 Polyester Thermoplastic Elastomers: Synthesis, Properties, and Some Applications. Wiley-VCH Verlag GmbH & Co. KGaA 2005.
386. Gojny F.H., Wichmann M.H.G., Kopke U., Fiedler B., Schulte K. Carbon nanotube-reinforced epoxy-composites: enhanced stiffness and fracture toughness at low nanotube content. Compos Sci Technol, 2004, 64(15), 2363–71.
387. Seidel G.D., Boehringer K.L., Lagoudas D.C. Analysis of clustering and interphase region effects on the electrical conductivity of carbon nanotube-polymer nanocompistes via computational micromechanics. Proceedings of SMASIS 2008 Ellicott City,USA' p.7 (2008).
388. Paszkiewicz S. Szymczyk A., Špitalski Z., Mosnáček J., Kwiatkowski K., Rosłaniec Z. Structure and properties of nanocomposites based on PTT-block-PTMO copolymer and graphene oxide prepared by in situ polymerization,. Europ Polym J,l 2014, 50, 69-77.
389. Szymczyk A. Paszkiewicz S., Roslaniec Z. Influence of intercalated organoclay on the phase structure and physical properties of PTT–PTMO block copolymers. Polym Bull, 2013, 70, 1575-1590.

List of figures

List of tables

"Polymer hybrid nanocomposites containing carbon nanoparticles. *In situ* synthesis and physical properties"

PhD Thesis

Sandra Paszkiewicz

Abstract

The main objective of this PhD thesis was to attempt the use of the enormous potential of hybrid carbon conductive nanoparticles and their extraordinary mechanical and thermal properties to obtain polymer nanomaterials, based on condensing polyesters (PET, PTT) and thermoplastic elastomers (PTT-PTMO) by *in situ* polymerization. The influence of the addition of carbon nanotubes, graphenes, and mixtures of both, on the mechanical, electrical and processing properties was observed. In addition, the effect of different varieties of graphene on barrier properties of thermoplastic polyesters has been examined. To obtain polymer hybrid nanocomposites, two kinds of single walled carbon nanotubes, and six different types of graphenes, varying in flake size, but also in the number of platelets were used. Investigated materials are classified as nanocomposites, a new group of engineering materials with promising, but not fully known physical properties, requiring the use of appropriate methods of production due to the size and properties of the dispersed phase.

The subject of research presented in the doctoral thesis was to confirm the possibility of obtaining polymer hybrid nanocomposites containing nanoparticles differ in shape (aspect ratio) (1D and 2D), which due to the high aspect ratio and a specific high surface area show a strong tendency to agglomeration, which is difficult to provide the effective distribution in the polymer matrix. Resulting in the process of chemical synthesis of the polymer matrix (*in situ*) polymer hybrid nanocomposites were characterized by a high degree of uniformity of the structure and improved physical properties. Efficiency of *in situ* polymerization in obtaining hybrid nanomaterials has been evaluated through synthesis of thermoplastic polyesters (PET and PTT) along with thermoplastic elastomers (PTT-PTMO). The effect of the addition of nanofillers, either of each individual, as well as mixtures of both, on the properties of the polymer matrix was assessed by morphology analysis, phase transitions and crystal structure, thermal stability, barrier properties (for 2D nanoparticles), mechanical strength and electrical conductivity.

Implementation of this PhD thesis has brought a lot of new information about obtaining and characterization of polymer nanocomposites. Conditions for preparing 1D and 2D nanoparticle dispersions in a liquid substrate has been established using ultrasonic vibration alternately with a mechanical stirrer (and additionally for 2D nanostructures a few hours' use of weak ultrasounds) and conducting the synthesis depending on the type of polymer matrix. It was also shown that the addition of single-wall carbon nanotubes and graphene nanoplatelets with a concentration of not higher than 0.6 wt % to the condensation polymers allows obtaining lightweight, electrically conductive composite materials with improved thermal stability and improved mechanical properties. Additionally, for nanocomposites based on PTT-PTMO the positive hybrid effect has been observed, for both, improvement in mechanical properties and electrical conductivity. The observed synergistic hybrid effect may be a response to the demands posed by modern materials for various

industries and are the result of the phenomena occurring in the polymer in the presence of carbon nanoparticles and the effects on the verge of a filler- filler and filler-polymer. The knowledge gained in the course of the carried out work is an important cognitive and contribute to the development and application of this new group of composite materials.

“Hybrydowe nanokompozyty polimerowe z udziałem nanocząstek węglowych. Synteza *in situ* i właściwości fizyczne”

Praca doktorska
Sandra Paszkiewicz

Streszczenie

Głównym celem niniejszej pracy doktorskiej była próba wykorzystania ogromnego potencjału hybrydowych nanocząstek węglowych przewodzących prąd elektryczny i ich nadzwyczajnych właściwości mechanicznych i cieplnych do otrzymania nanomateriałów polimerowych, na bazie poliestrów kondensacyjnych (PET, PTT) oraz elastomerów termoplastycznych (PTT - PTMO) metodą polimeryzacji *in situ*. Oceniono wpływ dodatku nanorurek węglowych, grafenów oraz mieszaniny ich obu, na właściwości mechaniczne, elektryczne oraz ich przetwórstwo. Dodatkowo zbadano wpływ różnych odmian grafenów na właściwości barierowe poliestrów termoplastycznych. Do otrzymania badanych nanokompozytów wykorzystano dwa rodzaje jednościennych nanorurek węglowych oraz sześć różnych odmian grafenów, różniących się wielkością płatków, ale też ilością płytek. Badane materiały zaliczane są do nanokompozytów, nowej grupy materiałów inżynierskich o obiecujących, lecz nie w pełni poznanych właściwościach fizycznych, wymagających zastosowania odpowiednich metod produkcji ze względu na rozmiary oraz właściwości fazy rozproszonej.

Przedmiotem badań przedstawianych w rozprawie doktorskiej było potwierdzenie możliwości otrzymania hybrydowych nanokompozytów polimerowych, zawierających nanocząstki różniące się kształtem (współczynnikiem kształtu) (1D oraz 2D), które ze względu duży współczynnik kształtu oraz dużą powierzchnię właściwą wykazują silną tendencję do aglomeracji, co stanowi trudność w zapewnieniu efektywnej ich dystrybucji w osnowie polimerowej. Otrzymane w procesie syntezy chemicznej osnowy polimerowej (*in situ*) hybrydowe nanokompozyty polimerowe charakteryzowały się wysokim stopniem jednorodności struktury oraz polepszonymi właściwościami fizycznymi. Efektywność polimeryzacji *in situ* w otrzymaniu nanomateriałów hybrydowych została oceniona w zastosowaniu do nanokompozytów na bazie poliestrów termoplastycznych (PET, PTT) oraz elastomerów termoplastycznych (PTT-PTMO). Wpływ dodatku nanonapełniaczy, zarówno każdego z osobna, jak i mieszaniny ich obu, na właściwości osnowy polimerowej badano na podstawie analizy morfologii, przemian fazowych oraz struktury krystalograficznej, stabilności termicznej, barierowości (tylko dla nanocząstek 2D), wytrzymałości mechanicznej i przewodnictwa elektrycznego.

Realizacja niniejszej rozprawy przyniosła wiele nowych informacji na temat otrzymywania i charakterystyki nanokompozytów polimerowych. Ustalono warunki przygotowania dyspersji nanocząstek 1D oraz 2D w ciekłym substracie z wykorzystaniem drgań mieszadła ultradźwiękowego naprzemiennie z mieszadłem mechanicznym (oraz dodatkowo dla nanostruktur 2D wykorzystanie wielogodzinnego oddziaływania słabych ultradźwięków) oraz prowadzenie syntezy zależnie od rodzaju osnowy polimerowej. Wykazano ponadto, że dodatek jednościennych nanorurek węglowych oraz nanopłytek grafenowych o stężeniu nie wyższym niż 0.6 % wag. do polimerów kondensacyjnych

pozwala na otrzymanie lekkich, elektrycznie przewodzących materiałów kompozytowych o podwyższonej stabilności termicznej i polepszonych właściwościach mechanicznych. Dodatkowo dla nanokompozytów na bazie PTT-PTMO został zaobserwowany pozytywny efekt hybrydowy, zarówno w przypadku poprawy właściwości mechanicznych jak i przewodnictwa elektrycznego. Zaobserwowany synergiczny efekt hybrydowy może stanowić odpowiedź na wymagania stawianymi nowoczesnym materiałom przez różne gałęzie przemysłu i są wypadkową zjawisk zachodzących w polimerze w obecności nanocząstek węglowych oraz oddziaływań na granicy nanonapełniacz- nanonapełniacz oraz nanonapełniacz - polimer. Wiedza uzyskana w toku przeprowadzonych prac ma duże znaczenie poznawcze i stanowi wkład do rozwoju i aplikacji tej nowej grupy materiałów kompozytowych.

APPENDIX

List of publications from ISI Journal Master List:

1. **S. Paszkiewicz**, M. Nachman, A. Szymczyk, Z. Špitalski, J. Mosnáček, Z. Rosłaniec, *Influence of expanded graphite (EG) and graphene oxide (GO) on physical properties of PET based nanocomposites***,** Polish Journal of Chemical Technology, 2014, nr 4 (in press). IF=0.444
2. **S. Paszkiewicz**, A. Szymczyk, Z. Špitalski, J. Mosnáček, K. Kwiatkowski, Z. Rosłaniec, *Structure and properties of nanocomposites based on PTT -block-PTMO copolymer and graphene oxide prepared by in situ polymerization*, European Polymer Journal 2014, *50*(1), 69-77. IF 2.562
3. R. Pilawka, **S. Paszkiewicz**, Z. Rosłaniec, *Thermal degradation kinetics of PET/SWCNTs nanocomposites prepared by in situ polymerization*, Journal of Thermal Analysis and Calorimetry 2014, *115*(1), 451-460. IF 1.982
4. **S. Paszkiewicz**, A. Szymczyk, Z. Špitalský, J. Mosnáček, E. Janus, Z. Rosłaniec, *Wpływ dodatku ekspandowanego grafitu (EG) na przebieg syntezy i charakterystykę PETG*, Polimery 2013, 58(11-12), 47-53. IF 0.470
5. A. Szymczyk, **S. Paszkiewicz**, Z. Roslaniec, *Influence of intercalated organoclay on the phase structure and physical properties of PTT-PTMO block copolymers*, Polymer Bulletin 2013, *70*(5), 1575-1590. IF 1.332
6. **S. Paszkiewicz**, A. Szymczyk, Z. Špitalský, M. Soccio, J. Mosnáček, T. A. Ezquerra, Z. Roslaniec, *Electrical conductivity of poly(ethylene terephthalate)/expanded graphite nanocomposites prepared by in situ polymerization*, Journal of Polymer Science Part B: Polymer Physics 2012, *50*(23), 1645-1652. IF 2.221

Papers published in other journals:

1) **S. Paszkiewicz**, I. Pawelec, A. Szymczyk, Z. Rosłaniec, *SWCNTs/Poly(ethylene terephthalate glycol-modified) (PETG) nanocomposites: preparation and characterization of thin conductive films*, International Journal of Materials Engineering and Technology 2014, 11 (2), 139-148. IF=0.801
2) R. Pilawka, **S. Paszkiewicz**, Z. Rosłaniec Z., *Epoxy composites with carbon nanotubes*, Advances in Manufacturing Science and Technology, 2012, *36*(3), 67-79.
3) **S. Paszkiewicz**, Z. Rosłaniec, A. Szymczyk, Špitalský Z., Mosnáček J., *Struktura i właściwości termiczne nanokompozytów ekspandowany grafit(EG))/poli(tereftalan etylenu)(PET)*, Chemik. Nauka Technika Rynek, 2012, *66*(1), 21-31.
4) R. Pilawka , **S. Paszkiewicz**, *Epoxy-vinyl ester materials*, Kompozyty 2011, *11*(1) , 66-69.

Patents:

Paszkiewicz S., Pawelec I., Szymczyk A., Rosłaniec Z., Sposób wytwarzania termoplastycznego tworzywa elastomerowego przewodzącego prąd elektryczny, PL407550

Participation in international conferences:

1. **S. Paszkiewicz,** Z. Rosłaniec, *Carbon hybrid nanoparticles in polymer nanocomposites prepared by in situ polymerization*, CNPComp2013 – 6th International Conference On Carbon Nanoparticle Based Composites, Dresden, Germany, 22-25.05.2013- oral presentation
2. **S. Paszkiewicz**, A. Szymczyk, E. Piesowicz, M. Nachman, K. Kwiatkowski, Z. Rosłaniec, *Mechanical and thermal stability of PTT-b-PTMO/graphene nanocomposites, Joint* Conferences on Advanced Materials: FNMA'13 - The 10th Conference on Functional and Nanostructured Materials, IMIM'13 - The 12th Conference on Intermolecular and Magnetic Interactions in Matter, Poros Island, Greece, 8-12.09. 2013 - oral presentation
3. M. Nachman, **S. Paszkiewicz**, E. Piesowicz, Z. Rosłaniec, *Gradient filled segmented block copolymer urethane elastomers with improve abrasion resistance***,** Joint Conferences on Advanced Materials: FNMA'13 - The 10th Conference on Functional and Nanostructured Materials, IMIM'13 - The 12th Conference on Intermolecular and Magnetic Interactions in Matter, Poros Island, Greece, 8-12.09.2013- poster
4. W. Brostow, G. Broza, E. Piesowicz, M. Nachman, **S. Paszkiewicz**, Z. Rosłaniec, *Synthesis and characterization of poly(butylene terephthalate) nanocomposites reinforced with oxidized carbon nanotubes*, Joint Conferences on Advanced Materials: FNMA'13 - The 10th Conference on Functional and Nanostructured Materials, IMIM'13 - The 12th Conference on Intermolecular and Magnetic Interactions in Matter, Poros Island, Greece, 8-12.09.2013- poster
5. **S. Paszkiewicz**, A. Szymczyk, Z. Špitalský, J. Mosnáček, Z. Rosłaniec, *Morphology and non-isothermal crystallization of poly(etylene terephthalate) (PET)/graphite oxide (GO) nanocomposites*, The Annual World Conference on Carbon, Carbon 2013, Rio de Janeiro, Brasil , 14-19.07.2013- oral presentation
6. **S. Paszkiewicz**, A. Szymczyk, Z. Špitalský, J. Mosnáček, Z. Rosłaniec, *Polymer nanocomposites based on graphene derivatives prepared by in situ polymerization, 3rd* Nanomeasure Scientific Symposium, Nanomeasure 2013, Warszawa Poland, 24-25.06.2013- oral presentation
7. **S. Paszkiewicz**, A. Szymczyk, M. Soccio, T.A. Ezquerra, Z. Rosłaniec, *Few Layer graphene (FLG) nanocomposites based on poly(trimethylene terephthalate) (PTT) matrix: structure and properties*, ICCS17- 17th International Conference on Composite Structures, Porto, Portugal, 17-21.06.2013- oral presentation
8. **S. Paszkiewicz**, A. Szymczyk, Z. Špitalský, J. Mosnáček, Z. Rosłaniec, *Investigations of nano-scale organization in PTT-block-PTMO copolymer/graphite oxide nanocomposites during melting and crystallization*, 3rd International Symposium Frontiers in Polymer Science, Sitges n. Barcelona, Spain, 21-23.05.2013- poster
9. **S. Paszkiewicz**, A. Szymczyk, Z. Špitalský, J. Mosnáček, Z. Rosłaniec**,** *Thermoplastic elastomers containing plate filler: layered silicates and graphene sheets***,** A European Conference/Workshop on the synthesis, Characterization and Applications of Graphene, Mykonos, Greece, 27-30.09.2012 - oral presentation

10. A. Szymczyk, **S. Paszkiewicz**, Z. Rosłaniec, *Thermoplastic elastomers/Organoclay nanocomposites: Morphology, Thermal and Mechanical Properties*, 7th IUPAC International Conference on Novel Materials and their Synthesis (NMS-VII) & 21st International Symposium on Fine Chemistry and Functional Polymers (FCFP-XXI) International Year of Chemistry 2011 of IUPAC, Shanghai, China, 16-21.10.2011- poster
11. **S. Paszkiewicz**, A. Szymczyk, Z. Špitalský, M. Soccio, J. Mosnáček, T.A. Ezquerra. Z. Rosłaniec, *Synthesis and characterization of PET/expanded graphite nanocomposites,* 2th International Conference on the Science and Application of Nanotubes, Cambridge, England, 10-16.07.2011- poster
12. **S. Paszkiewicz**, A. Szymczyk, Z. Rosłaniec, *Polymer nanocomposites based on poly(ethylene terephthalate) and carbon nanotubes and exfoliated graphite,* Multiphase Polymers and Polymer Composites from Nanoscale to Macro Composites Conference and Training School, Paris, France, 7-10.06.2011 - poster

Participation in national conferences:

1. M. Nachman, **S. Paszkiewicz**, Z. Špitalský, J. Mosnáček, Z. Rosłaniec, *Influence of Expanded graphite (EG) and graphene oxide (GO) on the synthesis of PET/EG and PET/GO nanocomposites*, Materiały Polimerowe Pomerania-Plast 2013, Międzyzdroje, Poland 4-7.06.2013-poster
1. **S. Paszkiewicz**, R. Pilawka, Z. Rosłaniec, *Influence of carbon nanotubes reinforcement on the processing and mechanical properties of CNT/epoxy nanocomposites,* Materiały Polimerowe Pomerania-Plast 2013, Międzyzdroje, Poland, 4-7.06.2013- poster
2. M. Kwiatkowska, **S. Paszkiewicz**, A. Szymczyk, Z. Rosłaniec, *Wpływ geometrii nanonapełniaczy węglowych na przepuszczalność pary wodnej kompozytów na bazie poli(tereftalanu etylenu),* Materiały Polimerowe Pomerania-Plast 2013, Międzyzdroje, Poland, 4-7.06.2013- poster
3. A. Szymczyk, **S. Paszkiewicz,** Z. Rosłaniec**,** *Nanokompozyty polimerowe z udziałem grafenu,* Materiały Polimerowe Pomerania-Plast 2013, Międzyzdroje, Poland, 4-7.06.2013 – poster
4. **S. Paszkiewicz**, A. Szymczyk, Z. Špitalský, J. Mosnáček, Z. Rosłaniec**,** *Effect of Expanded graphite on the phase structure and electrical properties of PTT/EG nanocomposites,* VII International Scientific and Technical Conference Carbon Materials and Polymer Composites, Ustroń Jaszowiec, Poland, 13-16.11.2012 - oral presentation
5. **S. Paszkiewicz**, A. Szymczyk, Z. Špitalský, J. Mosnáček, Z. Rosłaniec, *Struktura i właściwości termiczne nanokompozytów EG/PET,* VI Konferencja Naukowo-Techniczna Materiały Węglowe i Kompozyty Polimerowe, Ustroń-Jaszowiec, Poland, 7-11.11.2011- oral presentation
6. **S. Paszkiewicz**, A. Szymczyk, Z. Špitalský, M. Soccio, J. Mosnáček, T.A. Ezquerra. Z. Rosłaniec, *In situ synthesis and characteristics of polymer nanocomposites based on*

poly(ethylene terephthalate) and exfoliated graphite, The FNMA 2011 Joint Conferences on Advanced Materials, Szczecin, Poland, 6-9.09.2011 - oral presentation

7. R. Pilawka, **S. Paszkiewicz**, *Epoxy-vinylester composites obtained from prepregs,* XI Międzynarodowa Konferencja Naukowo-Techniczna, Olsztyn, Poland, 16-19.05.2011 - oral presentation
8. R. Pilawka, **S. Paszkiewicz,** *Epoxy-vinyl ester materials,* XV Seminarium „Kompozyty 2011- Teoria i praktyka", Spała, Poland, 27-29.04.2011- oral presentation
9. R. Pilawka, **S. Paszkiewicz**, *Kompozyty epoksydowo-winyloestrowe o wysokiej wytrzymałości mechanicznej*, VIII Konferencja Technologie Bezodpadowe i Zagospodarowanie Odpadów w Przemyśle i Rolnictwie, Międzyzdroje, Poland 15-16.06.2010 - poster
10. R. Pilawka, **S. Paszkiewicz,** *Laminaty epoksydowo-winyloestrowe,* Konferencja Materiały Polimerowe Pomerania-Plast 2010, Kołobrzeg, Poland, 8-11.06.2010- poster

Conferences' reports:

1. **Paszkiewicz S**., 2013 *Konferencje i Targi: The Annual World Conference on Carbon, Carbon 2013(Międzynarodowa Konferencja Carbon 2013) Rio de Janeiro, Brazylia, 14-19 lipca 2013 r.,* Polimery, 58(11-12), 927-928
2. **S. Paszkiewicz**, *Z.* Rosłaniec, *2011 Konferencje i Targi: NT11 International Conference on the science and Application of Nanotubes (12. Międzynarodowa Konferencja Badania i Zastosowanie Nanorurek Węglowych NT11,* Cambridge, Anglia, 10-16 lipca 2011, Polimery, 56(10), 770-772